STUDIES OF COPPER AND GOLD VAPOUR LASERS

Graeme Lawrence Clark

A Thesis Submitted for the Degree of PhD
at the
University of St Andrews

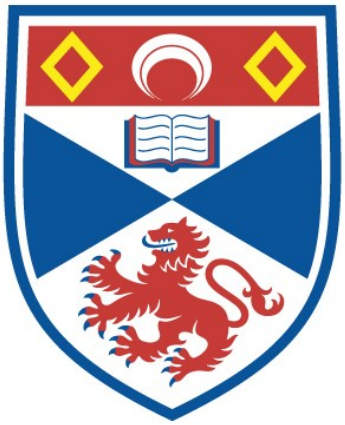

1988

STUDIES OF COPPER AND GOLD VAPOUR LASERS

A thesis presented by

Graeme Lawrence Clark, BSc

to the

University of St. Andrews

in application for the degree of

Doctor of Philosophy

January 1988

ProQuest LLC.
789 East Eisenhower Parkway
P.O. Box 1346
Ann Arbor, MI 48106 – 1346

DECLARATION

I, Graeme Lawrence Clark, hereby certify that this thesis has been composed by myself, and is a record of my own work, and that it has not been accepted in partial or complete fulfilment of any other degree or professional qualification.

I was admitted to the Faculty of Science of the University of St. Andrews under Ordinance General No. 12 in October 1983 and as a candidate for the degree of Ph.D. in October 1984.

Graeme Clark

CERTIFICATE

I certify that Graeme Lawrence Clark has spent nine terms at research work in the Physical Sciences Laboratory of St. Salvator's College, in the University of St. Andrews, under my direction, that he has fulfilled the conditions of Ordinance No. 16 (St. Andrews), and that he is qualified to submit the following thesis in application for the degree of Doctor of Philosophy.

A. Maitland

Research Supervisor

AUTHOR'S CAREER

The author was born in Johnstone, Scotland in 1961, and received his primary and secondary education in Glasgow. He obtained an honours degree in Natural Philosophy in 1983 from the University of Glasgow. In October 1983, he began his work on the project described here in the Physics Department of the University of St. Andrews, funded by the Science and Engineering Research Council. In October 1986, he joined EEV, working at St. Andrews both on this project and on a separate copper vapour laser development program. Since October 1987, he has been employed in the Gas Tubes Division of EEV in Chelmsford.

ACKNOWLEDGMENTS

I would like to thank my supervisor, Dr. Arthur Maitland, for his guidance, encouragement and friendship during the course of this work. Thanks for valuable discussions must also go to my colleagues past and present both at St. Andrews and at EEV and in particular : Roger, Ian, Robert, Janet, Andy K., Andy B., Natalie, Cliff and Colin.

The technical expertise of the mechanical workshop under Ron McCraw and the electronics workshop under Mike Robertson was essential to the success of this work. I thank everyone involved, especially for their hard work in the building of the gold vapour laser.

I am indebted to the Science and Engineering Research Council and to EEV for their financial support. In particular, I would like to thank Hugh Menown and Chris Neale of EEV for their support and patience.

Finally, I thank my family for their help and support, Lynn for her patience and understanding and all my friends for being my friends.

ABSTRACT

The work described in this thesis covers various aspects of pulsed copper and gold vapour lasers. The work is divided into four main parts : a computer model of the kinetics of the copper vapour laser discharge; construction and characterization of a copper vapour laser and a gold vapour laser system (to be used for photodynamic cancer treatment); analysis of the thermal processes occurring in the various forms of thermal insulation used in these lasers; and studies of the use of metal walls to confine a discharge plasma. The results of this work were combined in the design of the first copper vapour laser to use metal rather than an electrically insulating ceramic material for confinement of the discharge plasma. Laser action in copper vapour has been achieved in a number of metal-walled designs, with continuous lengths of metal ranging from 30 mm, in a segmented design, to 400 mm, where the discharge plasma was confined by two molybdenum tubes of this length. A theoretical explanation of the behaviour of plasmas in metal-walled discharge vessels is described.

CONTENTS

CHAPTER 1

1.1 THE COPPER VAPOUR LASER

1.1.1 INTRODUCTION

The copper vapour laser (CVL) is a high power, high efficiency laser, with output at 510.6 nm and 578.2 nm. A high repetition rate longitudinal electrical discharge in a buffer gas such as neon is used to excite the copper atoms to the upper laser levels. The discharge is also used to heat the active zone to about 1550°C, to produce the required copper vapour pressure of about 0.5 torr (Fig. (1.1)) [1]. The lower laser levels are metastable, so the population inversion is transient (self-terminating), and lasts only a few tens of nanoseconds. The laser must therefore be pulsed to allow time for the metastable levels to be deactivated between pulses.

Figure (1.2) shows a schematic outline of a CVL. The insulation is used to maintain a thermal gradient between the discharge and the outer wall of the laser, which is at room temperature. It must also confine the discharge to the zone between the electrodes and so materials which are both thermal and electrical insulators have been exclusively used until now. However, some of the work described in this thesis uses segmented metal tubes to confine the discharge and to provide thermal insulation.

1.1.2 HISTORICAL DEVELOPMENT

The first metal in which lasing was obtained in a self-terminating transition was lead [2]. This was followed by demonstrations of pulsed manganese [3] and copper [4] lasers. Since then,

a number of other metals have been shown to have self-terminating atomic laser transitions. Table (1.1) shows the optimum operating temperatures and the laser wavelengths for each metal. Of these, the CVL is the laser on which most work has been done.

The first CVLs used an oven to reach the required temperature. However, since they operated at low pulse repetition rates (< 1 kHz), only small output powers could be achieved, typically about 0.5 W [5]. Also, the total efficiency was low, because a large amount of power was needed to heat the oven.

A breakthrough in terms of both power output and efficiency was achieved when the energy from the capacitor discharge used to pump the laser was also used to heat the laser tube. This was done by increasing the repetition rate of the discharge by an order of magnitude. An output power of 15 W at 1% efficiency was obtained from the first discharge heated CVL [6]. The output power of the CVL is limited mainly by the size of the active volume, so that by increasing the bore diameter [7,8], output powers of over 100 W have been achieved [9].

1.1.3 ATOMIC STRUCTURE

The CVL has a typical efficiency of between 0.5% and 1%, which is high compared with other gas lasers with output in the visible part of the spectrum. A partial atomic energy level diagram (Fig. (1.3)) shows the reason for this. The first two sets of energy levels above ground are the lower and upper laser levels and the first allowed transition from ground is to the upper laser levels. Therefore there are no competing transitions and over half of the energy required to excite an atom to the ^2P states is returned as a laser photon. Although the ground to ^2D transition is radiatively forbidden, there

is still a significant cross-section for excitation by electron collision. Figure (1.4) [10] shows the excitation rates from ground of the $^2P_{3/2}$ and $^2D_{5/2}$ states. The voltage and current pulses must have fast risetimes in order to quickly achieve electron temperatures above 2 eV and thus avoid exciting the ^2D levels.

The lifetime of the ^2P to ground transition is about 10 ns, which would make achieving a population inversion difficult. As the density of copper atoms increases however, photons emitted when copper atoms make this transition are quickly absorbed by other ground state copper atoms. This process, known as radiation trapping (Section (3.9)) increases the effective lifetime of the ^2P states. At 1550°C, the copper density is about 10^{15} cm^{-3} and the effective lifetime of the ^2P to ground transitions is of the order of microseconds.

The laser transitions have longer lifetimes than the untrapped transitions to ground because an atom deexciting to the metastable levels must simultaneously move two electrons to different electron shells (Fig. (1.3)). However, as radiation trapping increases the upper laser level lifetime, the most likely radiative transition is to the ^2D states. The laser lines are shown in Fig. (1.3). The transition from $^2P_{3/2}$ to $^2D_{3/2}$ is allowed by the selection rules, but has only been observed once [11], and then only as superradiant emission.

1.1.4 KINETIC PROCESSES

1.1.4.1 EXCITATION AND IONIZATION

The upper laser levels are excited by inelastic collisions with electrons in the discharge. Once in the ^2P states, however, stimulated emission to the ^2D states is only one of a number of

possible processes. Excitation to higher lying energy levels followed by ionization, as well as ionization directly from the ^2P states are both important. This is shown by the high density of copper ions after the discharge pulse [12]. Superelastic relaxation processes, where slow electrons collide with excited atoms and gain energy by deexciting them, become increasingly important as the current density in the discharge rises. Increasing the discharge input energy eventually causes the laser output energy to saturate as superelastic collisions balance the excitation rate to the upper laser levels [13].

1.1.4.2 METASTABLE DEACTIVATION

Once a laser photon is emitted, the copper atom is left in the metastable ^2D state, and must return to the ground state before the next discharge pulse. The lifetime of the two metastable levels is dependent on a number of factors, including the dimensions of the discharge tube, the pressure and type of the buffer gas and the gas temperature.

In a CVL with bore diameter d and buffer gas pressure p such that $pd^2 < 100$ torr cm^2, the dominant deactivation mechanism is by wall collisions [14]. In narrow bore tubes ($d < 2$ cm), the lifetime of the metastable levels increases approximately linearly with the buffer gas pressure [14]. However, if neon is used, the ^2D lifetimes will decrease if the pressure rises high enough [15]. Neon has little direct effect on the copper laser levels [16], but it does reduce the electron temperature rapidly in the afterglow through elastic collisions. Since the cross-section for superelastic collisions increases as the electron energy falls (Section (3.5.2)), this becomes a significant deexcitation mechanism. At neon pressures above about 25 torr, the metastable lifetime falls to less than 25 μs [9]. There is also a large

cross-section for deactivation of the ^2D levels by other copper atoms [16].

1.1.4.3 PLASMA RECOMBINATION

For bore diameters of 1 cm or more, the factor limiting the output power of CVLs is not the lifetime of the ^2D levels, but the plasma recombination rate between discharge pulses [17]. This becomes increasingly important as the bore diameter increases. In Section (1.1.4.2), the ^2D lifetime is quoted as being less than 25 μs, so that pulse repetition rates of tens of kilohertz should be possible before the output pulse energy falls. However, maximum power output is usually obtained at between 5 and 10 kHz [9,18], and the energy per pulse decreases at even lower repetition rates [9] (Fig. (1.5)) [18].

The discharge circuit used with the CVL will always have an inductance associated with it, and this puts an upper limit on the rate at which energy can be deposited into the discharge. The slower the recombination rate, or the less time there is between pulses, the larger the electron density will be at the start of the following discharge pulse. Increasing the initial electron density has two effects: it reduces the rate of gain of energy of the electrons from the electric field and, at the same time, reduces the size of the electric field by decreasing the plasma impedance (Section (3.6)).

In order to run CVLs at high repetition rates, the operating temperature must be reduced, until at 200 kHz, the optimum wall temperature is only 1300°C [19]. By decreasing the wall temperature, the copper vapour density is reduced (Fig. (1.1)). This increases the electron mean free path, and so maintains the required electron temperature in the discharge. The recombination rate can also be increased by the addition of hydrogen (Section (1.3.4)) or by

arranging the charging circuit so that none of the capacitor charging current passes through the decaying plasma [19].

1.1.5 BUFFER GAS

As the walls of the discharge tube heat up, the buffer gas is used to carry the discharge between the electrodes. Once lasing starts, its main effect is to reduce the electron temperature in the afterglow with the result that the plasma recovers quickly. Usually, one of the noble gases is used, although lasing with H_2 added to neon has been observed [20]. Lasing has also been achieved with N_2 and H_2 as buffer gases [21]. Generally, it has been found that neon gives the highest power outputs [22]. Helium has also been used extensively, but its low mass means that it reduces the electron temperature through elastic collisions more than neon does. The heavier noble gases, Ar, Kr and Xe, produce a reduction in output power which is related to their excitation and ionization potentials. The lower these potentials are, the higher the rate of inelastic collisions with electrons becomes, so the electron temperature drops.

1.1.6 BASIC OPERATING CONDITIONS

Figure (1.6) [18] shows the variation of output power with temperature. The laser power initially rises because of the combined effect of the increasing copper density and the increasing lifetime of the upper laser levels. However, as the copper density rises, the electron temperature falls, and eventually drops below the threshold level for exciting the ^2P states. Also, the rising temperature increases the thermal population of the metastable levels and so reduces the size of the population inversion.

The ratio of energy in the green and yellow laser lines is affected by changes in the wall temperature. (Fig. (1.6)). Since the green line has the higher gain (58 dB/m compared with 42 dB/m for yellow [4]), the green pulse has more energy than the yellow one until the optimum temperature is reached [18]. For this reason, CVLs running at hundreds of kilohertz produce a laser output which is almost totally green, since they operate with much lower wall temperatures [19] (Section (1.1.4.3)). As the temperature rises and the total energy per pulse drops, the energy in the green pulse drops faster until there is more energy at 578 nm than at 510 nm. This is due to the increasing rate of collisional mixing of the ^2P states as the copper density rises [16], which decreases the $^2P_{3/2}$ population while increasing the $^2P_{1/2}$ population. At the same time, the thermal population of the $^2D_{5/2}$ state increases faster than that of $^2D_{3/2}$. The net result is to decrease the size of the population inversion for the green transition compared with the yellow one.

Figure (1.7) [23] shows the typical variation of output power with buffer gas pressure for constant supply voltage and frequency. A minimum pressure is required, both to keep the discharge between the electrode tips and stop it moving back towards the windows [8] and to prevent discharge instabilities [22]. Above this pressure, there is a fairly broad region where varying the buffer gas pressure has little effect. Eventually the output power drops, because of the reduction in the electron temperature as the frequency of elastic and inelastic electron-atom collisions increases.

1.2 METAL SEGMENTS

1.2.1 INTRODUCTION

The use of alumina in CVLs has a number of disadvantages. The main problem is the presence of large amounts of impurities which require prolonged outgassing procedures for their removal. Also, alumina tubes are conveniently available only in a limited number of standard diameters. Finally, although the melting point of high purity alumina is about 1950°C, it creeps at temperatures as low as 1500°C. In prolonged operation, this can cause the tube to sag and so reduce the output power [8].

If a metal with a high melting point and low vapour pressure at CVL operating temperatures, such as molybdenum (Fig. (1.1)), is used, it is possible to design a segmented system which uses only a small amount of alumina (Section (2.8.4)), or a system using metal tubes and no alumina (Section (7.2.3)). The thermal insulation is provided by concentric rings of molybdenum and/or layers of zirconia felt. In the segmented design, alumina rings are used to separate the segments and provide electrical insulation. The discharge plasma is confined by the molybdenum and in the tubular design, the ratio of the length of metal to the length of the insulating gap is 40:1 (Section (7.2.3)). The main source of contamination now comes from the surface oxide layer of the Mo, which is easily removed, and from the zirconia felt, which is outside the discharge zone. By adding layers of Mo sheet to the segmented design, the diameter of the discharge can be reduced without substantially altering the inner wall temperature.

Metal segments have been used before, but only in DC discharges. The most common application was in argon ion lasers [24]. The high

thermal conductivity of the metal allowed the heat dissipated by the discharge to be easily removed. Argon ion lasers using metal segments of 1.2 cm ID and 4 cm long have been demonstrated [25].

1.2.2 METAL SEGMENT THEORY

No theoretical work has been done on the physics of metal segments in pulsed discharges. A theory to determine the maximum length of a segment has, however, been worked out for DC discharges in some of the noble gases [26,27].

Figure (1.8(a)) shows the voltage drop along both the axis and the wall of a discharge tube which has a dielectric wall. Electrons diffuse to the wall much faster than ions, so that while the discharge is being established, the walls become negatively charged. This negative charge tends to attract positive ions and repel electrons with the result that the electron and ion currents to the wall become equal. The discharge wall therefore has a negative potential with respect to the plasma and a positive ion space charge sheath lies between the wall and the plasma. In equilibrium, the net current to the walls at every point is zero.

If floating metal segments are placed in a gas discharge, the voltage drop from one electrode to the other along an axial line next to the walls of the segments should be similar to that of Fig. (1.8(b)). Each part of a segment is at the same potential, so that although the net current to the segment in equilibrium must be zero, the current to each point will be different. At the anode end of each segment, the ion current will be greater than the electron current, and vice-versa at the cathode end.

For a given set of conditions in a discharge (type of gas, gas pressure, electric field), there is a maximum segment length. As can

be seen from Fig. (1.8(c)), if the segment is too long, a section of it will be at a positive potential with respect to the plasma. If this happens, a significant amount of the discharge current will flow through the segments and arc between them. By assuming a Maxwellian distribution of electron energies and negligible ionisation and recombination in the positive ion sheath, it can be shown [26] that the maximum segment length in an established neon discharge is given by

$$d_{max} = 1.1\ T_e / X \quad \text{metres} \quad , \qquad [1.1]$$

where T_e is the electron temperature and X (V/m) is the potential gradient on the discharge axis.

Equation [1.1] only applies to the case where the discharge is established, so that its usefulness in a pulsed CVL discharge is limited. Also, there is no theory to determine the optimum distance between segments.

1.3 HYDROGEN

1.3.1 INTRODUCTION

Hydrogen has been used in CVLs both on its own as a buffer gas and as an additive in a Cu-Ne mixture. When run with hydrogen as the buffer gas, the threshold temperature at which lasing starts is higher than when noble gases are used [21]. Also, the gas pressure must be lower than about 3 torr, or else lasing does not take place [15]. The addition of hydrogen in small quantities to a CVL using Ne as a buffer gas causes both the optimum pulse repetition rate and the output power to increase [20]. Reference [17] mentions a 4 cm diameter CVL which uses a Cu-Ne-H_2 mixture to obtain 60 W average power.

1.3.2 HYDROGEN CROSS-SECTIONS

Figure (1.9) shows the main inelastic cross-sections for electron impact collisions with both atomic [28,29] and molecular [30-32] hydrogen. It can be seen that excitation to the vibrational levels of H_2 [30] competes with excitation to the ^2P (and higher) levels of Cu, whereas the threshold for inelastic collisions with atomic hydrogen is above the electron temperatures reached in CVLs. Although the cross-section for excitation to the Cu ^2P levels is an order of magnitude larger than that to the vibrational levels of H_2, the rates for these two processes will be roughly equal when the H_2 pressure rises above 2-3 torr at the CVL operating temperature. The competition between these processes is complicated by the large dissociation cross-section of H_2 [32]. The electron energy distribution suffers large losses in an H_2 discharge, due to the large elastic cross-section for collisions with the molecules [33] and the low molecular mass, as well as the large vibrational cross-sections at low energies. Therefore, if the H_2 density is too high, the electron temperature does not become high enough for the majority of molecules to be dissociated [34].

Hydrogen also has a large elastic scattering cross-section with Cu atoms. In narrow tubes, where the main relaxation process for the ^2D levels is via wall collisions, raising the H_2 pressure from 1 to 2 torr increases the $^2D_{5/2}$ lifetime from 40 to 75 μs [15]. Hydrogen must therefore reduce the rate of diffusion of Cu atoms to the walls. There is also a large cross-section for collisional mixing of the copper ^2P states which can change the ratio of power in the yellow and green laser lines [16].

The momentum transfer cross-section for H_2 is of the order of

10^{-15} cm^2 [33], whereas for Ne it is about a factor of three smaller [35]. From the plasma resistance equation (Section (3.6)), the addition of H_2 to a Ne discharge would be expected to increase the plasma resistance. Similarly, a pure H_2 discharge should have a larger resistance than a pure Ne discharge, for equal electron and gas densities.

1.3.3 HYDROGEN BUFFER GAS

To operate a CVL with hydrogen as the buffer gas, it is obvious from Section (1.3.2) that the hydrogen molecules must be dissociated or else the rate of inelastic collisions becomes too high. If the pressure is low enough for a large proportion of the molecules to be dissociated, then lasing is possible. However, the pulse energy may be reduced compared with neon because of the lower mass and lower lying energy levels of atomic hydrogen.

1.3.4 HYDROGEN AS AN ADDITIVE

The effect on the optimum PRF of adding small amounts of hydrogen to neon can be understood with reference to Figure (1.10) [35,36]. Since the rates of volume recombination (Section (1.4.5)) and metastable deactivation increase as the electron temperature decrease, the addition of hydrogen to neon must reduce the electron temperature in the afterglow faster than pure neon can, due to its large elastic scattering cross-section and small mass. The density of the hydrogen additive can only be increased to a certain level before the laser power drops for the reasons given in Section (1.3.2).

The addition of hydrogen to a mixture of a metal and a noble gas has been studied for a He-Na-H_2 pulsed discharge [37]. For a He

pressure of 6 torr, the addition of 2 torr of H_2 significantly reduced both the electron temperature and density in the initial stages of the discharge. This was attributed to the inelastic losses from excitation and dissociation of the hydrogen molecules. There is also an interaction between H_2 and Ne. Adding small percentages (0.1% to 1.0% by volume) of H_2 to Ne deexcites the Ne metastable levels. As the density of H_2 increases, the peak electron density decreases [38] since the main ionization path for neon is by two-step ionization via the metastable levels. This has resulted in a Ne-H_2 laser [39] where the hydrogen was present as an impurity in a Ne discharge.

1.4 THE COPPER VAPOUR LASER DISCHARGE

1.4.1 INTRODUCTION

In the CVL discharge, a high electric field is applied across the gas in the laser tube by an external circuit. This field accelerates free electrons in the gas until they have sufficient energy to ionize atoms and so produce more electrons. The field remains at a high level until the discharge impedance falls as the gas breaks down. The energy stored in the circuit is then dissipated in the plasma until the electric field has dropped to below the level required to sustain the discharge. The plasma then moves from a conducting to a non-conducting state as the ions and electrons recombine.

1.4.2 PASCHEN'S LAW AND PREIONIZATION

In a homogeneous electric field, the breakdown voltage of a gas-filled cavity is dependent on both the type of gas and the product of the gas pressure and the distance between the electrodes. This

dependence is known as Paschen's law and is shown in Fig. (1.11) [40] for neon. However, the breakdown voltage in a pulsed discharge is partially governed (for a constant gas pressure) by the risetime of the pulse. Since it takes the gap a finite time to break down, it is possible to increase the voltage across the cavity to more than the breakdown value predicted by Paschen's law. The higher the voltage is at breakdown, the more energy there is that can be dissipated in the discharge before its impedance collapses.

Paschen's law does not take into account preionization of the discharge volume. If the gas is "seeded" with electrons prior to the discharge, the discharge will develop through the regions occupied by the preionization electrons. To obtain a uniform discharge with no arcing, the whole of the discharge volume must be preionized. In a CVL, the discharge is unstable when the tube is cold, and resembles a "twisting wire" [41]. As the tube heats up, however, the discharge becomes uniform due to the high electron density left from the previous pulse. If there is no preionization, the discharge is not uniform, even when hot, and lasing is very weak [42]. Therefore, at high pulse repetition rates, each discharge pulse acts as the preionization source for the following one. This allows CVLs to be constructed with unusual cross-sectional shapes (e.g. annular [43]) and yet still have a homogeneous discharge and laser output. Preionization also allows the CVL to be operated at much higher buffer gas pressures than would be allowed by Paschen's law for the cold, unionized gas. There are a number of examples of CVLs being run with buffer gas pressures of the order of an atmosphere, discharge gaps of tens of centimetres and breakdown voltages of less than 20 kV [44,45].

Although the electric field in the CVL discharge is not homogeneous, and the cavity does not break down at the voltages predicted in Fig. (1.11), Paschen's law still holds qualitatively. If

the buffer gas pressure is too low, the discharge will extend right out to the windows. As the pressure increases, the discharge gradually contracts until it is confined between the tips of the electrodes.

1.4.3 PULSED DISCHARGES IN LONG TUBES

The development of discharges in long insulating tubes [46,47] is important in understanding why metal segments do not conduct in the initial stages of the discharge before a positive ion sheath has had time to build up.

The discharge in a tube with its length much greater than its diameter starts with the ionization of the gas around the high-voltage electrode. An ionization wave front moves from the high-voltage electrode to the earthed electrode, leaving behind a conducting plasma. The region between the ionization wave front and the high voltage electrode can be regarded as a discharge with an increasing length. The ionization wave acts as a cathode, and propagates by ionizing the region ahead of it. It does this by accelerating electrons with its associated electric field and also by photoionization. Behind the wave front, a current flows in the plasma from the high-voltage electrode and charges up the walls. This current is given by [46],

$$I = C_o \, v \, V \quad , \qquad [1.2]$$

where v is the velocity of the ionization wave, V is the voltage on the high voltage electrode and C_o is the capacitance per unit length of the capacitor formed by the walls of the discharge tube and the nearest earthed object. The ionization wave velocity is dependent on

the gas, the geometry of the discharge gap and the experimental conditions.

1.4.4 CATAPHORESIS AND DIFFUSION

During the operation of a CVL, copper is gradually lost from the high temperature zone by the combined effects of diffusion and cataphoresis. This puts a limit on the length of time lasing can be achieved with a single fill of copper. Usually, 5 or 10 g of copper will last for a few hundred hours under conditions which produce maximum output power. The rate of diffusion of copper is determined by the buffer gas pressure, the discharge cross-sectional area and the axial temperature gradient. Commercial CVLs run at higher than optimum buffer gas pressures to prolong the time between copper refills.

In a discharge containing a mixture of a metal vapour and a noble gas, the metal is driven to the cathode end by a process called cataphoresis [48]. In this process, the constituent with the lowest ionization potential flows to the cathode end in the form of an ion current. To reduce the loss of copper by this method, the buffer gas can be flowed in the opposite direction.

In the absence of a discharge, cataphoresis will have no effect so that diffusion determines the copper distribution in the afterglow. The relative effect of these two processes will depend on factors such as the pulse repetition rate, temperature gradients, the electric field strength during the discharge, the buffer gas pressure and the initial distribution of copper in the laser.

1.4.5 RECOMBINATION PROCESSES

Depending on the diameter of the discharge and the buffer gas pressure in the CVL, there are two main forms of plasma recombination : wall and volume recombination. Wall recombination occurs under conditions of ambipolar diffusion as electrons and ions move at equal rates to the wall. There, they recombine in fast three-body processes with the atoms or molecules of the wall. When the wall temperature is below about 1200°C, there is very little copper in the discharge, so that only volume recombination processes involving neon need be considered. However, once the copper density becomes significant, the density of neon ions drops and afterglow processes involving copper ions become more important.

In a pure neon discharge, the dominant recombination process depends on the neon pressure. At low neon pressures (< 5 torr), ambipolar diffusion dominates, and molecular ions are not present [49]. As the pressure increases, dissociative recombination becomes more important until eventually Ne_2^+ ions are the principal afterglow ions [50].

When copper vapour appears in the discharge, the density of neon ions drops and the kinetic processes in the afterglow become more complicated. A number of processes are believed to occur [51], but an estimate [51] of the rate constants suggests that the following processes are the most important.

$$Cu^+ + e^- + Ne \rightarrow Cu^* + Ne \qquad (1)$$

$$Cu^+ + Cu + Ne \rightarrow Cu_2^+ + Ne \qquad (2)$$

$$Cu_2^+ + e^- \rightarrow Cu^* + Cu \qquad (3)$$

REFERENCES FOR CHAPTER 1

1 Rosebury F., HANDBOOK OF ELECTRON TUBE AND VACUUM TECHNIQUES, p142, ADDISON-WESLEY (1965)

2 Fowles G.R., Silfvast W.T., APPL. PHYS. LETT. 6, 236 (1965)

3 Piltch M., Walter W.T., Solimene N., Gould G., Bennett Jr. W.R., APPL. PHYS. LETT. 7, 309 (1965)

4 Walter W.T., Piltch M., Solimene N., Gould G., BULL. AMER. PHYS. SOC. 11, 113 (1966)

5 Walter W.T., IEEE J.Q.E. 4, 355 (1968)

6 Isaev A.A., Kazaryan M.A., Petrash G.G., JETP LETT. 16, 27 (1972)

7 Isaev A.A., Lemmerman G.Yu., SOV. J.Q.E. 7, 799 (1977)

8 Smilanski I., Kerman A., Levin L.A., Erez G. OPT. COMM. 25, 79 (1978)

9 Grove R.E., LASER FOCUS July, 45 (1982)

10 Kushner M.J., Warner B.E., J. APPL. PHYS. 54, 2970 (1983)

11 Weaver L.A., Liu C.S., Sucov E.W., IEEE J.Q.E. 10, 140 (1974)

12 Batenin V.M., Klimovskii I.I., Lesnoi M.A., Selezneva L.A. SOV. J.Q.E. 10, 563 (1980)

13 Tenenbaum J., Smilanski I., Lavi S., Levin L.A., Erez G. OPT. COMM. 36, 391 (1981)

14 Miller J.L., Kan T., J. APPL. PHYS. 50, 3849 (1979)

15 Bokhan P.A., Solomonov V.I., SOV. J.Q.E. 3, 481 (1974)

16 Chen H., Erbert G., J. CHEM. PHYS. 78, 4985 (1983)

17 Bokhan P.A., SOV. J.Q.E. 15, 622 (1985)

18 Marazov O., Stoilov St., Borisov V., Draganov Iv., Ivanov S. J. PHYS. E : Sci. Instrum. 17, 127 (1984)

19 Soldatov A.N., Fedorov V.F., SOV. PHYS. J. 26, 844 (1983)

20 Bokhan P.A., Silant'ev V.I., Solomonov V.I.
SOV. J.Q.E. 10, 724 (1980)

21 Ferrar C.M., IEEE J.Q.E. 10, 655 (1974)

22 Lesnoi M.A., SOV. J.Q.E. 14, 142 (1984)

23 Isaev A.A., Kazaryan M.A., SOV. J.Q.E. 7, 253 (1977)

24 Labuda E.F., Gordon E.I., Miller R.C., IEEE J.Q.E. 1, 273 (1965)

25 Wang C.P., Lin S., J. APPL. PHYS. 43, 5068 (1972)

26 Maitland A., J. PHYS. D: Appl. Phys. 4, 907 (1971)

27 Cornish J.C.L., Maitland A.
J. PHYS. D: Appl. Phys. 6, 1899 (1973)

28 McGowan J.W., Williams J.F., Curley E.K.
PHYS. REV. 180, 132 (1969)

29 McGowan J.W., Clarke E.M., PHYS. REV. 167, 43 (1968)

30 Schulz G.J., PHYS. REV. 135, A988 (1964)

31 Rapp D., Englander-Golden P., J. CHEM. PHYS. 43, 1464 (1965)

32 Corrigan S.J.B., J. CHEM. PHYS. 43, 4381 (1965)

33 Henry R.J.W., Lane N.F., PHYS. REV. 183, 221 (1969)

34 Shaw T.M., J. CHEM. PHYS. 30, 1366 (1959)

35 Cherrington B.E., GASEOUS ELECTRONICS AND GAS LASERS
PERGAMON PRESS (1979)

36 de Heer F.J., McDowell M.R.C., Wagenaar R.W.
J. PHYS. B: Atom. Molec. Phys. 10, 1945 (1977)

37 Nazarov V.N., Eikhvald A.I., OPT. SPECTROSC. 56, 347 (1984)

38 Martin R.J., Rowe J.E., J. APPL. PHYS. 39, 4289 (1968)

39 Dezenberg G.J., Willett C.S., IEEE J.Q.E. 7, 491 (1971)

40 Meek J.M., Craggs J.D., ELECTRICAL BREAKDOWN OF GASES
p558 (1978) JOHN WILEY AND SONS

41 Smilanski I., Erez G., Kerman A., Levin L.A.
OPT. COMM. 30, 70 (1979)

42 Gabay S., Smilanski I., IEEE J.Q.E. 16, 598 (1980)

43 Kan T., Ball D., Schmitt E., Hill J.
APPL. PHYS. LETT. 35, 676 (1979)

44 Marasov O.R., Stoilov St., OPT. COMM. 46, 221 (1983)

45 Burmakin V.A., Evtyunin A.N., Lesnoi M.A.
SOV. J.Q.E. 9, 939 (1979)

46 Abramov A.P., Mazan'ko I.P., SOV. PHYS. TECH. PHYS. 25, 446 (1980)

47 Abramov V.P., Ishchenko P.I., Mazan'ko I.P.
SOV. PHYS. TECH. PHYS. 25, 449 (1980)

48 Sosnowski T.P., J. APPL. PHYS. 40, 5138 (1969)

49 Sauter G.F., Gerber R.A., Oskam H.J., PHYSICA 32, 1921 (1966)

50 Bates D.R. (Editor), ADVANCES IN ATOMIC AND MOLECULAR PHYSICS
VOL. 6, 15 (1970) ACADEMIC PRESS

51 Borovich B.L., Nalegach E.P., Rybin V.M. Yurchenko N.I.
SOV. J.Q.E. 14, 1632 (1984)

FIGURE 1.1 : VAPOUR PRESSURE CURVES OF Mo AND Cu

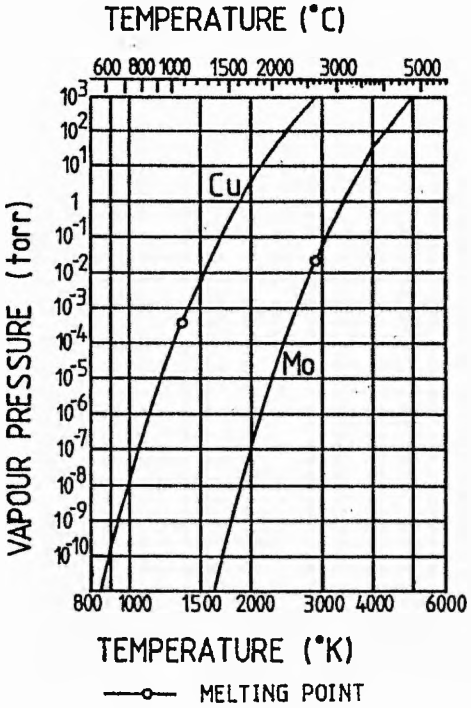

TABLE 1.1

SELF-TERMINATING LASER TRANSITIONS

ELEMENT	WAVELENGTH (nm)	OPTIMUM TEMPERATURE (°C)
Cu	510·6 , 578·2	1550
Fe	452·9	1700
Au	312·2, 627·8	1600
Mn	534·1,1290·0	1200
Pb	722·9	900
Ba	1130,1500	800
Tl	535·1	750
Ca	534·9, 5547	700
Sr	6457	600

FIGURE 1.2 : SCHEMATIC OUTLINE OF CVL

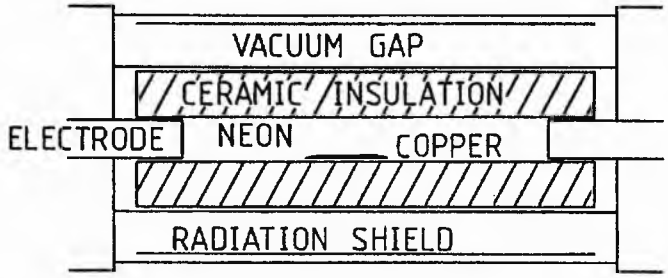

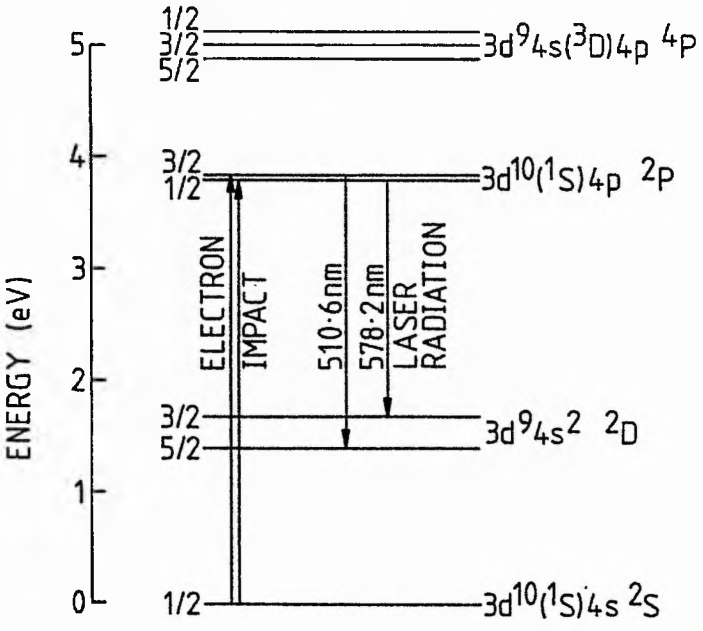

FIGURE 1.3: PARTIAL ENERGY LEVEL DIAGRAM OF COPPER

FIGURE 1.4: COPPER ELECTRON IMPACT EXCITATION RATES

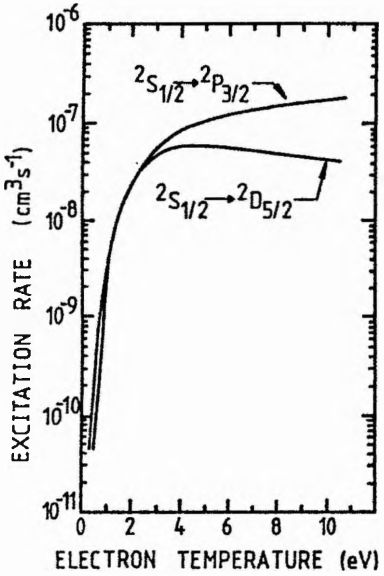

FIGURE 1.5: DEPENDENCE OF POWER AND PULSE ENERGY ON FREQUENCY

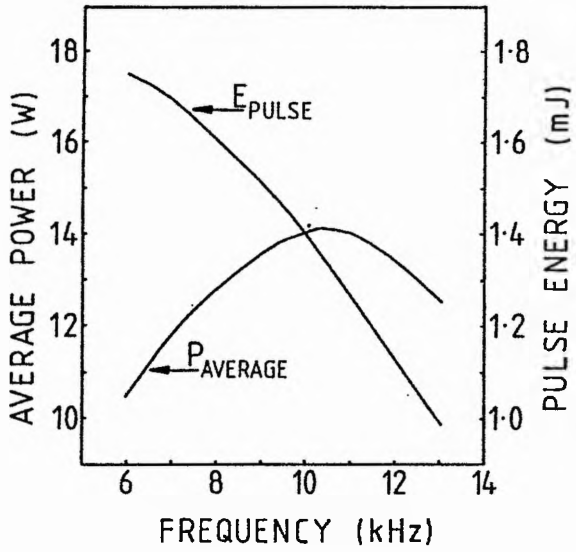

FIGURE 1.6: DEPENDENCE OF LASER POWER ON DISCHARGE TUBE TEMPERATURE

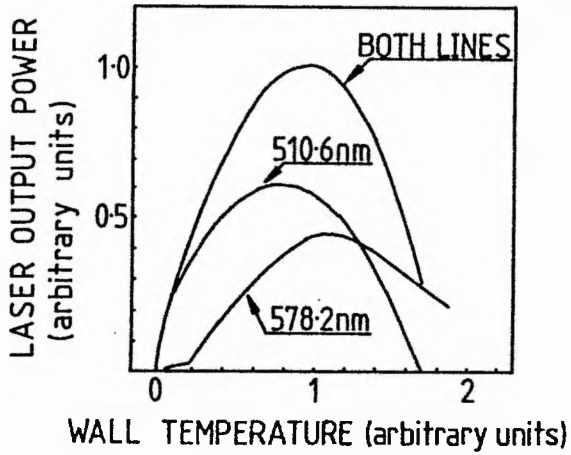

FIGURE 1.7: DEPENDENCE OF LASER POWER ON NEON BUFFER GAS PRESSURE

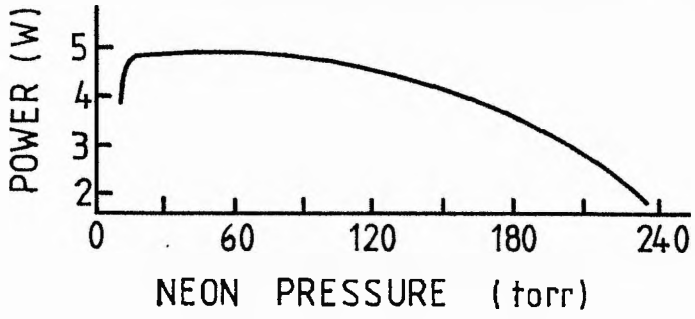

FIGURE 1.8: AXIAL AND WALL POTENTIALS IN A GAS DISCHARGE WITH DIFFERENT WALLS

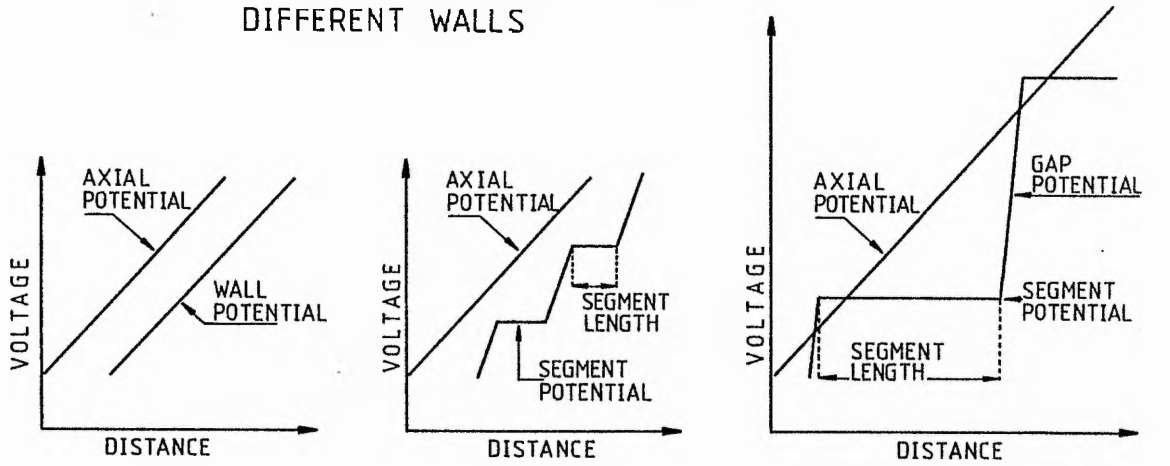

FIGURE 1.9: INELASTIC CROSS-SECTIONS FOR H AND H_2

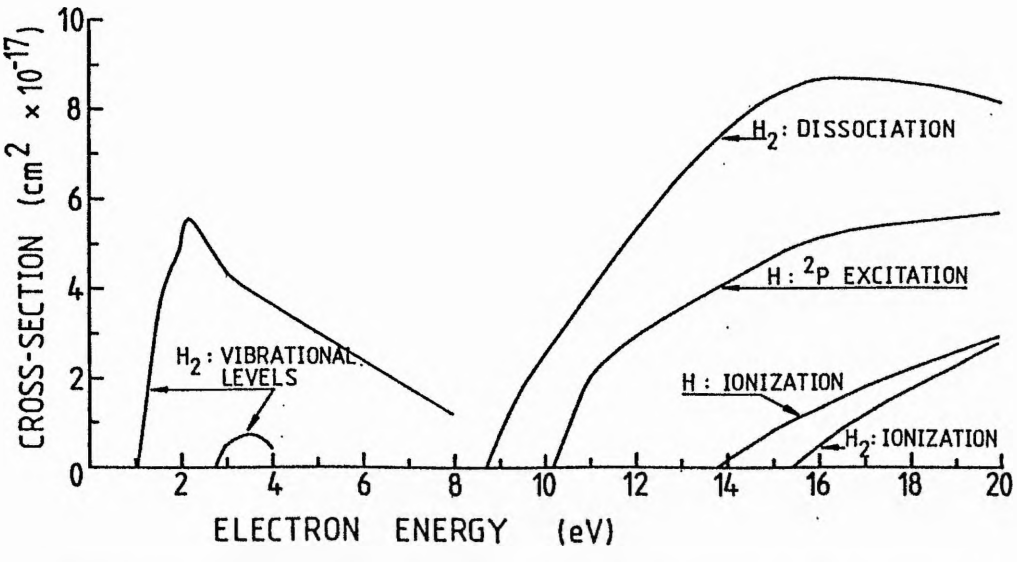

FIGURE 1.10: TOTAL ELASTIC SCATTERING CROSS-SECTIONS FOR NEON AND ATOMIC HYDROGEN

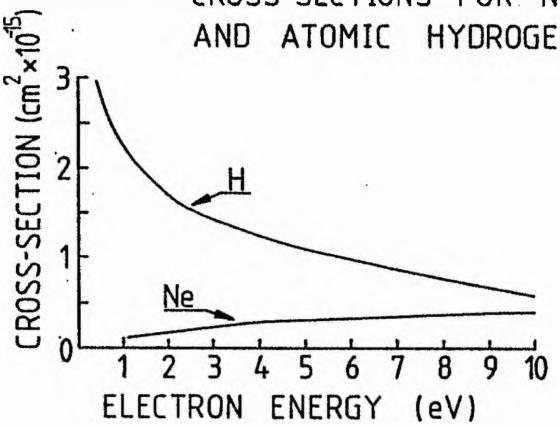

FIGURE 1.11: PASCHEN CURVE FOR NEON

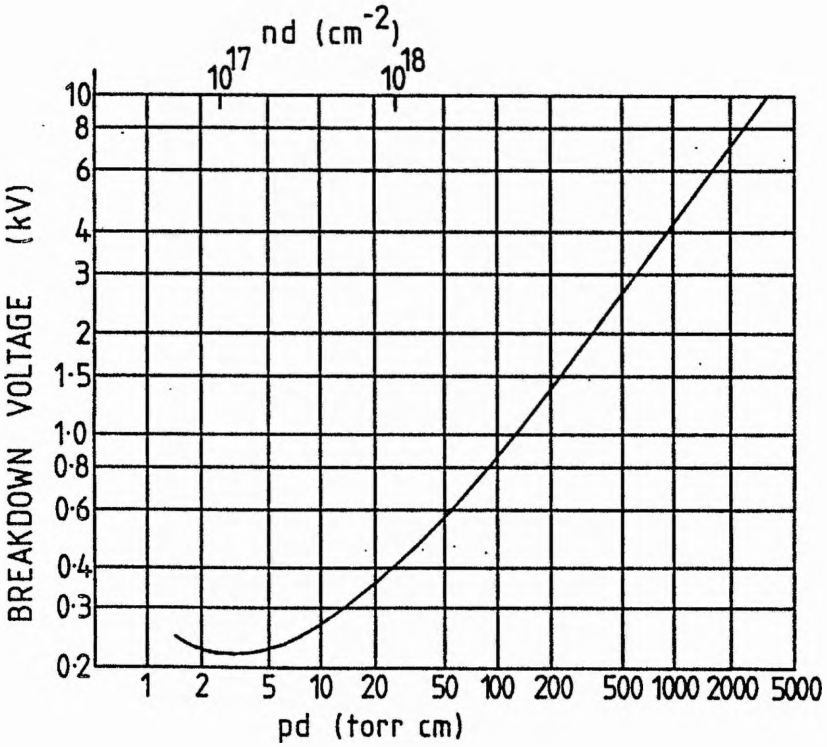

CHAPTER 2

2 THE COPPER VAPOUR LASER SYSTEM

2.1 INTRODUCTION

The CVL system can be divided up into a number of components as shown schematically in Fig. (2.1). Apart from the water cooling supply, the laser output power was dependent on all the other components in the system. Also, the operation of, and the components in, the electrical circuit were affected by the operation of the laser itself.

2.2 CIRCUIT COMPONENTS

The circuit used to run the laser is shown in Fig. (2.2). The DC power supply was rated to 10 kV, 1.0 A. The 5 μF capacitor was used to smooth the output from the power supply in the event of any sudden fluctuations of the load. A 1 MΩ resistor was connected across this capacitor to allow it to discharge when the power supply was switched off. The charging inductor L_c was designed according to the principles described in Appendix (A.4). A diagram of the charging inductor is shown in Fig. (2.3). By adding or removing layers of wire and/or changing the width of the air gap, the inductance could be altered within a certain range of values. The ferrite cores used were U-cores (type FX3860, Philips), with dimensions of 100x57x25 mm^3. The ferrite material was manganese-zinc ferroxcube, grade A16 (3C8, Philips), which has a low dissipation loss. The charging diode D was a KHP25 (Electronic Devices, Inc) high voltage diode rated to 25 kV reverse bias voltage and 2.25 A average forward current. Strontium

titanate ($SrTiO_4$) capacitors were used, either TDK type UHV-9 or Murata type DHS60 N4700 202M-40. These were rated to 40 kV DC, and had a measured capacitance of 1.8 nF. The TDK capacitors were 32 mm wide with a diameter of 60 mm. The Murata ones were slightly wider. Their small size allowed them to be mounted close to the laser cathode to reduce the circuit inductance. Figure (2.4) shows the characteristics of $SrTiO_4$ capacitors [1]. The main advantage of these capacitors was their low dissipation factor. There was a drop in capacitance with temperature, but this was not a problem. When running, the capacitors typically reached a temperature of about 40°C, corresponding to a 10% drop in capacitance. Barium titanate ($BaTiO_4$) capacitors have also been used. Figure (2.5) shows their operating characteristics [1]. The higher dissipation factor of this type caused severe overheating problems. Both CX1535 and CX1625 (EEV) thyratrons have been used. Their operation is described in more detail in Sections (2.3) and (2.4). Appendix (B) contains a general description of thyratrons and their operation. The charging inductor, charging diode and thyratron were all mounted under oil, whereas the capacitors were mounted on or next to the laser cathode. The thyratron anode was connected to the storage capacitor C_s by an 80 cm length of 50Ω coaxial cable (type URM74, BICC) which could carry up to 4.6 kW at 20°C [2]. The braid screen of the cable was connected to the thyratron cathode and to the earthed side of the peaking capacitor. The bypass charging element could be either a resistor or an inductor. A 200Ω high-wattage resistor and a 110 μH air-cored inductor have both been used (separately).

2.3 THYRATRON CX1535

The CX1535 is a hydrogen-filled, triple grid (pentode) thyratron

with a metal-ceramic body (Appendix (B)). There are two versions, one being oil-cooled by total immersion and capable of holding off 25 kV, while the other is air-cooled and is rated to only 18 kV. Both types have been used in the CVL discharge circuit. Figure (2.6) shows a schematic outline of the CX1535 and the connections to the discharge circuit, heater and trigger supplies. Grids 1 and 2 switch the tube on and grid 3 enables the thyratron to recover quickly so that it can be run at repetition rates of up to 100 kHz [3]. The thyratron is mounted by means of the cathode flange.

2.3.1 GRID STRUCTURE

Grid 1 (G1) preionizes the G1-cathode volume, as well as isolating grid 2 (G2) from the cathode plasma during the recovery stage after conduction. Therefore, the density of plasma around the cathode does not appreciably affect the current flowing in the G2 circuit during recovery. By applying a negative bias voltage to G2, the thyratron is kept non-conducting, since the bias shields the plasma around the cathode from the large positive voltage on the anode. The thyratron switches to the conducting state when a sufficiently large positive voltage pulse is applied to G2. Grid 2 is therefore known as the control grid. Grid 3 (G3) is a shield grid, which, together with G1, shields G2 from the rest of the tube. It was connected to the cathode by a 5Ω, high wattage, resistor to reduce the capacitance between the anode and G2. This was necessary to allow the thyratron to run at high repetition rates. At high rates of rise of the anode voltage, a large capacitance between G2 and the anode would tend to make the grid voltage follow the anode voltage positive and so trigger the thyratron.

2.3.2 HEATER CIRCUIT

The heater circuit for the CX1535 is shown in Fig. (2.7) [4]. Usually, 6.3 V AC is applied to both heater terminals, with the cathode being the common connection. The getter is used to remove contaminants from the thyratron. The replenisher is the gas reservoir (Appendix (B.1)). The barratter is an iron, wire-wound constant-current device with a large temperature coefficient of resistance. A change in current causes the temperature to change, so the resistance alters to keep the current at a constant level. The resistors R_1 and R_2 are used to vary the current through the replenisher. They are set by EEV so that, at the recommended heater voltage, the gas pressure is as high as possible without causing recovery problems. The capacitors C_1 and C_2 are used to protect the heater circuits against spikes generated when the thyratron breaks down. Large spikes could penetrate the insulation around the reservoir and so cause a short-circuit between the cathode and reservoir heaters. The capacitors C_1 and C_2 both consist of three, 0.47 μF capacitors in parallel.

2.3.3 COOLING

The CX1535 can be cooled either by total immersion in oil or by forced-air cooling. In each case, the maximum allowed temperature of the thyratron body is 150°C. Both of these cooling methods have been used, and Fig. (2.8) shows the arrangement used in each case.

Air cooling was provided by a fan blowing onto the base, to cool the reservoir heater circuit, and by a hose blowing compressed air into the anode cup. This form of cooling was not successful, as the anode cup became red hot at high power levels. However, the

overheating was not due to lack of cooling on the anode, but to insufficient cooling on the base. If the base temperature rose above the recommended maximum, the amount of current flowing through the replenisher dropped, which caused the gas pressure to drop and so increased anode dissipation for the reasons outlined in Appendix (B).

To improve the cooling, the thyratron was totally immersed in oil. A pump was used to direct warm oil through a cooler. The stream of cold oil which emerged from the cooler removed heat from the thyratron base. The anode cup was cooled by convection. With the thyratron cooled in this way, there were no dissipation problems.

2.3.4 TRIGGERING

Two different trigger units have been used. One, an ALCYON unit, supplied pulses to both G1 and G2. The G1 pulse was 400 V high, with a 0.1 μs risetime (between 25% and 75% of the peak) and a pulsewidth (FWHM) of 2.6 μs. The G2 pulse was also 400 V, but with a risetime of 0.15 μs and a 1.1 μs pulsewidth. The G2 bias was -100 V. The trigger pulses were supplied to each grid via a 220Ω, 11 W, wire-wound resistor. Wire-wound resistors were used to protect the trigger supply from high voltage spikes generated on the grids when the thyratron switched. The G2 pulse was delayed by 1 μs with respect to the start of the G1 pulse to allow time for the G1-cathode region to break down. This provided a large initial amount of plasma around the cathode so that breakdown proceeded rapidly when G2 was triggered. The second trigger unit was a 2 kV sub-modulator. This supplied a 93 mA DC priming current to G1 via a 1.5 kΩ, 30 W wire-wound resistor. This DC current kept the G1-cathode region permanently ionized. The G2 bias was -150 V. A 3.7 kV pulse was applied to G2 via a 500Ω, 10 W wire-wound resistor to trigger the thyratron.

2.3.5 RECOVERY

Once conduction in the thyratron ceases, the plasma starts to recombine, and the G2 voltage starts to fall from the arc level to the bias level. The plasma recombination processes occur mainly on the grid surfaces, so that the flow of ions to G2, attracted by the increasingly negative voltage there, must be equalled by an electron current flowing in the opposite direction from the grid supply. As the electron current increases, the inductance of the wire-wound resistor in series with G2 will induce a positive voltage on the grid, which slows the rate of rise of the negative bias. However, since the volume of plasma about G2 is very small, the ion current soon reaches a peak value and so the full bias voltage appears on G2. When the ion current starts to fall, the electron current follows, causing a negative voltage to be induced at the grid, which makes the grid more negative than the bias voltage. The ions are therefore accelerated faster to the grid. When the plasma has recovered, the electron and ion currents fall to zero and the G2 voltage returns to the bias level.

Figure (2.9) shows the voltage at G2 when the thyratron is filled with gas, but there is no voltage on the anode. Breakdown of the G2-cathode gap can be seen to occur and then as the plasma starts to recombine, the voltage at the grid falls to the bias level. For a short time (about 200 ns here), the ion and electron currents are steady, so G2 is at the bias level. As the current falls, the voltage drops below the bias level until the plasma has recovered and the current flow ceases. The increase in the negative voltage on G2 can significantly reduce the recovery time.

2.4 THYRATRON CX1625

A CX1625 has also been used in the CVL discharge circuit (Fig. (2.10)). This is a hollow-anode (Appendix (B.4)), oil-cooled, deuterium filled, metal/ceramic pentode thyratron. In normal operation it is limited to 1 kHz maximum repetition rate. However, it can be adapted to operate at up to 8 kHz.

For high repetition rate operation, grid 0 (G0) was supplied with a 0.5 A DC current through a 300Ω high wattage resistor. This current kept the region between G0 and the cathode permanently ionized. The thyratron was kept in the non-conducting state by a bias voltage of -150 V applied to G1, which shielded the anode from the G0-cathode plasma. The anode was connected to G2 by a thick piece of copper braid, which effectively made G2 act as the anode, so that the high voltage gap was between G1 and G2. The thyratron was triggered by applying a 3.7 kV pulse to G1 via a 100Ω wire-wound resistor.

The cathode and reservoir heaters were supplied from separate transformers so that the gas pressure could be adjusted independently of the cathode heater voltage. The cathode heater was kept at 6.6 V and 37.5 A and the reservoir heater at about 6.3 V, 7 A.

The heaters dissipate roughly 300 W and the tube itself dissipates between 100 and 300 W/A average anode current, depending on the rate of rise and fall of the anode current. To dissipate these thermal powers effectively, the thyratron was cooled by totally immersing it in oil. The cooling arrangement was the same as that shown in Fig. (2.8(a)) for the CX1535.

2.5 CVL CIRCUIT

2.5.1 CHARGING CIRCUIT

The charging circuit is shown in Fig. (2.11(a)). The storage capacitor C_s is charged inductively from the high voltage power supply via L_c, the diode and the bypass charging element. The size of the charging inductor depends both on the time to be allowed for charging and the size of C_s. For resonant charging, where the circuit discharges at the same time as the peak voltage on C_s is reached, L_c is given by equ. [A.14]. The voltage on C_s and the current through the diode are shown in Fig. (2.12) for the cases where L_c is less than, equal to, and greater than, L_r, the size of inductor required for resonant charging. The presence of the diode allows the circuit to be run at lower frequencies by stopping current reversal and so maintaining the peak voltage on C_s.

Inductive charging has two main advantages over resistive charging. The losses in the circuit are lower and the rate of increase of the voltage on the thyratron anode is lower immediately after the discharge pulse, which allows the thyratron time to recover. If resistive charging is used, a large proportion (>50%) of the available power is dissipated in the resistor. Also, the rate of rise of voltage on the thyratron anode is very high, which can cause the thyratron to start conducting again without a trigger pulse being applied.

The choice of bypass charging element affects both the performance of the laser and the charging circuit. Once copper vapour starts to diffuse through the discharge volume, the plasma conductivity rises, both during the discharge and in the afterglow. A

significant proportion of the charging current will therefore flow through the decaying plasma if the impedance of the bypass charging element is too high. A high level of ionization is therefore maintained in the afterglow which lowers the plasma impedance at the start of the following discharge pulse. For this reason, the output power can drop if a resistor is used [5]. The use of an inductor, with its lower impedance during the charging cycle, reduces the current flowing through the plasma. However, the laser power will also drop if the circuit is arranged so that none of the charging current flows through the decaying plasma [5]. A small current is therefore desirable to maintain the preionization at the optimum level.

The choice of bypass charging element affects the performance of the charging circuit mainly when the tube is cold or when contaminants are present in large amounts. In both of these cases, the impedance of the discharge is high for the duration of the discharge pulse, so that some of the energy will be dissipated in the circuit components rather than in the discharge. If a resistor is used, the energy is dissipated over a period with a time constant dependent on the impedance of the discharge plasma and the resistor in parallel, which may be of the order of microseconds. In this case, the load is over-matched, so that the large impedance produces a positive reflection on the thyratron anode which can cause the thyratron to fail to recover. If an inductor is used, the discharge voltage can oscillate for many microseconds with a time constant T_d determined by the size of the inductor and the peaking capacitor. This time constant is given by

$$T_d = 2\pi(C_p L_b)^{1/2} \quad . \qquad [2.1]$$

This also produces a reflection but in this case a negative voltage

appears at the thyratron anode. Since the CX1535 is unidirectional, this voltage will remain on the anode and on the following cycle will cause C_s to be charged up to a voltage V_c given by

$$V_c = 2V_s - v(0) \quad , \qquad [2.2]$$

where V_s is the power supply voltage and v(0) is the voltage on the thyratron anode at the start of the charging cycle (Appendix (A.2)). If the negative voltage becomes too large, the thyratron will start to dissipate too much power and may overheat. When the CX1625 thyratron is used, inverse voltages are quickly removed, and C_s always charges up to twice the supply voltage.

2.5.2 DISCHARGE CIRCUIT

The discharge circuit is shown in Fig. (2.11(b)). When the thyratron is triggered, the anode voltage falls to the arc drop level and C_s starts to discharge. The voltage across the laser increases as the charge on C_s is transferred to C_p. If the impedance of the inductor L_b is high enough, only an insignificant amount of the discharge current will flow through it. The voltage across the laser increases until the gas breaks down, at which point C_p discharges into the laser. Any energy left in C_s also discharges into the laser. In order to reduce the risetime of the current pulse, C_p is chosen to be smaller than C_s.

2.5.3 CIRCUIT INDUCTANCE

In order to obtain a fast rising current pulse, the inductance of the discharge circuit is minimized. By using a peaking capacitor, the

inductance of the thyratron is removed from the laser discharge loop. The inductance is further reduced by mounting C_p close to the laser, and by adding a coaxial return around the laser.

The discharge loop is almost totally coaxial, so the inductance of that part of it can be estimated from

$$L = \frac{\mu_o}{8} + \frac{\mu_o}{2} \ln(r_2/r_1) \quad , \qquad [2.3]$$

where μ_o is the permittivity of free space, r_2 is the radius of the outer conductor (the coaxial return) and r_1 is the radius of the inner conductor. If the current density across the discharge is uniform, the inductance of the coaxial system is 330 nH/m. However, when the discharge constricts, the current geometry changes, causing an increase in the inductance.

There is also an inductance associated with the discharge itself, which decreases as the gas breaks down. The plasma inductance is inversely proportional to the electron density (Section (3.6)). Therefore, when contaminants are released by outgassing, the electron density in the discharge increases at a lower rate, due to the presence of molecular species and electro-negative gases. Also, the current geometry may change. The presence of contaminants therefore results in a higher discharge inductance. Since the inductance of the coaxial system is low, an uncontrolled increase in inductance will have a large effect. The characteristic frequency w_q of the discharge loop is given by

$$w_q^2 = \frac{1}{LC} - \frac{R^2}{2L^2} \quad , \qquad [2.4]$$

where L, C and R apply to the discharge loop as a whole. Therefore, if we have

$$R > (2L/C)^{1/2} \quad , \qquad [2.5]$$

the discharge will be aperiodic. If, however, the inductance increases for the above reasons, so that R is such that

$$R < (2L/C)^{1/2} \quad , \qquad [2.6]$$

the discharge current and voltage will oscillate and energy will be deposited in the inductance of the loop outside the discharge.

2.5.4 DISCHARGE IMPEDANCE

The discharge impedance is dependent on a number of factors : the power deposited, which is dependent on the size of C_s and/or the voltage to which C_s is charged; the amount of preionization; the circuit inductance; the current geometry; the buffer gas pressure and type and the presence of contaminants or copper vapour. As the discharge tube heats up, these parameters vary, and so the impedance changes. In an ideal system, the load impedance should be exactly matched to the output impedance of the pulse forming network for maximum power transfer. However, since the CVL discharge impedance changes by orders of magnitude each time the gas breaks down, it is difficult to exactly match the circuit to the load. In this system, matching is taken to be when the voltage pulse is as in Fig. (2.13), with only a slight overswing.

2.6 LASER HEAD

2.6.1 LASER HEAD DESIGN

The laser design is shown in Figs. (2.14), (2.15) and (2.16). The thermal insulation is placed inside the quartz tube, which is 1 metre long, with inner and outer diameters of 56 and 60 mm respectively. The gap between the quartz and pyrex tubes is evacuated to reduce heat losses by conduction and convection. The quartz tube can be replaced easily, so different insulation configurations can be used in the same system. Pyrex (or Duran) tubing is used for the outer tube because it is at a much lower temperature (less than 300°C) than the inner one. The pyrex tube is 94.6 cm long with inner and outer diameters of 7.5 and 8.0 cm respectively. These two tubes fit into the end flange assemblies (Fig. (2.15)). The pyrex tube is shorter than the quartz one because it sits in the brass flange while the quartz tube extends beyond it to sit in the stainless steel flange. The evacuated gap is isolated both from the discharge cavity and the atmosphere by o-ring seals. The quartz-pyrex gap is evacuated from the anode end through a connection in the anode flange. Molybdenum foil is wrapped round the inside of the pyrex tube to act as a radiation shield. A water-cooled coaxial return, made up of two concentric brass tubes with the water flowing between them, runs from the anode flange to within 16 cm of the cathode flange. The coaxial return serves the dual purpose of reducing the inductance associated with the discharge and of removing heat radiated from the quartz through the pyrex. The coaxial return is supported at one end by the anode flange and at the other by a leg resting on the aluminium rail on which the laser is mounted.

The stainless steel end flanges contain the electrodes, the buffer gas input and output connections and the window mounts. The

electrodes are simply sheets of molybdenum rolled up and inserted into the end flanges. The buffer gas enters at the cathode end, flows through the cavity, and leaves at the anode end, thus reducing the cataphoretic effects on the copper ions and removing contaminants. Spectrosil B windows, 40 mm in diameter and 5 mm thick are mounted in nylon flanges at 5-10^{o} from normal incidence. The nylon ensures that the discharge cannot reach the windows and the small angle of incidence prevents them from forming secondary optical cavities. When running, this causes a small amount of the laser beam to be reflected off the windows away from the plane of the main laser beam. Both steel flanges have a water jacket welded onto the main structure. The cathode is the high voltage end and is insulated from the aluminium rail by a nylon block 6 cm high. The anode flange is mounted onto the rail by steel legs and the coaxial return is supported at its end by a single leg whose height can be adjusted to take the weight of the return off the pyrex tube.

The bypass charging element is mounted between the cathode flange and the near end of the coaxial return. The peaking capacitors are mounted on the cathode flange and are connected to the coaxial return by a wide strip of copper sheet.

The mirrors are mounted outside the laser. A flat aluminium mirror is used as a total reflector with a quartz flat as the output coupler. The mirrors are placed 2 m apart.

2.6.2 LASER HEAD ASSEMBLY

The laser head is assembled by placing the quartz tube which contains the insulation inside the pyrex tube. Both of these tubes are placed inside the coaxial return. The coaxial return is then placed on the aluminium rail, supported at one end by its leg, and at

the other by a lab-jack. The cathode flange is fixed, so the coaxial return must be brought up to it. With about 15 cm of the pyrex/quartz tubing protruding from the cathode flange end of the coaxial return, the thin locking flange (Fig. (2.15)) is slid onto the pyrex tube. An o-ring is then fitted onto the pyrex tube and the tube is slotted into the support flange (Fig. (2.15)). The quartz tube is then pushed through the support flange and an o-ring placed around it. The whole assembly is pushed towards the cathode flange. The threaded rods protruding from the cathode flange slot into the holes in the locking and support flanges. The quartz tube slots into the cathode flange. Care must be taken to ensure that the quartz tube is centred to avoid breaking it. The same process is then repeated at the anode end: first the pyrex o-ring (the locking flange is part of the coaxial return), then the brass flange with the quartz tube running through it and finally the quartz tube's o-ring is put on. The anode flange is then moved into position and the threaded rods on it slid into the holes in the brass flange and end flange of the coaxial return. Again, the quartz tube must be carefully centred in the anode flange.

In order to take the laser head apart, the above process is carried out in reverse. The electrodes can be inserted into the end flanges by removing the windows and pushing the Mo sheet in from the ends. To load the laser with copper, an open-ended plastic tube containing the copper wire pieces is inserted into the laser tube. The copper is pushed out with a rod as the plastic tube is withdrawn along the length of the laser tube to ensure a uniform distribution.

2.7 VACUUM AND GAS SUPPLY SYSTEM

Two rotary pumps are used to evacuate the laser. One is connected to the vacuum gap between the quartz and pyrex tubes while the other

one evacuates the discharge cavity. It was found to be necessary to use two pumps in order to prevent some of the buffer gas diffusing into the vacuum gap. If this happens, the pressure in the gap rises, and discharges become possible there. Also, for the gap to be effective as an insulator, the pressure must be as low as possible to ensure that radiation is virtually the only heat loss process. To control both the rate of flow and pressure of the buffer gas, a Swagelok bellows metering valve (SS-4BMG) is placed between the cathode gas input and the gas bottle together with a Swagelok bellows valve (SS-4BK) between the anode and the rotary pump. To prevent the discharge going to the gas supply, the supply is connected to the cathode via a 1m long glass coil and a 1m length of plastic tubing. A Leybold-Heraeus Diavac-K pressure gauge, measuring from 1 mbar to atmospheric pressure, is placed between the glass coil and the metering valve.

2.8 THERMAL INSULATION

2.8.1 INTRODUCTION

The thermal insulation must satisfy a number of criteria. First, it must allow an inner wall temperature of 1550^{o}C to be maintained without requiring more power than the discharge circuit can handle. Secondly, the insulation should provide a uniform inner wall temperature over as much of the length of the discharge tube as possible. Finally, since the maximum safe operating temperature of quartz is about 1000^{o}C, the insulation between the discharge and the quartz wall must allow a temperature difference of more than 500^{o}C. These criteria have been satisfied successfully both by using a wholly ceramic insulation configuration and a segmented metal-ceramic one.

Most CVLs use ceramic insulation [6-8]. However, a number have used layers of metal foil (to act as radiation shields) placed in a vacuum outside the ceramic tube which confined the discharge [9,10]. The use of multilayer radiation shields outside a ceramic tube has not been successful because the large dielectric stresses induced across the ceramic tube caused it to fracture [11].

2.8.2 MATERIALS

There are four materials used in the high temperature zone of the CVL described in this thesis : they are alumina, zirconia, quartz and molybdenum.

Alumina (Al_2O_3) is a ceramic material which combines high strength, low thermal conductivity, low electrical conductivity and a high maximum service temperature. However, its large coefficient of thermal expansion (Fig. (2.17)) [12] makes it susceptible to fracture when it is heated or cooled too rapidly or nonuniformly. Figures (2.18) [13] and (2.19) [14] show the thermal conductivity and electrical resistivity, respectively. Recrystallized alumina tubing (99.8% pure) is used. This type of alumina has a maximum service temperature of 1950°C. However, at temperatures close to this, it softens and creeps, causing the tube to distort. As alumina heats up, various impurities outgas and can affect the operation of the laser. Impurities detected when a CVL using an alumina tube is operating include gases such as N_2, O_2 and H_2, and low vapour pressure metals, such as Na and Ca [15].

Zirconia (ZrO_2) has a melting point of about 2700°C and a very low thermal conductivity. Pure zirconia is monoclinic and undergoes a phase change to the tetragonal crystal form at about 1000°C, causing a drop in volume of 7%. It reverts to the monoclinic state when the

temperature drops below 1000°C again. To prevent this, about 6% of a suitable metal oxide is added to convert the crystal structure to the stable cubic form. This prevents the change in volume, but lowers the melting point to about 2600°C. Stabilized zirconia has a very low coefficient of thermal expansion. The zirconia used in the laser is in the form of ZIRCAR zirconia felt (type ZYF). The felt is white and easily tears, making it difficult to use in large quantities. It is stabilized by the addition of 8% by weight of yttria (Y_2O_3). The thermal conductivity in various atmospheres is shown in Fig. (2.20) [16]. The dotted line shows the values used in our calculations (Chapter 5). The melting point is 2590°C, but the felt loses its flexibility after being heated to 1370°C. It has a vapour pressure of 8×10^{-12} torr at 1370°C. As the temperature increases, the electrical resistance decreases (Fig. (2.19)).

Fused quartz has a melting point of 1750°C, but should be kept below 1100°C to avoid devitrification. Since its coefficient of thermal expansion is very low (5.4×10^{-7} K^{-1}), it is resistant to thermal shock.

Molybdenum is of interest as a material for use in CVLs because of its high melting point (2617°C) and low vapour pressure over the CVL operating range (Fig. (1.1)). It is ductile and easily worked. Above 760°C, it forms an oxide which evaporates as it is formed [17], so that an air-leak in a CVL using molybdenum segments would seriously damage them. The emissivity is low (Figure (2.21)) [18] and so molybdenum is a suitable material for a radiation shield.

2.8.3 CERAMIC INSULATION

The ceramic insulation configuration is made up of a 2.0 cm I.D., 2.85 cm O.D. recrystallised alumina tube with zirconia felt (2.5 mm

thick) wrapped around it to a diameter of about 5.5 cm. Care must be taken to ensure that the fragile felt is not torn. The felt and alumina are then pushed into the quartz tube. To stop any of the discharge current running between the felt and the quartz wall, extra felt is forced in at each end to block any gaps.

2.8.4 SEGMENTED INSULATION

The general form of the segmented insulation is shown in Fig. (2.22). The thermal insulation in a segment consists of concentric molybdenum cylinders made from 3 cm wide strips of sheet ten thousandths of an inch thick. The strips are of different lengths so that, when rolled into a tubular shape, they form 3 cm long cylinders of different diameters. The ends of the strips are not joined, they merely butt together. Dimples are punched in each strip to reduce the amount of contact between concentric rings, so that ideally, the rings act as multilayer radiation shields. To reduce the thermal conductivity between concentric rings, the outer surface of each ring can be flame sprayed with zirconia and strips of zirconia felt placed between concentric rings. In Fig. (2.22), three insulating layers, each made up of a strip of zirconia felt held between concentric molybdenum rings, are placed inside an alumina ring (5.5 mm wide, 4.4 cm I.D.) for support. In turn, the alumina ring is placed inside the quartz tube. Another insulating layer is placed between adjacent alumina rings. This outer layer's inner diameter is such that it does not touch the layer held by the alumina ring. Therefore, there is no continuous metal path between the electrodes longer than the length of a metal segment. The effective length of a segment can be increased by removing alumina rings and pushing the 3 cm long segments together.

2.8.5 FLAME SPRAYING

Flame spraying is a process by which one material can be coated with a different material without heating the surface being coated. The process is applied here to coat the molybdenum rings with stabilized zirconia to reduce the radial thermal conductivity of a segment. The flame spraying system used is a CastoDyn System 2000 (Eutectic Co.). The coatings applied are first a bond coat (Metaceram 29029S) and then a low thermal conductivity ceramic coat (Metaceram 28085). The bond coat is a Ni-based alloy with 6% Al added. The ceramic coat is made up of ZrO_2 and CaO in the ratio 60:40. The maximum temperature at which this ceramic material can be used is quoted as 1000°C [19]. At the gun's outlet, the coating material is uniformly fed into an oxy-acetylene flame in powder form and sprayed on to the surface to be coated which has to be thoroughly cleaned for the coatings to adhere. The Mo rings were cleaned by sand-blasting them. The rings were then placed round a metal bar. which was rotated while the rings were sprayed to ensure an even coat thickness. The inside surface of each Mo ring was only occasionally discoloured, showing that little oxidation of the Mo took place. The resulting coat is very strong and has withstood numerous thermal cycles to CVL operating temperatures without flaking off.

REFERENCES FOR CHAPTER 2

1 : MURATA MFG CO. LTD. : DHS SERIES CAPACITORS DATA SHEETS

2 : BICC CABLESELECTOR No. E19 DATA SHEET (NOV. 1978)

3 : EEV HYDROGEN THYRATRON PRODUCT DATA HANDBOOK (1985)

4 : Pirrie C.A., EEV, Private communication (1986)

5 : Karras T.W., PROC. INT. CONF. LASERS 1980, 139, STS PRESS (1981)

6 : Bokhan P.A., Nikolaev V.N., Solomonov V.I.
SOV. J.Q.E. 5, 96 (1975)

7 : Marazov O., Stoilov St., Borisov V., Draganov Iv., Ivanov S.
J. PHYS. E : Sci. Instrum. 17, 127 (1984)

8 : Piltch M., Gould G., REV. SCI. INSTRUM. 37, 925 (1966)

9 : Miller J.L., Kan T., J. APPL. PHYS. 50, 3849 (1979)

10 : Alger T.W., LAWRENCE LIVERMORE NATIONAL LAB. REPORT
No. UCRL-83649 (1980)

11 : Andrews A., Oxford Lasers, Private communication (1986)

12 : Coors Technical Data Sheet (1985)

13 : Kingery W.D., Francl J., Coble R.L., Vasilos T.
J. AMER. CERAMIC SOC. 37, 107 (1954)

14 : Espe W., MATERIALS OF HIGH VACUUM TECHNOLOGY, VOLUME 2,
p569 (1968) Pergamon Press

15 : Karras T.W., PROC. INT. CONF. LASERS 1980, p168, STS Press (1981)

16 : Zircar Products Technical Data, Bulletin No. ZPI-207 (1984)

17 : Brady G.S., Clauser H.R., MATERIALS HANDBOOK VOLUME I, p496
McGraw Hill, 11th Edition (1977)

18 : Goldsmith A., Waterman T.E., Hirschhorn H.J.
HANDBOOK OF THERMOPHYSICAL PROPERTIES OF SOLID MATERIALS
VOLUME 1, pI-M-4, Pergamon Press (1961)

19 : Witts L., Eutectic Co., Private communication (1987).

FIGURE 2.1 : COPPER VAPOUR LASER SYSTEM

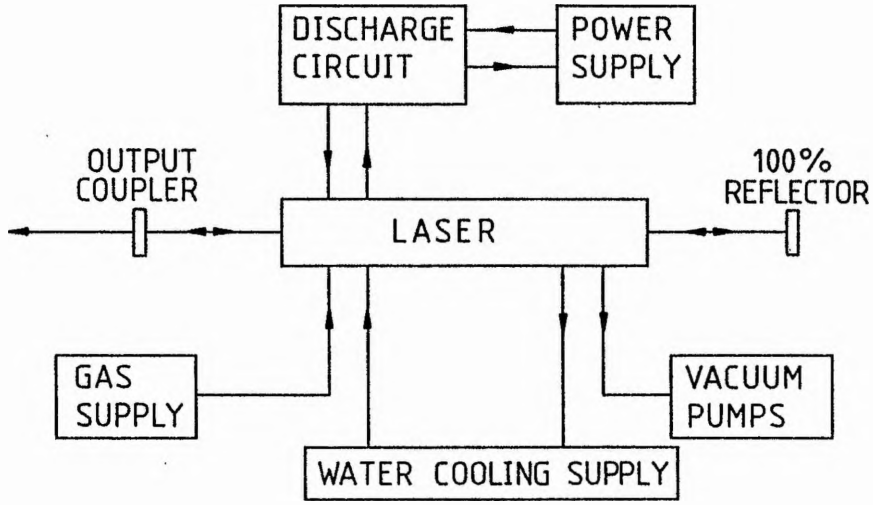

FIGURE 2.2 : LASER CIRCUIT

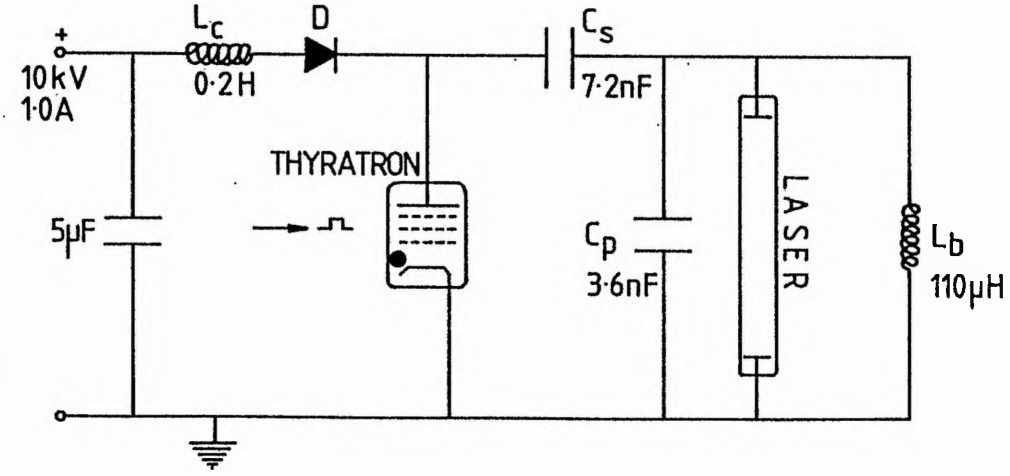

FIGURE 2.3 : CHARGING INDUCTOR

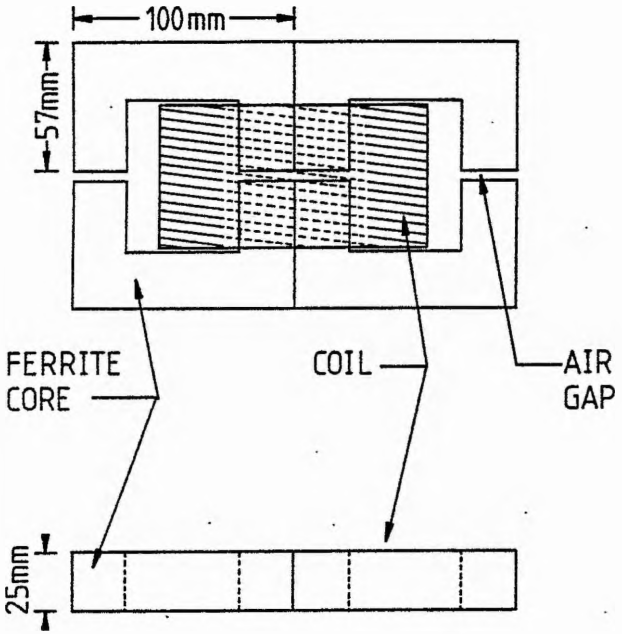

FIGURE 2.4: DISSIPATION FACTOR AND CAPACITANCE DATA FOR $SrTiO_4$ CAPACITORS

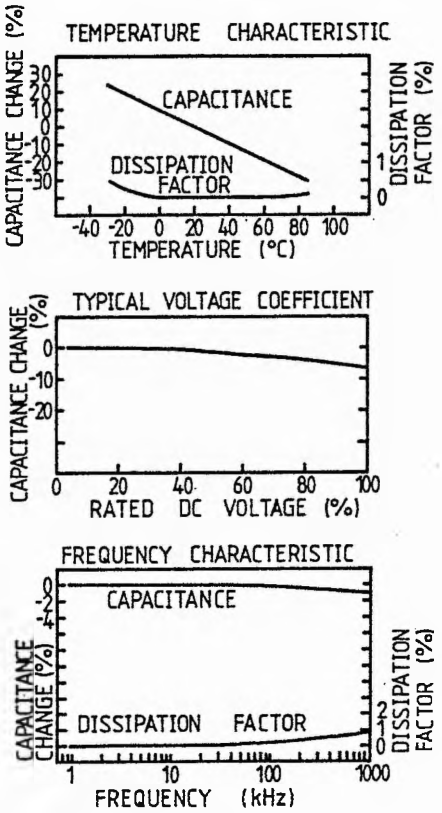

FIGURE 2.5: DISSIPATION FACTOR AND CAPACITANCE DATA FOR $BaTiO_4$ CAPACITORS

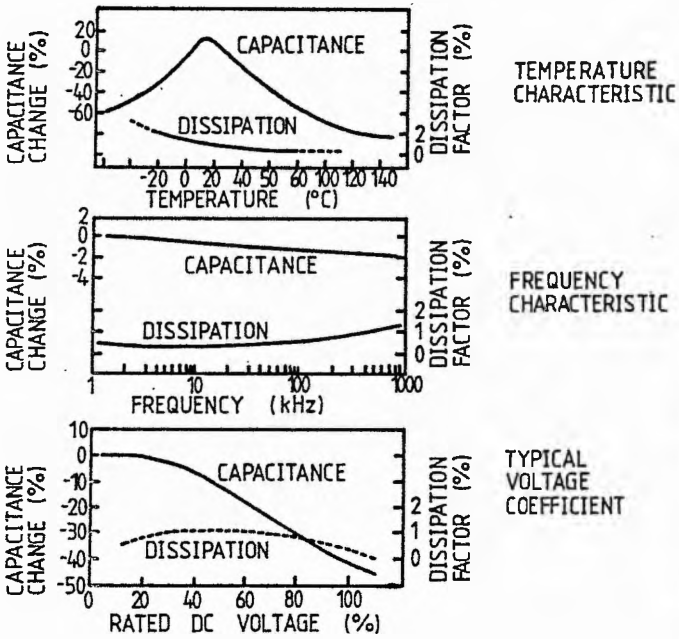

FIGURE 2.6 : SCHEMATIC OUTLINE OF THE CX1535 THYRATRON

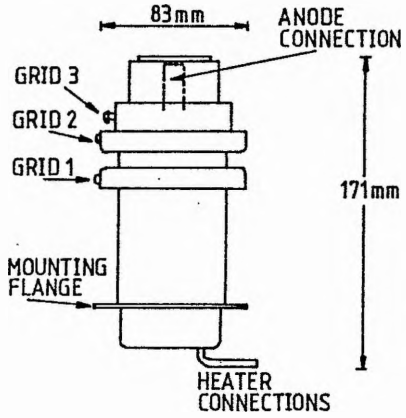

FIGURE 2.7: HEATER CIRCUIT FOR THYRATRON CX1535

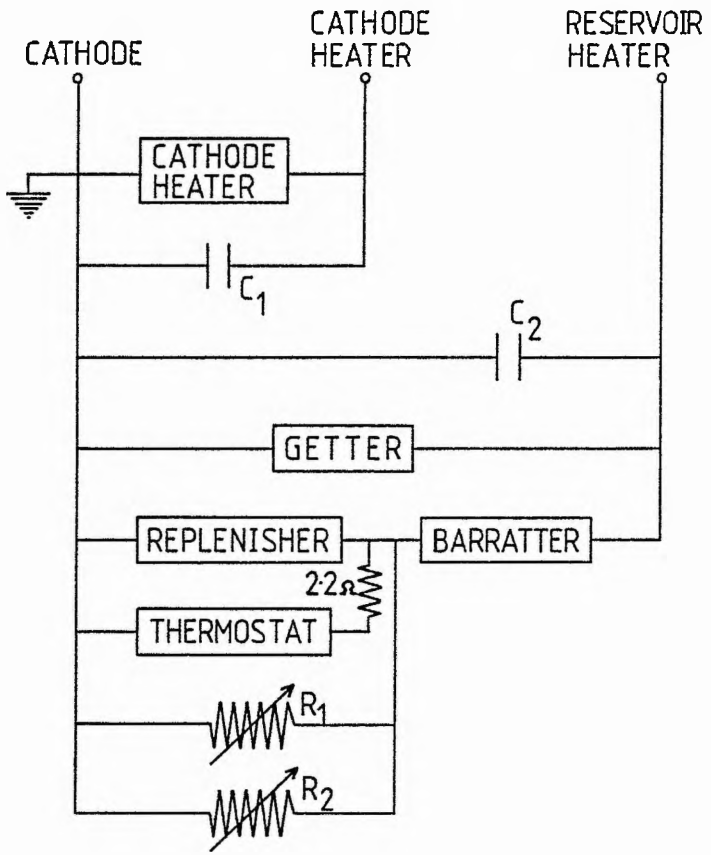

FIGURE 2.8: THYRATRON COOLING

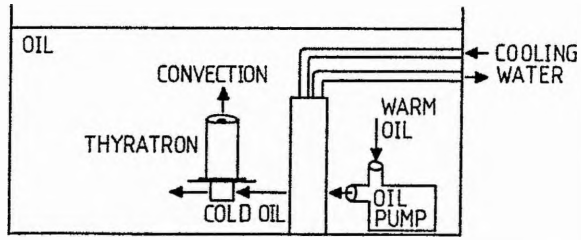

(a) OIL COOLING

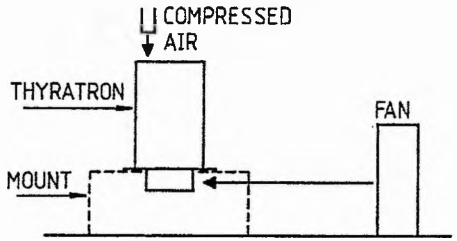

(b) FORCED-AIR COOLING

FIGURE 2.9 : GRID 2 VOLTAGE

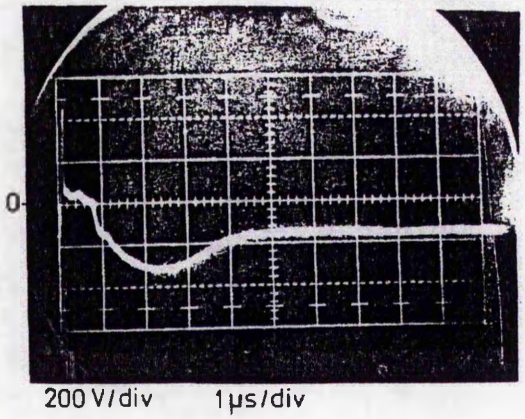

FIGURE 2.10 : SCHEMATIC OUTLINE OF THE CX1625 THYRATRON

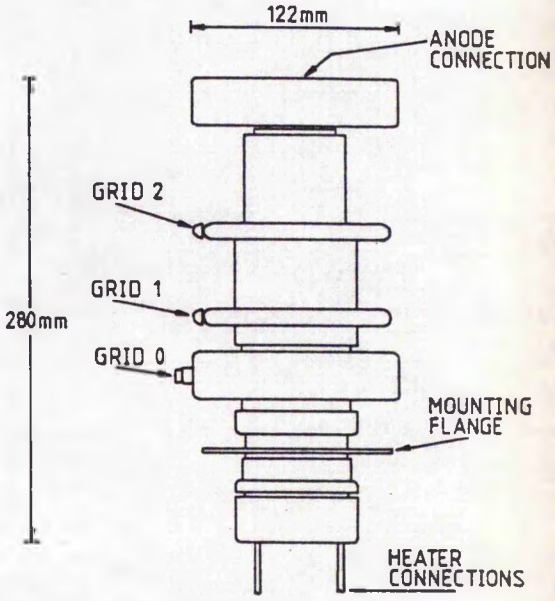

FIGURE 2.11: CHARGE (a) AND DISCHARGE (b) CIRCUITS

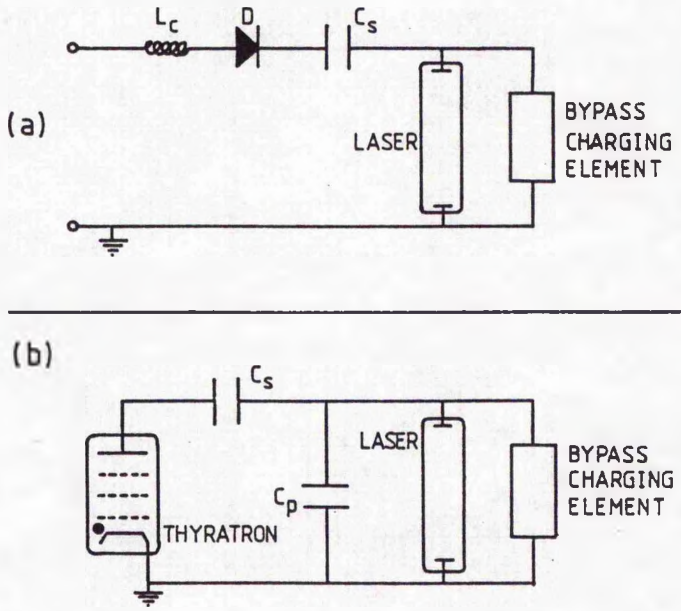

FIGURE 2.13 : "MATCHED" VOLTAGE PULSE

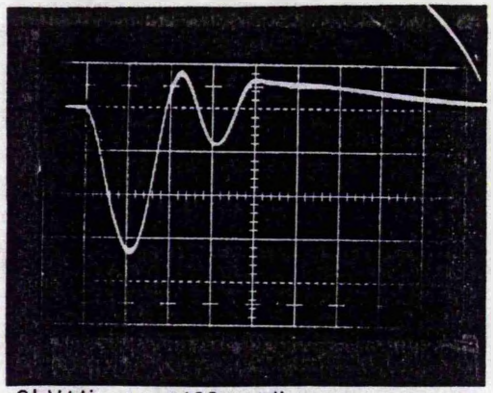

2kV/div 100ns/div

FIGURE 2.12: VOLTAGE AND CURRENT FOR AN INDUCTIVELY CHARGED CAPACITOR

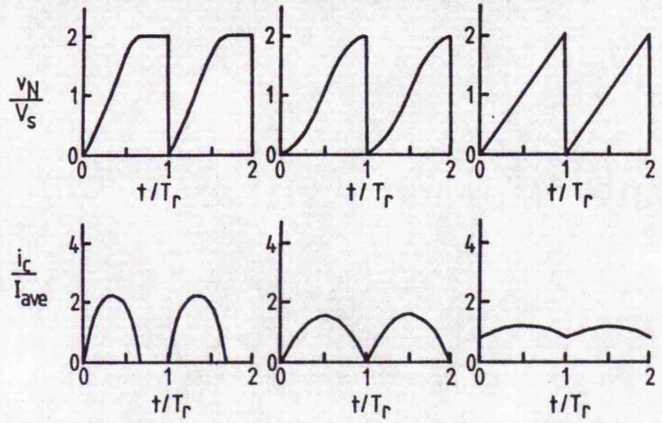

CHARGING DIODE USED ; $v_N(0) = 0$

FIGURE 2.14: FLANGE COMPONENTS (SIZES IN mm)

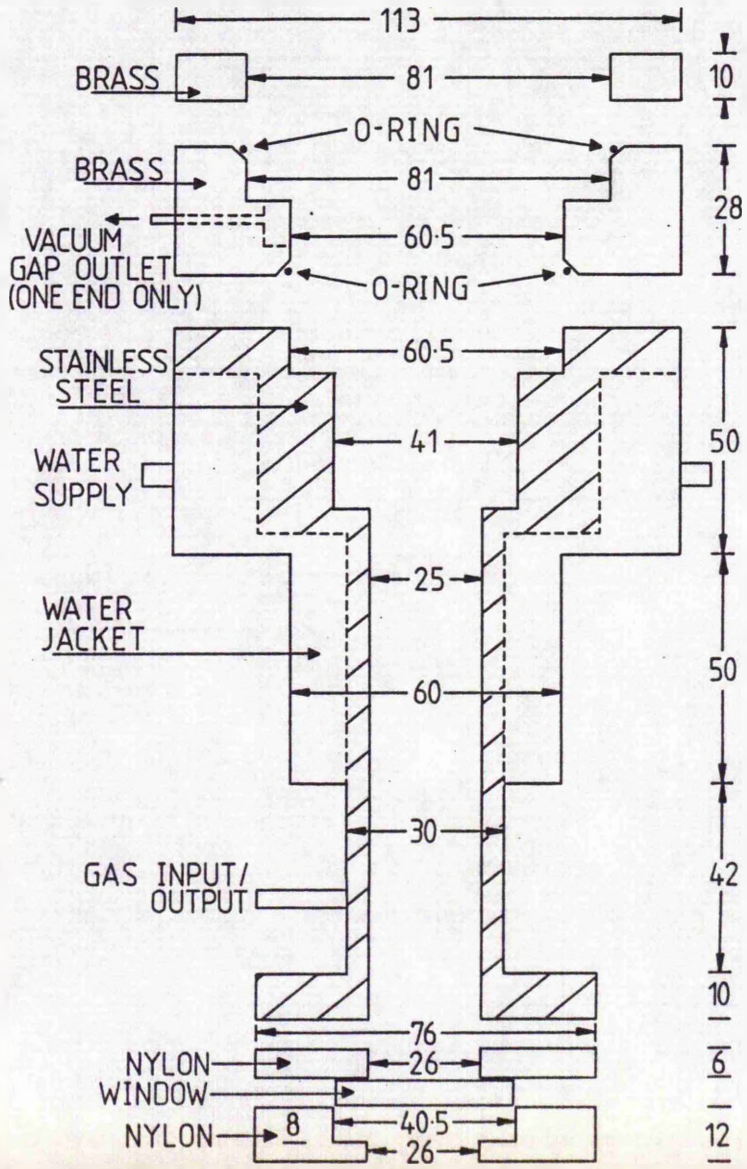

FIGURE 2.15: FLANGE ASSEMBLY

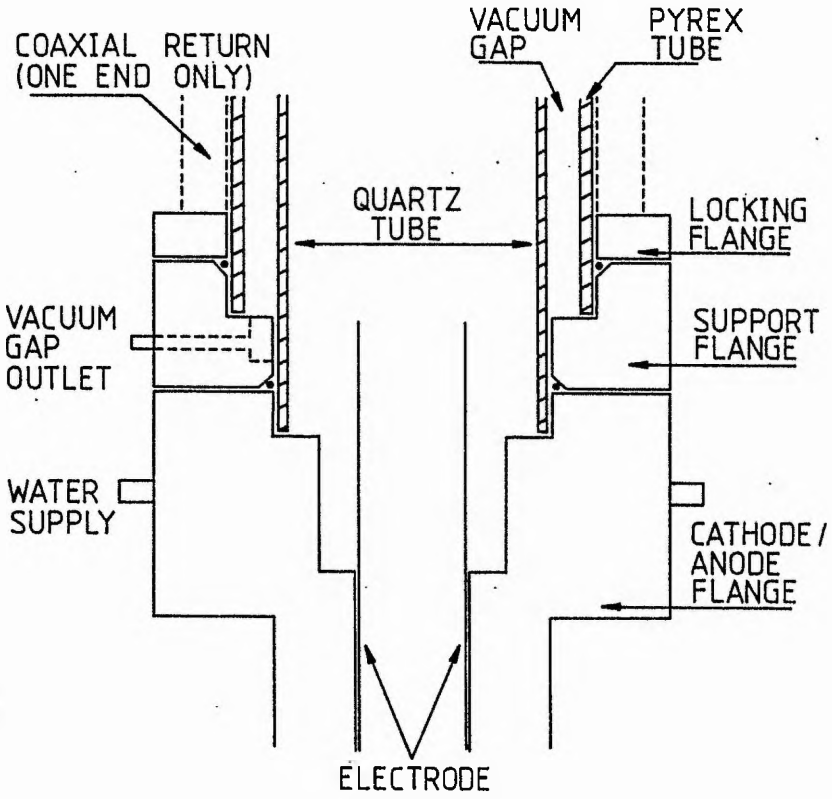

• : O-RINGS

FIGURE 2.16: LASER ASSEMBLY

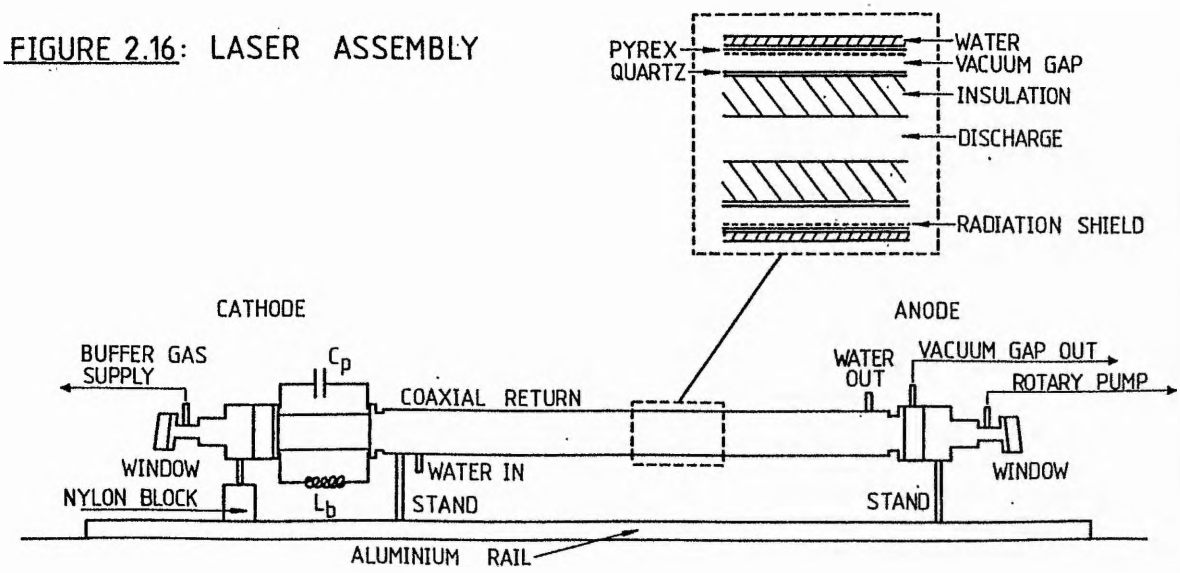

FIGURE 2.17 : THERMAL EXPANSION OF ALUMINA AD-999

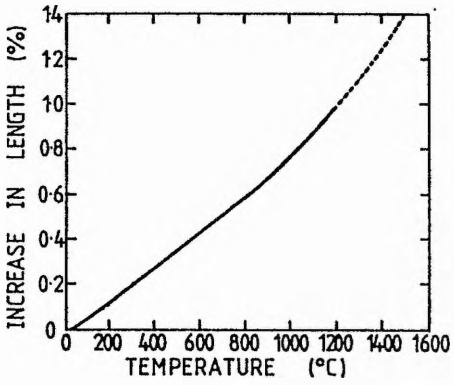

FIGURE 2.18: THERMAL CONDUCTIVITY OF ALUMINA

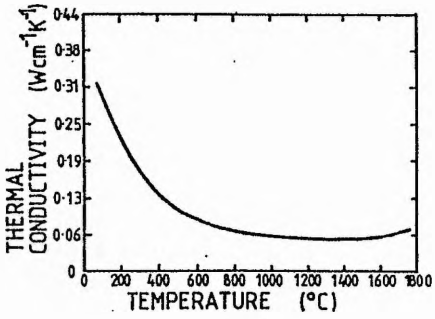

FIGURE 2.19 : ELECTRICAL RESISTIVITY OF CERAMICS AS A FUNCTION OF TEMPERATURE

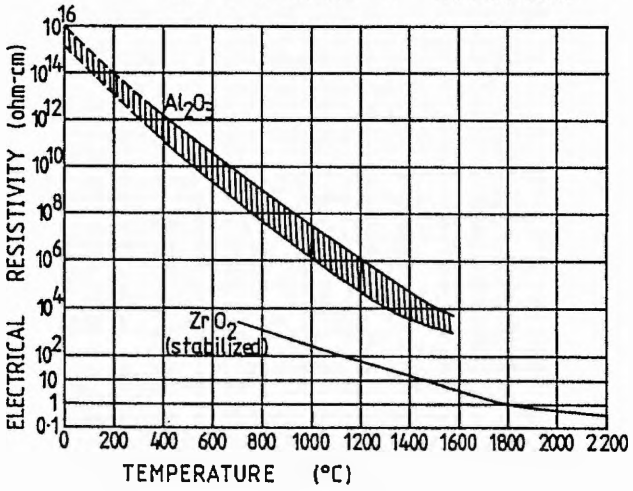

FIGURE 2.20: THERMAL CONDUCTIVITY OF ZIRCAR TYPE ZYF ZIRCONIA FELT IN VARIOUS ATMOSPHERES

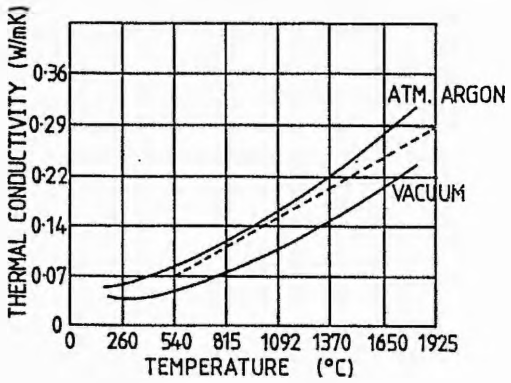

-------VALUES USED IN COMPUTER MODEL

FIGURE 2.21: TEMPERATURE DEPENDENCE OF MOLYBDENUM EMISSIVITY

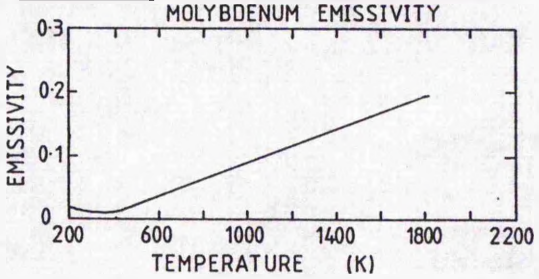

FIGURE 2.22(a): SCHEMATIC LONGITUDINAL CROSS-SECTION OF SEGMENTED INSULATION

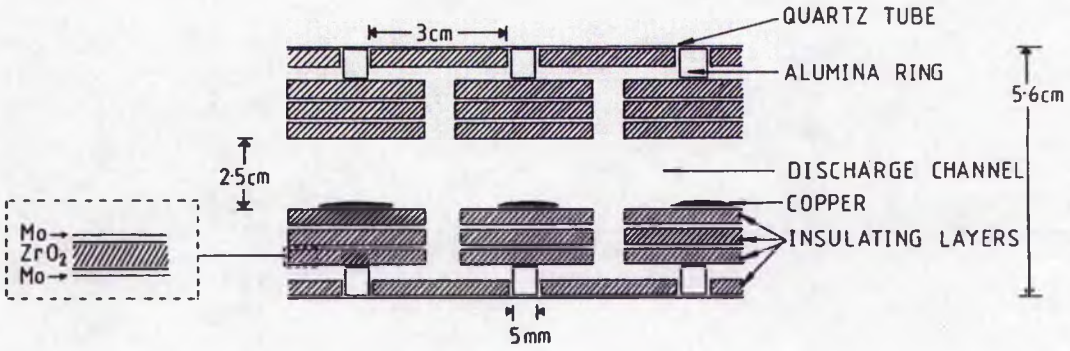

FIGURE 2.22(b): SCHEMATIC TRANSVERSE CROSS-SECTION SHOWING INSULATING LAYERS HELD INSIDE ALUMINA RING

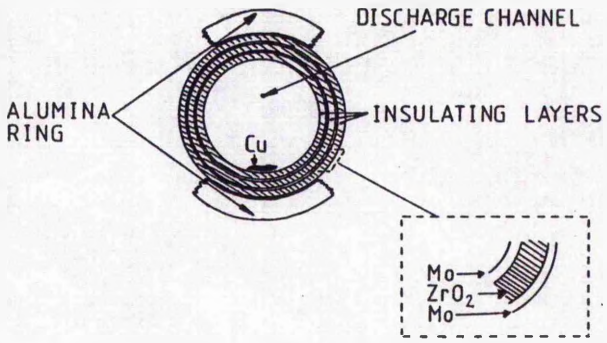

CHAPTER 3

3 COPPER VAPOUR LASER COMPUTER MODEL

3.1 INTRODUCTION

A number of detailed models of CVLs have been written [1-5]. Of these, Reference [2] provides the most accurate results by modelling both the discharge and the afterglow over a number of cycles until the initial conditions in two consecutive pulses converge. This method provides the model with realistic initial conditions, but uses a lot of computer time. The models which consider only the discharge pulse take less time to run, but must assume initial conditions and so reduce the accuracy of their results.

The model described in this chapter is designed to be simple, to reduce the amount of computer time required, and yet to be sufficiently detailed to provide qualitatively good results. It has been written from a kinetics viewpoint to enable the characteristics of the plasma to be studied under various conditions. The model simulates the operation of a CVL and its discharge circuit for up to 500 ns after the start of the discharge pulse. Only copper and neon are included. The wall temperature can be varied to simulate the operation of the system as it heats up. To account for the axial temperature gradient, the discharge is divided into a central hot zone and an outer cool zone.

Figure (3.1) shows an outline of the program structure, and the program itself is given in Appendix (C).

3.2 INITIAL CONDITIONS

Initial conditions for a number of variables are set up at the start of the program. The Cu vapour density n_{Cu} in the hot zone is given by [2]

$$n_{Cu} = 1.23 \times 10^{7} \exp(0.01236\ T_{w}) \quad cm^{-3} \quad , \qquad [3.1]$$

where T_w is the wall temperature. The Ne density n_{Ne} is calculated from the gas equation

$$n_{Ne} = \frac{p_{Ne}\ V}{R\ T_g} \quad , \qquad [3.2]$$

where p_{Ne} is the Ne pressure as measured outside the laser, V is the volume, R is the gas constant and T_g is the gas temperature. The gas temperature in the cool zone is assumed to be half the value in the hot zone. During the discharge, the gas temperature will increase rapidly to a maximum, and then slowly decrease. In the model, the gas temperature is assumed to increase by 50% in the first 100 ns, and then decrease at a slower rate, approximately following the decrease in the electron temperature. The neon and copper densities change in proportion to the change in the gas temperature. The interpulse processes are not considered in this model, so the initial electron density must be assumed. The initial gas, electron and wall temperatures are set equal to each other. Apart from the metastable levels of Cu, the populations of each level of Cu and Ne are assumed to be in thermal equilibrium with each other at the start. The population of each metastable level can be set to any value.

The dimensions of the laser and the initial values used are shown in Tables (3.1) and (3.2). Each of these values can be changed at the start of the program if required.

3.3 ATOMIC ENERGY LEVELS

Figures (3.2) and (3.3) show the energy levels included in the model. The model of the Cu atom contains seven energy levels : the ground state ($^2S_{1/2}$); the four laser levels (^2D and ^2P states); a pseudo state; and the ion ground state. The pseudo state lumps together all the energy levels between the upper laser levels and the ion ground state to make calculations easier. The simplified Ne atom is made up of a metastable, a resonance and a pseudo state between ground and the ion level. The metastable and resonance levels have the same excitation energy and represent the 3s states of neon. The pseudo state lumps together all the 3p levels. The use of a pseudo state has been found to be sufficient to model the higher levels of the Cu and Ne atoms [4].

Figures (3.2) and (3.3) also show the transitions included in the model. The processes included in the Cu atom are : electron impact excitation from ground to every energy level; superelastic relaxation from every level back to ground; excitation and superelastic relaxation between the upper laser levels and the pseudo state; ionization from every level; spontaneous emission from the pseudo state to the upper laser levels and from there to ground; and spontaneous and stimulated emission between the upper and lower laser levels. The lower laser levels are metastable and so are assumed to have an infinite lifetime for radiative decay. Electron excitation from the metastable levels to the upper laser levels and the pseudo state is two orders of magnitude less significant than the processes

included above [4] and so they are neglected. Since the model only calculates rate processes for 500 ns after the start of the discharge pulse, it is assumed that processes which affect the population of the Cu ionic ground state, such as recombination and diffusion, can be neglected. The processes affecting the Ne atom are similar : electron impact excitation to, and superelastic relaxation from, every level; ionization from every level to the ion ground state; spontaneous emission from the pseudo state to the metastable and resonance states; and spontaneous emission from the resonance state to ground.

3.4 DISTRIBUTION FUNCTION

In order to simplify the calculations needed for the rate equations, the electron energy distribution is assumed to be Maxwellian. The equation describing this distribution is

$$f(E_e) = 2n_e \left[E_e/\pi(kT_e)^3\right]^{1/2} \exp(-E_e/kT_e) \quad , \qquad [3.3]$$

where n_e is the number density of electrons, E_e is the electron energy, T_e is the electron temperature, and k is Boltzmann's constant. Figure (3.4) shows the Maxwellian distribution as a function of energy.

The average velocity $\langle v_e \rangle$ of the electron distribution at a temperature T_e is given by

$$\langle v_e \rangle = \frac{1}{n_e} \int_0^\infty v_e \, f(E_e) \, dE_e \quad , \qquad [3.4]$$

where v_e is the velocity of an electron of energy E_e and is given by

$$v_e = (2 E_e / m_e)^{1/2} \quad . \qquad [3.5]$$

From equ. [3.4], the average velocity of the electron distribution can be shown to be given by

$$\langle v_e \rangle = (8\ k\ T_e\ /\ \pi\ m_e)^{1/2} \quad . \qquad [3.6]$$

The number of electrons with energy greater than the threshold energy E_{12} for a process is given by

$$n' = \int_{E_{12}}^{\infty} f(E_e)\ dE_e \quad . \qquad [3.7]$$

Strictly, a Maxwellian distribution can be used only when the system in question is in thermodynamic equilibrium. Once inelastic processes such as excitation and ionization start to become important however, the proportion of electrons in the tail of the distribution drops below that of a Maxwellian distribution. The result of using a Maxwellian distribution is that all inelastic processes are probably overestimated, and the higher the energy required for the process, the larger the error is in the calculation of the rate of that process. Therefore, the rates of ionization of Ne are overestimated with respect to those of Cu, and the rate of excitation of the ^2P levels is overestimated with respect to the ^2D levels. However, all previous CVL computer models have used a Maxwellian distribution with results which are judged to be satisfactory.

3.5 CROSS-SECTIONS

3.5.1 COPPER AND NEON CROSS-SECTIONS

The cross-sections for excitation and ionization are assumed to

be zero up to the threshold energy and are then given by the values in Table (3.3). The excitation cross-sections for copper are taken from Ref. [4]. The $^2P_{1/2}$ and $^2D_{3/2}$ cross-sections are not given in Ref. [4] and so are calculated using the $^2P_{3/2}$ and $^2D_{5/2}$ cross-sections given in Ref. [4] and the ratio of the ^2P and ^2D cross-sections from Ref. [1]. The momentum transfer and elastic scattering cross-sections for copper are shown in Table (3.4) [6]. The excitation cross-section from ground to the metastable level of neon [7] is assumed to be equal to that of the cross-section from ground to the resonance level [8]. The excitation cross-sections for the pseudo state from both ground and the metastable and resonance levels are taken to be the sum of the cross-sections to each of the 3p levels of the real atom [9]. The neon elastic scattering cross-section given in Table (3.2) is from Ref. [10a], and the momentum transfer cross-section is assumed to be approximately equal to this. The ionization cross-sections for copper [11] and neon [12] are in Table (3.3). Ionization cross-sections from levels above ground are calculated using [1]

$$\sigma_{xi} = (E_{0i} / E_{xi})^2 \sigma_{0i} \quad , \qquad [3.8]$$

where E_{0i} and E_{xi} are the threshold energies for ionization from the ground state and the level x respectively and σ_{0i} is the ionization cross-section from ground.

3.5.2 DETAILED BALANCE

The cross-sections for superelastic relaxation processes are calculated using the principle of detailed balance [10b]. If a system is in thermodynamic equilibrium, the excitation and deexcitation rates must be equal. Therefore, we have

$$n_e\, n_0\, \bar{\sigma}_{01}(E_1+dE)\, f(E_1+dE)\, v(E_1+dE) = n_e\, n_1\, \bar{\sigma}_{10}(dE)\, f(dE)\, v(dE) \quad , \qquad [3.9]$$

where f is the Maxwellian distribution, v is the electron velocity, 0 and 1 represent the lower and upper states and E_1 is the energy difference between the states. With reference to Fig. (3.5), dE is defined to be either the electron energy (for superelastic collisions) or the difference between the electron energy and the threshold energy for the process (for inelastic collisions), depending on the process under consideration. Equation [3.9] can be rearranged using equs. [3.3] and [3.5] to give

$$\bar{\sigma}_{10}(dE) = \frac{n_0}{n_1}\,\frac{(E_1+dE)}{dE}\,\frac{\exp[-(E_1+dE)/kT_e]}{\exp(-dE/kT_e)}\,\bar{\sigma}_{01}(E_1+dE) \quad . \qquad [3.10]$$

For a system in equilibrium at a temperature T_e, the populations of two energy levels are related by the equation

$$n_1 = n_0 \left[\exp(-E_1/kT_e)\right] g_1 / g_0 \quad , \qquad [3.11]$$

where g_0 and g_1 are the statistical weights of the two levels and E_1 is the difference in energy between them. Substituting equ. [3.11] into [3.10] gives a relation between the excitation and superelastic cross-sections, which is

$$\sigma_{10}(dE) = \frac{(E_1 + dE)}{dE}\,\frac{g_0}{g_1}\,\sigma_{01}(E_1+dE) \quad . \qquad [3.12]$$

Since the cross-sections are dependent only on the electron energy,

this result can be used in a non-equilibrium situation, even though it has been derived for a system in thermodynamic equilibrium. It can be seen from equ. [3.12] that the lower the electron energy, the higher the cross-section for a given superelastic process will be.

3.6 LASER PLASMA

The conductivity of a plasma in which the electrons have a Maxwellian energy distribution, and where there is a DC electric field across the plasma, is given by [1]

$$\sigma_p = \frac{n_e e^2 \langle v_e \rangle}{3kT_e \sum_i N_i \sigma_{mi}} \quad , \qquad [3.13]$$

where σ_{mi} is the cross-section for momentum transfer collisions with atoms of density N_i. The resistance of the plasma is given by [1]

$$R_p = \frac{d}{\sigma_p A} \quad , \qquad [3.14]$$

where d is the length of the plasma zone and A is its cross-sectional area. The plasma inductance is given by [1]

$$L_p = \frac{m_e d}{n_e e^2 A} \quad . \qquad [3.15]$$

When the wall temperature is high enough, the hot zone is occupied by a mixture of the buffer gas and Cu vapour, both of which are assumed to be uniformly distributed. The cool zone is occupied solely by the buffer gas at a temperature below that required for the

production of copper vapour. The total plasma resistance and inductance is the sum of the respective values in each zone.

3.7 CIRCUIT EQUATIONS

The CVL discharge circuit is modelled by the circuit shown in Fig. (3.6). In the model, i_1 is the discharge current from the storage capacitor C_s which charges the peaking capacitor C_p and i_2 is the discharge current from C_p which flows into the laser when the gas breaks down. The thyratron is modelled by a reverse-biased voltage V_s which decays exponentially with a time constant t_{on} to represent the thyratron switch-on time. Therefore, V_s is given by

$$V_s = V_o \exp(-t/t_{on}) \quad , \qquad [3.16]$$

where t is the time after the trigger pulse is applied to the thyratron and V_o is the initial voltage on C_s. The thyratron is only allowed to pass current in one direction. The lumped inductances and resistances of loops 1 and 2 are represented by L_1, L_2, R_1 and R_2. The plasma inductance and resistance are represented by L_p and R_p, respectively. The bypass inductor is omitted because it is assumed that a negligible amount of current flows through it during the discharge.

The equations governing the rate of change of current and voltage in the circuit are

$$di_1/dt = (V_{cs}-V_s-V_{cp}-i_1R_1) / L_1 \quad , \qquad [3.17]$$

$$di_2/dt = (V_{cp}- i_2(R_2+R_p)/(L_2+L_p) \quad , \qquad [3.18]$$

$$dV_{cs}/dt = - i_1 / C_s \quad , \quad [3.19]$$

$$dV_{cp}/dt = (i_1 - i_2) / C_p \quad , \quad [3.20]$$

$$V_p = (L_p \, di_2/dt) + (R_p \, i_2) \quad , \quad [3.21]$$

where V_{cs}, V_{cp}, V_p are the voltages across C_s, C_p and the laser plasma, respectively. Table (3.5) shows the circuit values used.

3.8 RATE EQUATIONS

When calculating rate equations for the excitation and ionization of atoms, only those electrons with energy greater than the threshold energy of the process can be included in the rate equation. The velocity of these electrons will be different from the average velocity of the whole distribution, which is given by equ. [3.6], since only a part of the distribution is being considered. The average velocity of electrons in a Maxwellian distribution with energy greater than or equal to E_{12} is given by

$$\langle v' \rangle = \frac{1}{n'} \int_{E_{12}}^{\infty} v_e \, f(E_e) \, dE_e \quad , \quad [3.22]$$

where n' is the number of electrons in this part of the distribution (equ. [3.7]), and $f(E_e)$ is given by equ. [3.3]. When the integral in equ. [3.22] is calculated, the average velocity of the electrons with an energy greater than or equal to the threshold energy for the process is given by

$$\langle v' \rangle = \frac{n_e}{n'} \left[\frac{8kT_e}{m_e} \right]^{1/2} [1+(E_{12}/kT_e)] \exp(-E_{12}/kT_e) \quad . \quad [3.23]$$

In order to calculate the changing populations of the various energy levels used in the model, rate equations of the form

$$R = N_1 N_2 \sigma \langle v \rangle \quad , \qquad [3.24]$$

are used. This equation gives the total number of collisions per second per unit volume between particles of type 1 and 2, where N is the number density of the particles, σ is the cross-section for the process and v is the relative velocity of the two particles. It is assumed that σ is independent of the particle energy and that the velocity of electrons is much greater than the velocity of atoms and ions, so that v_e can be substituted for v in collisions between electrons and atoms.

Most of the rate equations describe interactions between electrons and Cu or Ne atoms. Two versions of equ. [3.24] are used, depending on whether the whole, or only part, of the electron distribution can take part in the process. It is assumed that all electrons can take part in elastic and superelastic processes, so that the average electron velocity is given by equ. [3.6], and equ. [3.24] becomes

$$R = N n_e \sigma (8kT_e/\pi m_e)^{1/2} \quad . \qquad [3.25]$$

For processes such as excitation and ionization, only a fraction of the electron distribution is involved, so equ. [3.23] is used. The rate equation is then given by

$$R' = R\,[1+(E_{12}/kT_e)]\exp(-E_{12}/kT_e) \quad , \qquad [3.26]$$

where R is given by equ. [3.25].

3.9 RADIATION TRAPPING

Under conditions of radiation trapping, the effective lifetimes of the copper ^2P levels are increased by the trapping factor F_t, which is given by

$$F_t = \frac{A_{21}\ (\text{trapped})}{A_{21}\ (\text{untrapped})} \quad , \qquad [3.27]$$

where A_{21} is the Einstein coefficient for spontaneous emission between levels 2 and 1. The trapping factor for an infinite cylinder of radius R is given by [13]

$$F_t = \frac{1.60}{k_{21}\ R\ (\pi \ln(k_{21}R))^{1/2}} \quad , \qquad [3.28]$$

where k is the absorption coefficient of photons emitted between levels 2 and 1. The absorption coefficient is given by

$$k_{21} = \frac{1}{4\pi}\sqrt{\frac{\ln(2)}{\pi}}\ \frac{\lambda_{21}^2\ A_{21}\ N_1\ g_2}{\Delta\nu_D\ g_1} \quad , \qquad [3.29]$$

where λ_{21} is the wavelength, N_1 is the density of atoms in the lower state, g is the statistical weight of the level, A_{21} is the untrapped Einstein coefficient and $\Delta\nu_D$ is the Doppler linewidth (FWHM). The Doppler linewidth of a transition between two levels of an atom of mass M in equilibrium at a temperature T is given by

$$\Delta\nu_D = \frac{2.35}{\lambda_{12}} \sqrt{\frac{kT}{M}} \quad . \qquad [3.30]$$

Assuming Doppler broadening to be the main broadening mechanism in the CVL, the linewidths of the two transitions can be calculated from equ. [3.30]. The untrapped Einstein coefficients are taken as 9.60 ns^{-1} and 10.24 ns^{-1} for the $^2P_{3/2}$ and $^2P_{1/2}$ transitions to ground, respectively [14]. The absorption coefficients k_a can then be shown to be given by

$$k_a\,(^2P_{3/2}\text{-}^2S_{1/2}) = 3.32 \times 10^{-15}\ N / \sqrt{T} \quad , \qquad [3.31]$$

and

$$k_a\,(^2P_{1/2}\text{-}^2S_{1/2}) = 1.57 \times 10^{-15}\ N / \sqrt{T} \quad , \qquad [3.32]$$

where N is the density of ground state copper atoms. By substituting equs. [3.31] and [3.32] into equ. [3.28], the effect of radiation trapping on the copper ^2P levels' lifetimes can be calculated. The effective lifetimes are given by

$$t\,(\text{trapped}) = t\,(\text{untrapped})\ k_a\ R\ (\pi \ln(kR))^{1/2} / 1.60 \quad , \qquad [3.33]$$

where t (trapped) is the effective lifetime of the trapped level, t (untrapped) is the untrapped lifetime and k_a is the relevant absorption coefficient from equ. [3.31] or [3.32].

3.10 ELECTRON ENERGY EQUATIONS

The changing electron temperature is determined by the flow of

energy into and out of the electron distribution. There are five processes included in the model which affect the electron temperature : power gain from the electric field (P_F); power gain from superelastic collisions (P_{SEL}); power loss from elastic collisions (P_{EL}) and power loss from excitation (P_{EX}) and ionization (P_{ION}) processes. The temperature change per second of the electron distribution is given by

$$d(1.5\ k\ T_e) = P_F + P_{SEL} - P_{EL} - P_{EX} - P_{ION} \quad . \qquad [3.34]$$

The power gain per unit volume from the electric field is given by

$$P_F = \sigma_p^- F^2 \quad , \qquad [3.35]$$

where σ_p^- is the plasma conductivity (equ. [3.13]) and F is the electric field. The elastic and superelastic terms involve the whole of the electron distribution. In an elastic collision, the electron loses a fraction dE of its energy, which is given by

$$dE = 2\ m_e\ E_e\ /\ M \quad , \qquad [3.36]$$

where M is the mass of the atom and E_e is the electron energy. In a superelastic collision, the electron collides with an atom in an excited state, causing it to deexcite to some lower energy level. The energy lost by the atom is transferred to the electron. Therefore the energy gain per second per unit volume for these two processes is given by

$$P_{EL} = N\, n_e\, \sigma_{EL}\, (2m_e/M)\, \langle v_e E_e \rangle$$

$$= 2\, N\, n_e\, \sigma_{EL}\, \frac{2m_e}{M} \left[\frac{8(kT_e)^3}{m_e} \right]^{1/2} \quad , \qquad [3.37]$$

and

$$P_{SEL} = N\, n_e\, \sigma_{SEL}\, E_{12}\, \langle v_e \rangle \quad , \qquad [3.38]$$

where $\langle v_e \rangle$ is given by equ. [3.6]. The excitation and ionization terms only involve part of the electron distribution. The energy loss per second per unit volume by excitation and ionization is given by

$$P_{EX} = N\, n'\, \sigma_{12}\, E_{12}\, \langle v' \rangle \quad , \qquad [3.39]$$

and

$$P_{ION} = N\, n'\, \sigma_{xi}\, E_{xi}\, \langle v' \rangle \quad , \qquad [3.40]$$

where n' and $\langle v' \rangle$ are given by equs. [3.7] and [3.23], respectively.

At the end of each iteration of the program, the electron temperature is recalculated using equ. [3.34]. It is assumed that any new electrons produced by ionization have the average electron energy. Since there are two temperature zones included in the model, the above equations are calculated for each zone separately.

3.11 STIMULATED EMISSION

The model has been written mainly in terms of kinetic processes, so the routines for calculating the laser output are very simple. The

transitions from the upper to the lower laser levels have a known spontaneous emission lifetime [1]. It is assumed that spontaneously emitted photons can be emitted in any direction with equal probability, so only those photons which travel towards the end mirrors contribute to the growth of the laser pulse. If an average Cu atom is located in the middle of the hot zone, on the central axis of the laser, then the number of spontaneously emitted photons, n_{spont}, travelling towards the end mirrors is given by

$$n_{spont} = n_t \, r^2 / 4R^2 \quad , \qquad [3.41]$$

where n_t is the number of spontaneous emissions, r is the radius of the end mirror and R is the distance from the middle of the laser to the end mirrors. The rate equation for stimulated emission is given by

$$R_{lase} = N_u \, n_{ph} \, c \, \sigma_{stim} \quad , \qquad [3.42]$$

where N_u is the density of atoms in the upper laser level, n_{ph} is the number of photons in the cavity travelling towards a mirror with a wavelength equal to the laser wavelength, c is the speed of light and σ_{stim} is the cross-section for stimulated emission. Stimulated emission gives rise to gain if we have

$$g_l \, N_u \geqslant g_u \, N_l \quad , \qquad [3.43]$$

where g is a statistical weight and u, l refer to the upper and lower laser levels respectively. The rate at which laser photons are coupled out of the cavity by a mirror of reflectivity R is given by

$$R_{out} = n_{lase}\, c\, (1 - R) / l_c \quad , \qquad [3.44]$$

where n_{lase} is the density of laser photons and l_c is the distance between the mirrors.

3.12 RESULTS

The advantage of the computer model described in the preceding sections is that one parameter at a time can be altered in order to obtain a better understanding of how the laser works. Figures (3.7) to (3.14) show the dependence of the plasma resistance and Figs. (3.15) to (3.19) the dependence of the electron density and peak electron temperature on various system variables. In each case, the other variables are held constant with values as given in Table (3.2(a)), unless otherwise stated. The three curves on the resistance and electron density graphs show the values of these variables at different times after the start of the discharge.

As the wall temperature (and hence the gas temperature) rises, the gas density falls. This causes the plasma resistance to fall (Fig. (3.15)), since the resistance is proportional to the density of gas atoms (equ. [3.14]). There is a marked drop in the plasma resistance at about 1300°C, where the temperature becomes high enough for a significant copper vapour density to be produced. This decrease in resistance is due to the lower ionization potential of copper compared with neon, which causes an increase in the electron density (Fig. (3.15)). The model also shows an increase in the plasma resistance as the temperature increases past the optimum level. As the copper vapour density increases, the peak electron temperature drops (Fig. (3.18)), and eventually falls below the level required for ionization. The corresponding drop in the electron density

(Fig. (3.19)) causes the rise in resistance. Increasing the buffer gas pressure causes the plasma resistance (Fig. (3.8)) to rise, whereas the peak electron temperature falls (Fig. (3.17)), due to the increasing rate of elastic and inelastic collisions with the neon atoms. The electron density curve (Fig. (3.16)) has a different form, reaching a peak and then slowly decreasing. The dependence of the plasma resistance on the voltage to which C_s is charged has also been calculated. A higher voltage is required at low temperature. (Fig. (3.9)) than at 1500°C (Figs. (3.10) and (3.11)) to achieve the same amount of excitation and ionization. By varying the amount of insulation along the length of the tube, the length of the zone with sufficient copper vapour in it for lasing can be altered. Increasing the length of the hot zone to the electrodes would result in the lowest possible plasma resistance as shown in Fig. (3.12). In Fig. (3.13), the sizes of the storage and peaking capacitors are varied. When C_s is smaller than C_p, the plasma resistance is quite large, due partly to there being insufficient energy in the pulse to achieve the same degree of ionization and excitation, and partly to a mismatch in energy transfer between the capacitors. As C_s increases, the resistance falls, but further increases in C_s produce smaller reductions in the plasma resistance, again because there is a mismatch between the capacitors. The plasma resistance and peak electron temperature both depend on the initial electron density (Figs. (3.14) and (3.19) respectively). Varying the density of electrons at the start of the discharge gives an indication of the effect of changing the length of the afterglow period or the effectiveness of the afterglow processes. Increasing the PRF, or reducing the effectiveness of the plasma recombination processes, eventually causes the electron temperature to drop below the level required to excite the upper laser levels (Fig. (3.19)). At the same time, the plasma

resistance falls (Fig. (3.14)), making matching more difficult.

The variation of plasma resistance (Fig. (3.20)) and inductance (Fig. (3.21)) with time during a single discharge pulse is of interest in determining the action of the bypass charging element and the factors limiting the current risetime. The model shows that the initial resistance, and hence the resistance over much of the afterglow, is of the order of hundreds of ohms. Bypass resistors are usually chosen to be about 200 ohms, in which case, a significant amount of the charging current will flow through the laser plasma. A bypass inductor of 100 uH, however, will only have an impedance of a few ohms at 10 kHz and so will carry almost all of the charging current. Once the plasma starts to break down, the inductance falls quickly to a few nanohenries (Fig. (3.21)). Therefore, under ideal conditions, with a low contaminant density, the factor limiting the current risetime is the external circuit inductance rather than the plasma inductance.

Figures (3.22) to (3.25) show the results of calculations to determine the maximum metal segment length at the peak of the voltage pulse, using equ. [1.1]. There is a strong dependence on the wall temperature (Fig. (3.22)) and neon pressure (Fig. (3.24)). The main factor which increases the maximum metal segment length in these cases is a reduction in gas density. Fig. (3.22) shows that the maximum segment length drops when the wall temperature becomes high enough for copper vapour to be produced. This effect has not been observed experimentally, probably because the introduction of the copper vapour changes the discharge conditions, whereas for the purpose of the calculations shown in Fig. (3.22), the discharge conditions (apart from the wall temperature), were taken to be constant over the entire temperature range. Figure (3.23) shows that at high initial electron densities, the maximum segment length increases markedly. This effect

will compensate for the drop in segment length shown in Fig. (3.22). The voltage to which C_s is charged has a comparatively small effect (Fig. (3.25)). Taken together, these results suggest that in order to maximise the metal segment length, the discharge should be run at very high repetition rates and/or low buffer gas pressures.

Figures (3.26) and (3.27) show the variation in the maximum metal segment length during a single discharge pulse for different wall temperatures and neon pressures. The discharge voltage pulse across the laser cavity is also shown. In Fig. (3.26), the segment length drops rapidly as the discharge voltage rises because the electron temperature is still at a low level. However, breakdown between the segments at this point in the discharge is unlikely because the electric field is not very high. In the next stage of the discharge, both the voltage and the electron temperature rise rapidly together, so that the maximum segment length stays constant. If there is any breakdown between segments, it probably occurs at this stage, when the electric field in the discharge is at, or close to, its peak. Before the discharge voltage reaches its peak, and the discharge current starts to flow, small arcs between segments caused by the high electric field may produce a large preionization density within the segments. This will allow the main discharge current to penetrate through the segments. As discussed in Section (7.2.2), a segment length of 12 cm was used successfully with neon. With this length, the neon pressure had to be less than 6 torr when the tube was cold or else some of the discharge current could be seen to arc between segments. This simple theory (equ. [1.1]) therefore provides an accurate result. At high temperatures and electron densities (Fig. (3.27)), the neon pressure can be increased significantly before the maximum segment length drops. This result is important because unless the laser bore is very narrow, a neon pressure of greater than

20 torr is usually required for a stable discharge and optimum operation of the laser.

The relative densities of copper and neon ions during the discharge pulse changes as the wall temperature increases from 1300°C to 1500°C (Fig. (3.28)). Whereas the ionization of neon is the main source of electrons at 1300°C, the density of neon ions has fallen significantly at 1500°C. At this temperature, the copper atom density is about 10^{15} cm^{-3}, so that about 10% of the copper atoms are ionized when the discharge ends. Figure (3.29) shows the variation in the densities of the atomic copper levels during a discharge pulse. The effect of stimulated emission on the populations of the ^2P and ^2D levels can clearly be seen. Only a few percent of the copper atoms contribute to the laser pulse and the higher lying levels (the pseudo state) are populated at a lower rate than the laser levels are.

REFERENCES FOR CHAPTER 3

1 : Walter W.T., Solimene N., Kull G.M.
PROC. INT. CONF. LASERS 1980, 148, STS PRESS (1981)

2 : Kushner M.J., IEEE J.Q.E. 17, 1555 (1981)

3 : Harstad K.G., IEEE J.Q.E. 16, 550 (1980)

4 : Kushner M.J., Warner B.E., J. APPL. PHYS. 54, 2970 (1983)

5 : Harstad K.G., IEEE J.Q.E. 19, 88 (1983)

6 : Trajmar S., Williams W., Srivastava S.K.
J. PHYS. B : Atom. Molec. Phys. 10, 3323 (1977)

7 : Mityureva A.A., Penkin N.P., OPT. SPECTROSC. 55, 229 (1983)

8 : Salinger S.N., Rowe J.E., J. APPL. PHYS. 39, 4299 (1968)

9 : Frish S.E., Revald V.F., OPT. SPECTROSC. 15, 395 (1963)

10 : Cherrington B.E., GASEOUS ELECTRONICS AND GAS LASERS
Pergamon Press (1980) (a) p23 (b) p55

11 : Pavlov S.I., Rakhovskii V.I., Fedorova G.M.
SOV. PHYS. JETP 25, 12 (1967)

12 : Rapp D., Englander-Golden P., J. CHEM. PHYS. 43, 1464 (1965)

13 : Holstein T., PHYS. REV. 83, 1159 (1951)

14 : Weaver L.A., Liu C.S., Sucov E.W., IEEE J.Q.E. 10, 140 (1974)

TABLE 3.1 : LASER DIMENSIONS

Discharge length	90 cm
Hot zone length	50 cm
Discharge diameter	2 cm
Optical cavity length	200 cm
Mirror reflectivity	0.1

TABLE 3.2 : INITIAL VALUES OF VARIABLES

	Neon pressure	20 torr
(a)	Hot zone wall temperature	$1500^{\circ}C$
	Hot zone electron density	2×10^{11} cm^{-3}
	Cool zone electron density	10^{11} cm^{-3}
	Hot zone gas temperature	1800 K
	Hot zone electron temperature	1800 K
	$^2D_{5/2}$ Population	10^{12} cm^{-3}
	$^2D_{3/2}$ Population	1.55×10^{11} cm^{-3}
(b)	Hot zone wall temperature	$1300^{\circ}C$
	Hot zone electron density	10^{10} cm^{-3}
	Cool zone electron density	5×10^{9} cm^{-3}
	Hot zone gas temperature	1600 K
	Hot zone electron temperature	1600 K
	$^2D_{5/2}$ Population	10^{10} cm^{-3}
	$^2D_{3/2}$ Population	1.08×10^{9} cm^{-3}

TABLE 3.3 : CROSS-SECTIONS AND LIFETIMES

TRANSITION	CROSS-SECTION ($\times 10^{-16}$ cm^2)	LIFETIME (ns)
COPPER		
$^2S_{1/2}$ - $^2D_{5/2}$	3.3	∞
$^2S_{1/2}$ - $^2D_{3/2}$	2.2	∞
$^2S_{1/2}$ - $^2P_{1/2}$	3.5	10.24 (untrapped)
$^2S_{1/2}$ - $^2P_{3/2}$	7.5	9.60 (untrapped)
$^2S_{1/2}$ - PS	2.4	100
$^2D_{5/2}$ - $^2P_{3/2}$	0.0	770
$^2D_{3/2}$ - $^2P_{1/2}$	0.0	370
$^2P_{1/2}$ - PSEUDO	40	20
$^2P_{3/2}$ - PSEUDO	48	10
$^2S_{1/2}$ - ION	3.0	∞
NEON		
GROUND - METASTABLE	0.06	∞
GROUND - RESONANCE	0.06	2.0
GROUND - PSEUDO	0.02	∞
METASTABLE - PSEUDO	60	1.0
RESONANCE - PSEUDO	60	1.0
GROUND - ION	0.2	∞

TABLE 3.4 : ELASTIC AND MOMENTUM TRANSFER CROSS-SECTIONS

ELASTIC SCATTERING	CROSS-SECTION ($\times 10^{-16}$ cm^2)
Copper	80
Neon	3

MOMENTUM TRANSFER

Cu (^2S)	80
Cu (^2D)	4
Cu (^2P)	10
Cu (PSEUDO)	6
Ne (GROUND)	2
Ne (METASTABLE)	0.4
Ne (RESONANCE)	0.4
Ne (PSEUDO)	0.4

TABLE 3.5 : CIRCUIT VALUES

L_1	1.2 μH
L_2	0.8 μH
C_s	6.5 nF
C_p	3.2 nF
V_c	10 kV
R_1	1 ohm
R_2	1 ohm
t_{on}	10 ns

FIGURE 3.1 : PROGRAM STRUCTURE

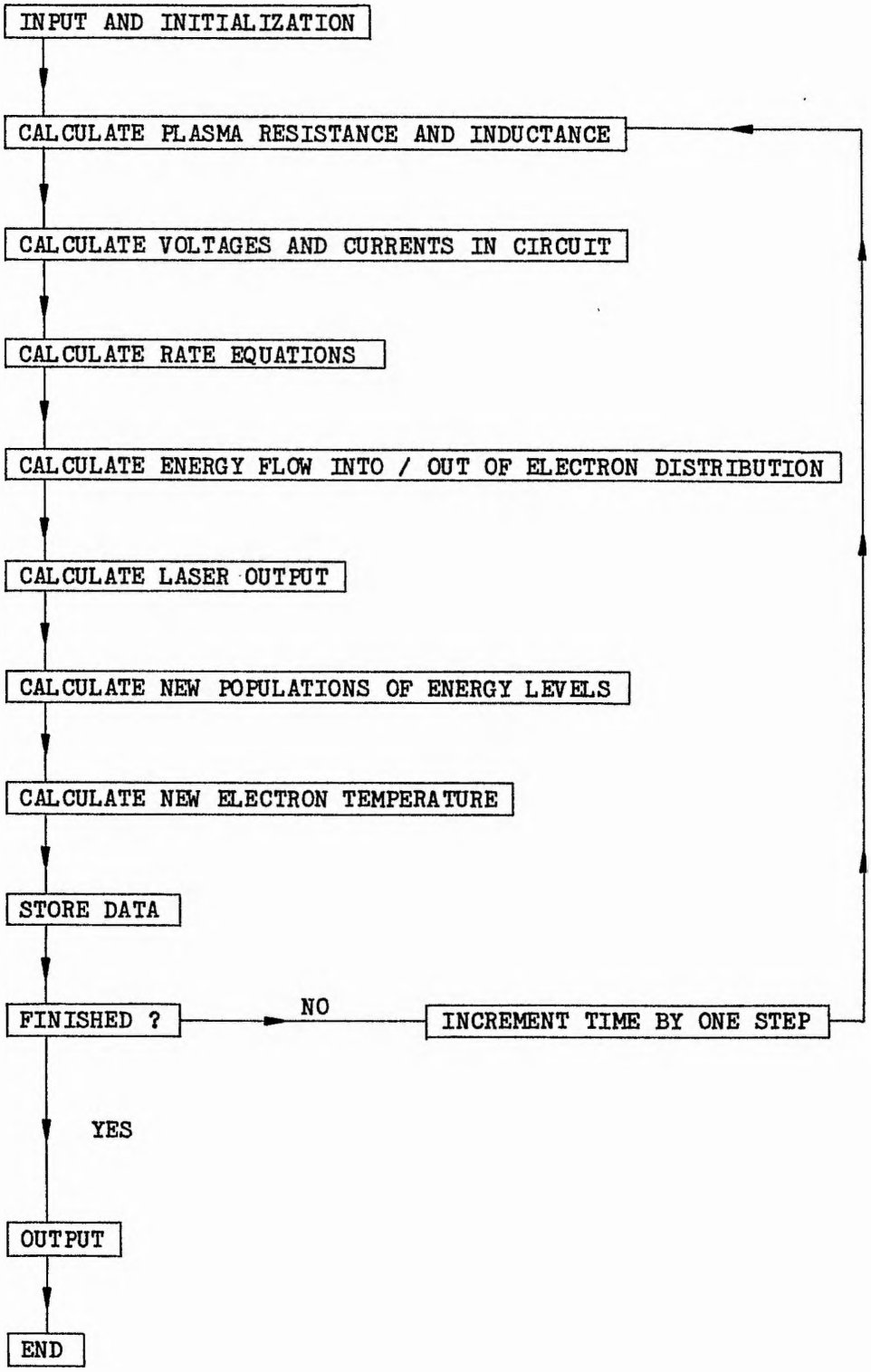

FIGURE 3.2 : COPPER ENERGY LEVELS AND PROCESSES INCLUDED IN MODEL

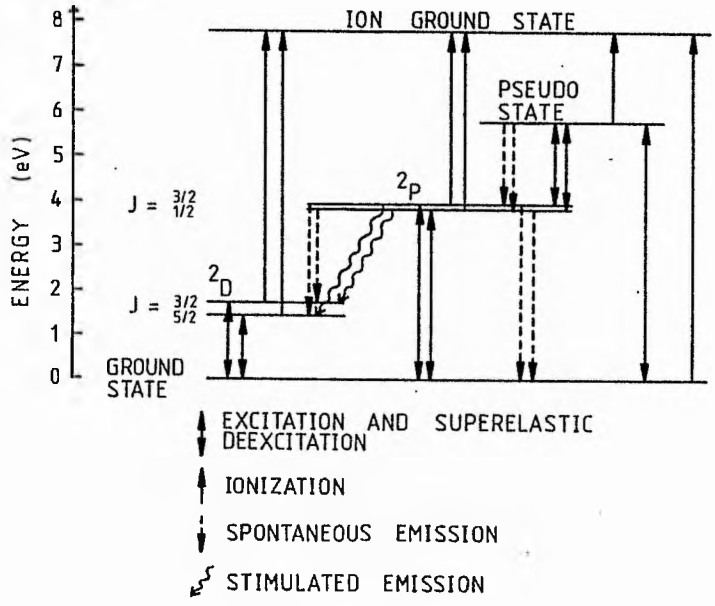

FIGURE 3.3 : NEON ENERGY LEVELS AND PROCESSES INCLUDED IN MODEL

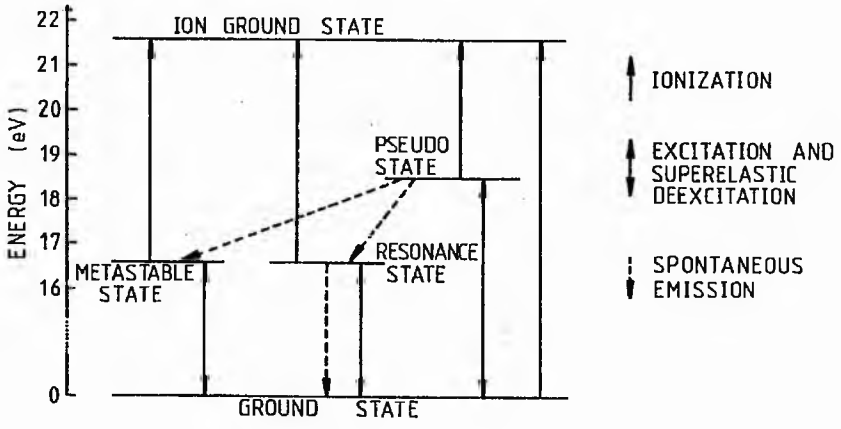

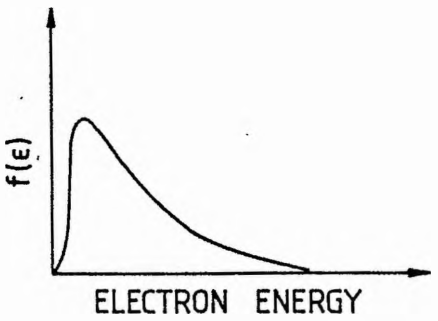

FIGURE 3.4 : RELATIVE MAXWELLIAN ELECTRON ENERGY DISTRIBUTION

FIGURE 3.5 : EXAMPLE ENERGY GAIN/LOSS IN SUPERELASTIC/EXCITATION PROCESSES

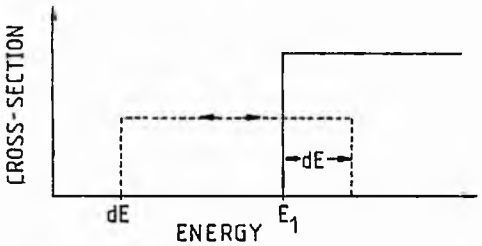

FIGURE 3.6 : DISCHARGE CIRCUIT MODEL

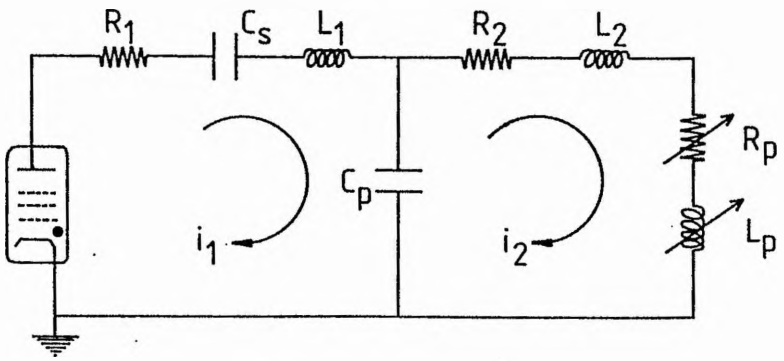

FIGURE 3.7 : DEPENDENCE OF PLASMA RESISTANCE ON WALL TEMPERATURE

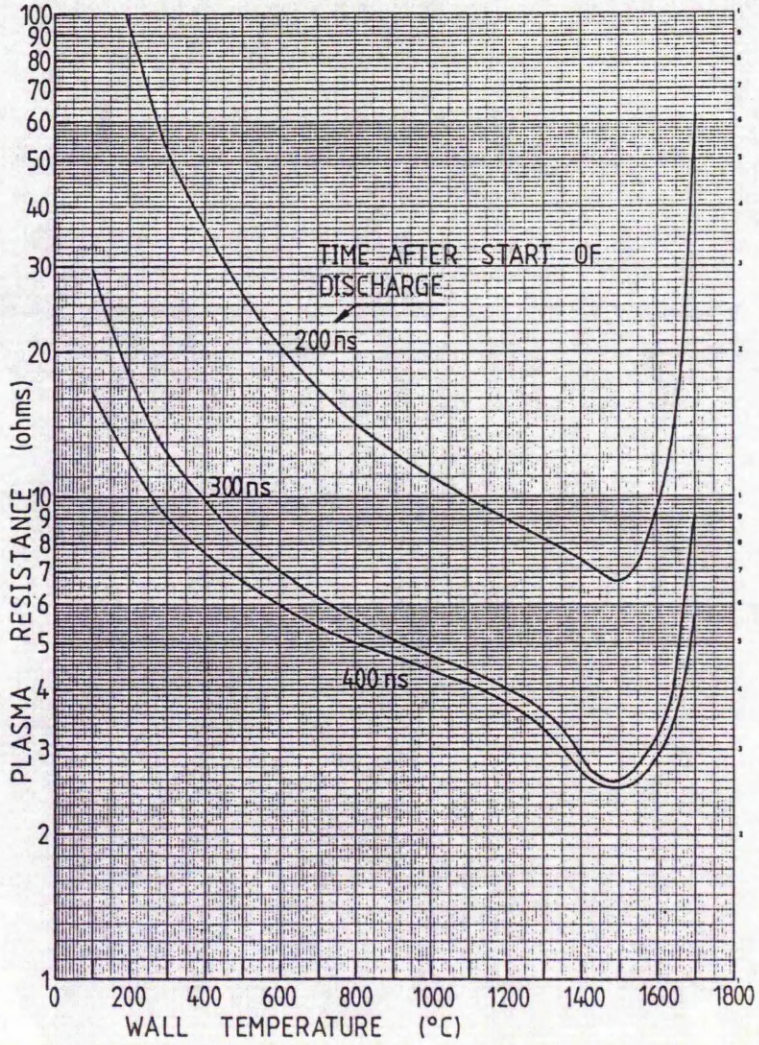

FIGURE 3.8 : DEPENDENCE OF PLASMA RESISTANCE ON NEON PRESSURE

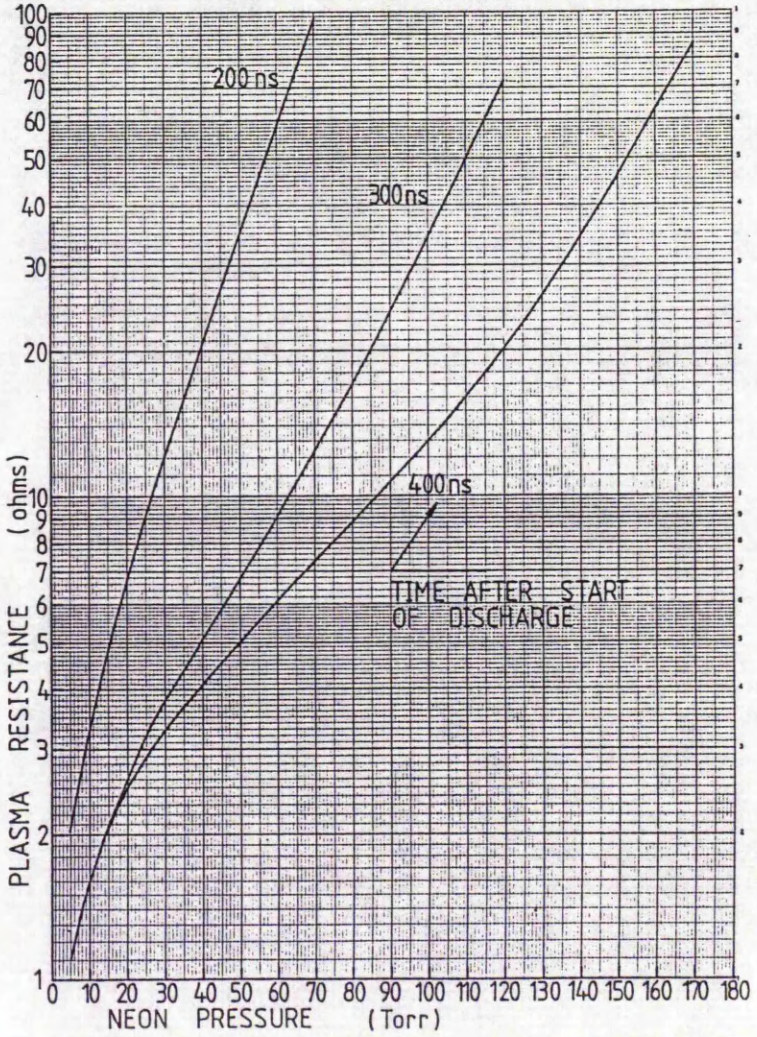

FIGURE 3.9 : DEPENDENCE OF PLASMA RESISTANCE ON CHARGING VOLTAGE ON C_s

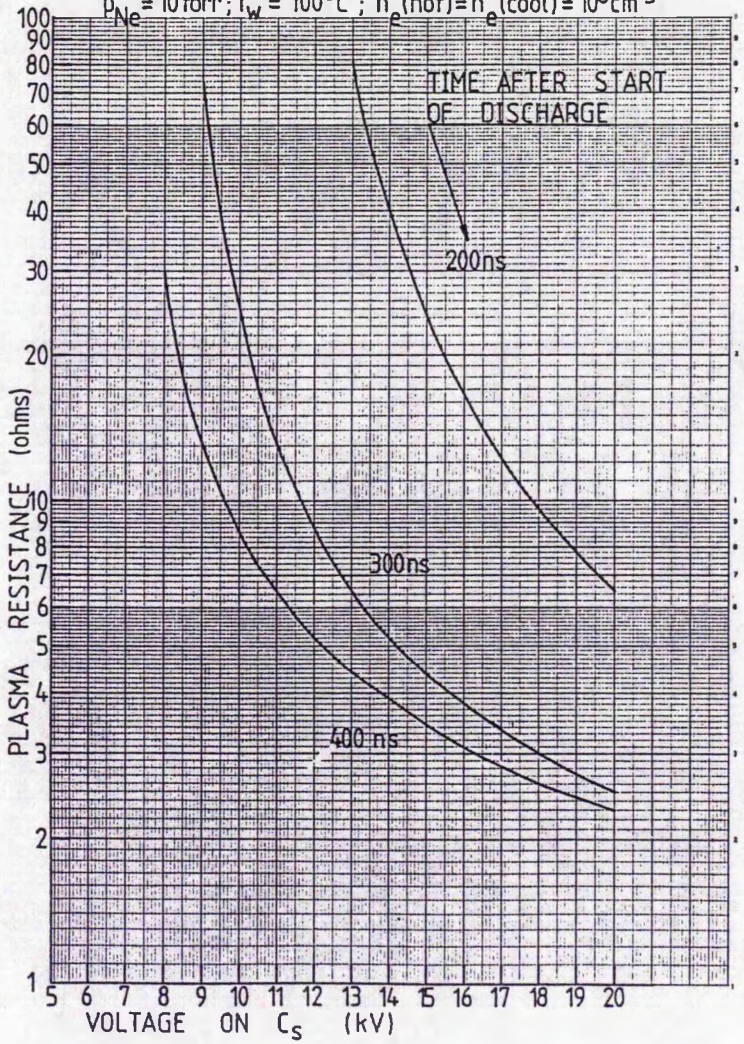

FIGURE 3.10 : DEPENDENCE OF PLASMA RESISTANCE ON CHARGING VOLTAGE ON C_s

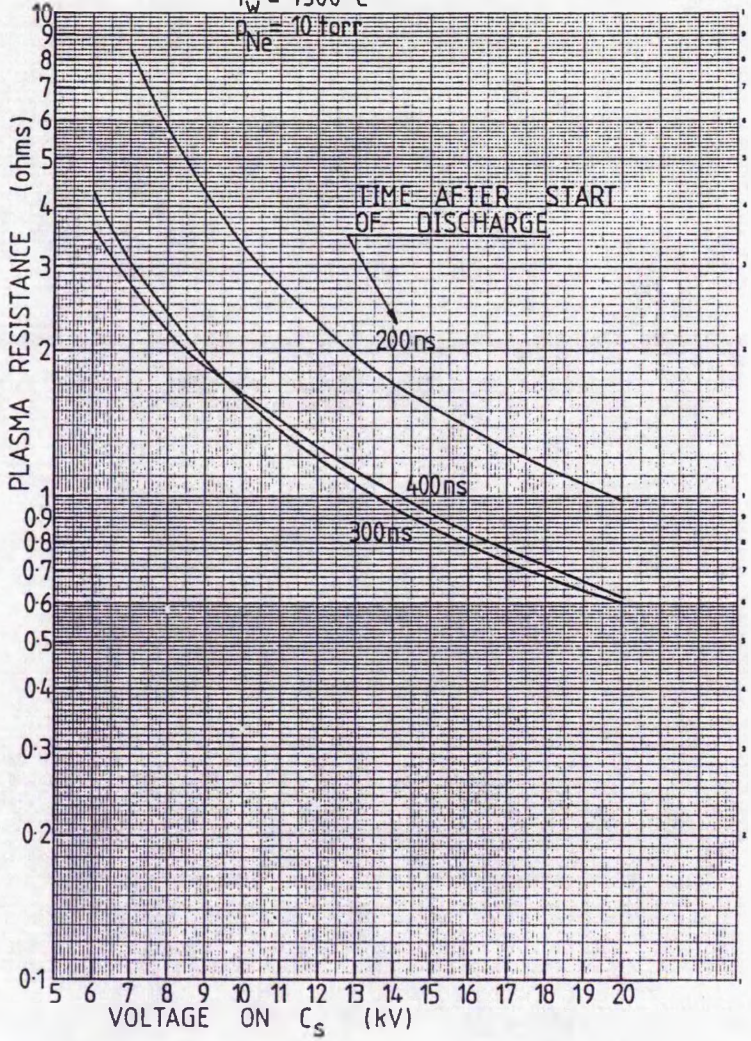

FIGURE 3.11 : DEPENDENCE OF PLASMA RESISTANCE ON CHARGING VOLTAGE ON C_s

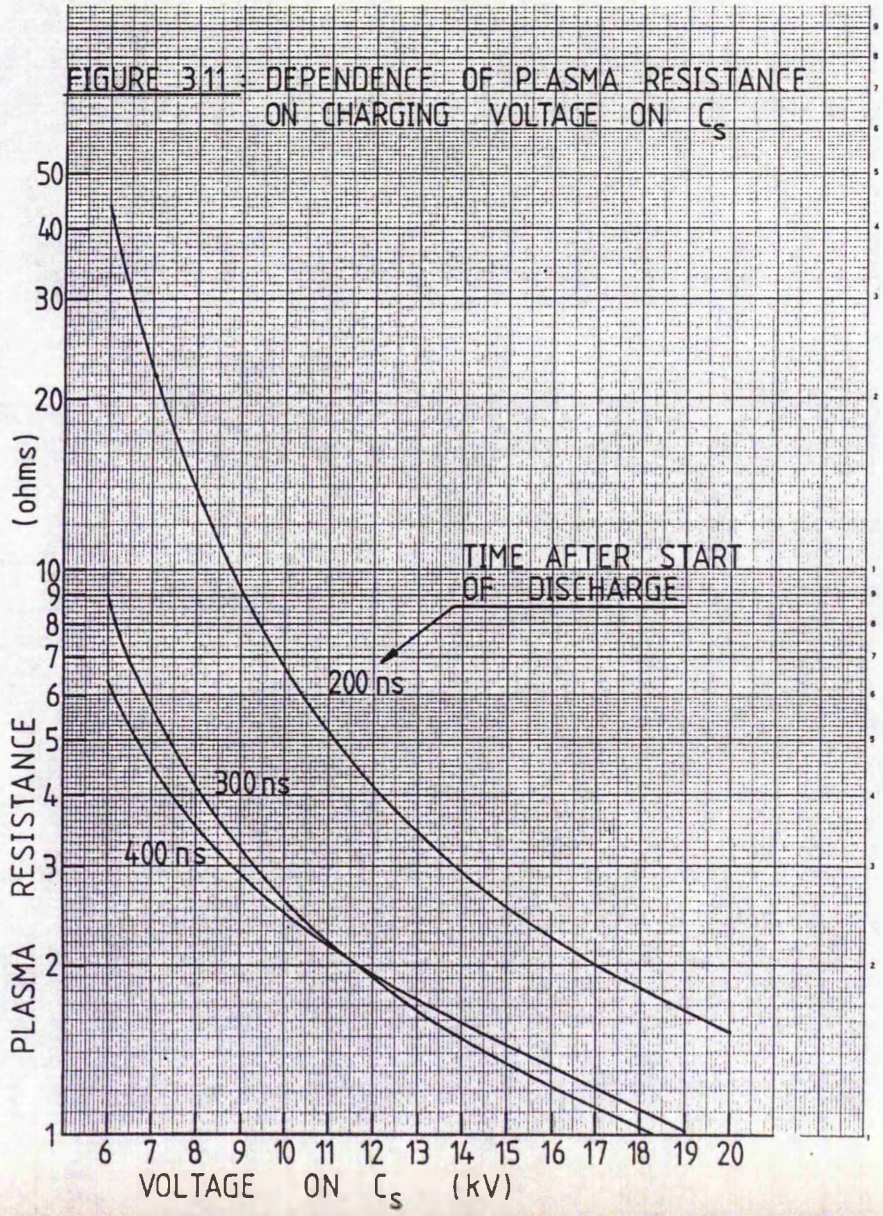

FIGURE 3.12 : DEPENDENCE OF PLASMA RESISTANCE ON HOT ZONE LENGTH

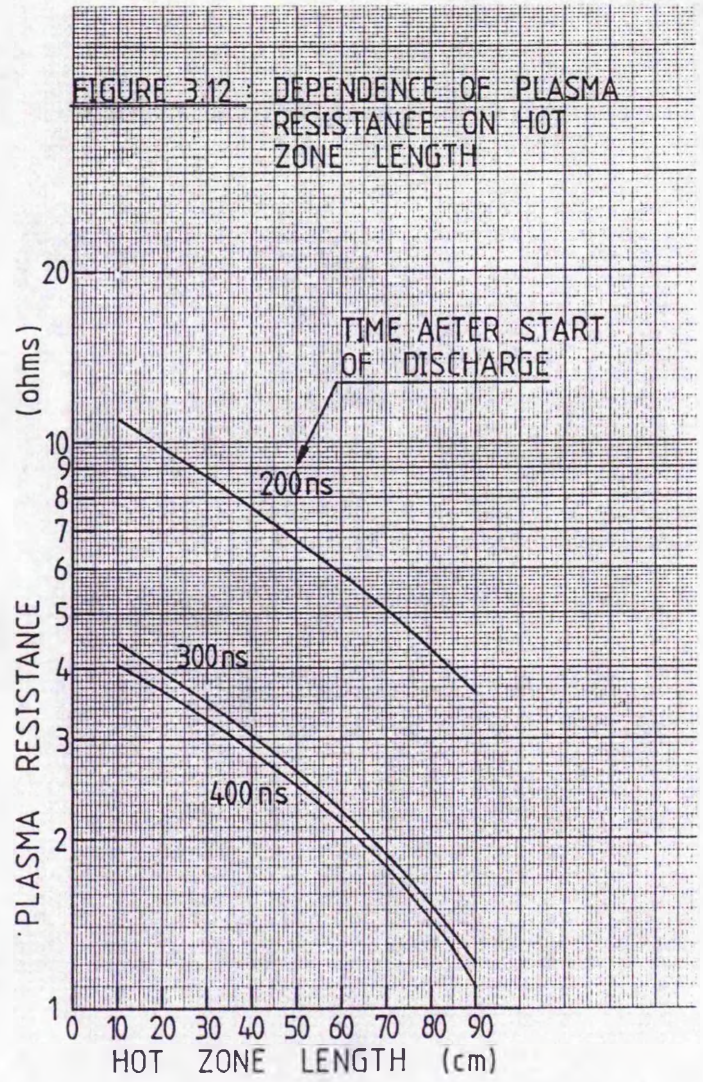

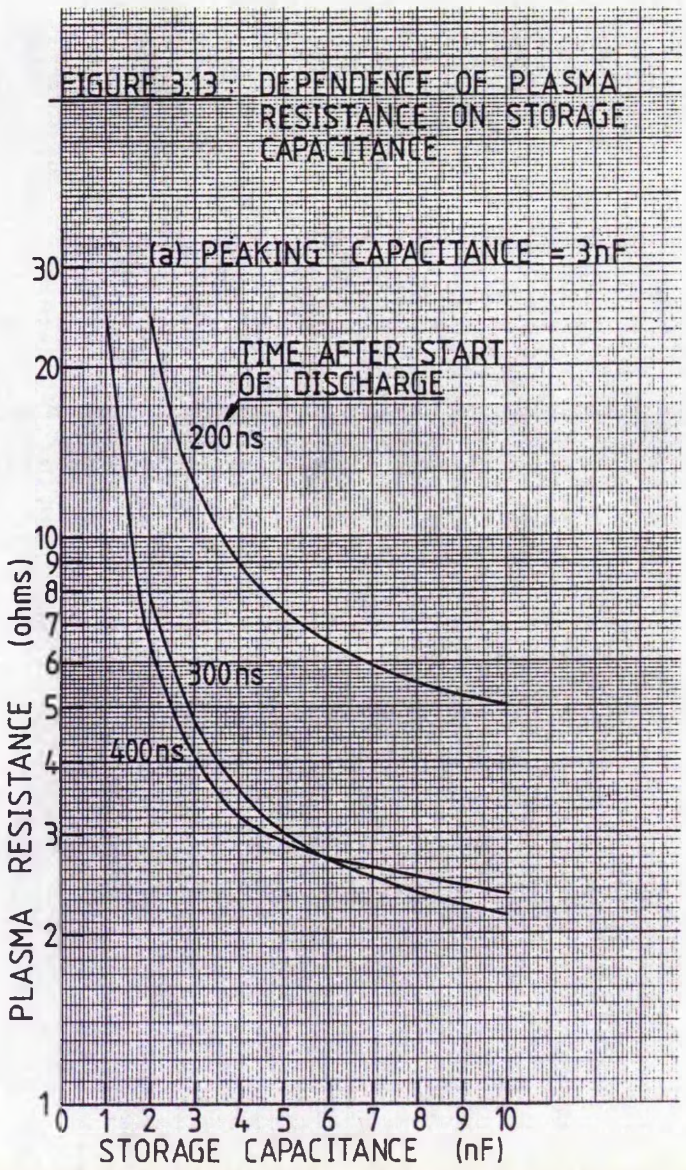

FIGURE 3.13 : DEPENDENCE OF PLASMA RESISTANCE ON STORAGE CAPACITANCE

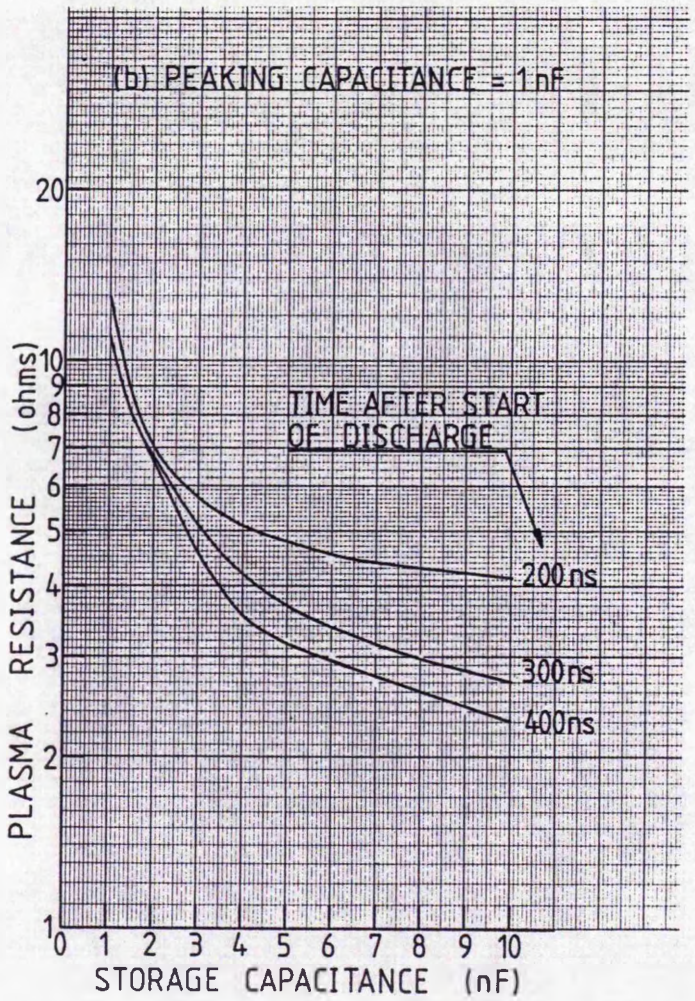

FIGURE 3.14 : DEPENDENCE OF PLASMA RESISTANCE ON INITIAL ELECTRON DENSITY

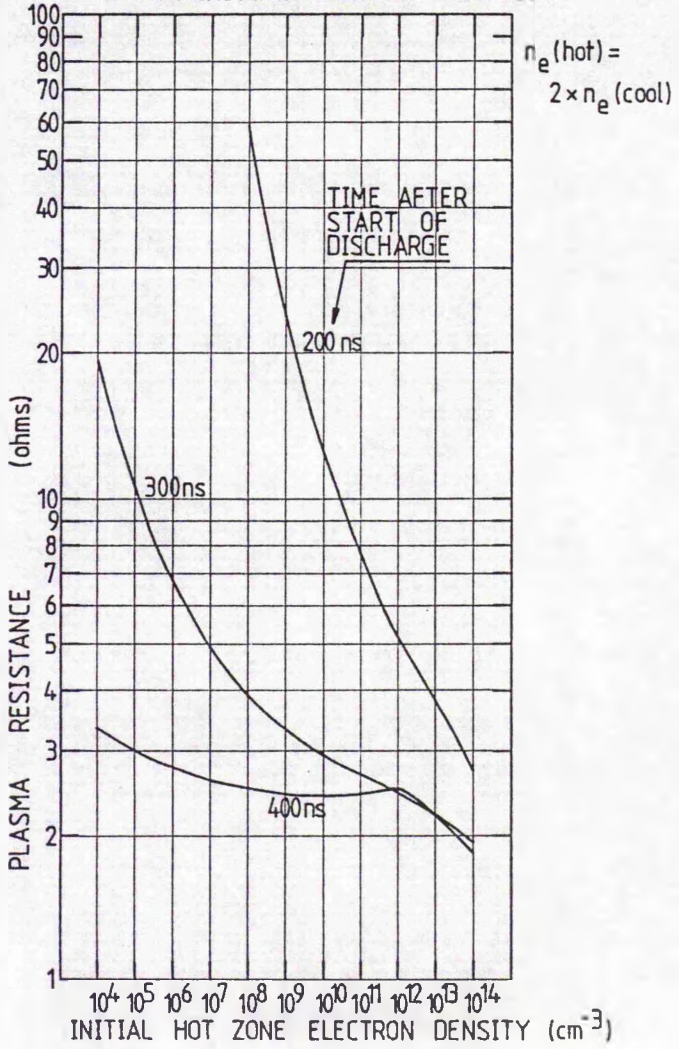

FIGURE 3.15 : DEPENDENCE OF ELECTRON DENSITY ON WALL TEMPERATURE

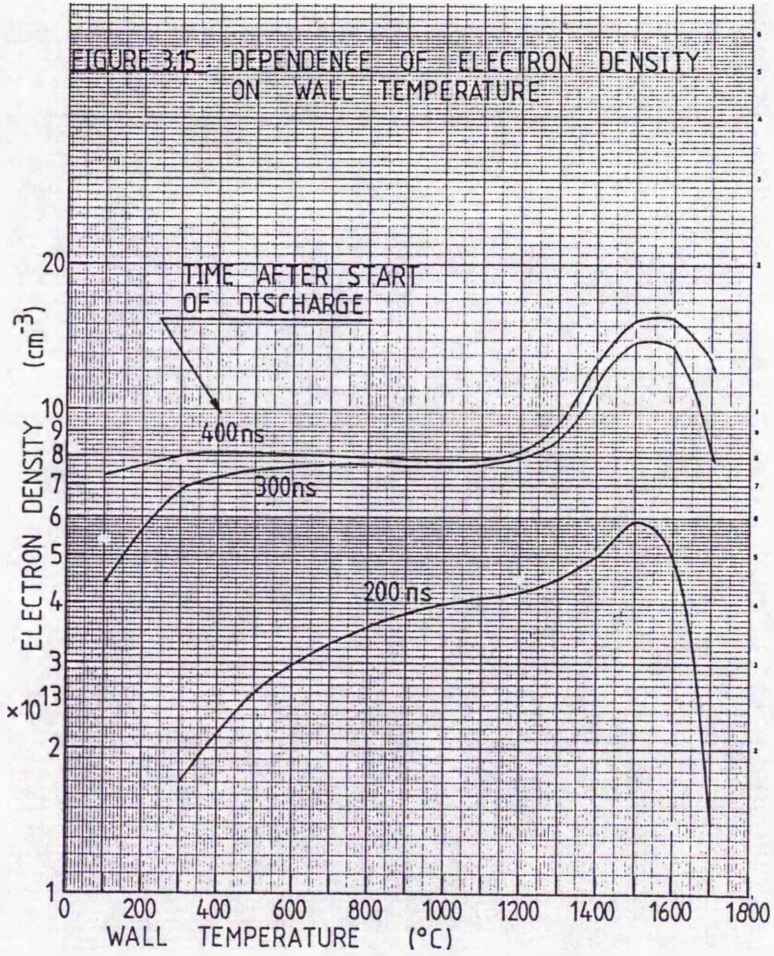

FIGURE 3.16: DEPENDENCE OF ELECTRON DENSITY ON NEON PRESSURE

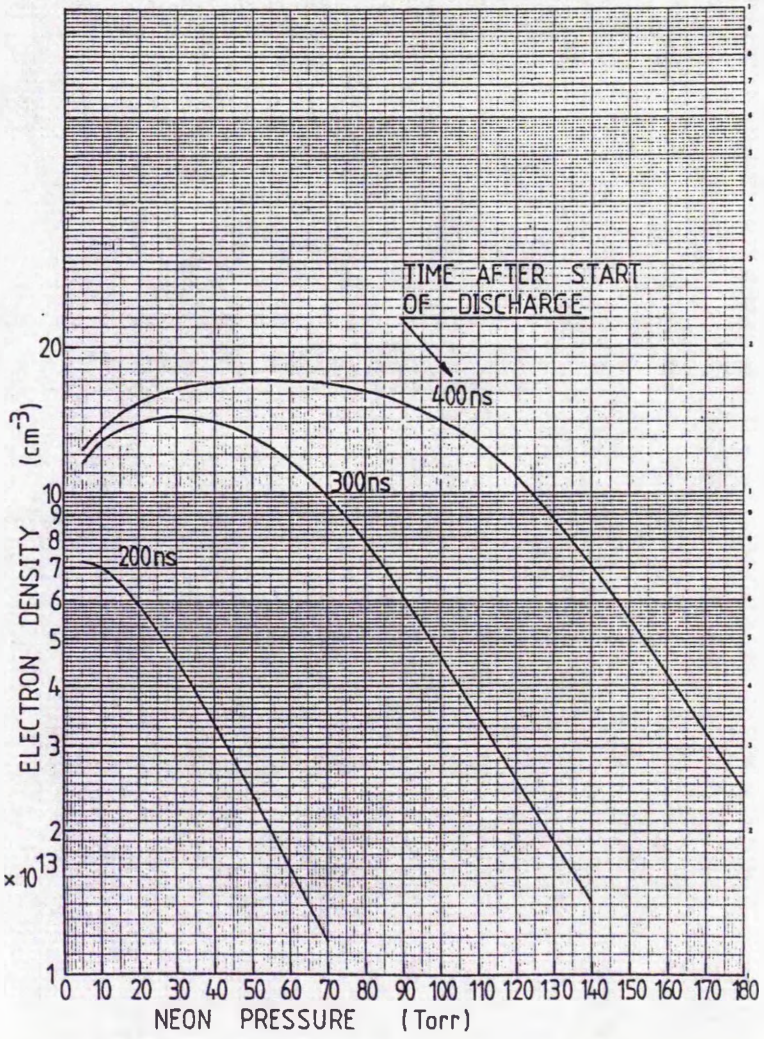

FIGURE 3.17: DEPENDENCE OF PEAK ELECTRON TEMPERATURE ON NEON PRESSURE

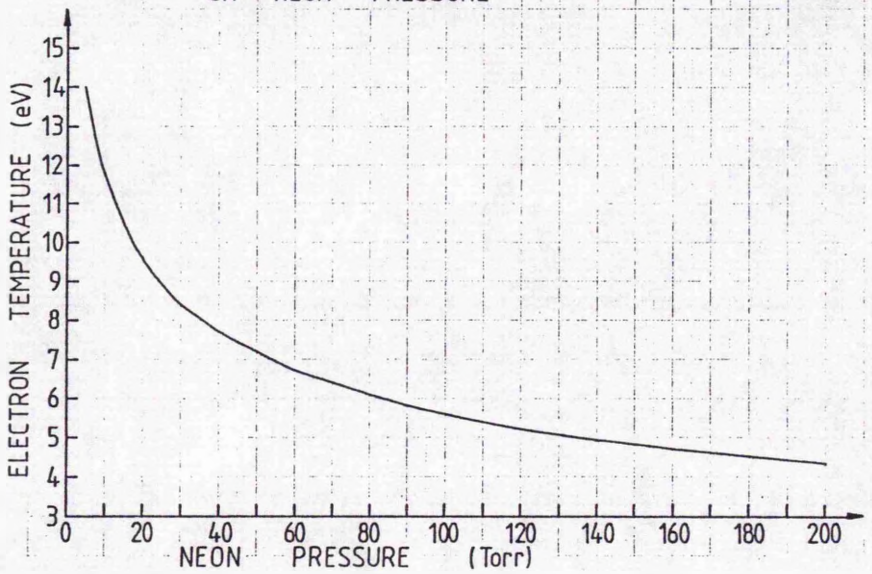

FIGURE 3.18 : DEPENDENCE OF PEAK ELECTRON TEMPERATURE ON WALL TEMPERATURE

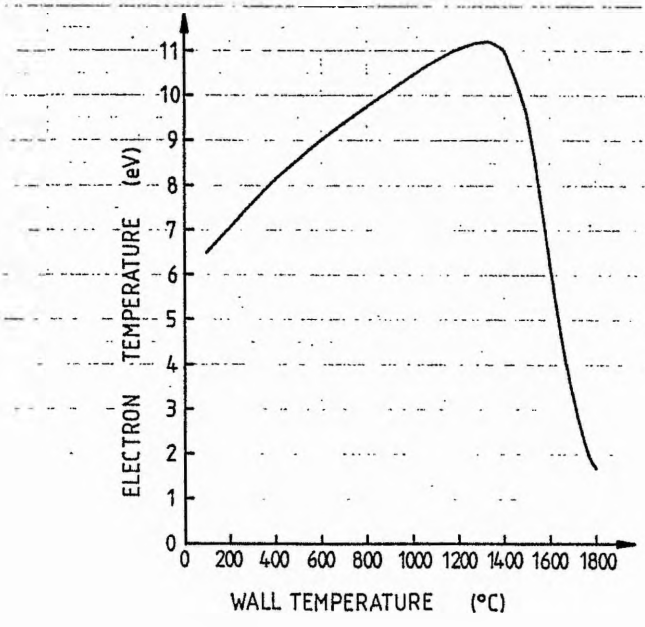

FIGURE 3.19 : DEPENDENCE OF PEAK ELECTRON TEMPERATURE ON INITIAL ELECTRON DENSITY

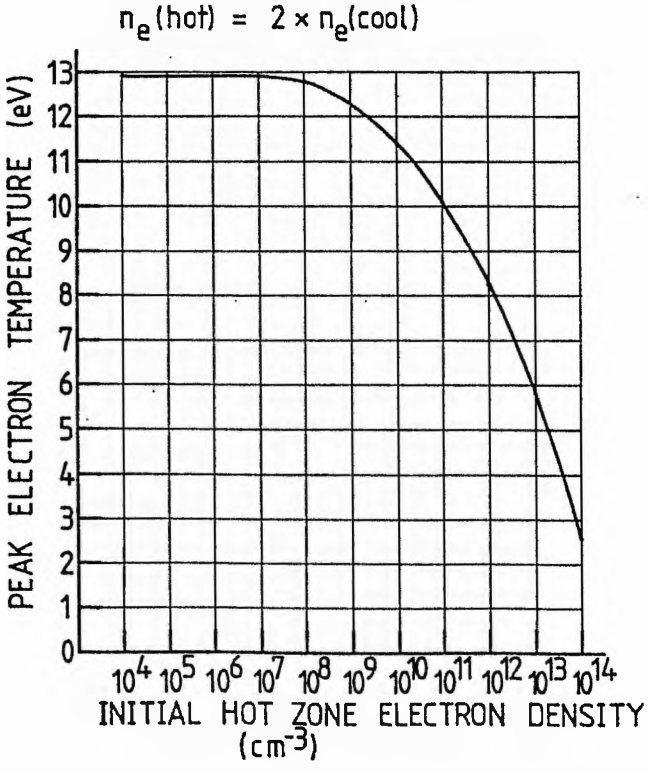

FIGURE 3.20 : VARIATION OF PLASMA RESISTANCE WITH TIME

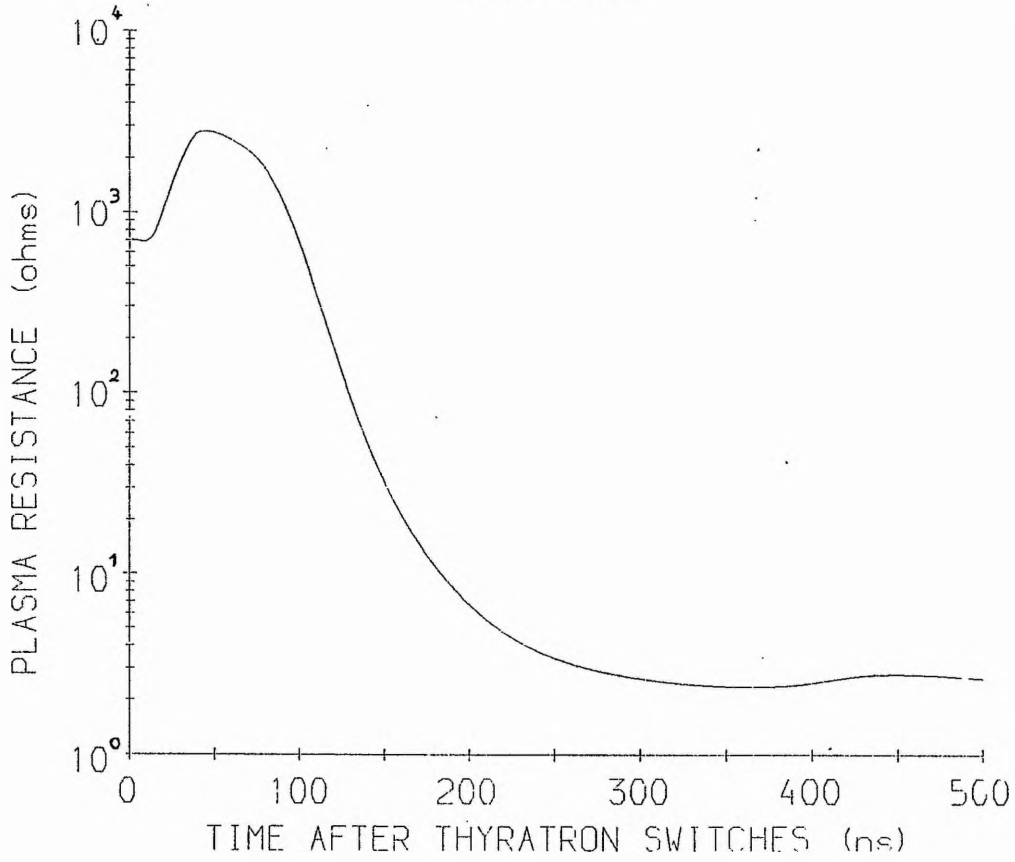

FIGURE 3.21 : VARIATION OF PLASMA INDUCTANCE WITH TIME

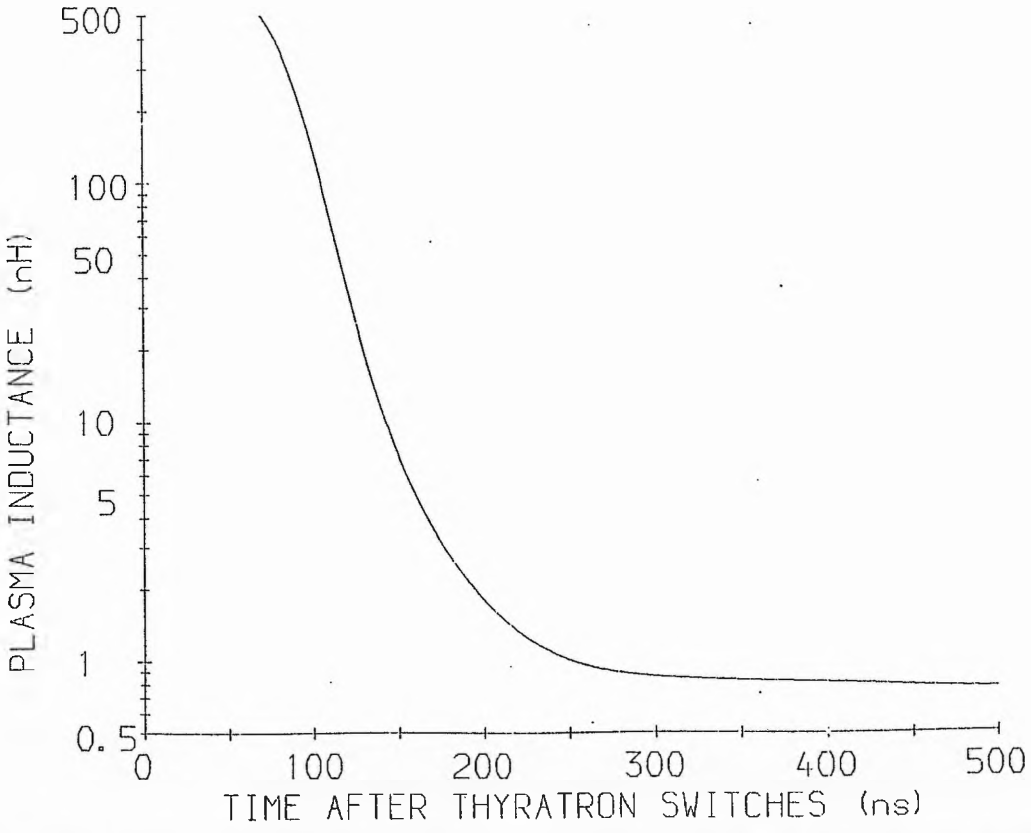

FIGURE 3.22: DEPENDENCE OF MAXIMUMUM METAL SEGMENT LENGTH (AT PEAK VOLTAGE) ON WALL TEMPERATURE

(a) p_{Ne} = 10 torr (b) p_{Ne} = 20 torr

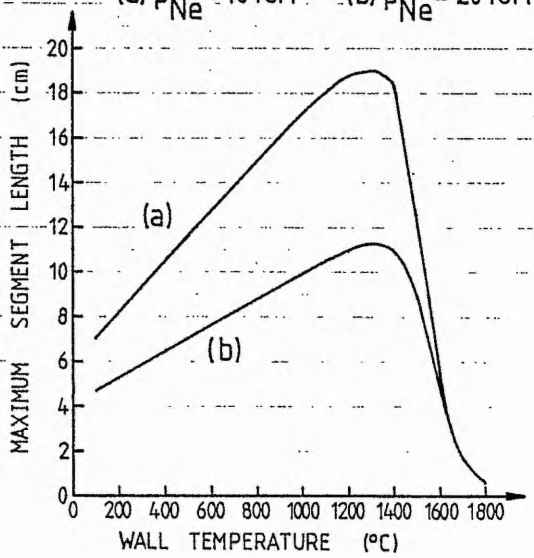

FIGURE 3.23: DEPENDENCE OF MAXIMUM SEGMENT LENGTH (AT PEAK VOLTAGE) ON INITIAL HOT ZONE ELECTRON DENSITY

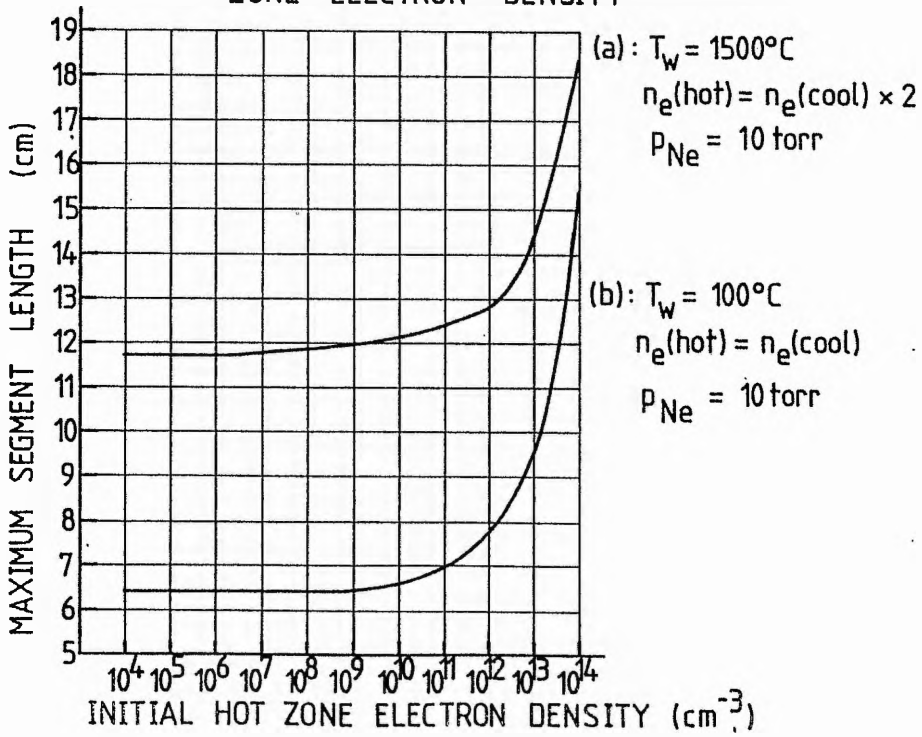

FIGURE 3.24: DEPENDENCE OF MAXIMUM SEGMENT LENGTH (AT PEAK VOLTAGE) ON NEON PRESSURE (a) T_w = 100°C ; n_e(hot)= 10^8 cm^{-3} n_e(cool)= 10^8 cm^{-3} (b) T_w = 1500°C ; n_e(hot) = 2×10^{11} cm^{-3} n_e(cool) = 10^{11} cm^{-3}

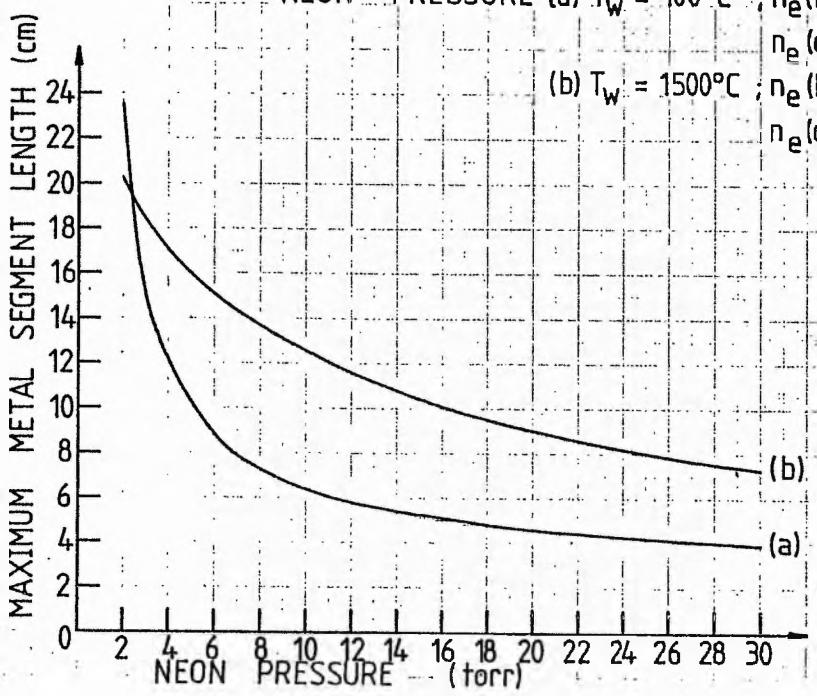

FIGURE 3.25: DEPENDENCE OF MAXIMUM SEGMENT LENGTH (AT PEAK VOLTAGE) ON CHARGING VOLTAGE ON C_s

(a) T_w = 100°C ; n_e(hot) = n_e(cool) = 10^8 cm^{-3}

(b) T_w = 1500°C ; n_e(hot) = 2×10^{11} cm^{-3} ; n_e(cool) = 10^{11} cm^{-3}

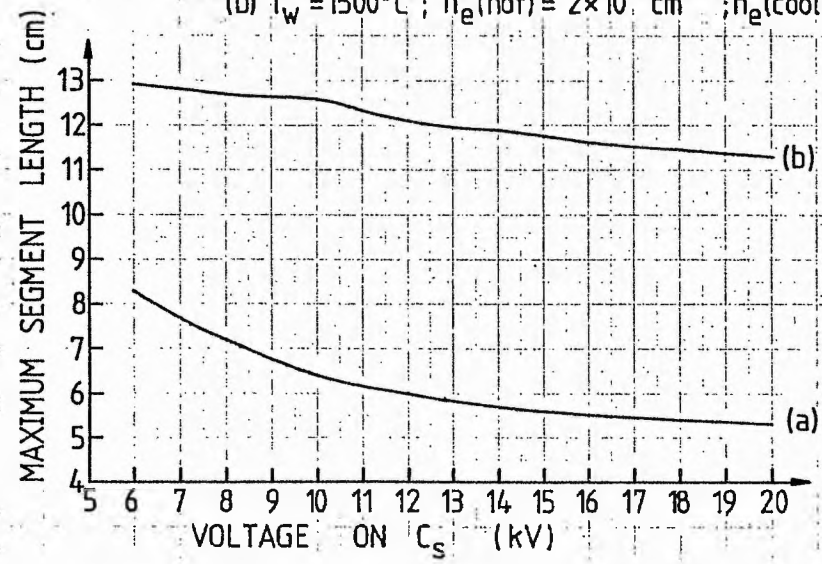

FIGURE 3.26 : VARIATION OF MAXIMUM METAL SEGMENT LENGTH WITH TIME. DISCHARGE VOLTAGE PULSE ALSO SHOWN.
T_{wall} = 100°C ; n_e(hot) = n_e(cold) = $10^8 cm^{-3}$

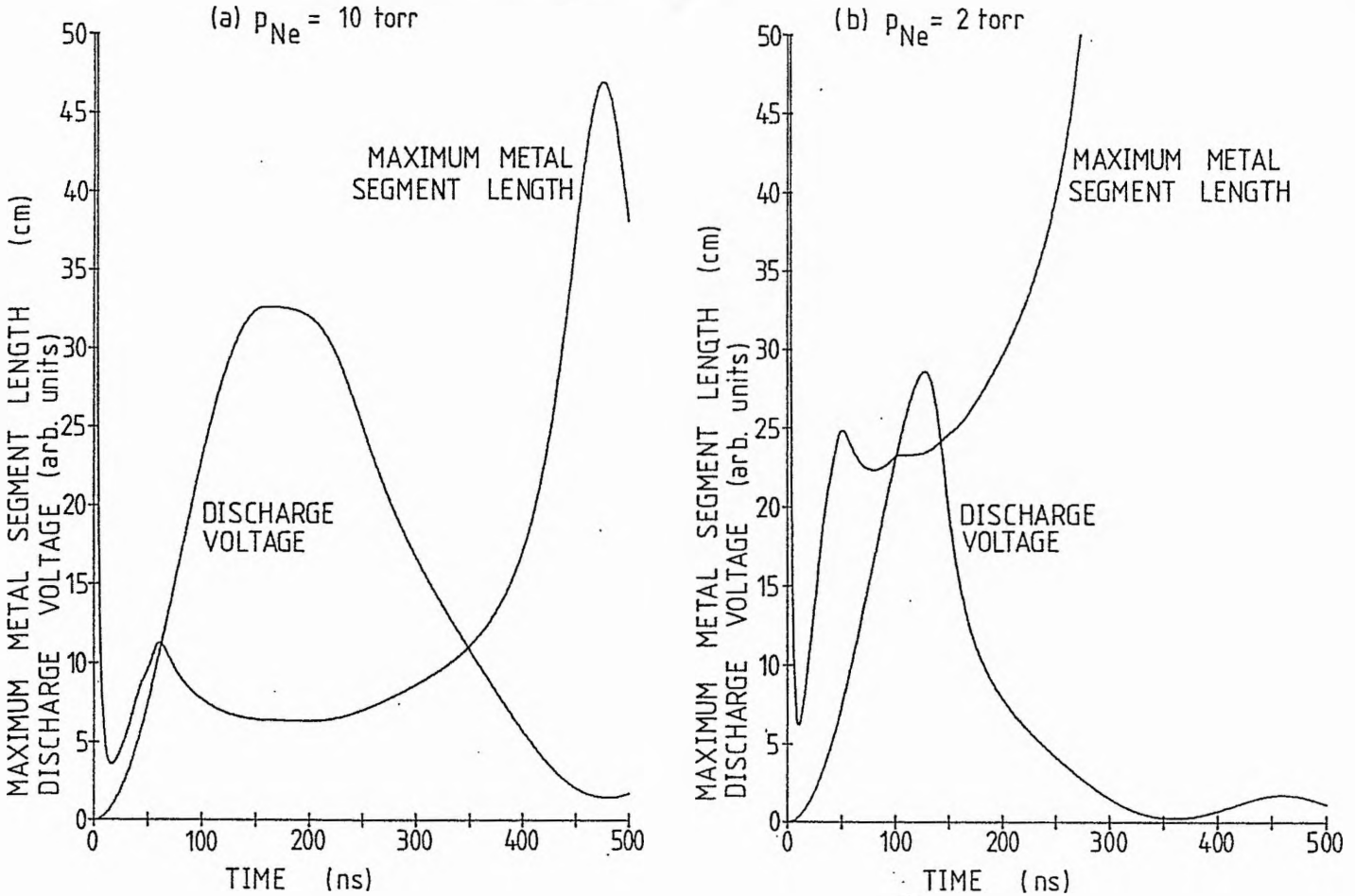

FIGURE 3.27 : VARIATION OF MAXIMUM METAL SEGMENT LENGTH WITH TIME. DISCHARGE VOLTAGE PULSE ALSO SHOWN.

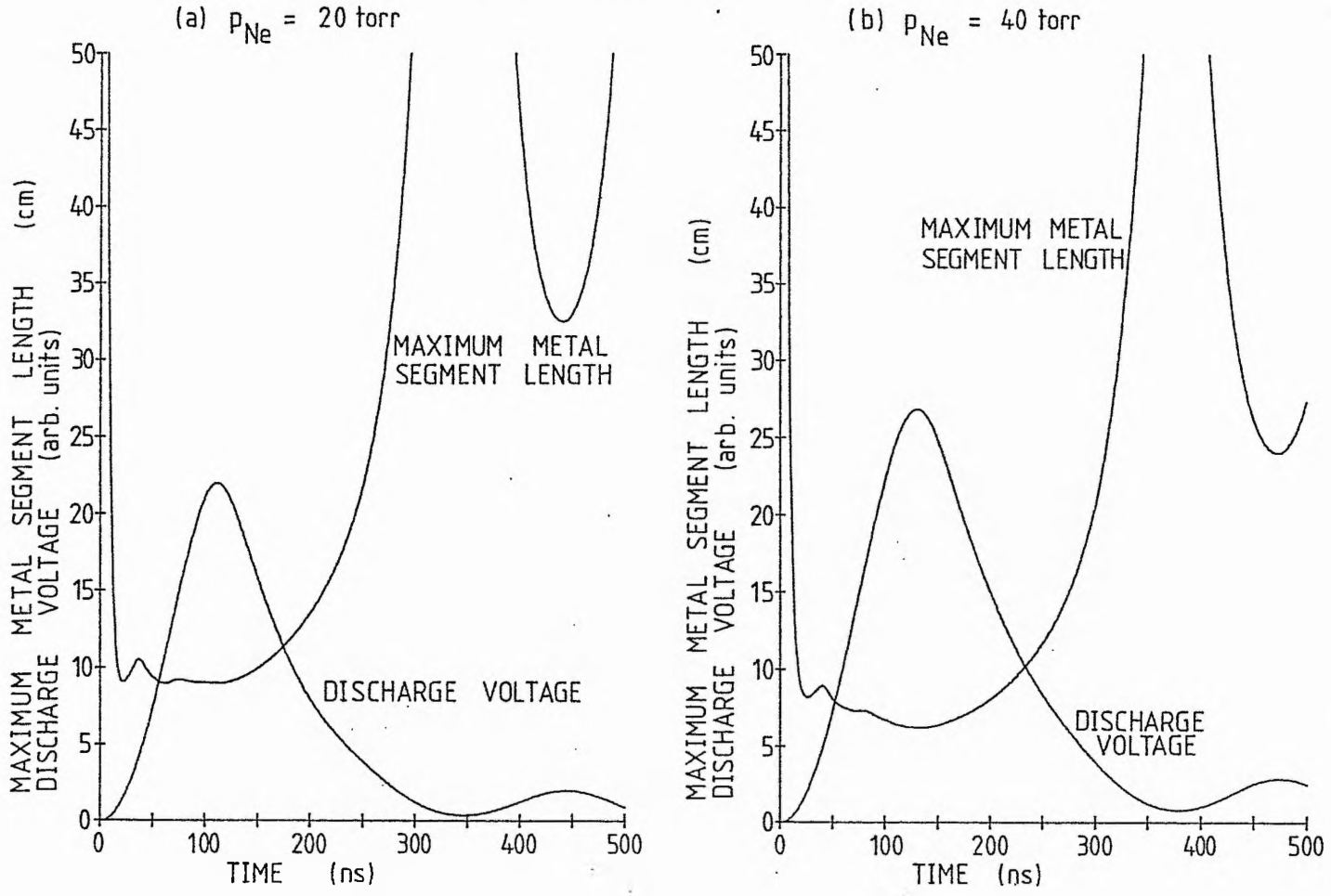

FIGURE 3.28 : VARIATION OF COPPER WITH TIME

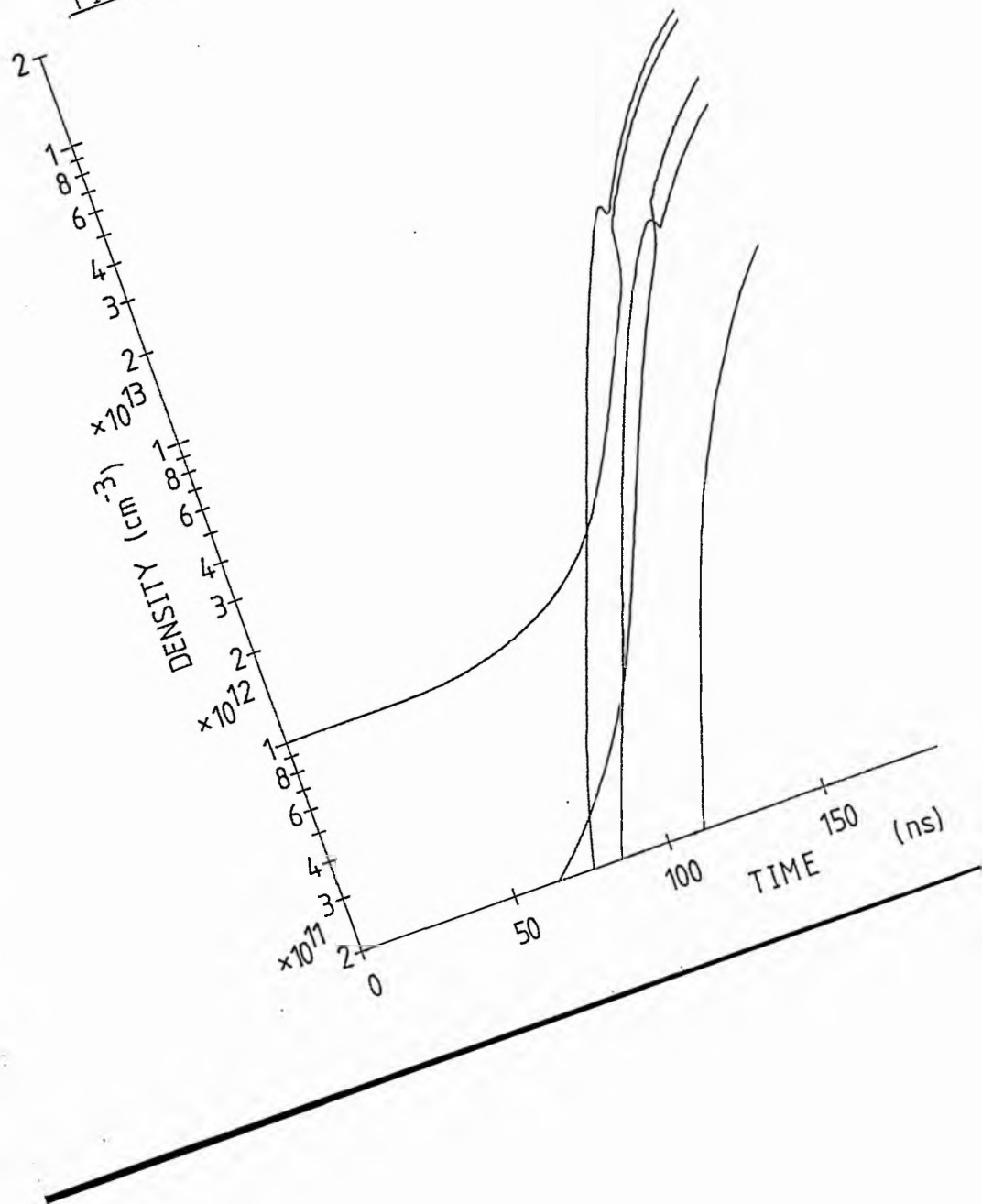

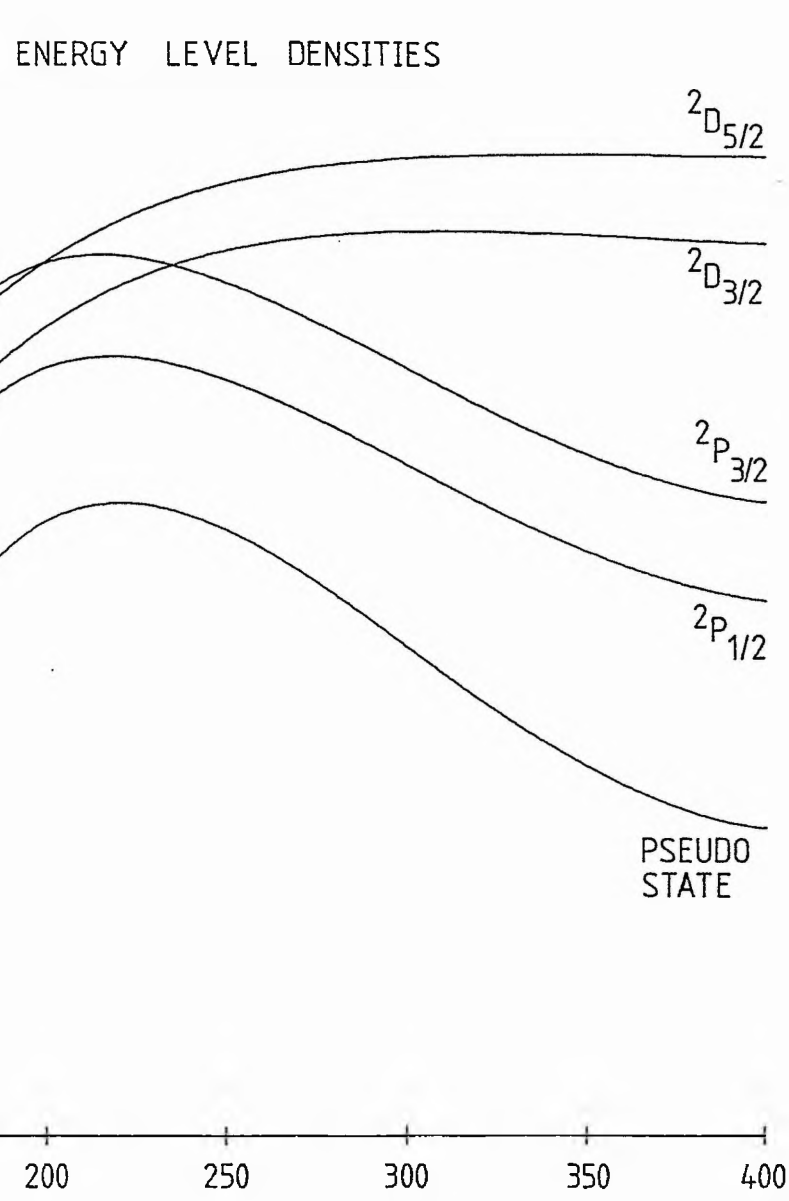
ENERGY LEVEL DENSITIES
$^2D_{5/2}$
$^2D_{3/2}$
$^2P_{3/2}$
$^2P_{1/2}$
PSEUDO STATE
200
250
300
350
400

FIGURE 3.29 : VARIATION OF ION DENSITY WITH TIME

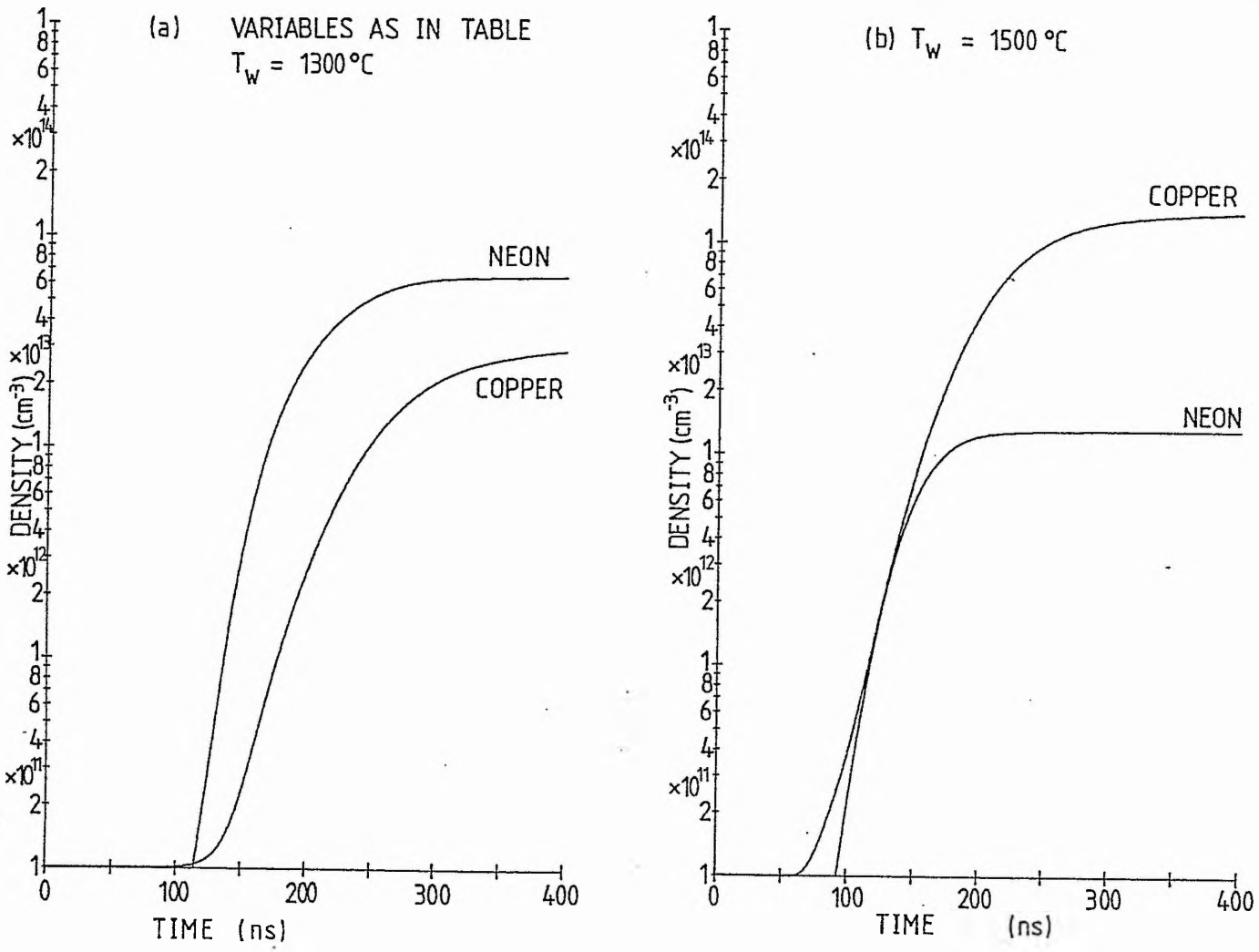

CHAPTER 4

4 COPPER VAPOUR LASER RESULTS

4.1 INTRODUCTION

This chapter describes and discusses the results of experiments run on the CVL. In the first section, the gaseous contaminants found in the CVL are described. The characteristics of the charging and discharge circuits are then described in some detail. The other sections describe the effects of the buffer gas on the operation of the laser.

4.2 CONTAMINANTS IN THE CVL

A mass spectrometer (Kratos MS10S) was attached to the laser gas handling system at the gas outlet on the laser head in order to identify the contaminants evolved when the discharge was run. Since the mass spectrometer was attached to the system outside the hot zone, only species which are gaseous at room temperature could be detected. The thermal insulation in the laser head consisted of a recrystallised alumina tube (TSL Thermal Syndicate) within 3 cm long Mo segments.

A background scan of the residual gases in the mass spectrometer was run. The species detected were H_2O, N_2, O_2 and CO_2. Water vapour and nitrogen were the main contaminants and were approximately 2% of the levels detected when the discharge was run. When the laser was filled with neon, the ratio of Ne^{20} to Ne^{22} was found to be 10:1, as expected.

A DC discharge was run for 120 hours to allow the variation in the contaminant concentration with time to be monitored. When the

discharge current stabilized, the mean power dissipated in the discharge was 1.7^{+}_{-} 0.1 kW. Neon at between 25 and 28 torr was slowly flowed through the tube to remove the contaminants. The temperature of the inner wall of the alumina tube was 1100°C when 1.75 kW was dissipated in the discharge.

The species detected while the discharge was running were H_2O, Ne^{20}, Ne^{22}, N_2, O_2, CO_2 and occasionally H_2 (the mass spectrometer was temperamental in detecting H_2). Figure (4.1) shows the variation of contaminant concentration with time. The points on the graph were plotted by measuring the heights of the contaminant peaks relative to the height of the Ne^{22} peak.

The results show that the gaseous contaminants consisted of water vapour and atmospheric species, with water vapour as the main contaminant. Although it is assumed that the alumina tube was the main source of these impurities, this was not proved. Once the oxide layers and surface water vapour were removed from the Mo electrodes and segments, these should not have been a source of any further contamination. However, the stainless steel end flanges and quartz tube may provide significant amounts of impurities. Although the flanges are water-cooled, their inner surfaces may become quite hot, especially the flange containing the cathode. Metallic elements from the steel flanges have been deposited on the end windows under certain conditions (Section (7.2.3)), so it is not unreasonable to assume that they could also be a source of gaseous contaminants. Ideally, an optical spectrometer should have been used to see if metallic elements such as Na and Ca, which are known impurities in alumina [1], were present in the discharge.

4.3 DIAGNOSTICS

Measurements were made of the laser cathode and thyratron anode voltage, the laser current, laser pulse duration, average laser power and tube temperature.

The voltage waveforms were measured with a Tektronix P6015 High Voltage Probe. This attenuates the voltage by a factor of 1000 and has a risetime of 5 ns [2]. The current pulses were measured with a T&M Research Products current probe (type W-4-001-2.5FC). This has a very low inductance, which is essential for measuring currents which have a very high rate of rise. The probe's resistance is 1mΩ and its risetime is 8 ns [3]. Both the current and voltage pulses were displayed on a Tektronix 543B oscilloscope (not simultaneously). A 50Ω BNC termination was used to match the current probe to the oscilloscope. The voltage probe was calibrated and compensated [4] by displaying the oscilloscope calibrator output through the probe.

The laser pulse was observed using the experimental arrangement shown in Fig. (4.2). An ITL photodiode (type TF1850M20) was used. This required a bias voltage of -3 kV. The spectral response of the photodiode is shown in Fig. (4.3) [5]. The photodiode risetime was 100 ps. The diameter of the photocathode was 18 mm, so some of the CVL pulse was lost, but it was assumed that the spatial profile of the beam was uniform. The photodiode was placed in a metal box to screen out the RF noise generated by the laser and pulse circuitry. The coaxial cable running from the photodiode to the oscilloscope was wrapped around a ferrite core to reduce the amount of noise entering the oscilloscope through the cable's screen. In order to avoid saturating the photodiode, the laser beam was split by using a quartz flat to deflect 10% of the laser beam to the photodiode. Strips of

brass mesh then further reduced the intensity of the beam if required.

The laser power meter consisted of a thermopile detector attached to a Comark microvoltmeter. It was calibrated against a Coherent power meter (accurate to within 10%) with an argon ion laser used as the calibration source. The voltage produced by the detector was dependent on the temperature difference between the detector and the surroundings. The power meter was therefore placed far enough away from the laser to avoid any heating effects caused by thermal radiation coming through the laser window. In order to screen out any radiated noise, the power meter was placed in a copper box and the meter reading was observed through a fine copper mesh.

The discharge tube temperature was measured with a Minolta/Land Cyclops 52 Infra-red Thermometer. This had a temperature range from 600°C to 3000°C. The thermometer had an emissivity compensation control to ensure accurate temperature readings for surfaces with different emissivities. The thermometer's optics could focus to a spot of diameter less than 5 mm at distances of up to 100 cm. The thermometer was calibrated against the melting point of copper. A piece of copper wire was inserted into the centre of the tube with the wire's tip on the tube's axis. As the tube heated up, the copper wire was regularly inspected. When the base started to melt and the wire collapsed, the discharge was switched off and the temperature of the alumina wall adjacent to the copper wire read as 1100°C (of 1083°C MP of Cu) with the emissivity set at 0.4. Ideally, another metal should have been used to check that the alumina's emissivity did not alter as the temperature was increased to 1550°C. However, this would have rendered the alumina tube useless for use in a CVL. The error in temperature measurements made in the centre of the tube was estimated to be 20°C.

4.4 DISCHARGE CIRCUIT

4.4.1 CHARGING INDUCTOR

The charging inductor was made from a nylon bobbin and four ferrite U-cores (Section (2.2)), clamped so that they form the core shown in Fig. (2.3). Pieces of mylar were placed between the U-cores to form the "air" gap. More mylar was placed round the central leg of the core and the nylon bobbin to increase the breakdown voltage between the ferrite and the windings. Single strand 0.6 mm^2 insulated wire (RS) was wound round the bobbin.

The required inductance was calculated to be 0.169 H for a resonant frequency of 10 kHz and a storage capacitance of 6 nF. For a maximum supply voltage of 9 kV, the peak current was calculated to be 1.7 A from equ. [A.20]. The volume of the air gap required to stop the inductor saturating with a maximum magnetic flux density of 0.3 T was 6.8 cm^3 from equ. [A.29]. The three air gaps shown in Fig. (2.3) had a total area of 25 cm^3, so the required air gap length was 2.7 mm (neglecting fringing). The number of turns needed was 380 from equ. [A.31]. With the bobbin wound and an air gap length of 2.3 mm, the inductance was measured to be 0.160 H. Taking into account the effect of fringing at the air gaps (equ. [A.25]), the effective core area was 29.2 cm^2. Hence the effective air gap volume was 6.7 cm^3 as required. The inductance of the charging inductor was changed for later experiments by altering the width of the air gap.

With C_s at 9 nF, C_p at 3.6 nF, and a CX1535 thyratron, the duration of the charging voltage wave was studied as a function of the power supply voltage. The inductance, L_c, in this case, was measured to be 0.29 H. The charging period was calculated to be 160 μs. The

circuit was run at 140 Hz to avoid heating the capacitors and so changing their capacitance. Photograph (4.1) shows the charging voltage waveform at a supply voltage of 5.25 kV. The charging period was 160 μs, as expected. However, as the power supply voltage was increased, the length of the charging period decreased, until, with a supply voltage of 7.05 kV, it was 115 μs (Photo. (4.2)). This reduction in the charging period was due to core saturation as the peak current increased. In Photo. (4.2), it can be seen that the slope of the curve increased at about 40 μs after the start of the charging cycle, where the core started to saturate as the peak current passed through the windings. Although the circuit appeared to operate well even when the core was saturating, the inductor was altered to stop this by increasing the length of the air gap.

The voltage probe was placed between the charging inductor and diode to look at the voltage there at the end of the charging cycle. Photograph (4.3) shows that after C_s has been charged up, the voltage oscillated with a period of 60 μs. The charging diode prevented current reversal in the circuit after C_s was fully charged. The voltage across L_c then fell to zero by discharging the energy stored in its coils to ground via the stray capacitance. The charging inductance in this case was 0.38 H, so its stray capacitance to ground was calculated to be 0.24 nF.

Photograph (4.4) shows the charging waveform when the CX1625 thyratron was used. The neon pressure was 4 torr. The insulation was made up of the 3 cm long Mo segments. The capacitors were charged to 10.0 kV, from a power supply voltage of 5.3 kV. The charging inductor's efficiency was, therefore, 94%.

4.4.2 BYPASS CHARGING ELEMENT

When the hollow anode thyratron type CX1625 was used, the bypass charging element was a 200Ω, high wattage, resistor. However, this arrangement caused problems with thyratron recovery when a CX1535 was substituted. With a bypass resistor, if the first discharge pulse did not break the gas down properly, the load seen by the circuit included the 200Ω resistor for a large part of the pulse. This overmatched load reflected energy back to the discharge circuit, producing a positive voltage at the thyratron anode which caused the thyratron to fail to recover ("hang up"). When the 200Ω resistor was changed to a 5Ω one to improve the matching, the CX1535 operated perfectly.

Bypass inductors were tried both to avoid the recovery problems and to reduce the power dissipated in the bypass resistor. Results of experiments suggested that the required bypass inductor should be air-cored to avoid saturation and should also be as large as practicable to reduce the amount of discharge current flowing through it. A 110 μH inductor was made. Assuming a 100 ns risetime current pulse, this had an impedance of about 3.5kΩ during the initial stages of the discharge. During the charging cycle, its impedance was calculated to be about 7Ω (for a PRF of 10 kHz), so the power dissipated was much less than with a bypass resistor. When the discharge was run, the inductor never became hot.

4.4.3 EFFECT OF CONTAMINANTS

If the rate of heating of the thermal insulation was too great and/or the flow rate of the buffer gas was too low, then as contaminants outgassed and entered the discharge, they increased the

discharge impedance. This increase in impedance caused less power to be dissipated in the plasma and more to be dissipated elsewhere in the circuit. A large proportion was dissipated at the thyratron anode by the negative voltage which appeared there after the discharge pulse (Appendix (B.3)). Some energy was left stored in the C_p-L_b loop, which then oscillated (Photo. (4.5)) with a period given by equ. [2.1]. The resistance of this loop was very small, so the oscillations were only slightly damped and could last for hundreds of microseconds. These oscillations were then superimposed on the charging waveform as shown in Photo. (4.6).

One consequence of the increase in the discharge impedance as contaminants were evolved was that one or more filamentary discharges ran between the outside of the zirconia felt and the quartz tube. These discharges started at the cathode flange and ran to a point approximately level with the start of the coaxial return. At this point, the discharges spread out and became more diffuse. Adding more zirconia felt at each end of the tube to try to block off these discharge paths was unsuccessful. After a number of runs, these filamentary discharges "burned" paths through the outside of the felt. If the gas flow rate was increased, the arcs reduced in intensity and would stop if the flow rate was high enough or the plasma was clean enough.

4.4.4 VOLTAGE AND CURRENT PULSES

Photographs (4.7(a)) to (4.7(f)) show the evolution of the voltage pulse across the laser as the ceramic insulation heated up. The Ne pressure was 20 torr. Photographs (4.7(a)) to (4.7(e)) were taken at the same PRF (4 kHz), with a supply voltage of 3.5 kV. The thyratron used was a CX1535. Photograph (4.7(a)) was taken shortly

after the discharge was switched on. As the discharge plasma heated up, the impedance of the plasma fell, and the voltage pulse narrowed. However, at the same time, the density of contaminants increased until it was high enough to reverse the fall in impedance. This caused a larger reflection from the load to the thyratron anode, so the charging voltage on C_s increased. This larger voltage on C_s together with the higher discharge impedance combined to increase the peak voltage across the laser (Photo. (4.7(b))). As still more contaminants entered the discharge, the voltage pulse widened (Photo. (4.7(c))) and the proportion of power dissipated in the circuit components increased. Gradually the density of contaminants decreased as they were carried away by the flowing buffer gas so the discharge impedance started to fall again (Photo. (4.7(d))). At the same time, the current drawn from the power supply dropped. In Photo. (4.7(e)), the effect of the contaminants had disappeared. The impedance of the plasma continued to fall as the gas temperature rose and copper vapour diffused through the discharge cavity. Photograph (4.7(f)) shows the voltage pulse at a PRF of 6.1 kHz, after lasing had started.

As the discharge tube heated up, the current pulses also changed. Photographs (4.8) to (4.11) show this. In Photo. (4.8), there were contaminants in the discharge (there were oscillations on the voltage pulse after the main pulse). The current pulse trace was affected by noise so only the overall current pulse shape could be determined. The pulse appeared to have a broad base (about 400 ns), with a low peak value (400 A, neglecting the initial spike). In Photo. (4.9), most of the contaminants had been removed. The current pulse had narrowed to about 300 ns at the base and increased in height to about 600 A. Gradually, the characteristic double hump pulse shape emerged (Photo. (4.10)) until it was clearly there in Photo. (4.11)

when lasing had started. The first peak was due to the charge on C_p discharging into the plasma and the second peak was due to the remaining charge on C_s discharging into the plasma. In Photo. (4.11), the pulse height was 1200 A.

Photographs (4.12) and (4.13) show the current and voltage in the laser when the discharge was overmatched. The negative part of the voltage pulse was nearly 1.5 μs wide and then became positive, but did not oscillate. Instead, it showed a resistive decay as the remaining charge on the capacitors discharged into the plasma.

When the storage capacitor was reduced to 3.6 nF (= C_p), the current waveform was as in Photo. (4.14), showing good matching between the capacitors, with comparatively little aftercurrent from C_s. The discharge voltage was an almost perfectly matched pulse (Photo. (4.15)). To reach the required temperature with this arrangement, the supply voltage was increased to 6.1 kV and the PRF to 9.3 kHz.

With storage and peaking capacitors of 9 nF and 3.6 nF respectively, ceramic insulation, 3.8 kV supply voltage and a PRF of 5 kHz, the current pulse at peak lasing power appeared as in Photo. (4.16). The oscillation after the second hump of the current pulse shows that the load was undermatched. Photograph (4.17) shows the reduction in height of the current pulse when the laser temperature was higher than optimum; also, the positive overswing after the second hump had decreased in height. This shows that the discharge impedance increased as the copper vapour density rose past its optimum value. The laser output was almost wholly yellow at this point.

The highest recorded power from the ceramic insulated CVL was 11.2 W. The PRF was 4.8 kHz, the supply voltage 4.4 kV, the storage capacitance 7.2 nF and the Ne pressure 50 torr. The efficiency (laser

power divided by supply power) was 0.6%.

4.5 DEPENDENCE OF LASER POWER ON SUPPLY POWER

Although a Minolta/Land thermometer was available for the measurement of the discharge tube temperature, it was not possible to obtain the dependence of the laser power on the tube temperature. This was because of the difficulties associated with observing the discharge tube wall while the CVL was lasing. Instead, the laser power was measured as a function of the power drawn from the supply.

For the experiments using metal segments, the storage capacitance was 9 nF, the peaking capacitance was 3.6 nF and the neon pressure was kept between 10 and 15 torr. The results shown in Fig. (4.4) were taken from experiments where the insulation consisted of the 12 cm segments described in Section (2.8.4). For the results in Fig. (4.4(a)), a Mo heat shield was used, whereas in Fig. (4.4(b)), the heat shield was Al. In Fig. (4.4(a)), the optimum temperature was not reached due to the limitations of the power supply. In Fig. (4.4(b)), the lower emissivity of the Al heat shield increased the thermal efficiency of the insulation. Lasing was thus achieved for a lower supply power. However, part of the Al heat shield melted (point A on the graph), reducing the temperature. More power then had to be supplied to raise the temperature and laser power to their former levels. At point B on the graph, the power drawn from the supply drops from 2.56 kW to 2.52 kW. This was due to the changing impedance of the load as the walls cooled and the copper vapour density dropped.

Figure (4.5) shows the laser power and efficiency as a function of the power drawn from the supply for two different PRFs. In this experiment, ceramic insulation (Section (2.8.3)) was used with a Mo

heat shield. The storage and peaking capacitances were 7.2 nF and 3.6 nF respectively. The Ne pressure was kept between 20 and 40 torr. At 3.3 kHz, the peak laser power was achieved at a higher supply power than at 4.1 kHz. This was due to the higher supply voltage, and hence larger electric field, which was used at the lower PRF.

With 1.94 kW drawn from the power supply, the discharge was switched off and the peak wall temperature measured with the infra-red thermometer to be 1550°C.

4.6 LASER PULSE WITH NEON BUFFER GAS

Photographs (4.18) to (4.20) show the changing shape of the laser pulse as the wall temperature and output power increased. The PRF was 4.6 kHz and the neon pressure kept between 20 and 30 torr. The laser powers in Photos. (4.18), (4.19) and (4.20) were 0.4 W, 4.7 W and 9 W, respectively. As the temperature rose, the pulse width narrowed and both the energy per pulse and the peak power increased. In Photo. (4.20), the FWHM of the pulse was 36 ns and the peak power was 54 kW.

In Photos. (4.21) and (4.22), the PRF was increased to 8 kHz. In order to keep a constant power supplied to the laser, the supply voltage was reduced. The storage and peaking capacitors were unaltered. In Photo. (4.21), the laser power output was 2.4 W and the wall temperature was below optimum; a prominent spike had appeared at the start of the pulse. In Photo. (4.22), the laser power was 8.9 W, and the power drawn from the supply was 1.8 kW. The pulse shape was the same as for Photo. (4.20), but the FWHM had decreased to 28 ns. However, since the energy per pulse had also decreased, the peak power was only 40 kW. In Photo. (4.23), the PRF was switched to 1.4 kHz and

the photograph taken before the wall temperature had dropped significantly. The beam attenuation in front of the photodiode was the same as for Photo. (4.22), so the energy per pulse had increased.

To study the effect on the laser pulse of increasing the PRF without reducing the supply voltage, the storage capacitance was reduced to 3.6 nF. Photograph (4.24) shows the laser pulse at 9.3 kHz, a charging voltage of 10.5 kV and a neon pressure of 50 torr. The laser power was only 1.8 W for a supply power of 1.94 kW. The pulse shape was different to that of Photo. (4.22), which was taken at a comparable PRF (8 kHz). The main difference between the two cases was the power drawn from the supply. At this high PRF, the supply power was probably higher than optimum, resulting in the lower laser power.

Photograph (4.25) shows the effect on the laser pulse of running the discharge with a very high neon pressure. In this case, the neon pressure was 280 torr, the PRF was 4.8 kHz and the laser power was 2.5 W. The temperature was near optimum. The supply voltage was higher to compensate for the drop in supply current caused by the high pressure.

The changing shape of the pulse with temperature was due to the combined effects of the two laser lines. Initially, only the green line lased, then, as the temperature increased, so did the strength of the yellow line. Since the yellow pulse has been found to be delayed with respect to the green pulse [6], this would explain the increasing height of the centre of the pulse as being due to the emergence of the yellow laser line.

The change in the pulse shape with PRF was probably due to the change in the electron density at the start of the each discharge pulse. At higher PRFs, the higher electron density increases both the excitation rate and the rate of superelastic collisions. This

produces both the faster rising front edge and the faster falling tail. Also, at higher electron densities, the electron temperature falls, eventually resulting in a drop in the pulse energy. Finally, the gas temperature rises, resulting in a higher metastable population at the start of the discharge. At higher buffer gas pressures, the large radial temperature gradient in the plasma produces a larger thermal population of the lower laser levels. These effects combine to produce the observed reduction in laser pulse energy and width as the PRF and/or the neon pressure was increased.

4.7 BUFFER GAS EFFECTS

4.7.1 DEPENDENCE OF LASER POWER ON NEON PRESSURE

Figures (4.6) and (4.7) show how the laser power varied as the neon pressure was increased. The storage and peaking capacitors were 7.2 nF and 3.6 nF, respectively. The difference between the two graphs was that in Fig. (4.6), the power drawn from the power supply was kept constant by adjusting the supply voltage, whereas in Fig. (4.7), the power drawn was allowed to vary with pressure. The laser power in Fig. (4.7) therefore dropped as the pressure increased, partly because the power drawn from the supply, and hence the wall temperature, decreased. Figure (4.8) shows the decrease both in the charging voltage on C_s and in the power drawn from the supply as the neon pressure rose. The power supply voltage was 4.5 kV. Below 100 torr, there was a large reflection from the load to the thyratron, causing C_s to charge up to more than twice the supply voltage (Section (2.5.1) and equ. [2.2]). The drop in the supply power as the buffer gas pressure increased was not compensated for by the improvement in matching between the load and the circuit. The

charging voltage in Fig. (4.8(b)) was calculated by measuring the temperature of C_s and then estimating the actual value of C_s from Fig. (2.4). When running, C_s reached a temperature of 45°C, corresponding to a 10% drop in capacitance. In Fig. (4.6), the initial rise in power was due to an increase in the tube temperature caused both by the improved matching and the higher dissipation per unit length as the higher pressure moved the discharge closer to the electrode tips. After this, as the neon density increased, the larger elastic and inelastic losses in the discharge caused the gradual decrease in power. The small fluctuations in the curve were due to small variations in the power drawn from the supply. In the experiment, the power drawn varied by $\pm$20 W from a mean value of 1.61 kW. The vertical error bars were obtained using Fig. (4.5) to calculate the proportional variation in output power over this range. Another source of error was the variation in the flow rate of neon as the pressure rose. This altered the rate of loss of contaminants and the rate of heat loss by gaseous conduction.

Lasing was achieved at up to atmospheric pressure of neon. As the pressure rose, the intensity of the green line decreased, until at 760 torr, only the yellow line was visible, at a power of 30 mW.

The above results show that the coupling between the discharge circuit and the laser plasma was strongly influenced by the buffer gas pressure. This applied during both the discharge and the charging cycles.

4.7.2 ADDITION OF HYDROGEN TO NEON

Research grade hydrogen was added to the gas supply system to observe the effect on the voltage and laser pulses of adding H_2 in small amounts to a copper-neon discharge. The results are shown in

Photos. (4.26) to (4.29). Photographs (4.26) and (4.27) were taken with 50 torr of Ne in the laser, a supply voltage and current of 4 kV, 0.42 A, a PRF of 6.1 kHz and a laser output power of 5 W. The efficiency was therefore 0.30%. Hydrogen was then let slowly into the laser through a needle valve. With less than 1 torr partial pressure of H_2 in the system, the supply current dropped to 0.39 A, the laser power to 4 W and the efficiency to 0.26%. The voltage and laser pulses were as in Photos. (4.28) and (4.29). Comparing Photos. (4.26) and (4.28), it can be seen that the effect of adding H_2 was to increase the discharge impedance. This increase reduced the size of the reflection to the thyratron anode so that C_s charged to a slightly lower voltage, causing the supply current to fall. The reduction in laser power was due more to a drop in the wall temperature than to the effect of hydrogen on the laser processes. The laser pulse in Photo. (4.29) had the same pulsewidth as in Photo. (4.27), but a slightly different shape. The pulse risetime decreased with the addition of H_2. The bumps in the laser pulses were 12 ns apart, which corresponded to the cavity round trip time. The vertical scales in the two photographs were different. As more H_2 was let into the system the supply current fell further. If a large partial pressure of H_2 was let into the system, lasing ceased almost immediately and the current drawn from the power supply dropped sharply. The speed at which this happened can be explained by the hydrogen atoms or molecules reducing the electron temperature to a level below that required for lasing. Alternatively, the H_2 molecules deexcited the copper upper laser levels in inelastic collisions.

4.7.3 HYDROGEN BUFFER GAS

Photographs (4.30) to (4.32) show the variation of the discharge

current with hydrogen pressure. The wall temperature in this case was kept at less than 1100°C to avoid producing copper. The supply voltage was 5.3 kV and the PRF was 2 kHz. As the H_2 pressure was decreased from 7.5 torr (Photo. (4.30)) to 1 torr (Photo. (4.31)), the height of the current pulse increased. At the highest pressure, there was a lot of amplitude jitter, showing that the discharge impedance was varying between pulses. The oscillations 200 ns after the start of the pulse show that energy was still being dissipated due to reflections from the load. As the pressure decreased, more of the discharge power was dissipated in the plasma (Photo. (4.31)) and less in the circuit components. The jitter had also disappeared. At pressures below 1 torr, the current pulse height continued to increase, but the jitter increased as well (Photo. (4.32)). With 1.5 torr of H_2, lasing only started when the supply power reached 1.8 kW, which was close to the optimum for neon. The laser beam was not steady, but varied strongly in intensity. As the pressure was reduced, the average power increased from 0.7 W at 1.4 torr to a maximum of 5.1 W at less than 0.75 torr (the pressure gauge would not read below this level). Photograph (4.33) shows the laser pulse at 0.75 torr, with 1.9 kW drawn from the supply. The average power was 3 W. Both the green and yellow lines lased, but their relative powers were not measured.

Photograph (4.34) shows the laser pulse at 2.2 torr, for a supply power of 1.9 kW and an output power of less than 100 mW. The low power output was due to the high pressure.

In order to study the effect on the laser pulse of running at higher PRF's, C_s was changed to the same size as C_p (i.e. 3.6 nF). Photographs (4.35) and (4.36) show the laser pulses for storage capacitances of 7.2 nF and 3.6 nF, respectively. The PRFs were 4.7 kHz and 9.8 kHz, and the average powers were 5.4 W and 4.9 W,

respectively. The hydrogen pressure was less than 0.75 torr in both cases. The faster rising front edge of the pulse in Photo. (4.36) was due to the effect on the initial electron density of running at a higher PRF. The pulsewidth in Photo. (4.36) is slightly less than in Photo. (4.35) (25 ns and 30 ns, respectively).

4.7.4 CONCLUSION

The effect of the buffer gas is extremely complicated, since it affects the operation of the discharge circuit, the afterglow processes and the radial temperature gradient in the discharge, as well as the discharge kinetics during the discharge pulse. In turn, the optimum buffer gas pressure depends on the tube diameter [7] and the copper vapour density [8]. There is probably also a dependence on the contaminant density, which is related to the rate of flow of the buffer gas, the type of insulation used and its cleanliness. Therefore, making sense of a comparison between the use of Ne and H_2, or a mixture of the two gases in various circumstances is very difficult. In effect, each gas and every gas mixture will be likely to have different optimum operating conditions.

The results in Section (4.7.2) show that adding small amounts of H_2 to Ne increased the discharge impedance. Whether this was due to a higher plasma recombination rate in the afterglow, which affected the electron/ion density at the start of the following pulse, or to larger elastic and/or inelastic losses during the discharge, or to both, is unknown at present. From a theoretical viewpoint (Section (1.3.2)), the higher elastic scattering cross-section suggests that hydrogen will affect both the discharge and afterglow processes. It is also known that the addition of hydrogen improves the radial intensity distribution of the laser beam by increasing the power output from the

axial regions [9]. Although this improvement is attributed to an increase in the rate of volume deexcitation of the ^2D levels, it is equally likely to be due to the high thermal conductivity of H_2 which lowers the radial temperature gradient in the plasma. This is because the larger the radial temperature gradient, the higher the plasma temperature will be, and hence the lower the density of copper atoms on the axis (equ. [3.2]).

When hydrogen was used on its own, the dependence of the laser power on pressure was similar to when it was used as an additive. This suggests that when hydrogen is added to neon, the importance of the neon gas is significantly reduced. The conclusions to be drawn from Section (4.7.3) are limited to the facts that the CVL lased, with power levels and laser pulses similar to those obtained with neon. However, the discharge circuit and buffer gas pressure were not optimized for use with either neon or hydrogen, so the maximum attainable power is not known. It should be noted that, for an optimum hydrogen pressure of about 0.75 torr (as measured outside the discharge), the density of hydrogen in the discharge at a temperature of 2000 K is 3.6×10^{15} cm^{-3}. This is only 1.4 times the estimated copper vapour density of 2.6×10^{15} cm^{-3} (from equ. [3.1], for a wall temperature of 1550°C). At these low pressures, the discharge kinetics in the hot zone may be dominated by processes involving copper vapour and hydrogen may only have a secondary role. However, it is still needed to carry the discharge from the electrodes to the copper vapour.

The use of hydrogen, with its higher impedance and thermal conductivity, suggests that, compared with neon, larger bore diameters and repetition rates may be used. However, further work in a properly decontaminated system, with a suitable pressure gauge, is required before this can be confirmed.

REFERENCES FOR CHAPTER 4

1 : Karras T.W., PROC. INT. CONF. LASERS, 168 (1980)

2 : McDuff G., PhD Thesis, Chapter 3, 1987

3 : T&M Research Products Current Probe Data Sheet, P12, 1981

4 : Tektronix P6015 Probe Instruction Manual 1974

5 : ITL Sub-nanosecond Photodiode Operating Instructions

6 : Isaev A.A., Kazaryan M.A., SOV. J.Q.E. 7, 253 (1977)

7 : Grove R.E., LASER FOCUS, p45 July 1982

8 : Marasov O.R., Stoilov St., OPT. COMM. 46, 221 (1983)

9 : Huang Z-G., Namba K., Shimizu F.
JAP. J. APPL. PHYS. 25, 1677 (1986)

PHOTOGRAPH 4.1 : CHARGING VOLTAGE

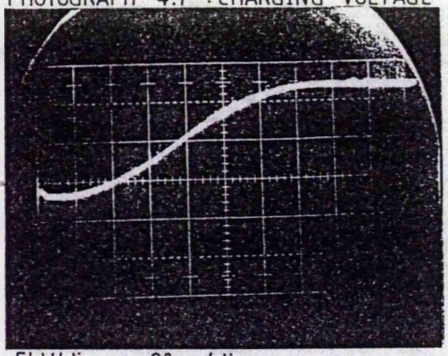

5kV/div 20μs/div

PHOTOGRAPH 4.2 : CHARGING VOLTAGE

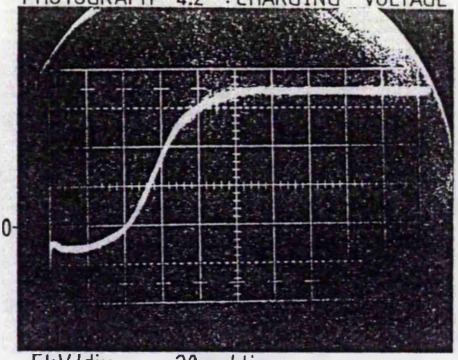

5kV/div 20μs/div

PHOTOGRAPH 4.5 : LASER VOLTAGE

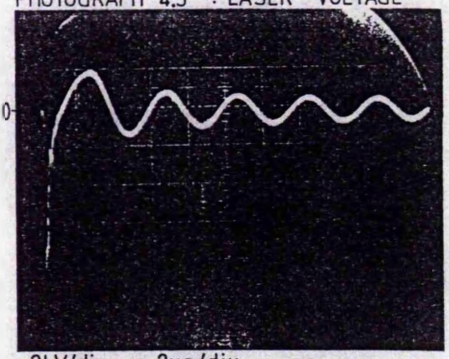

2kV/div 2μs/div

PHOTOGRAPH 4.6 : CHARGING VOLTAGE

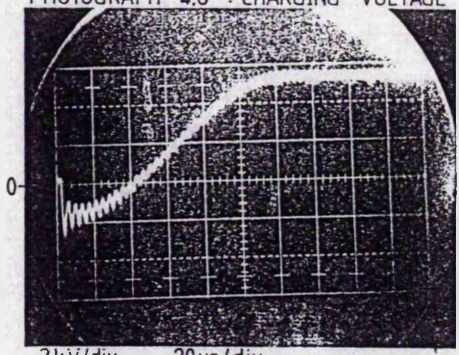

2kV/div 20μs/div

PHOTOGRAPH 4.7 (c)

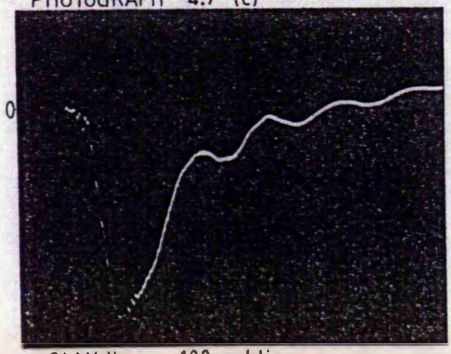

2kV/div 100ns/div

PHOTOGRAPH 4.7 (d)

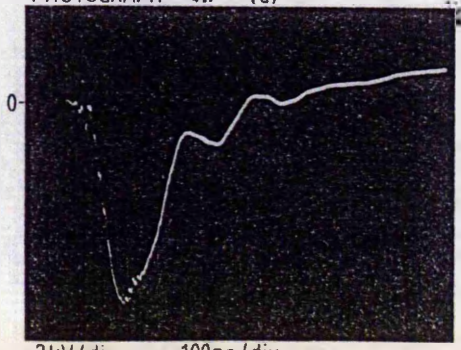

2kV/div 100ns/div

PHOTOGRAPH 4.3 : VOLTAGE BETWEEN L_r AND DIODE

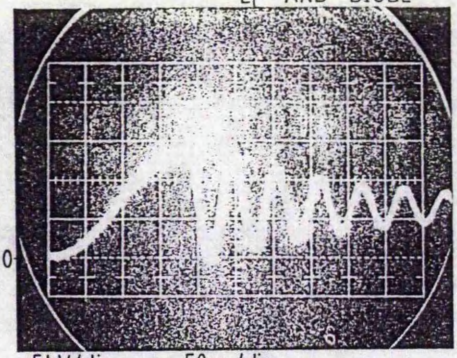

5kV/div 50μs/div

PHOTOGRAPH 4.4 : CHARGING VOLTAGE

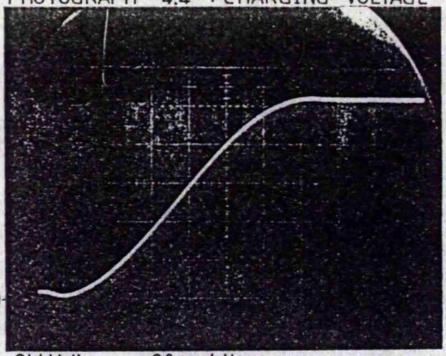

2kV/div 20μs/div

PHOTOGRAPH 4.7 :LASER VOLTAGE (a)

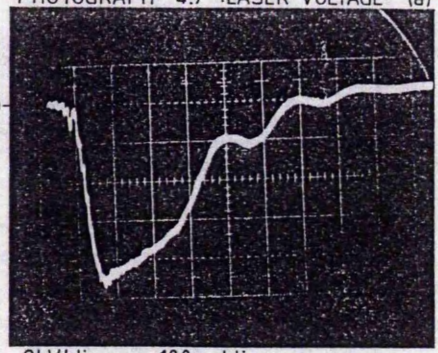

2kV/div 100ns/div

PHOTOGRAPH 4.7 (b)

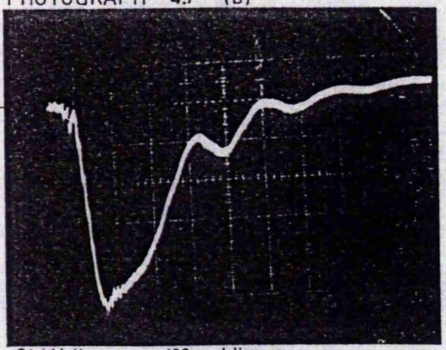

2kV/div 100ns/div

PHOTOGRAPH 4.7 (e)

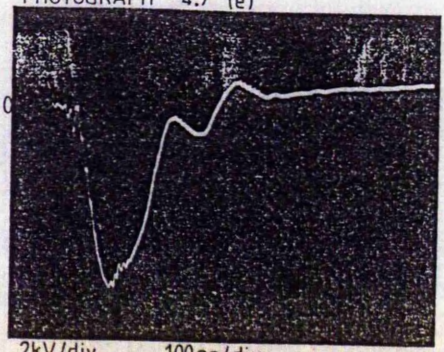

2kV/div 100ns/div

PHOTOGRAPH 4.7 (f)

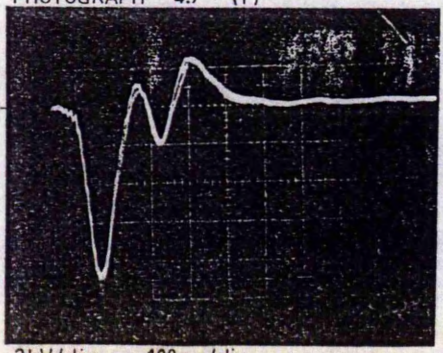

2kV/div 100ns/div

PHOTOGRAPH 4.8 : LASER CURRENT

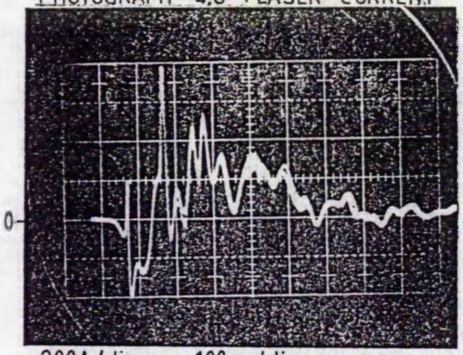

200A / div 100ns / div

PHOTOGRAPH 4.9 : LASER CURRENT

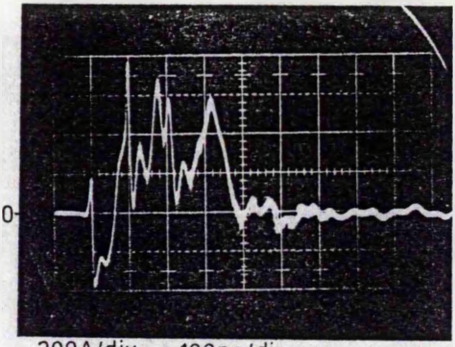

200A/div 100ns/div

PHOTOGRAPH 4.12 : LASER CURRENT

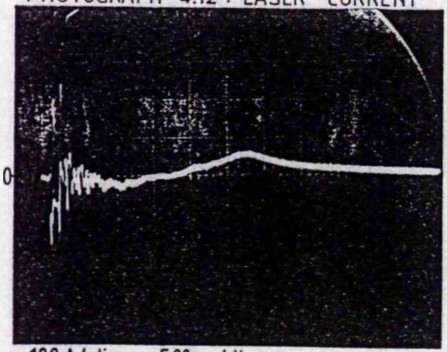

100A/div 500ns/div

PHOTOGRAPH 4.13 : LASER VOLTAGE

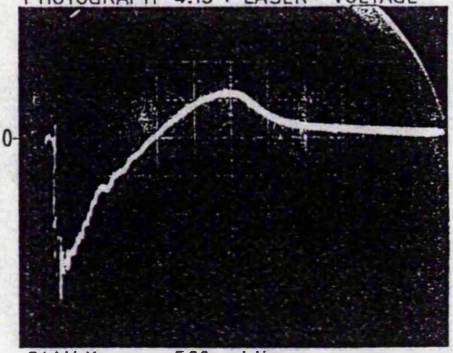

2kV/div 500ns/div

PHOTOGRAPH 4.16 : LASER CURRENT

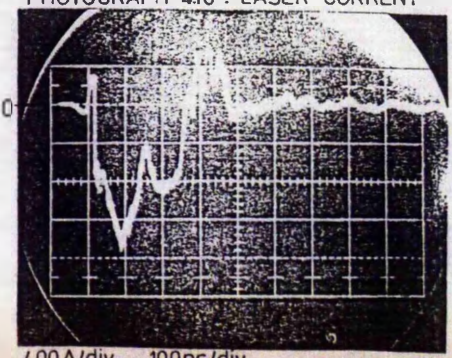

400A/div 100ns/div

PHOTOGRAPH 4.17 : LASER CURRENT

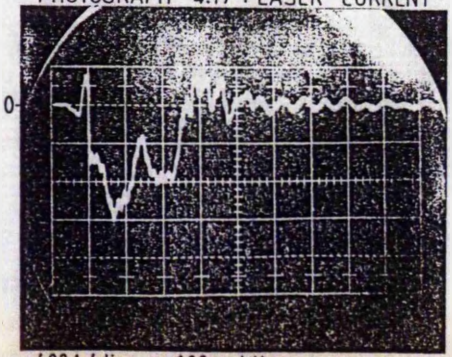

400A/div 100ns/div

PHOTOGRAPH 4.10 : LASER CURRENT

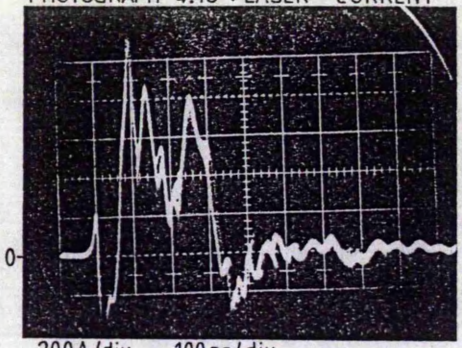

200A/div 100ns/div

PHOTOGRAPH 4.11 : LASER CURRENT

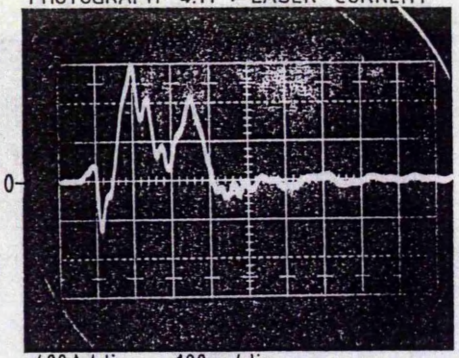

400A/div 100ns/div

PHOTOGRAPH 4.14 : LASER CURRENT

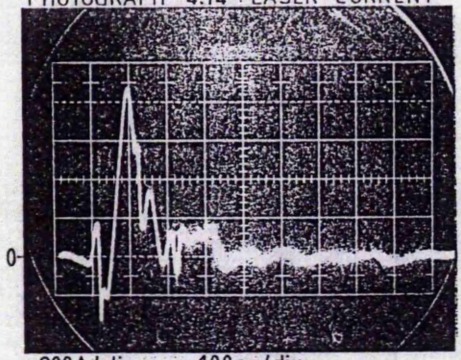

200A/div 100ns/div

PHOTOGRAPH 4.15 : LASER VOLTAGE

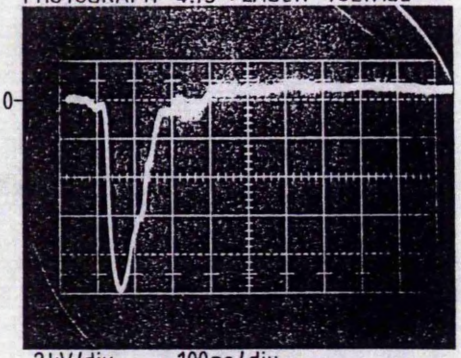

2kV/div 100ns/div

PHOTOGRAPH 4.18 : LASER

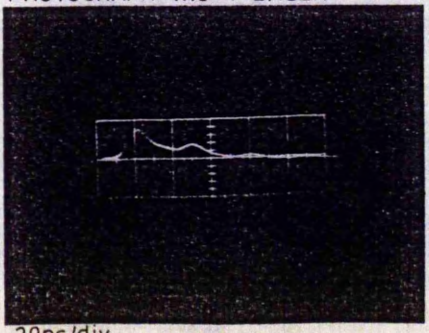

20ns/div

PHOTOGRAPH 4.19 : LASER

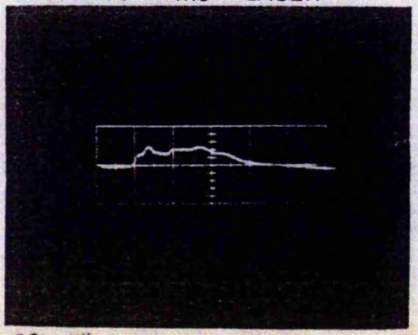

20ns/div

PHOTOGRAPH 4.20 : LASER

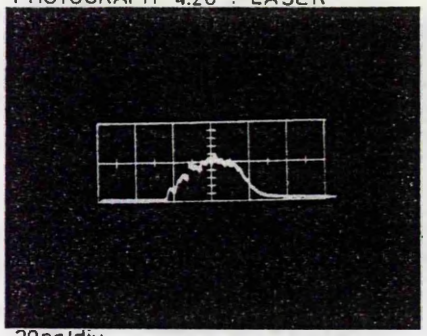

20ns/div

PHOTOGRAPH 4.21 : LASER

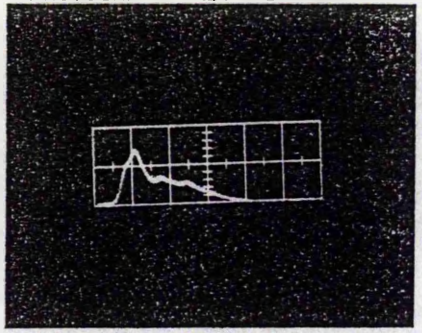

20ns/div

PHOTOGRAPH 4.22 : LASER

20ns/div

PHOTOGRAPH 4.23 : LASER

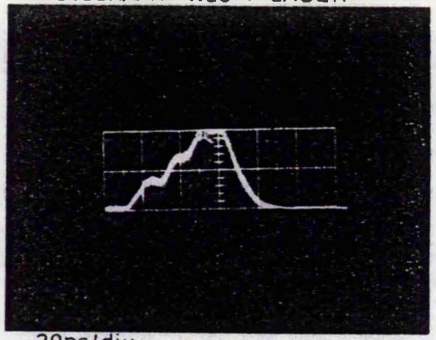

20ns/div

PHOTOGRAPH 4.24 : LASER

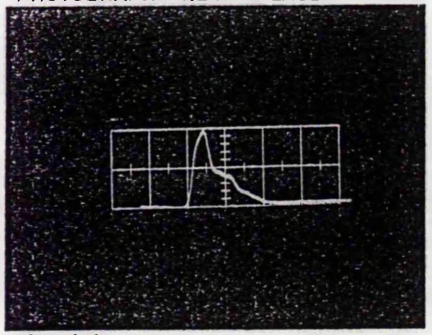

20ns/div

PHOTOGRAPH 4.25 : LASER

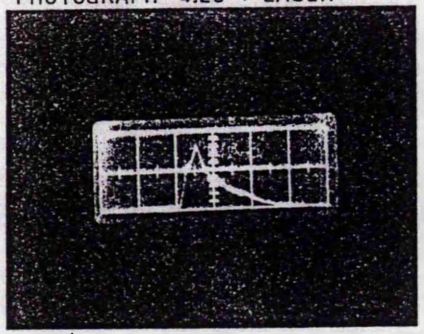

20ns/div

PHOTOGRAPH 4.26 : VOLTAGE

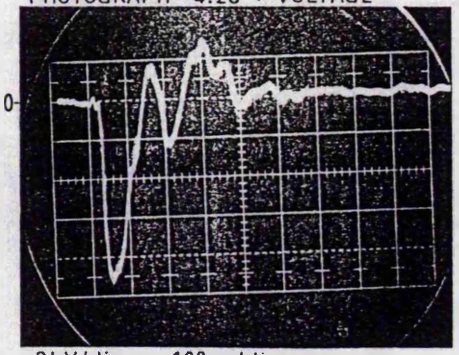

2kV/div 100ns/div

PHOTOGRAPH 4.27 : LASER

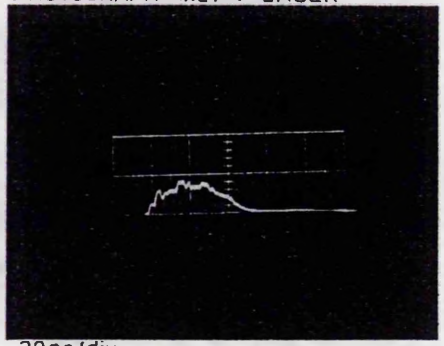

20ns/div

PHOTOGRAPH 4.28 : VOLTAGE

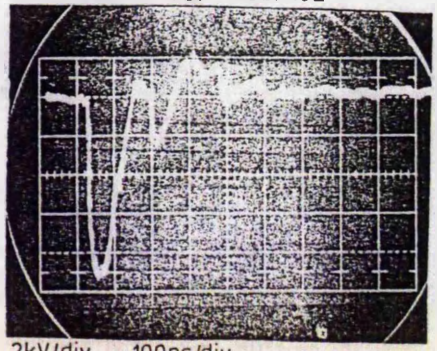

2kV/div 100ns/div

PHOTOGRAPH 4.29 : LASER

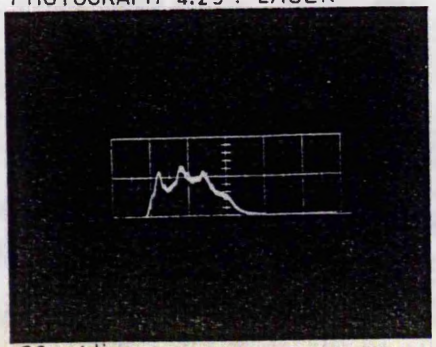

20ns/div

PHOTOGRAPH 4.30 : CURRENT

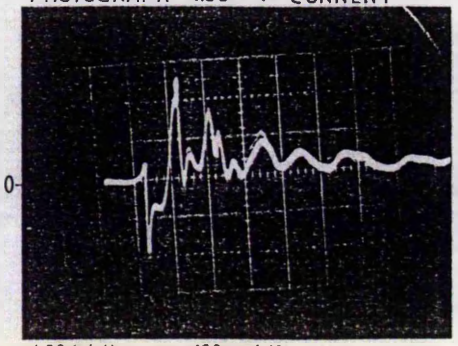

400A/div 100ns/div

PHOTOGRAPH 4.31 : CURRENT

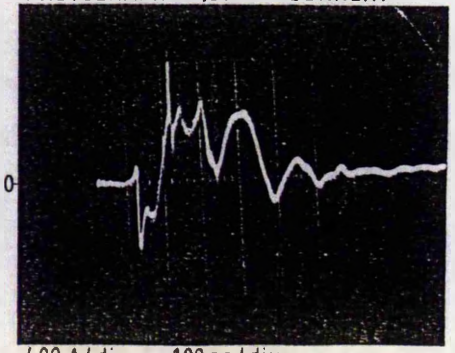

400 A/div 100ns/div

PHOTOGRAPH 4.32 : CURRENT

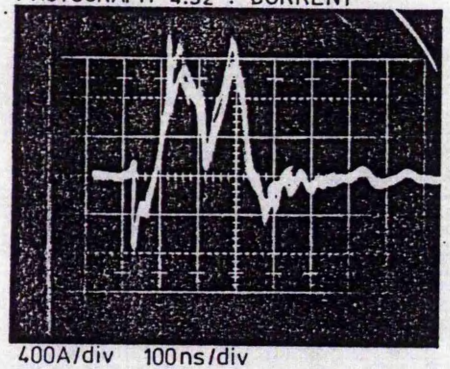

400A/div 100ns/div

PHOTOGRAPH 4.33 : LASER

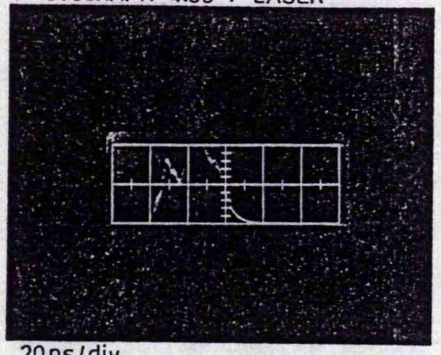

20ns/div

PHOTOGRAPH 4.34 : LASER

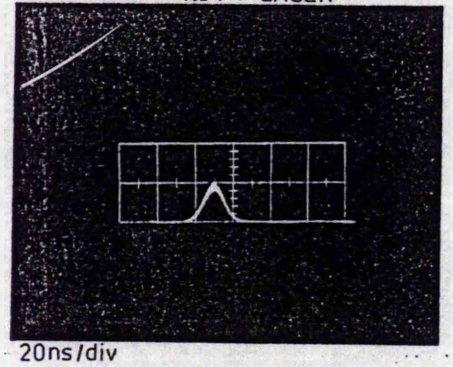

20ns/div

PHOTOGRAPH 4.35 : LASER

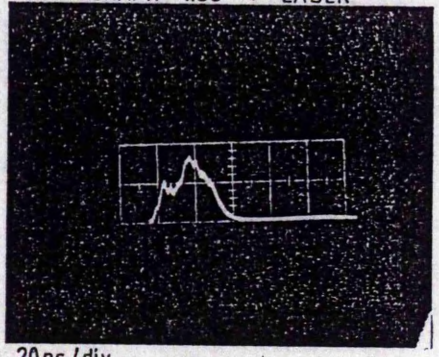

20ns/div

PHOTOGRAPH 4.36 : LASER

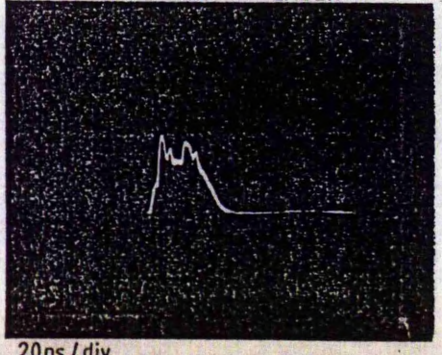

20ns/div

FIGURE 4.1 : VARIATION OF CONTAMINANT CONCENTRATION WITH TIME

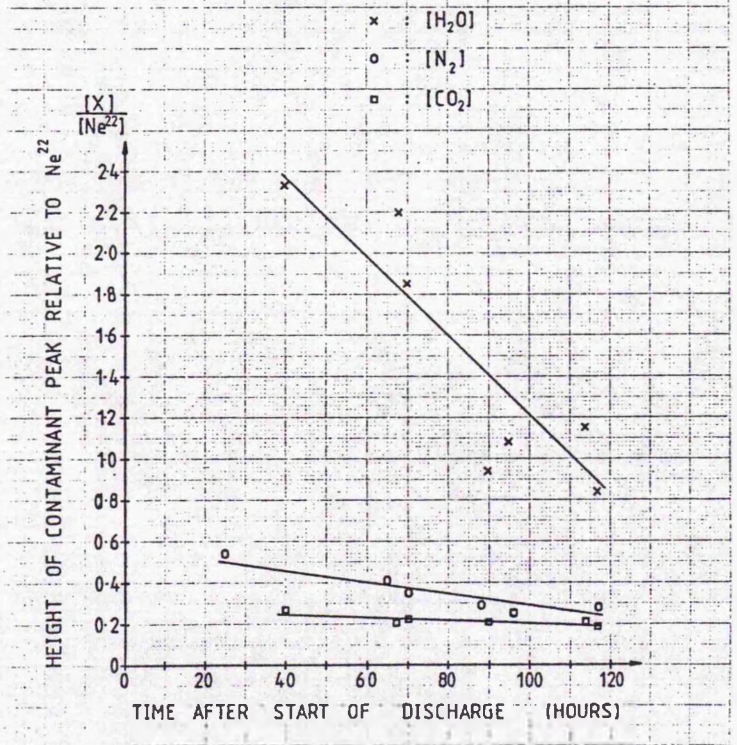

FIGURE 4.2 : SCHEMATIC DIAGRAM OF EXPERIMENTAL ARRANGEMENT USED TO MEASURE LASER PULSE

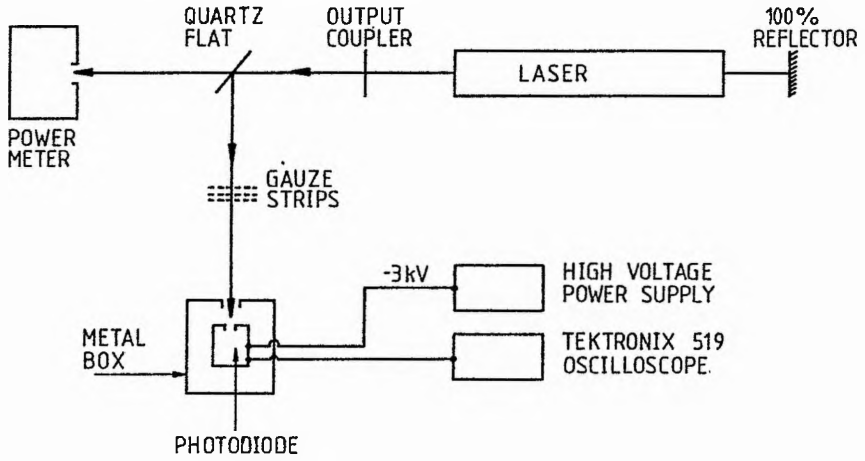

FIGURE 4.3 : WAVELENGTH SENSITIVITY OF PHOTODIODE TF1850M20

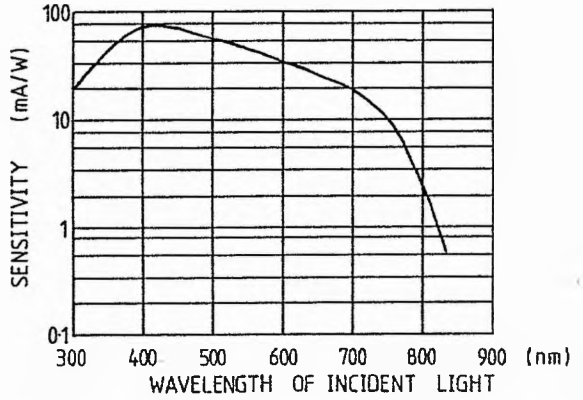

FIGURE 4.4 : VARIATION OF LASER POWER WITH POWER DRAWN FROM SUPPLY ; 12cm LONG SEGMENTS
(a) Mo HEAT SHIELD
(b) Al HEAT SHIELD

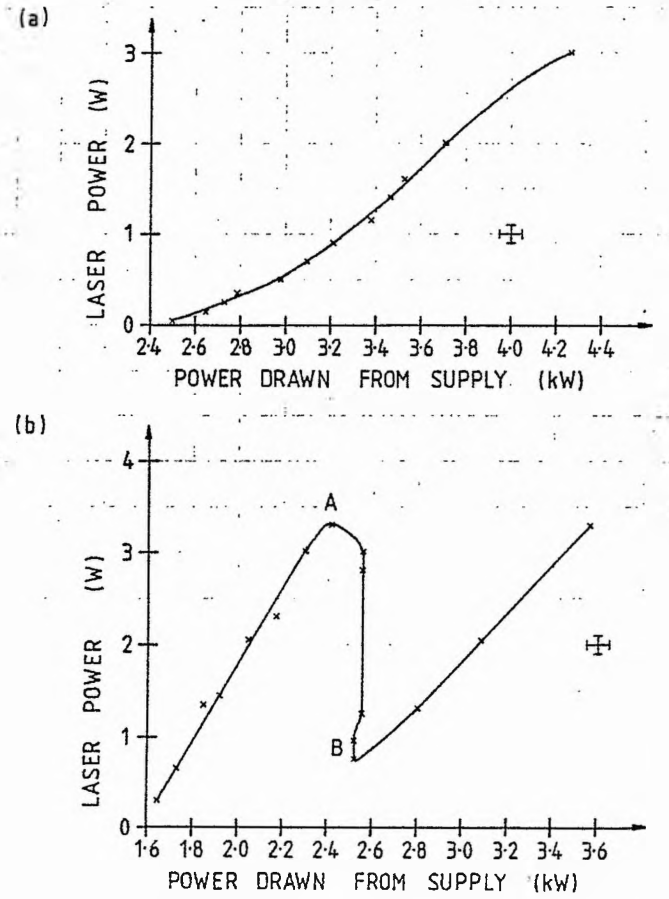

FIGURE 4.5 : VARIATION OF LASER POWER WITH POWER DRAWN FROM THE SUPPLY AT TWO REPETITION RATES ; CERAMIC INSULATION ; Mo HEAT SHIELD

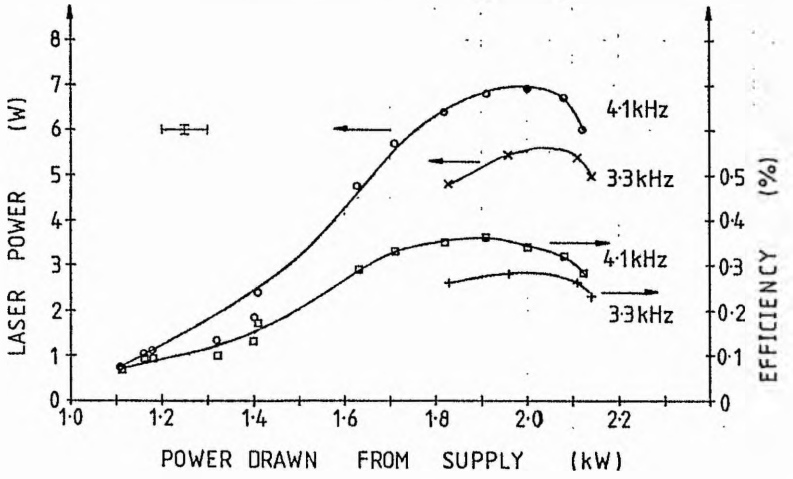

FIGURE 4.6 : DEPENDENCE OF LASER POWER ON NEON PRESSURE ; SUPPLY POWER KEPT CONSTANT

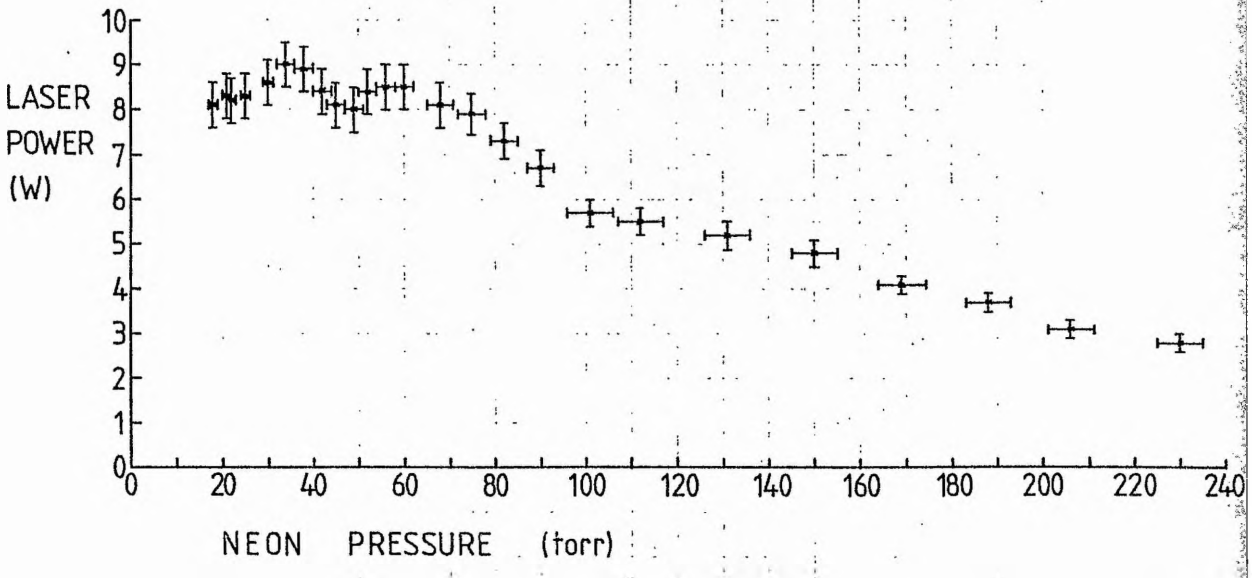

FIGURE 4.7 : DEPENDENCE OF LASER POWER ON NEON PRESSURE ; POWER SUPPLY CURRENT ALLOWED TO VARY WITH PRESSURE

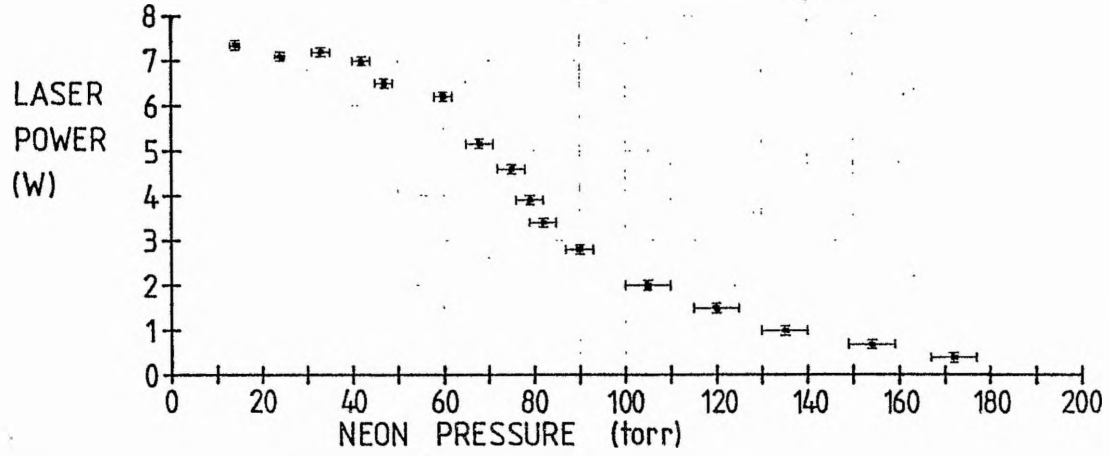

FIGURE 4.8 : DEPENDENCE OF SUPPLY POWER AND C_s VOLTAGE ON NEON PRESSURE

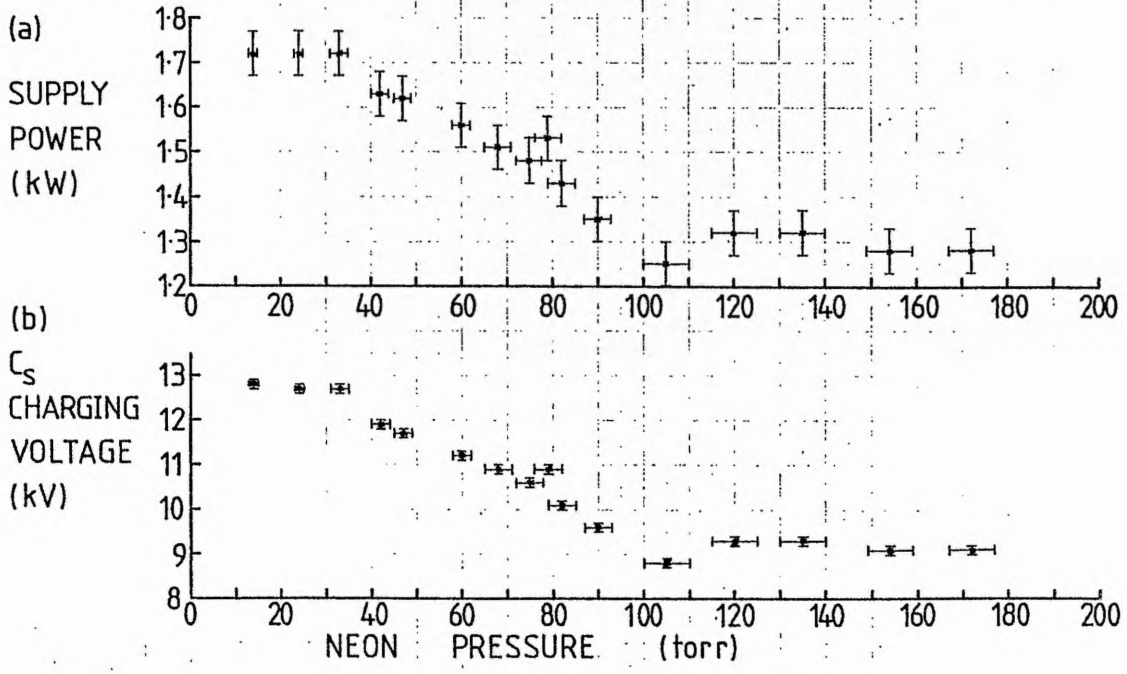

CHAPTER 5

5 THERMAL INSULATION FOR THE CVL

5.1 INTRODUCTION

This chapter analyzes the thermal processes which occur in the CVL. The first section gives the heat transfer equations used in the computer models. The other sections describe the various insulation configurations used in the CVL, their thermal characteristics and the results of the computer programs written to model their behaviour under various conditions.

5.2 THERMAL PROCESSES

The power radiated from a body with surface area A_1 at a temperature T_1 to a body at a temperature T_2 is given by [1]

$$P_{rad} = A_1 F_A F_e \sigma (T_1^4 - T_2^4) \quad , \qquad [5.1]$$

where F_A is the radiation shape factor, F_e is the emissivity factor and σ is Stefan's constant. The total amount of heat radiated from the first surface is not necessarily completely absorbed by the second, unless the second surface completely encloses the first. Also, since the second surface is radiating heat at some temperature, the first surface will absorb some of this. Therefore, the radiation shape factor is used as a measure of the net amount of radiant energy transferred between the two surfaces. Figure (5.1) [2] shows the radiation shape factor for concentric cylinders of finite length. The emissivity factor is used to allow for the effect of the emissivity of

non-black bodies. This factor depends on the configuration and relative positions of the two bodies, as well as being dependent on their emissivities. For the case of infinite cylinders, the emissivity factor is given by [1]

$$F_e = \frac{1}{1/e_1 + A_1/A_2(1/e_2 - 1)} \quad , \qquad [5.2]$$

where e is the emissivity, and A is the area of surfaces 1 and 2.

The power per unit length transported radially by conduction in an infinitely long cylinder is given by

$$P_{rcon} = \frac{2 \pi k (T_1 - T_2)}{\ln(r_2/r_1)} \quad , \qquad [5.3]$$

where k is the thermal conductivity, T is the temperature, r is the radius and the subscripts 1, 2 refer to the inner and outer surfaces respectively.

The power conducted linearly over a distance d between two points at temperatures T_1 and T_2 is given by

$$P_{lcon} = \frac{A k (T_1 - T_2)}{d} \quad , \qquad [5.4]$$

where A is the cross-sectional area of the conductor.

The power transported by convection is given by [3]

$$P_{conv} = A h (T_s - T_g) \quad , \qquad [5.5]$$

where h is the convective heat transfer coefficient, A is the surface

area, T_s is the surface temperature and T_g is the temperature of the surroundings.

5.3 POWER DISSIPATED IN THE DISCHARGE

In order to compare the results of the computer models with experiment, it is necessary to know the amount of power being dissipated per centimetre in the discharge. However, although the power drawn from the supply is known, the proportion dissipated in the laser is not. Also, it is not known whether the power is dissipated uniformly over the length of the discharge. Finally, the exact length of the discharge is not known.

The proportion of the supply power which reaches the discharge is estimated by combining the following factors: the charging circuit is 94% efficient (Section (4.4.1)); the thyratron dissipates approximately 10% of the power which it switches; the rest of the discharge circuit (capacitors, loop resistances, etc) is assumed to dissipate 5% of the power passing through it. Therefore, the total circuit efficiency is estimated to be 80%. The discharge length is assumed to be 100 cm, which is slightly longer than the distance between the electrodes (90 cm), but since the discharge is not necessarily confined between the tips of the electrodes, this is a reasonable approximation. Finally, the power dissipated is assumed to be uniform over the length of the discharge.

5.4 MOLYBDENUM SEGMENTS AS INSULATION

5.4.1 INTRODUCTION

The Mo segments described in Section (2.8.4) were designed to

produce a large temperature gradient between the inner and outer rings by reducing conduction losses to a minimum. Molybdenum has a low emissivity (Fig. (2.21)) so by arranging a number of concentric Mo rings, the segments were designed to be able to maintain temperatures high enough for lasing to occur with the available input power.

In the gap between two concentric Mo rings, heat energy is transferred from the hotter to the colder by a number of processes. Radiation, convection, gaseous conduction and conduction through points of contact (such as the dimples) may all be significant. The full heat transfer equation is given by

$$P_{total} = P_{rad} + P_{rcon} + P_{lcon} + P_{conv} \quad , \qquad [5.6]$$

where the terms on the right hand side are the power transferred by radiation, radial conduction, linear conduction and convection respectively. These terms are given by equs. [5.1] to [5.5]. Heat is conducted radially both by the buffer gas and through the dimples. Equation [5.3] is used for gaseous conduction and equ. [5.4] is used for conduction through the dimples and other points of contact.

By substituting sample values into equ. [5.6], an estimate of the relative importance of the four heat transfer processes was obtained. Taking two concentric Mo rings, each 3 cm long, with diameters of 40 mm and 42 mm and at temperatures of 1300 K and 1200 K respectively, the heat transferred by each process is given in Table (5.1). Table (5.2) shows the values of the other variables used in the calculations. It was assumed that the only contact between the Mo rings was at the eight dimples, each of which has a cross-sectional area of 1 mm^2. From this estimate, it was assumed for the purpose of the computer model that convection losses are negligible. However, radiation, gaseous conduction and conduction through points of contact

were all taken into account.

Figure (5.1) shows that, taking an average over the values of R_1 and R_2 for the different radii of the Mo rings, the radiation shape factor for an isolated 3 cm long segment is 0.92 and for an isolated 12 cm segment it is 0.96.

5.4.2 COMPUTER MODEL

A computer model was written to estimate the temperatures achievable for various input powers. The program is listed in Appendix (D). There are two versions of the program. One models a segment made solely of Mo rings, and the other models the effect of using flame-sprayed Mo rings. The gaps between the segments are neglected by assuming that the segments are isolated.

The temperature of the radiation shield is fixed at 400 K. The effects of the quartz and pyrex are neglected. The temperature of the outer Mo ring is calculated using equ. [5.1] by assuming that radiation is the only heat loss process across the vacuum gap. The temperature of each ring is then calculated in turn using equs. [5.1] to [5.4]. The variation of the emissivity of Mo with temperature (Fig. (2.21)) is taken into account. An approximate initial value of the emissivity is used to calculate the ring temperature. The emissivity of Mo at that temperature is then calculated using the values given in Fig. (2.21). If the assumed and calculated emissivities differ by more than a set amount, the assumed emissivity is adjusted and the temperature recalculated. When agreement is reached, the program moves on to the next ring. The values of the Ne and Mo thermal conductivity used in the model are shown in Table (5.2).

In order to adapt the metal segment heat transfer program to the

case of segments which have been flame-sprayed with zirconia, the emissivity of the outer surface of each ring is changed to 0.5 [4] and the conductivity of the zirconia is taken to be 2 $Wm^{-1}K^{-1}$ [5]. In fact, the true thermal conductivity of the sprayed zirconia layer is unknown, being dependent on the density of the layer, which in turn depends on the spraying technique used [6]. The thickness of the flame-sprayed surface is 0.12 mm. Assuming that all the power transferred by conduction goes through the dimples, equ. [5.4] is rewritten to take account of the altered thermal conductivity, and so becomes

$$P_{1con} = A\,(T_1-T_2) \,/\, ((d_1/k_1) + (d_2/k_2)) \quad , \qquad [5.7]$$

where d_1 is the height of the Mo dimple, d_2 is the thickness of the zirconia coating and k_1 and k_2 are their respective thermal conductivities.

5.4.3 COMPUTER MODEL RESULTS

Figures (5.2) and (5.3) show the temperatures predicted by the model for isolated 3 cm and 12 cm wide segments which have not been flame-sprayed. In each case, as the emissivity of the heat shield is reduced, both the inner and outer wall temperatures rise, as expected. The temperature gradient across the segment falls with decreasing emissivity of the heat shield because of the rise in the emissivity of Mo with temperature. In Figs. (5.4) and (5.5), the same graphs are plotted, but with the ten innermost Mo rings flame-sprayed on their outer surface. This significantly reduces the power required to reach a given temperature by reducing conduction losses through points of contact between adjacent rings.

Figures (5.6) to (5.9) show the effect of contact between concentric rings and the effect of the different heat transfer processes for both flame-sprayed and non-flame-sprayed segments. Comparing Figs. (5.6) and (5.8), it can be seen that flame-sprayed rings reduce the heat loss through points of contact. The "no contact" temperatures in Fig. (5.8) are smaller than in Fig. (5.6) because of the higher emissivity of the zirconia layer compared with Mo. Heat loss by gaseous conduction has been included in Figs. (5.6) and (5.8). Gaseous conduction is a major heat loss process, as can be seen in Figs. (5.7) and (5.9). In the flame-sprayed segment, more heat is lost through gaseous conduction than by conduction through the dimples. The effect of using the segments in a vacuum, with no contact between concentric rings, is shown in the "radiation only" curves.

5.4.4 EXPERIMENTAL RESULTS

The initial insulation configuration consisted of ten flame-sprayed Mo rings held inside the alumina ring, with four non-sprayed rings outside. The segments were 3 cm long. There was no radiation shield in the vacuum gap. The inner wall temperature did not become high enough for laser action even with 3.9 kW drawn from the power supply, but the Cu did melt in some of the segments, showing that in some parts of the tube, the temperature had risen above $1083^{\circ}C$.

A 2.5 mm thick piece of zirconia felt was placed inside the innermost ring of each segment with another flame-sprayed Mo ring placed inside the felt. Lasing started when the circuit was drawing 3.9 kW from the power supply. The insulation was then changed to that shown in Fig. (2.22), with more felt and fewer Mo rings. The supply

power required for lasing to start in this case was 3.3 kW.

The segments were then rearranged in groups of four to form 12 cm long segments and a Mo heat shield was placed in the vacuum gap. The power required for lasing to start dropped significantly, with 1 W of laser power when 2.36 kW was drawn from the supply. When the supply power was increased to 2.86 kW, 8.4 W of laser power was produced. The laser was then disassembled and the segments inspected. The distribution of Cu on the innermost surface of each segment was as shown in Fig. (5.10). The distribution of Cu can be related to the local wall temperature when the discharge was running. Every piece of Cu had melted, but the Cu in segments 5 to 13, where the temperature was the highest, had flowed through the gaps in the segments and been absorbed by the zirconia felt. The highest temperatures were not in the centre because of the gap in the heat shield at the cathode end which allowed heat to escape. At the anode end, the heat shield extended to the anode flange. Temperatures were therefore higher on the anode side of the mid-point of the discharge.

The Mo heat shield was then replaced by an aluminium one. This resulted in a further improvement in the efficiency of the thermal insulation, so that 1.3 W of laser power was produced when 1.85 kW was drawn from the power supply.

Figure (5.11) shows the pattern of heating when 27 cm long segments were used. When the laser was disassembled, the Cu had melted in some segments, but in others, the Cu and Mo still had an oxide layer. Since molybdenum oxide evaporates at temperatures above 760^{o}C (Section (2.8.2)), there must have been a large axial temperature gradient at the anode end. When the discharge was running, the highest temperatures were in segments 11 to 17 and must have been greater than 1083^{o}C. The lower temperatures in segments 10 to 18 were due to the proximity of the gaps produced by the alumina

rings. The wall temperature was high enough to remove the oxide layer from both the Cu and Mo in segments 6 to 9 and 19 to 23, but not in the segments nearest the anode electrode. The low temperatures produced in segments 1 to 9 were probably because some of the discharge current conducted through the metal walls.

5.4.5 COMPARISON OF RESULTS

The computer model differs from the experimental reality by not taking the gaps between the segments into account. In the case of the discharge confined by 3 cm long segments, these gaps allow nearly 20% of the power dissipated in the discharge to radiate and conduct directly to the much cooler regions on the outside of the segments. Therefore, close agreement between the computer model and the experimental results is not expected.

When insulation consisting of 3 cm long, flame-sprayed Mo segments with no heat shield (modelled in Fig. (5.4(a))) was used, lasing temperatures were not achieved with up to 3.9 kW drawn from the supply. Using the assumptions given in Section (5.3), the power dissipated per unit length was 31.2 W/cm. According to the model, this should produce an inner wall temperature of 1840 K (Fig. (5.4(a))). In fact, it only melted the Cu, so while the temperature was at least 1083^{o}C, it was probably not much more than this.

5.5 CERAMIC INSULATION

5.5.1 INTRODUCTION

The ceramic insulation consisted of a recrystallised alumina tube

with zirconia felt wrapped round it. The alumina tube had an ID of 2.0 cm and an OD of 2.8 cm. The zirconia felt was in the form of sheets with dimensions 18"x24"x2.5 mm. Two of these sheets were required to fill the quartz tube. A Mo heat shield was inserted into the vacuum gap over a length of 85 cm from the anode flange end.

5.5.2 COMPUTER MODEL

A computer program was written to model the radial temperature gradient produced when the ceramic insulation described above was used. The program is listed in Appendix (D). The heat transfer processes included are radial conduction through the alumina and zirconia felt and radiation from the felt to the heat shield. Axial conduction and radiation to the end flanges are assumed to be negligible. The temperature of the heat shield is taken to be 400 K. Starting at this fixed temperature, the temperature of the outer surface of the zirconia felt is calculated for a given input power. The radiation shape factor is estimated to be 0.74 from Fig. (5.1). The emissivity of the zirconia felt is assumed to be 0.5 [4]. The program then moves through the zirconia to the alumina tube in 0.5 mm steps, calculating the temperature at each step using the thermal conductivity given in Fig. (2.20). Finally, the temperature on the inside of the alumina tube is calculated. The thermal conductivity of the alumina is taken to be 5.6 $Wm^{-1}K^{-1}$ [5].

5.5.3 COMPUTER MODEL RESULTS

Figure (5.12) shows the results of the model for different heat shield materials. In Fig. (5.12(a)), there is no heat shield, so the emissivity is assumed to be equal to that of the pyrex tube, which is

0.8 [7]. In Fig. (5.12(b)), the heat shield is Mo, with an emissivity of 0.05 [8]. In each graph, the temperatures shown are those of the inner wall of the alumina tube and the quartz tube, which is assumed to be equal to that of the outer surface of the zirconia.

When the emissivity of the heat shield is reduced, both the quartz and the alumina temperatures increase for a given input power. However, the temperature drop across the zirconia felt decreases because the thermal conductivity of the zirconia rises with temperature (Fig. (2.20)).

5.5.4 EXPERIMENTAL RESULTS

The ceramic insulation was more efficient than any of the configurations using Mo segments. With a Mo heat shield, only 1.1 kW from the power supply was required for lasing to start, and the optimum temperature of 1550°C was reached with 1.94 kW drawn from the supply (Fig. (4.5)). The highest temperature measured before lasing started was 1330°C. A 76% increase in the supply power was therefore required to raise the tube temperature by approximately 200°C.

5.5.5 COMPARISON OF RESULTS

In order to produce the optimum temperature, the model predicts that an input power of 11.3 W/cm (Fig. (5.12(b))) is needed. Using the assumptions of circuit efficiency and discharge length given in Section (5.3), this is equivalent to a total supply power of 1.41 kW. The actual power required was 1.94 kW. The wall temperature was measured at supply powers of 950 W and 750 W to be 1330°C and 1100°C respectively. The model predicts that the powers required to produce these temperatures are 990 W and 650 W respectively. Assuming that

the temperature measurements are accurate, the disagreement between theory and experiment has two main sources: the estimate of losses in the discharge circuit and the assumption that axial heat processes can be neglected. Before Cu vapour is produced, the load is not matched to the discharge circuit. This reduces the effective circuit efficiency used above by an amount which depends on the matching. At higher temperatures, axial and radial radiation losses become so important that it is no longer valid to neglect them. The variation of thermal conductivity with temperature for zirconia (Fig. (2.20)) shows an increase at higher temperatures. This is because, as the temperature rises, radiation losses through the felt's fibres increase so that more and more radiation is being lost from the interior of the felt directly to the heat shield. The effective radiation shape factor will therefore be smaller than the value used. Finally, the addition of Cu vapour to the discharge may increase its axial thermal conductivity.

5.6 CONCLUSION

The comparisons of results in Sections (5.4.5) and (5.5.5) show that the computer models describe the various forms of insulation with varying success. In the case of the Mo segments, this is partly because of the large variation in contact area which exists in reality between concentric rings. If adjacent rings were isolated, they would each have a different temperature gradient. While this effect is probably smoothed out in the discharge tube, the inner temperature of adjacent segments will still be slightly different. Another source of error in the description of the segments is the neglect of the effect which the gaps have. However, an equally serious error, which only shows up in the case of the ceramic insulation, is the neglect of

axial heat loss processes. This only seems to become important at lasing temperatures, but this is exactly where the model should be most accurate. In order to model the temperature gradients with greater accuracy, it will be necessary to include the axial processes, as well as improve the estimates of the actual proportion of the supply power which is dissipated in the discharge.

REFERENCES FOR CHAPTER 5

1 : Hsu S.T., ENGINEERING HEAT TRANSFER : D. Van Nostrand (1963)

2 : Chapman A.J., HEAT TRANSFER (3rd Edition) : Macmillan (1974)

3 : Alger T.W., Benett W.J., REV. SCI. INSTRUM. 53, 762 (1982)

4 : Espe W., MATERIALS OF HIGH VACUUM TECHNOLOGY
VOL. 2, p569, Pergamon Press (1968)

5 : Kingery W.D., Francl J., Coble R.L., Vasilos T.
J. AMER. CERAMIC SOC. 37, 107 (1954)

6 : Witts L., Eutectic Co., Private communication (1987)

7 : Goldsmith A., Waterman T.E., Hirschhorn H.J.
HANDBOOK OF THERMOPHYSICAL PROPERTIES OF SOLID MATERIALS
VOLUME III - CERAMICS, p201, Pergamon Press (1961)

8 : Goldsmith A., Waterman T.E., Hirschhorn H.J.
HANDBOOK OF THERMOPHYSICAL PROPERTIES OF SOLID MATERIALS
VOLUME I - ELEMENTS, pI-423, Pergamon Press (1961)

TABLE 5.1

THERMAL PROCESS	HEAT LOST (W)
P_{rad}	30
P_{rcon}	31
P_{lcon}	67
P_{conv}	1

TABLE 5.2

VARIABLE	VALUE	
T_g	1250 K	
c_1	0.3	
c_2	0.3	
h	5 $Wm^{-2}K^{-1}$	(Ref. 3)
k_g	0.08 $Wm^{-1}K^{-1}$	(Ref. 3)
k_{Mo}	84 $Wm^{-1}K^{-1}$	

FIGURE 5.1 : THE RADIATION SHAPE FACTOR FOR TWO CYLINDERS OF FINITE LENGTH

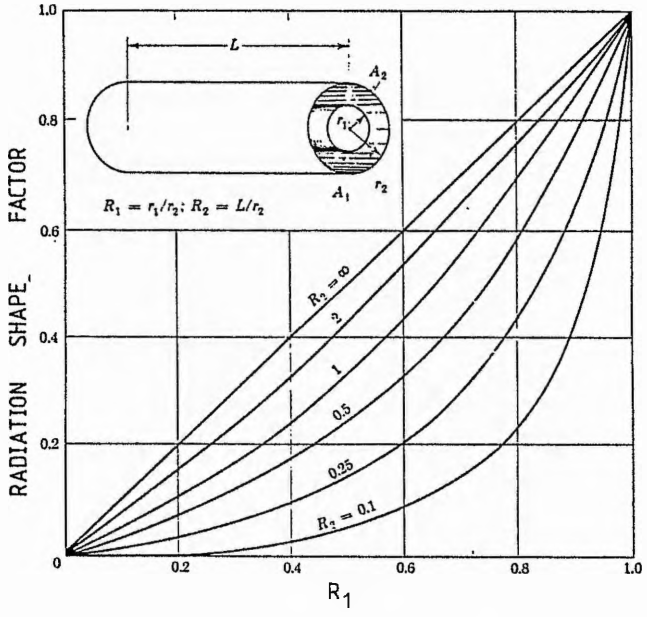

FIGURE 5.2 : CVL TEMPERATURES FOR VARIOUS INPUT POWERS, INSULATION CONSISTS OF 14 Mo RINGS IN A 3cm WIDE, 3cm ID SEGMENT GASEOUS CONDUCTION INCLUDED, 8mm^2 CONTACT BETWEEN RINGS (a) NO HEAT SHIELD (e=0.8)

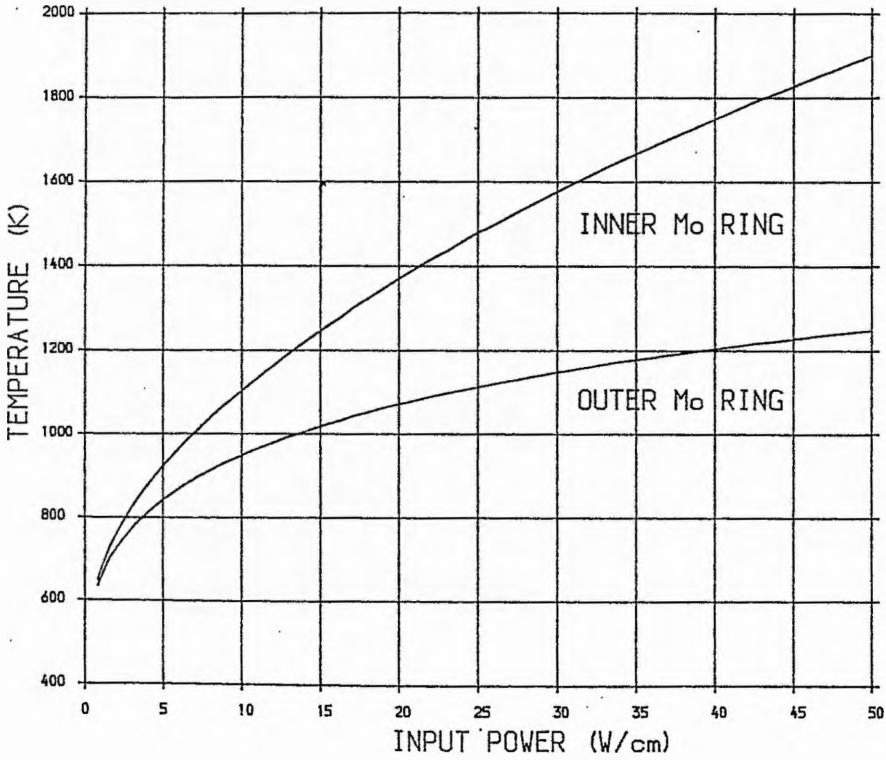

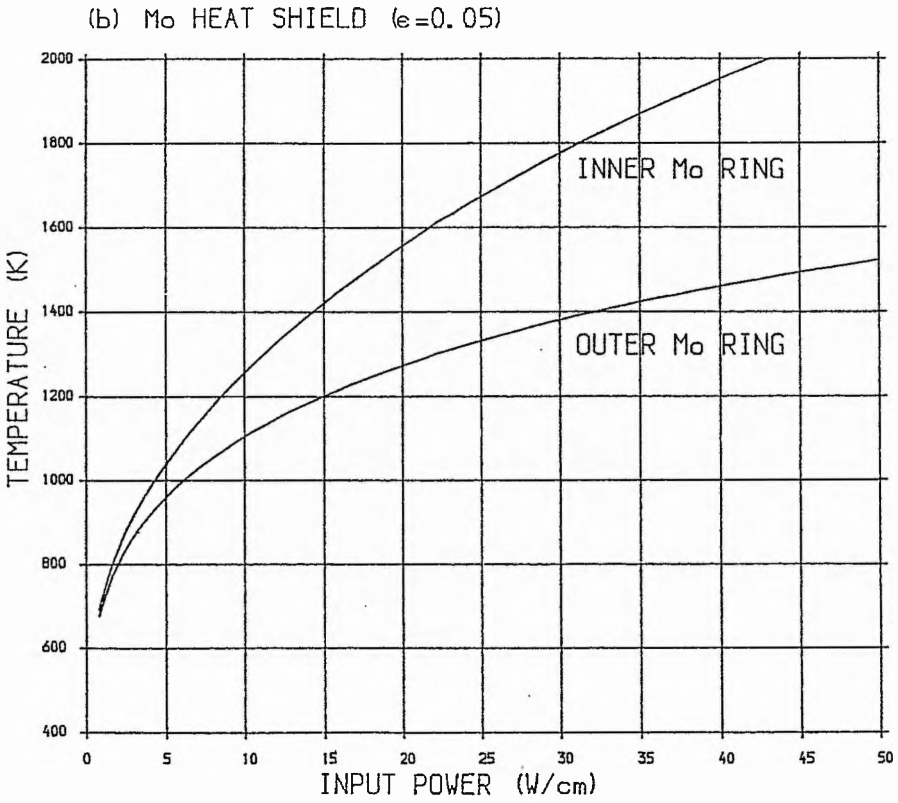
(b) Mo HEAT SHIELD (e=0.05)
INNER Mo RING
OUTER Mo RING
TEMPERATURE (K)
INPUT POWER (W/cm)
2000
1800
1600
1400
1200
1000
800
600
400
0
5
10
15
20
25
30
35
40
45
50

FIGURE 5.3 : CVL TEMPERATURES FOR VARIOUS INPUT POWERS, INSULATION CONSISTS OF 14 Mo RINGS IN A 12cm WIDE, 3cm ID SEGMENT GASEOUS CONDUCTION INCLUDED, 8mm^2 CONTACT BETWEEN RINGS

(a) NO HEAT SHIELD (ϵ=0.8)

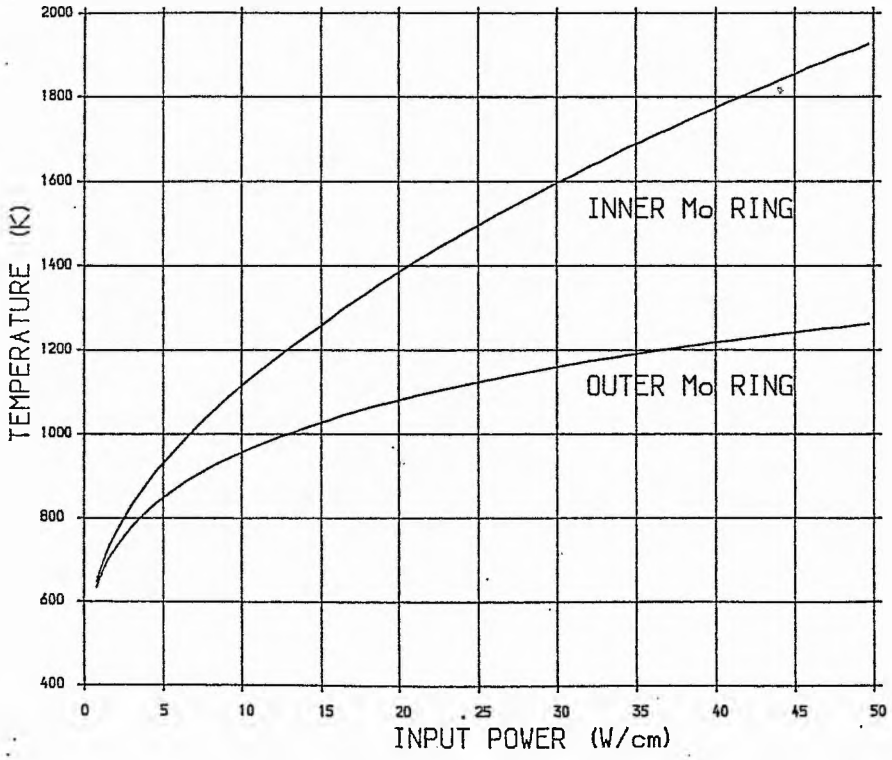

(b) Mo HEAT SHIELD (ϵ=0.05)

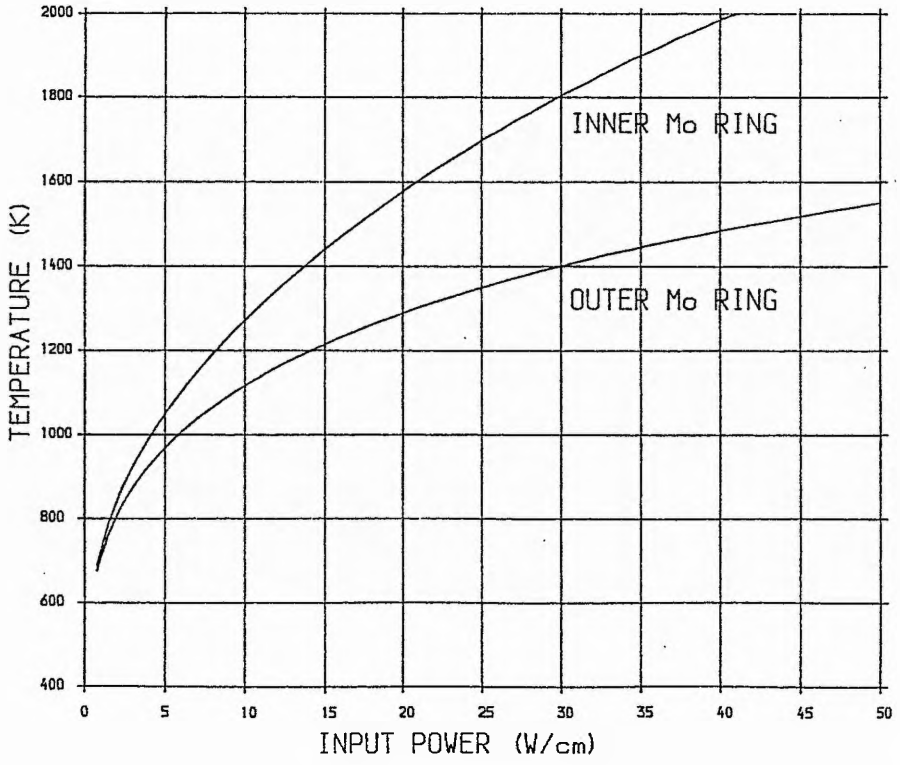

FIGURE 5.4 : CVL TEMPERATURES FOR VARIOUS INPUT POWERS; INSULATION CONSISTS OF 4 Mo RINGS AROUND 10 FLAME SPRAYED Mo RINGS IN A 3cm WIDE, 3cm ID SEGMENT, GASEOUS CONDUCTION 8mm^2 CONTACT BETWEEN RINGS. (a) NO HEAT SHIELD (e=0.8)

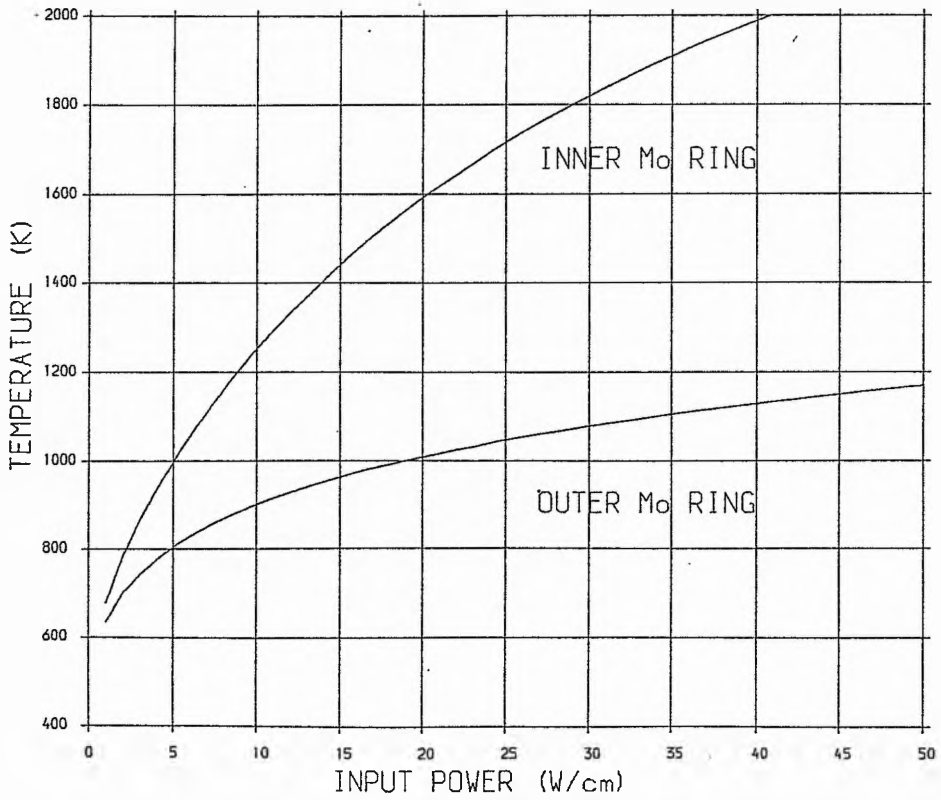

(b) Mo HEAT SHIELD (e=0.05)

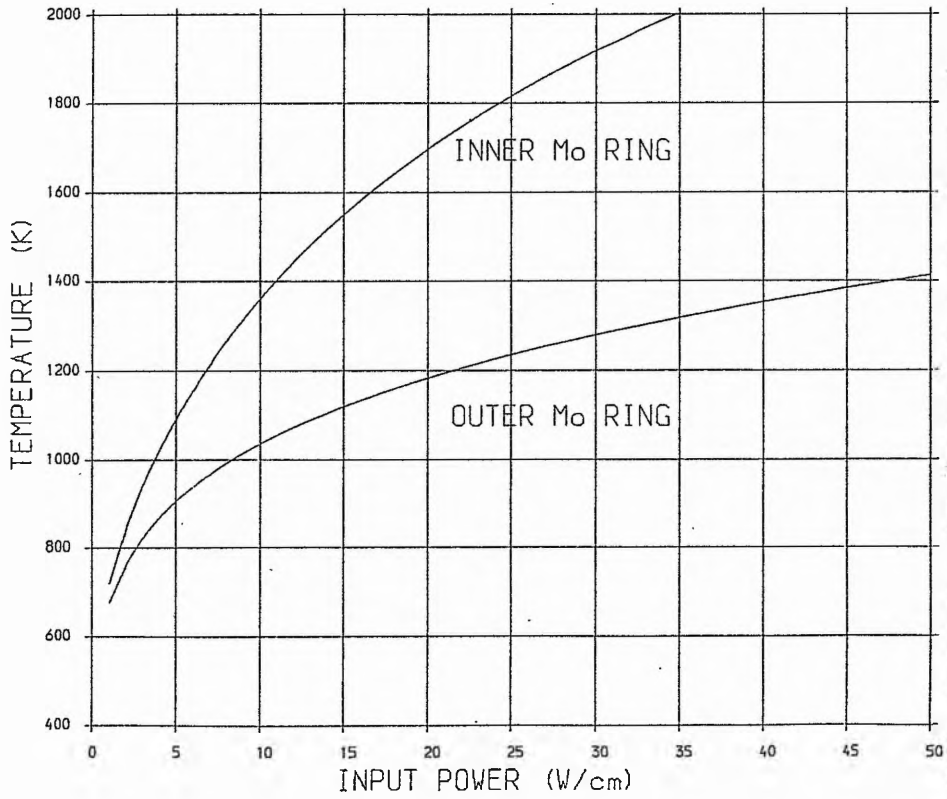

FIGURE 5.5 : CVL TEMPERATURES FOR VARIOUS INPUT POWERS, INSULATION CONSISTS OF 4 Mo RINGS AROUND 10 FLAME SPRAYED Mo RINGS IN A 12cm WIDE, 3cm ID SEGMENT; GASEOUS CONDUCTION; 8mm^2 CONTACT BETWEEN RINGS. (a) NO HEAT SHIELD (ϵ=0.8)

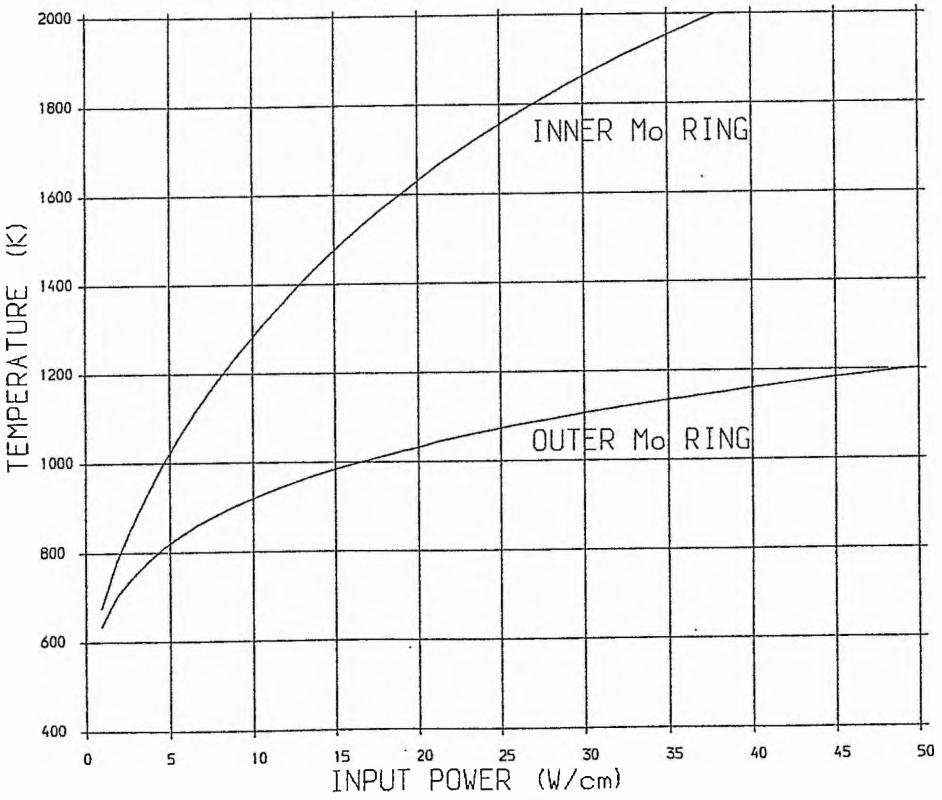

(b) Mo HEAT SHIELD (ϵ=0.05)

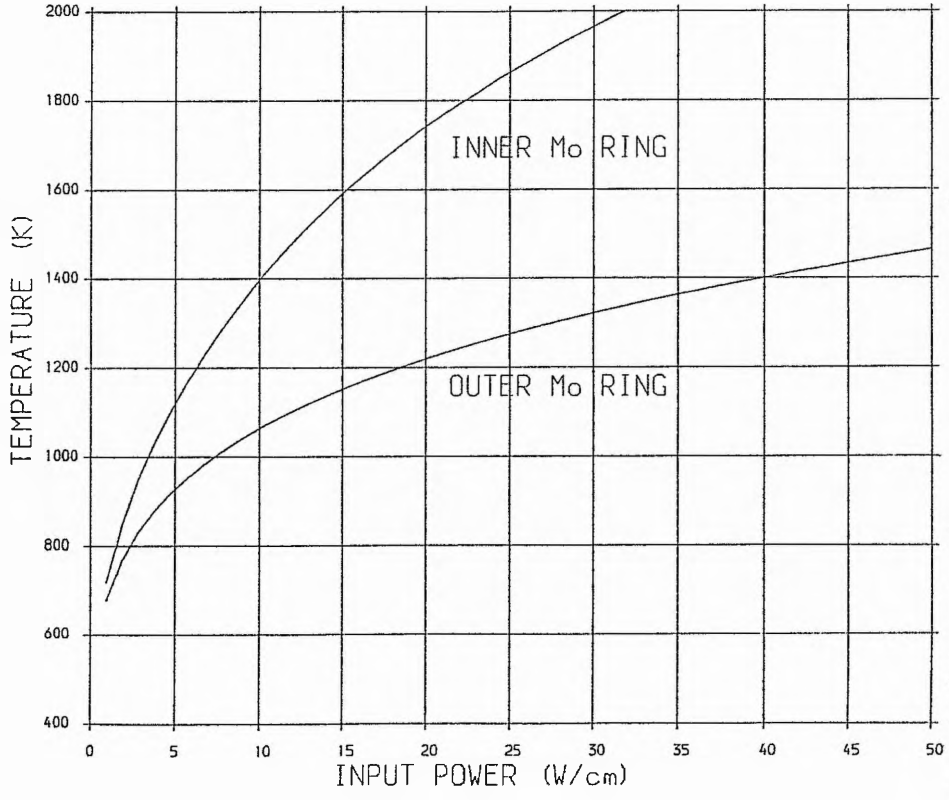

FIGURE 5.6 : CVL INNER WALL TEMPERATURES SHOWING THE EFFECT OF CONTACT BETWEEN CONCENTRIC RINGS, INSULATION CONSISTS OF 14 Mo RINGS IN A 3cm WIDE, 3cm ID SEGMENT Mo HEAT SHIELD (ϵ=0.05)

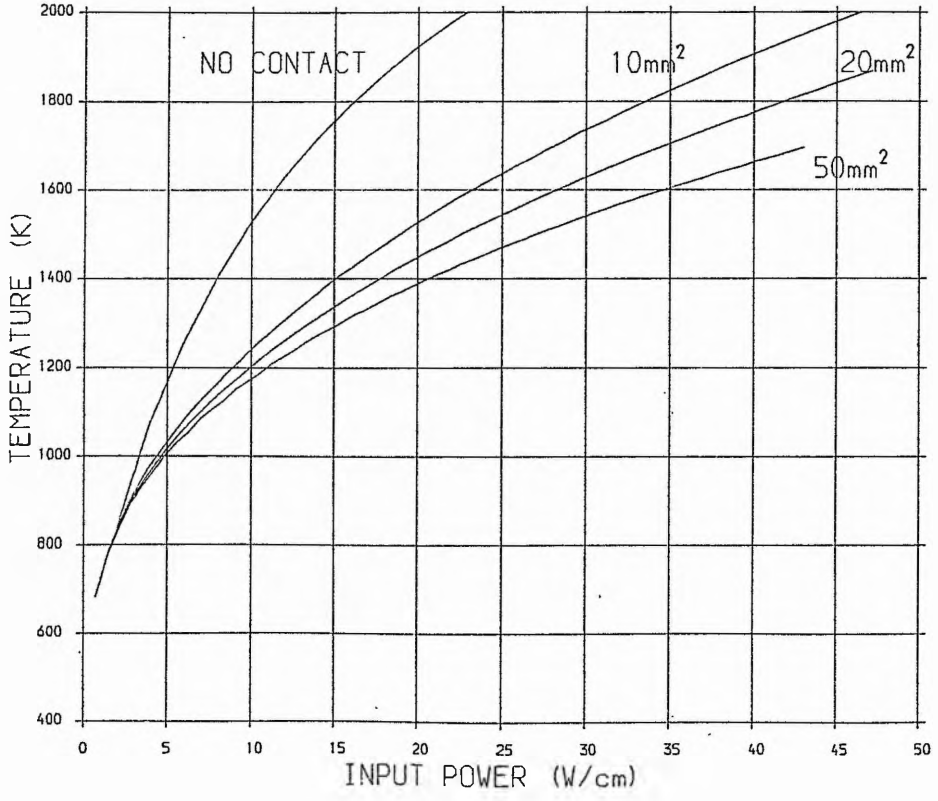

FIGURE 5.7 : CVL INNER WALL TEMPERATURES SHOWING THE EFFECT OF THE VARIOUS HEAT TRANSFER PROCESSES, INSULATION CONSISTS OF 14 Mo RINGS IN A 3cm WIDE, 3cm ID SEGMENT, Mo HEAT SHIELD (ϵ=0.05)

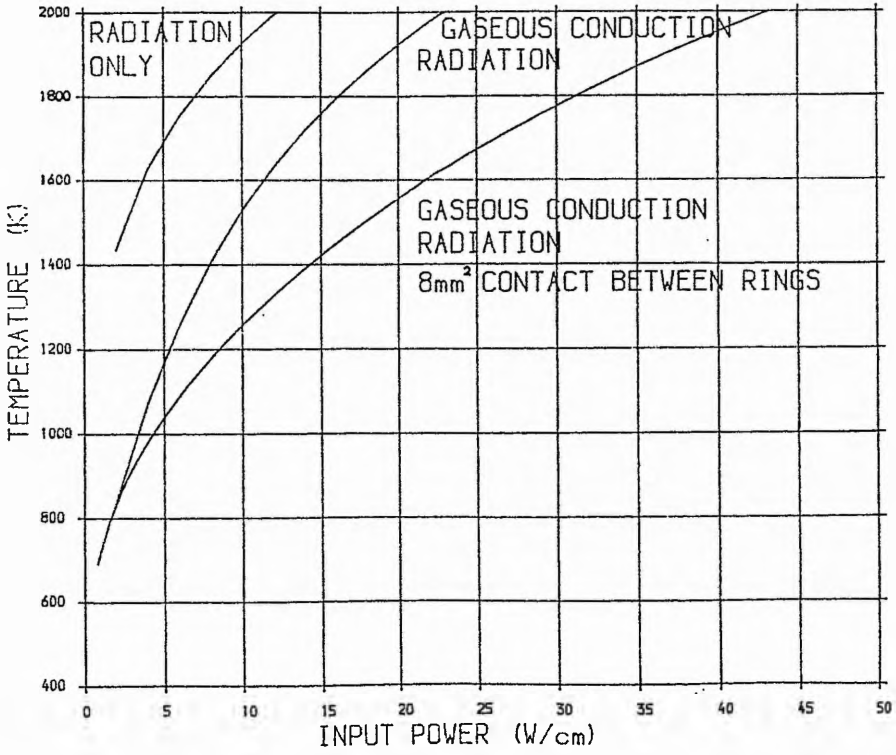

FIGURE 5.8 : CVL INNER WALL TEMPERATURES SHOWING THE EFFECT OF CONTACT BETWEEN CONCENTRIC RINGS; INSULATION CONSISTS OF 4 Mo RINGS AROUND 10 FLAME SPRAYED Mo RINGS IN A 3cm WIDE, 3cm ID SEGMENT; Mo HEAT SHIELD (e=0.05)

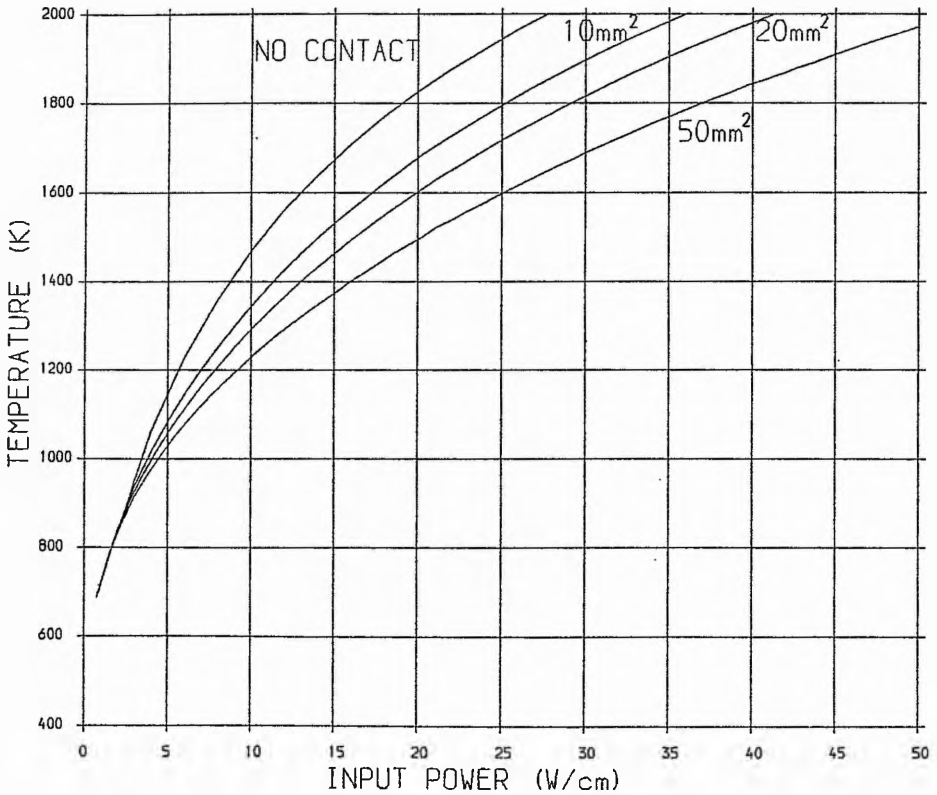

FIGURE 5.9 : CVL INNER WALL TEMPERATURES SHOWING THE EFFECT OF VARIOUS HEAT TRANSFER PROCESSES; INSULATION CONSISTS OF 4 Mo RINGS AROUND 10 FLAME SPRAYED Mo RINGS IN A 3cm WIDE, 3cm ID SEGMENT; Mo HEAT SHIELD (e=0.05)

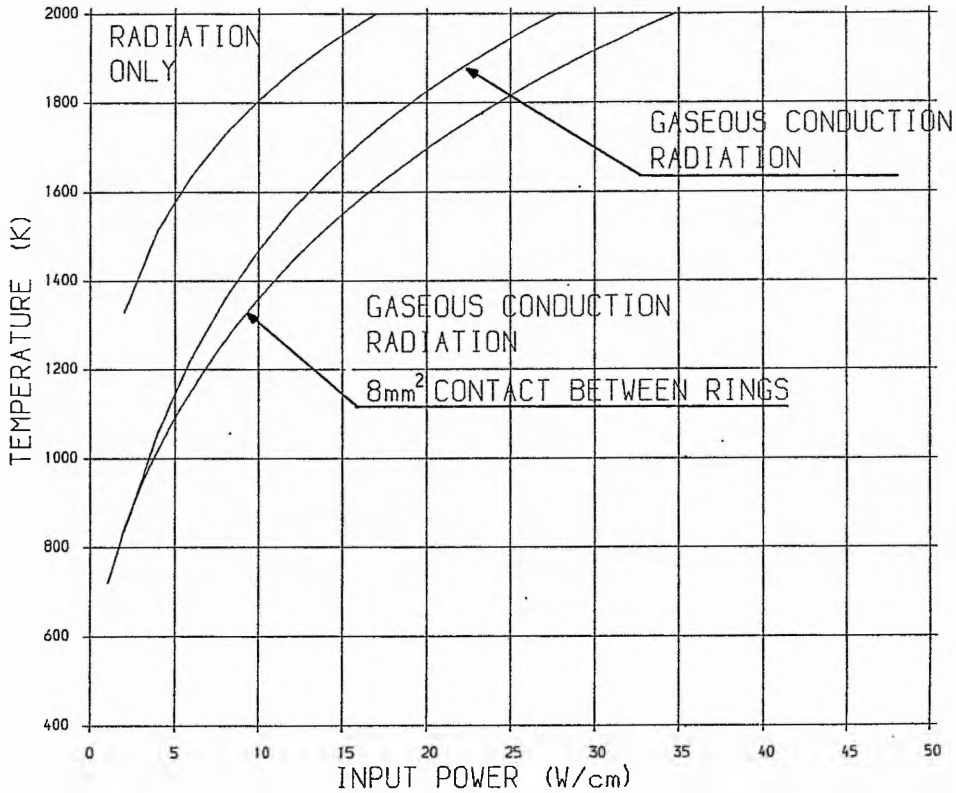

FIGURE 5.10 : SCHEMATIC DIAGRAM SHOWING THE DISTRIBUTION OF COPPER REMAINING INSIDE THE SEGMENTS AFTER 70 MINUTES LASING

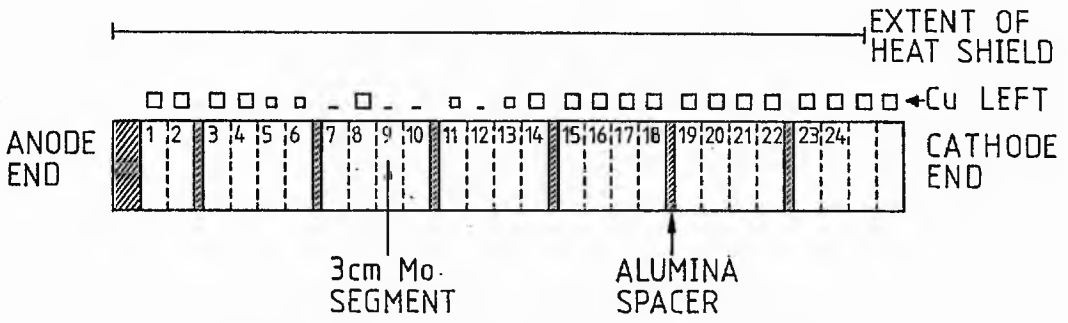

□ MOST OF THE COPPER LEFT (MELTED)

▫ LITTLE COPPER LEFT

\- NO COPPER LEFT

FIGURE 5.11 : SCHEMATIC DIAGRAM SHOWING THE HEATING EFFECT OF THE DISCHARGE ON THE COPPER AND THE INNER WALL OF EACH SEGMENT

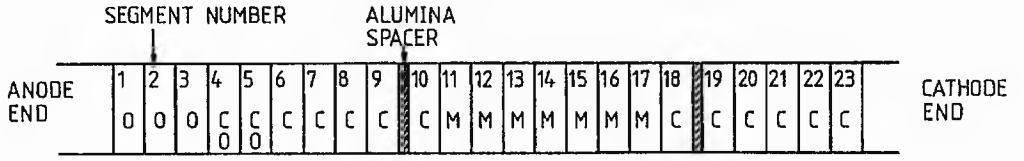

O : COPPER AND MOLYBDENUM OXIDISED

CO : COPPER CLEAN (OXIDE LAYER REMOVED) ; MOLYBDENUM OXIDISED

C : COPPER AND MOLYBDENUM CLEAN (OXIDE LAYER REMOVED)

M : COPPER MELTED

FIGURE 5.12 : CVL TEMPERATURES FOR VARIOUS INPUT POWERS, INSULATION CONSISTS OF AN ALUMINA TUBE WRAPPED IN ZIRCONIA FELT

(a) NO HEAT SHIELD (e=0.8)

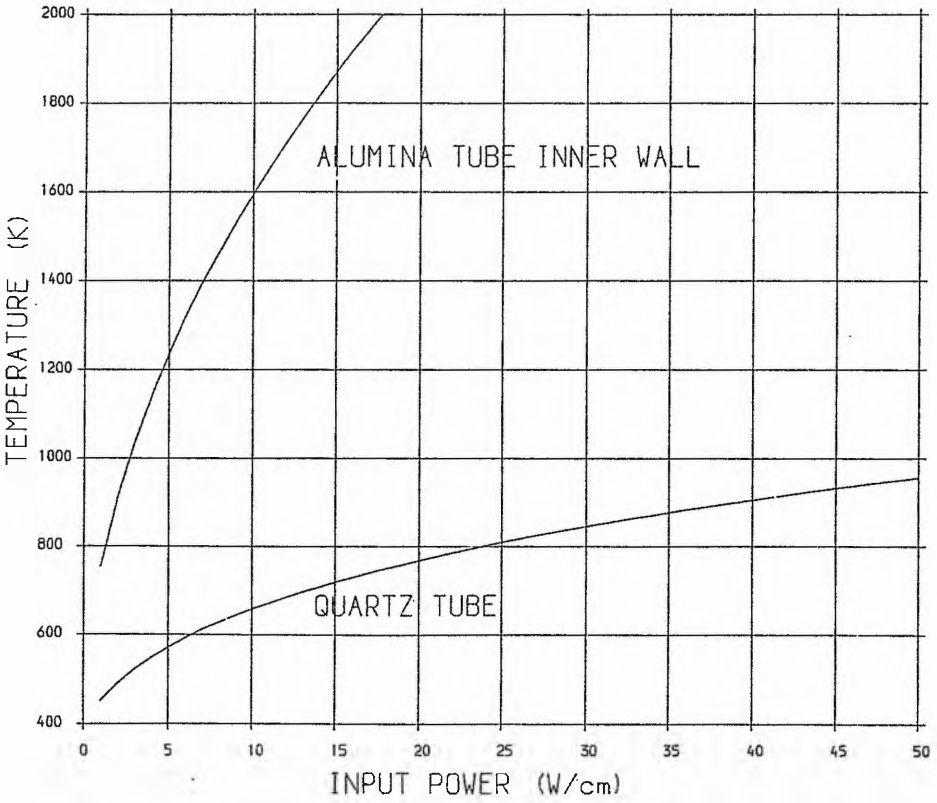

(b) MOLYBDENUM HEAT SHIELD (e=0.05)

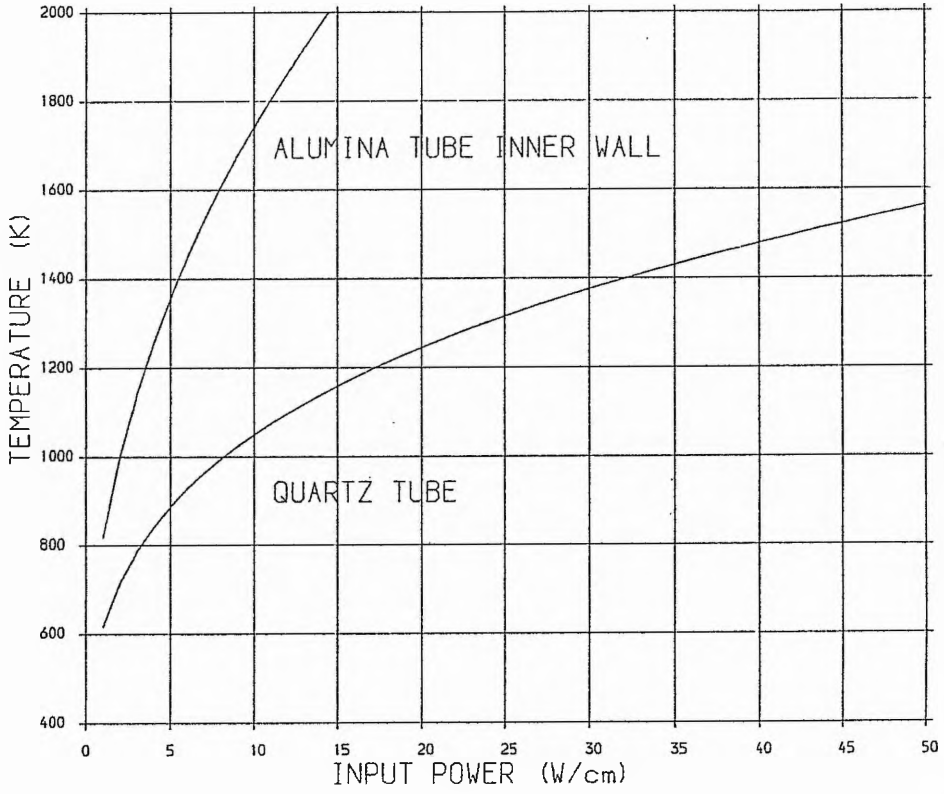

CHAPTER 6

6 GOLD VAPOUR LASER

6.1 INTRODUCTION

The gold vapour laser (GVL) [1-3] belongs to the same class of lasers as the CVL (Section (1.1.2)), but operates at a slightly higher temperature. The GVL system described in this chapter is designed to provide laser light at 628 nm for research into the treatment of cancer. Hematoporphyrin Derivative (HPD) [4,5] is a dye which, when injected into humans or animals, is flushed out of healthy tissue, but retained by cancerous tumours. Unlike most body tissue, HPD has a large absorption cross-section at 628 nm, so that the output of the GVL can be used to selectively irradiate the cancer tumour and destroy it without harming the surrounding healthy tissue. The short laser pulses produced by the GVL give high peak powers which may be an advantage in the treatment when compared with CW dye lasers of similar average power.

6.2 LASER SYSTEM

The gold vapour laser system is contained within a single chassis as shown in Photo. (6A). The laser head is mounted on top with the controls on an angled face along one side. Inside the chassis, the power supply components are placed at one end (Photo. (6B)), the thyratron oil box and cooling system in the middle (Photo. (6C)) and the vacuum system at the other end (Photo. (6D)). Power and water enter the chassis at ground level at one end. The whole chassis is mounted on wheels.

6.2.1 LASER HEAD

The laser head is exactly the same as that described in Section (2.6). Ceramic insulation is used, with zirconia felt wrapped round a recrystallised alumina tube (Purox, Morgan Refractories) which is 95 cm long, 25.5 mm ID and 32 mm OD. Molybdenum sheet is used both for the radiation shield in the vacuum gap and for the electrodes. The laser head is enclosed within a "perspex" box to shield the high voltage components.

6.2.2 VACUUM SYSTEM

The vacuum system consists of two rotary pumps (Edwards E2M5) with a number of gauges and valves, as shown schematically in Fig. (6.1). One pump keeps the discharge cavity under vacuum when the laser is off, to minimize the buildup of contaminant levels. It also removes the buffer gas and contaminants from the cavity when the laser is running. The other pump is used solely to evacuate the vacuum jacket. The solenoid valves (Edwards PV25EK) are wired up so that they shut if the power to the laser is interrupted, thus preserving the vacuum. The solenoid valve in the discharge cavity system can also be opened or closed manually from the front panel. The air admittance valves (Edwards PVA10EK) open if electrical power is lost. This allows air into the space between the pumps and the solenoid valves and so prevents oil being sucked back from the pumps into the system. The pressure gauge next to the pump in the cavity system is an Edwards Controller 503 with a PRM10K Pirani gauge head. This covers the pressure range from 1000 mbar to 10^{-3} mbar. The gauge also has a relay facility with two set points. The low pressure relay is

set to $2x10^{-2}$ mbar and is connected to a relay in the laser power supply. This relay is set so that operation of the laser is not possible if the cavity pressure is above $2x10^{-2}$ mbar. This prevents the laser being damaged by running it up to temperature while there is an air leak. The high pressure relay is set to 2 mbar to switch the system off if a leak develops while the laser is being run. A capsule dial gauge (Edwards CG3), which measures from 0 to 125 mbar is used to measure the buffer gas pressure in the discharge cavity. The buffer gas used is neon (BOC Research Grade). The pressure and flow rate are determined by the two fine control valves at each end of the cavity, with the coarse flow control valve shut. To evacuate the cavity, the coarse flow control valve is fully opened. The neon bottle regulator is left fully opened, and the neon is brought into the system by the ON/OFF valve. A pressure gauge on the front panel shows when the neon bottle is empty. The neon cylinder is size 5(D) (BOC). In the vacuum jacket system, the pressure gauge is an Edwards Thermocouple 507 with a thermocouple TC1 gauge head. There are no relays on this gauge. A leak in this system will only reduce the effectiveness of the thermal insulation. Both systems are connected between the solenoid valves and the laser head by flexible metal tubing (25 mm ID) and then a short length of green plastic tubing. The piping on the gas supply side is Swagelok 1/4". A metre and a half of green plastic tubing connects the cavity gas input (on the cathode flange) to the gas supply, to stop the discharge going to earth via the gas supply system.

6.2.3 THYRATRON

The thyratron used is a hollow anode EEV CX1625, as described in Section (2.4). However, the grid and heater supplies are different

from those used before.

The cathode and reservoir heaters are supplied from the same variac and transformer. The variac is a 0-240 V, 2 A transformer. The heaters require 6.6 V and 44.5 A, 37.5 A for the cathode heater and 7 A for the reservoir heater. The transformer (TEC) has a voltage ratio of 240:6.6 with a secondary current rating of 50 A. The heater tags on the thyratron are connected to the heater supply circuit as shown in Fig. (6.2). The capacitor C in Fig. (6.2) consists of three, 0.47 μF, 1000 V polypropylene capacitors connected in parallel. This protects the heater circuits from high voltage spikes generated when the thyratron switches.

The grid supply circuits are shown in Fig. (6.3). The three thyratron grids are numbered G0, G1 and G2, running from the cathode to the anode. The trigger unit output is labelled G1 and G2. The trigger unit G1 output voltage is 140 V DC and is connected to the thyratron G0 via an 820Ω, 50 W aluminium clad resistor to provide a 170 mA DC priming current. The required current is recommended by EEV to be between 150 and 200 mA. The trigger supply G2 output provides a bias of -200 V and the pulses required to switch the thyratron. It is connected to both G1 and G2 on the thyratron via the circuit shown in Fig. (6.3). The resistors are RS 17 W wire-wound ceramic ones. The capacitor is a 1000 V polypropylene capacitor. This circuit provides pulses to both G1 and G2, but only G2 is negatively biased. The 10 kΩ resistor keeps G1 at cathode potential in the interpulse period. As in Sections (2.3.4) and (2.3.5), the resistors are wire-wound to provide a large inductive impedance to spikes travelling back to the trigger unit and to aid in recovery of the thyratron. The cables running from the trigger unit to the thyratron are coaxial and are wound round a ferrite core five or six times to help to prevent spikes from going back to the trigger unit through the braid of the

cables.

The thyratron is mounted in a tank under oil. The tank also contains the grid supply circuits, the charging diode and the inlet and outlet pipes for the oil cooling system. The thyratron is mounted onto a stainless steel plate which, in turn, is mounted on a perspex base which sits about 12 cm above the base of the oil tank. Holes drilled in the steel plate allow oil to circulate in the tank. The perspex base isolates the thyratron from the tank, so that the tank partially screens the rest of the system from the RF noise radiated by the thyratron. The structure which supports the thyratron and other circuit components can be lifted out of the tank for easy maintenance. Steel legs in each corner of the tank slot into corresponding holes in the thyratron support structure to guide it into place. Cool oil is directed onto the thyratron end cover which contains the heater circuits. The cooling oil is removed from near the surface of the oil so that the oil is forced to move up from below the perspex base to cool the thyratron body. The grid supply circuits are mounted onto a perspex plate which is mounted vertically next to the thyratron. The storage capacitors are mounted above the oil and are connected to the thyratron anode by a stainless steel rod. A probe connection is included for monitoring the thyratron heater voltage. On two sides of the tank, welded to the rim, are supports on which the structure can be rested for inspection. The supports are flexible enough to be easily bent back as the structure is lifted out of the oil. When released, they spring back and support the structure.

6.2.4 CHARGE AND DISCHARGE CIRCUIT

The circuit is almost exactly the same as that used for the CVL

(Fig. (2.2)), with one or two minor changes. The 150 mH charging inductor L_c is made by TEC. It is rated to 10 kV, 1.0 A, and is designed to run at 10 kHz with air cooling. The storage capacitor C_s is mounted directly above the thyratron and is connected to the laser cathode by coaxial cable, instead of being mounted at the laser cathode as in the CVL. The earth of the whole system has been chosen to be on the aluminium rail on which the laser head is mounted rather than the thyratron cathode. The thyratron cathode is therefore floating. The laser chassis is earthed at a point on the rail next to the laser cathode end of the laser's coaxial return.

In order to protect various sensitive components, such as voltmeters, from the electrical noise generated by the discharge circuit, a number of noise reduction and protection techniques are used. To prevent high voltage spikes travelling along wires, they are wrapped around ferrite cores. Polypropylene capacitors (0.1 μF, 1000 V) are used to provide a low impedance path to ground for high voltage spikes. Finally, coaxial cable screening and metal boxes are used to reduce the amount of radiated noise.

6.2.5 POWER SUPPLY

The whole laser system is run from a three-phase power supply. The three-phase supply is transformed and rectified to produce the high voltage DC supply for charging the storage capacitors. The other components in the system which require single-phase power at 240 V, such as the vacuum pumps and trigger supply are run from one of the three phases. The circuit diagram is shown in Fig. (6.4).

The three phases, plus a neutral and an earth, enter the system via a three-phase plug. An isolating switch next to the plug connects the circuit to the supply. Each phase then goes through a fuse (F1 to

F3). A red lamp (ø1 to ø3), connected across each phase and positioned on the front control panel, shows that all three phases are on. There are a number of interlocks on the system, all connected through to relay G, which is placed in front of the standby switch in the circuit. The interlocks are for the three back panels, the laser head's perspex cover, the vacuum in the discharge cavity and the water pressure. Lights on the front control panel show that the interlocks are closed. These are wired in series so that if a door interlock is open, the vacuum and water lights will not come on, even though they may be OK. Both the vacuum and water pressure relay settings can be adjusted if required. When all the interlocks are shut, the standby ON switch can be pressed. The standby ON button on the front panel starts a fifteen minute timer and sends power to the trigger supply, the thyratron heaters and the oil pump. The fifteen minute delay is to allow time for the trigger supply and thyratron to warm up. An amber light on the front panel shows that power is being supplied to the thyratron heaters. After the fifteen minutes, relay F shuts and allows the high voltage to be switched on. A green light on the front panel shows that the system is ready. The variac voltage is displayed on a voltmeter on the front panel before the HT is turned on to show where the variac is set. After another set of fuses (F4 to F6) there is a transformer on each phase. These are 24:0.24 V transformers with a secondary current maximum of 20 A. By connecting the secondaries to each phase, and then rectifying the AC output, the AC current in each phase can be monitored. Relay H then trips out the high voltage supply if the AC current becomes too high. The HT ON switch is connected to contactor B. When B closes, there is a 0.2 second delay before contactor C closes and the full AC current reaches the transformer. This delay is needed because the state of the transformer's core is unknown. If it is in a saturated state, or the

initial current flow which charges up the circuit's stray capacitance causes it to saturate, the AC relay would cause the power to trip out. The resistor in parallel with contactor C allows a small current to flow while the transformer core stabilizes and the circuit's stray capacitance charges up. The transformer is a delta-star three-phase transformer (TEC), rated to 8 kV, 9 kVA. The high voltage output from the transformer is rectified by a three-phase diode bridge (GD Rectifiers). The six diodes in the bridge are each made up of two J-Ea 9000-0.7 modules in series. Each of the modules can hold off 9 kV and pass 0.7 A. The bridge is therefore rated to 18 kV, 2.1 A. The maximum DC voltage that this arrangement can produce is 10.8 kV. The DC overload relay is positioned on the earth side of the DC circuit. A 10Ω, 50 W resistor in series with the thyratron cathode and diode bridge produces a voltage drop across relay J in parallel with it. This relay will trip out the high voltage if the DC current becomes too large.

6.2.6 OPTICAL COMPONENTS

As in the CVL, the optical cavity consists of a total reflector (research quality, flat, circular aluminium mirror) and a flat Spectrosil B polished window as the output coupler. Both mirrors are mounted on standard gimbals (Ealing) which are mounted in turn on pins screwed into the rail. The output coupler is at the anode end. There is about 65 cm between the output coupler and the end of the rail to leave space for the optical components necessary for coupling the light into an optical fibre.

6.2.7 COOLING SYSTEM

The laser and thyratron are both water cooled; the laser directly and the thyratron indirectly. The water supply comes directly from the mains through a water relay (Flowline), which is preset to trip out the high voltage supply if the water pressure drops below a certain level. From there, the water runs through a heat exchanger which cools the oil flowing through the thyratron tank. The oil is circulated in this loop by a pump (Totton Electrical Products: type DP30/3).

6.3 RESULTS

6.3.1 CURRENT AND VOLTAGE WAVEFORMS

This section describes and explains the current and voltage waveforms which occur in the GVL under various experimental conditions. In each case, the supply voltage, PRF and neon pressure is given. Unless stated otherwise, the storage capacitance was 7.2 nF and the peaking capacitance was 3.6 nF. For the single trace photographs, a Tektronix 543B oscilloscope was used, whereas the dual trace photographs were taken from a Tektronix 555 dual trace oscilloscope. The voltage and current pulses were monitored with Tektronix P6015 High Voltage probes and a T&M Research Products current probe (type W-4-001-2.5FC) respectively.

Photographs (6.1) to (6.3) show the same discharge voltage pulse on three different timescales. The PRF was 1.3 kHz, the supply voltage was 4.1 kV and the neon pressure was 25 mbar. The voltage was not high enough to break down the neon sufficiently for the load to be

well-matched. Therefore, after the neon started to break down at the peak of the voltage pulse, the collapse of the voltage across the discharge gap only lasted for about 200 ns. The voltage pulse then showed three distinct types of oscillation, each characteristic of one loop in the discharge circuit. The first set of oscillations had a duration of 300 ns and can be seen most clearly in Photo. (6.2), starting 400 ns after the start of the pulse. These were due to the mismatch in energy transfer between C_s and C_p. From equ. [2.1], the inductance of the thyratron-C_s-C_p loop was calculated to be 0.95 μH, using the period of these oscillations and the capacitance of C_s and C_p in series. The second set of oscillations were those shown in the first 20 μs of Photo. (6.3). These were heavily damped, but the resonance period was estimated to be 5.6 μs from the duration of the first half-cycle of the oscillations. This corresponded to the period of the thyratron-C_s-L_b loop. The oscillations occurred because a hollow anode thyratron was used, and were damped because of the increasing resistance of the thyratron as the plasma in the hollow anode was used up in reverse conduction. The third set of oscillations had a period of 4 μs and were due to the remaining energy in the circuit oscillating in the C_p-L_b loop.

Photographs (6.4) to (6.6) show the thyratron anode voltage on different timescales when the load was overmatched as above. In this case, the storage capacitance was 3.6 nF, the supply voltage was 2.2 kV, the PRF was 2 kHz and the neon pressure was 15 mbar. In Photo. (6.4), the voltage drop to the arc level was as expected, but in Photo. (6.5), there were oscillations equivalent to those shown in Photos. (6.1) to (6.3). The first set, in the thyratron-C_s-C_p loop, can just be seen up to 2 μs after the start of the pulse in Photo. (6.5). Then, reverse conduction in the thyratron due to oscillations in the thyratron-C_s-L_b loop show as the negative swings

in Photo. (6.5), 4 and 10 μs after the start of the pulse. Finally, both these oscillations and those in the C_p-L_b loop can be seen superimposed on the charging voltage waveform in Photo. (6.6).

When the GVL was lasing and the load was well matched, the supply voltage could not be increased much above 6 kV without the thyratron "hanging up". Also, while the laser was heating up, the thyratron hung up at seemingly random intervals. Photograph (6.7) shows the thyratron anode voltage. The supply voltage was 6 kV, the PRF was 5 kHz and the neon pressure was 25 mbar. It can be seen that the anode voltage rose to between 200 and 400 V after 2 μs and then fell to about 100 V before starting to increase again as C_s charged up. There was a large amount of amplitude jitter in the waveform, due to discharge instabilities. Occasionally, the voltage rose above the reignition voltage and the thyratron "hung up".

Photographs (6.8) to (6.13) show the changing voltage waveform on the laser cathode as the laser heated up. As with the CVL, the pulse width narrowed and the pulse height fell as the matching improved and the discharge impedance dropped. In Photo. (6.12), the pulse height was only -4.6 kV. At this point, the neon was being flowed very fast through the cavity, so the density of contaminants was low. The resulting "pure" neon discharge had a very low impedance as shown by the low peak voltage. When the flow rate was reduced, the discharge pulse height increased (Photo. (6.13)) as the density of contaminants in the discharge rose.

The current pulse going through the thyratron when the laser was cold is shown in Photo. (6.14). The supply voltage was 5.25 kV, the PRF was 2 kHz and the neon pressure was 20 mbar. The first peak was the current flowing in the thyratron-C_s-C_p loop as C_s pulse charged C_p. At low laser temperatures, the discharge took longer to form, so there was a delay between the current which charged C_p and the second

peak, which was the remaining charge on C_s discharging into the laser. During the interval between these two current pulses, the current in the thyratron-C_s-C_p loop reversed, but the peak reverse current pulse was only one third of the peak forward pulse. The slower risetime of the second peak compared to the first one shows that the inductance of the thyratron-C_s-laser loop was larger than that of the thyratron-C_s-C_p loop. The smaller oscillations after the second peak were caused by the mismatch in the circuit so that current continued to oscillate after the main pulse. When the discharge was at its optimum temperature, there was little or no current oscillation in the circuit after the main pulse.

Photographs (6.15) to (6.23) show the thyratron anode voltage and current (the upper and lower traces, respectively, on the dual trace photographs) and the laser cathode voltage as the laser warmed up. The circuit conditions are shown under each photograph. As the PRF increased and the laser heated up, the delay between the two parts of the current pulse decreased. When the delay reached zero (Photo. (6.19)) the negative swing in the anode voltage started to disappear. Eventually, when the GVL was lasing, the current pulse had the expected double hump shape and the anode voltage only became slightly negative (Photo. (6.23)).

Photographs (6.24) to (6.30) show the laser cathode and thyratron anode voltages. In each photograph, the upper trace was the laser cathode voltage and the lower trace was the thyratron anode voltage. The extra noise on the traces compared with the other dual traces was due to the fact that the two probes were grounded at different points in the circuit. Therefore, there was coupling between the grounded screens of the two coaxial cables bringing the signals from the voltage probes to the oscilloscope. The neon pressure was kept between 20 and 24 mbar. Photographs (6.24) and (6.25) show the same

traces, but on a different timebase. The laser voltage was overmatched, as was expected when the laser was warming up. Photographs (6.26) to (6.30) then show the usual pattern as the laser heated up. The two traces follow each other almost exactly, showing that after the thyratron switched, the thyratron anode voltage was dependent on the laser cathode voltage, and hence on the impedance of the discharge.

Photographs (6.31) to (6.36) show how the thyratron anode voltage and current (Photos. (6.31), (6.33) and (6.35)) and the laser voltage (Photos. (6.32), (6.34) and (6.36)) varied with the PRF. Photographs (6.31) and (6.32) were taken at 400 Hz, Photos. (6.33) and (6.34) at 1 kHz and Photos. (6.35) and (6.36) at 2 kHz. In each case, the supply voltage was 6.3 kV and the neon pressure was 20 mbar. The discharge was run at 400 Hz and the photographs at higher PRFs were taken within one minute of increasing the frequency to avoid changing the wall temperature significantly. Increasing the PRF had no effect on the initial current pulse which charged up C_p from C_s because that was dependent solely on the voltage to which C_s was charged and the inductance of the loop. However, the second part of the current pulse did depend on the PRF. As the frequency increased, and the discharge impedance decreased (shown in the laser voltage pulses: Photos. (6.32), (6.34) and (6.36)), the current flowing from C_s into the discharge in a single pulse increased. At the same time, the amount of current left oscillating in the circuit after the second part of the current pulse decreased.

6.3.2 LASER PULSE

The laser pulse photographs were taken from a Tektronix 519 oscilloscope. The laser beam was directed into an ITL TF1850

photodiode (Section (4.3)) in an arrangement similar to that of Fig. (4.2) except that the photodiode was positioned directly in line with the laser.

Photographs (6.37) to (6.41) show the GVL laser pulse under different conditions. In Photo. (6.37), the laser was just above threshold and was still warming up. The PRF was 10 kHz and the neon pressure was 25 mbar. As the laser continued to heat up, the initial spike became larger and the pulse developed a broad tail. The GVL pulse at 1.5 W and 25 mbar of neon is shown in Photo. (6.38). The indentations in the pulse were 10.6 ns apart. The cavity length was 162 cm, so the interval between these indentations corresponded to the round trip time in the cavity. Something within the cavity was absorbing the laser light. Figure (6.5) shows the variation of the average laser power with the neon pressure, up to 100 mbar. Photographs (6.39) and (6.40) show the effect of pressure on the laser pulse and were taken at 50 and 100 mbar, respectively. The effect of increasing the pressure appeared to be to reduce the size of the population inversion after the initial spike so that the amount of energy in the tail of the pulse decreased. Finally, the PRF was decreased to 5 kHz and Photo. (6.41) was taken before the wall temperature had time to change. The neon pressure was 25 mbar. The pulse appeared to be almost exactly the same as that of Photo. (6.38), which was taken under the same conditions, but at 10 kHz. The average power at 5 kHz could not be measured. The absence of any change in the GVL pulse shape with the PRF is due to the energy level structure of gold (Fig. (6.6)). Since the lower level of the 628 nm transition lies over 2.5 eV above ground (compare this with the copper energy levels in Fig. (1.3)), the high gas temperature does not significantly populate the $^2D_{3/2}$ level. It is possible to run a GVL at PRFs of up to 20 kHz without any reduction in the laser efficiency [6]. However,

because the $^2D_{5/2}$ level lies close to ground, it is difficult to get the 312 nm line to lase.

6.4 FUTURE DEVELOPMENT

With the GVL system as described above, it was possible to get between 1 and 1.5 W consistently at a PRF of 10 kHz. If more power is required, it will be necessary to make some changes to the system.

The easiest method of obtaining more power is to increase the length of the active zone by smoothing out the axial temperature gradient. This could be done by replacing the Mo heat shield near each end with a higher reflectivity material. Secondly, hydrogen could be added in small amounts to the neon buffer gas (Section (4.7.2)). Finally, since the GVL can be run at higher PRFs than CVLs of comparable bore diameters with no reduction in the efficiency [6], the circuit could be altered to run at a higher PRF to obtain a higher average power. This would be an expensive alteration however, because the trigger unit would have to be modified and the charging inductor would have to be replaced.

REFERENCES FOR CHAPTER 6

1 : Errey K.H., LASER UND OPTOELEKTRONIK 15, 103 (1983)

2 : Markova S.V., Cherezov V.M., SOV. J.Q.E. 7, 339 (1977)

3 : Markova S.V., Petrash G.G., Cherezov V.M.
SOV. J.Q.E. 8, 904 (1978)

4 : Kessel D., DIGEST OF TECHNICAL PAPERS, CLEO 1987, 46 (1987)

5 : Atsumi K. (Editor), NEW FRONTIERS IN LASER MEDICINE AND SURGERY
p161, EXCERPTA MEDICA (1983)

6 : Lewis R.R., Harpin A.P.R., Kearsley A.J.
DIGEST OF TECHNICAL PAPERS, CLEO 1987, 26 (1987)

PHOTOGRAPH 6.1 : LASER VOLTAGE

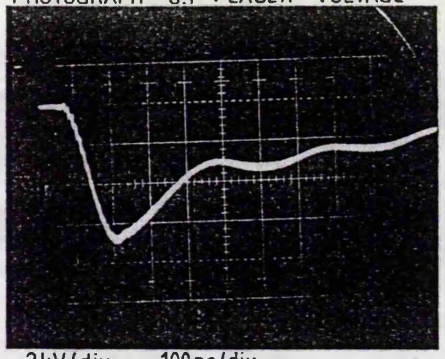

2kV/div 100ns/div

PHOTOGRAPH 6.2 : LASER VOLTAGE

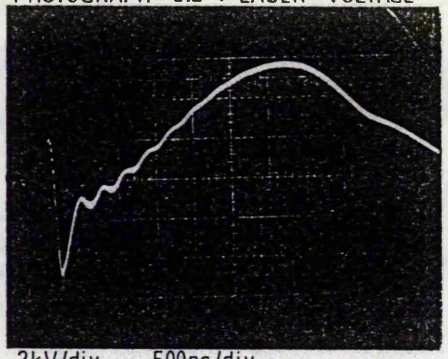

2kV/div 500ns/div

PHOTOGRAPH 6.3 : LASER VOLTAGE

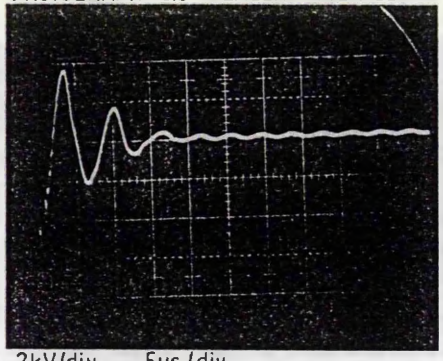

2kV/div 5µs/div

PHOTOGRAPH 6.4 : THYRATRON VOLTAGE

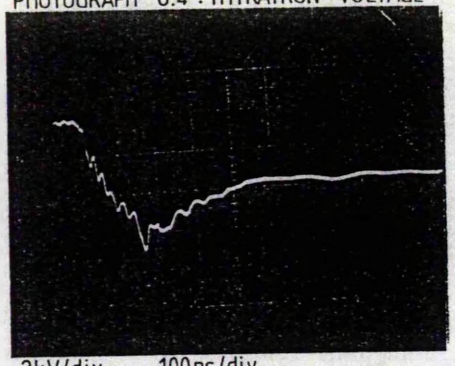

2kV/div 100ns/div

PHOTOGRAPH 6.5 : THYRATRON VOLTAGE

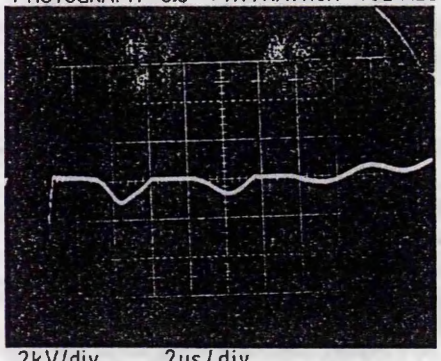

2kV/div 2µs/div

PHOTOGRAPH 6.6 : CHARGING VOLTAGE

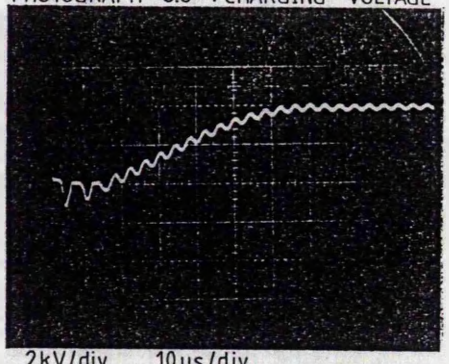

2kV/div 10µs/div

PHOTOGRAPH 6.7 : THYRATRON VOLTAGE

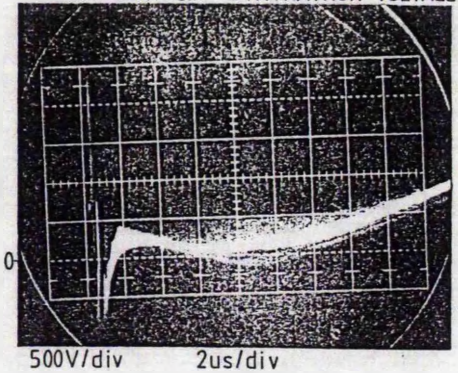

500V/div 2us/div

PHOTOGRAPH 6.8 : LASER VOLTAGE

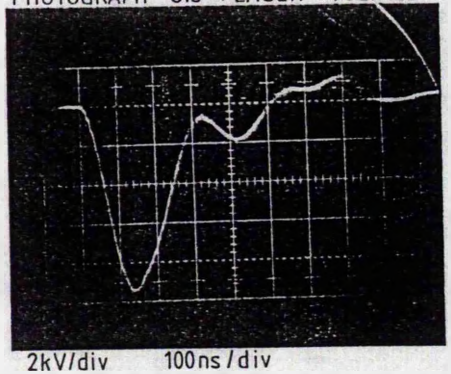

2kV/div 100ns/div

PHOTOGRAPH 6.9 : LASER VOLTAGE

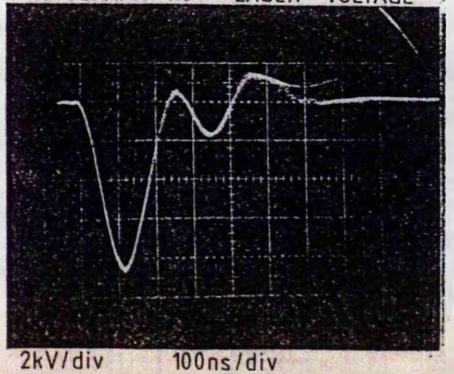

2kV/div 100ns/div

PHOTOGRAPH 6.10 : LASER VOLTAGE

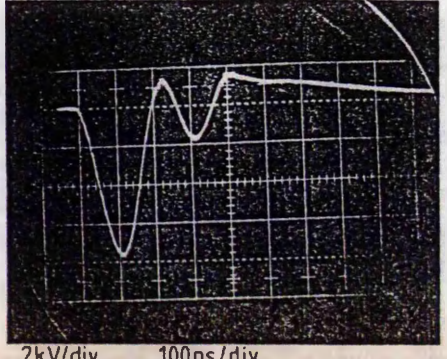

2kV/div 100ns/div

PHOTOGRAPH 6.11 : LASER VOLTAGE

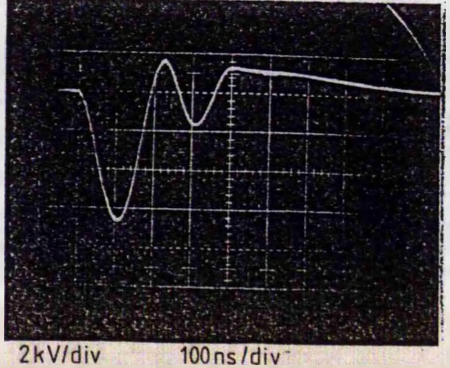

2kV/div 100ns/div

PHOTOGRAPH 6.12 : LASER VOLTAGE

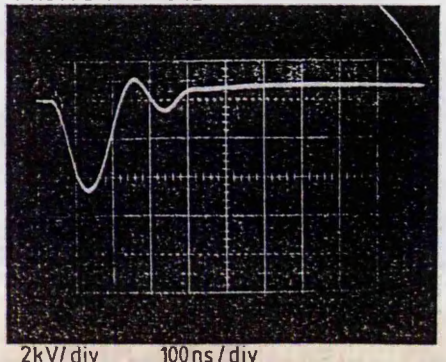

2kV/div 100ns/div

PHOTOGRAPH 6.13 : LASER VOLTAGE

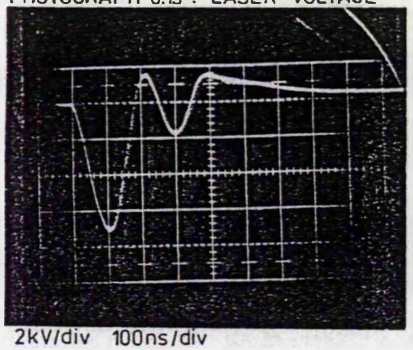

2kV/div 100ns/div

PHOTOGRAPH 6.14 : THYRATRON CURRENT

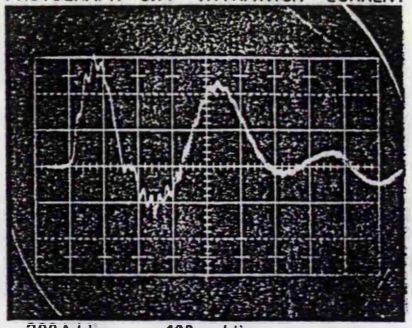

200A/div 100ns/div

PHOTOGRAPH 6.15 : (a) THYRATRON VOLTAGE
(b) THYRATRON CURRENT

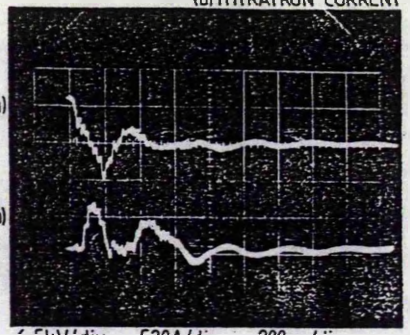

6·5kV/div 520A/div 200ns/div
6kV SUPPLY, 3kHz, 30mbar

PHOTOGRAPH 6.16 : LASER VOLTAGE

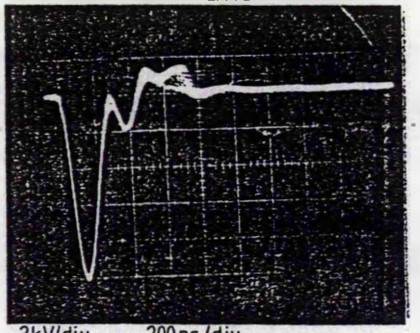

2kV/div 200ns/div
6kV SUPPLY, 3kHz, 30mbar

PHOTOGRAPH 6.17 : (a) THYRATRON VOLTAGE
(b) THYRATRON CURRENT

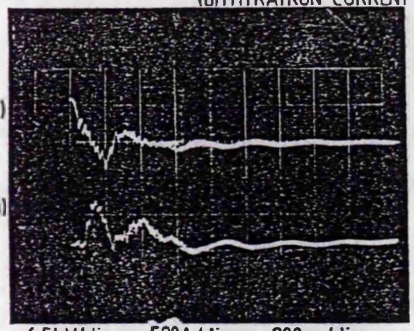

6·5kV/div 520A/div 200ns/div
5·4kV SUPPLY, 5kHz, 30mbar

PHOTOGRAPH 6.18 : LASER VOLTAGE

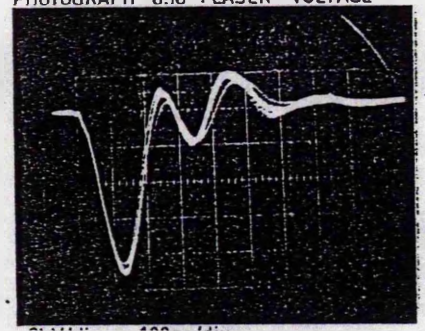

2kV/div 100ns/div
5·4kV SUPPLY, 5kHz, 30mbar

PHOTOGRAPH 6.19 : (a) THYRATRON VOLTAGE
(b) THYRATRON CURRENT

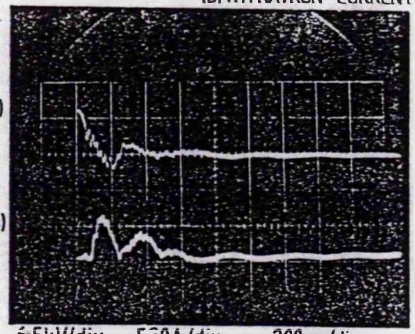

6·5kV/div 520A/div 200ns/div
5·4kV SUPPLY, 8kHz, 45mbar

PHOTOGRAPH 6.20 : LASER VOLTAGE

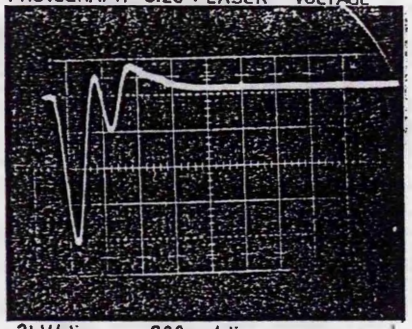

2kV/div 200ns/div
5·4kV SUPPLY, 8kHz, 45mbar

PHOTOGRAPH 6.21 : (a) THYRATRON VOLTAGE
(b) THYRATRON CURRENT

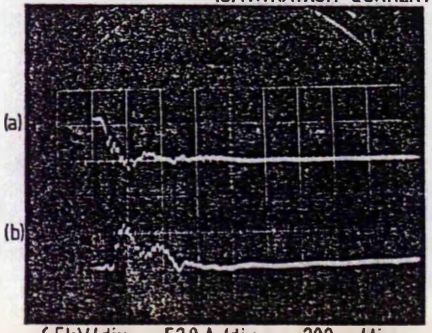

6·5kV/div 520A/div 200ns/div
5·2kV SUPPLY, 9kHz, 45mbar

PHOTOGRAPH 6.22 : LASER VOLTAGE

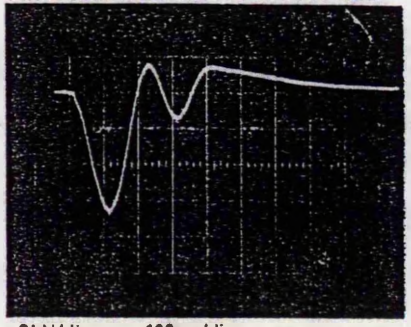

2kV/div 100ns/div
5·2kV SUPPLY, 9kHz, 45mbar

PHOTOGRAPH 6.23 : (a) THYRATRON VOLTAGE
(b) THYRATRON CURRENT

6·5kV/div 520A/div 100ns/div
5·9kV SUPPLY, 10kHz, 45mbar

PHOTOGRAPH 6.24 : (a) LASER VOLTAGE
(b) THYRATRON VOLTAGE

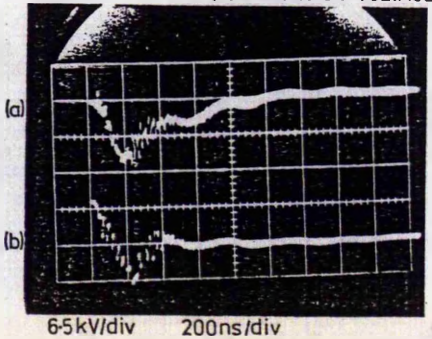

6·5kV/div 200ns/div

PHOTOGRAPH 6.25 : (a) LASER VOLTAGE
(b) THYRATRON VOLTAGE

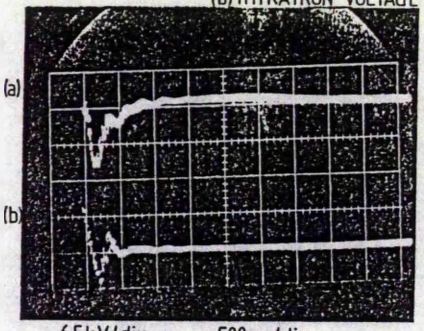

6·5kV/div 500ns/div

PHOTOGRAPH 6.26 : (a) LASER VOLTAGE
(b) THYRATRON VOLTAGE

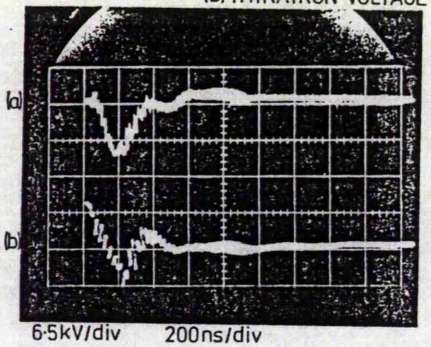

6·5kV/div 200ns/div

PHOTOGRAPH 6.27 : (a) LASER VOLTAGE
(b) THYRATRON VOLTAGE

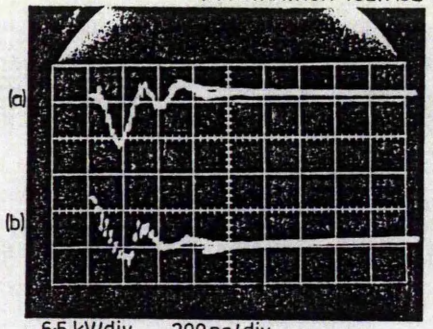

6·5 kV/div 200ns/div

PHOTOGRAPH 6.28 : (a) LASER VOLTAGE
(b) THYRATRON VOLTAGE

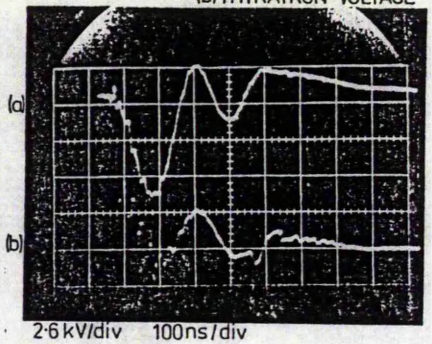

2·6 kV/div 100ns/div

PHOTOGRAPH 6.29 : (a) LASER VOLTAGE
(b) THYRATRON VOLTAGE

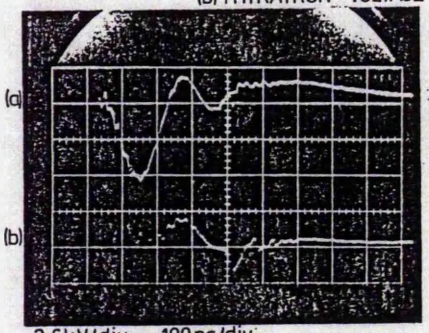

2·6kV/div 100ns/div

PHOTOGRAPH 6.30 : (a) LASER VOLTAGE
(b) THYRATRON VOLTAGE

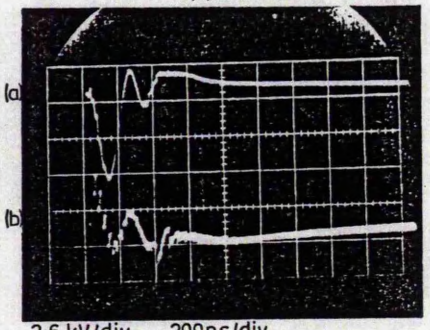

2·6 kV/div 200ns/div

PHOTOGRAPH 6.31 : (a) THYRATRON VOLTAGE
(b) THYRATRON CURRENT

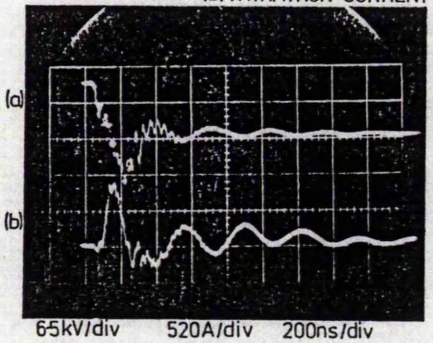

6·5kV/div 520A/div 200ns/div

PHOTOGRAPH 6.32 : LASER VOLTAGE

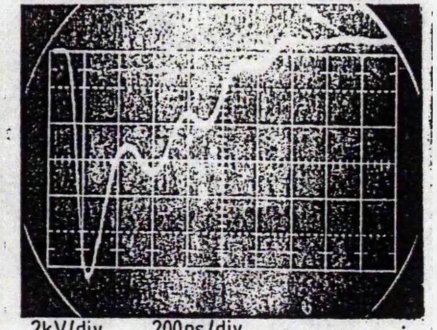

2kV/div 200ns/div

PHOTOGRAPH 6.33 : (a) THYRATRON VOLTAGE
(b) THYRATRON CURRENT

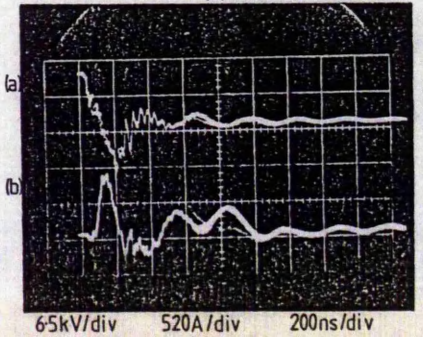

6·5kV/div 520A/div 200ns/div

PHOTOGRAPH 6.34 : LASER VOLTAGE

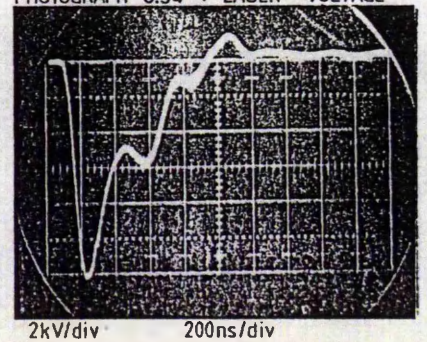

2kV/div 200ns/div

PHOTOGRAPH 6.35 : (a) THYRATRON VOLTAGE
(b) THYRATRON CURRENT

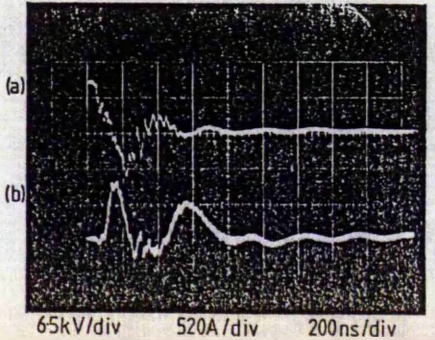

6·5kV/div 520A/div 200ns/div

PHOTOGRAPH 6.36 : LASER VOLTAGE

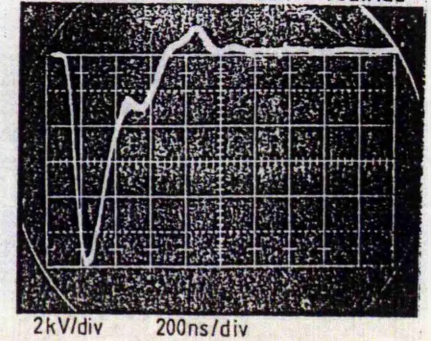

2kV/div 200ns/div

PHOTOGRAPH 6.37 : LASER

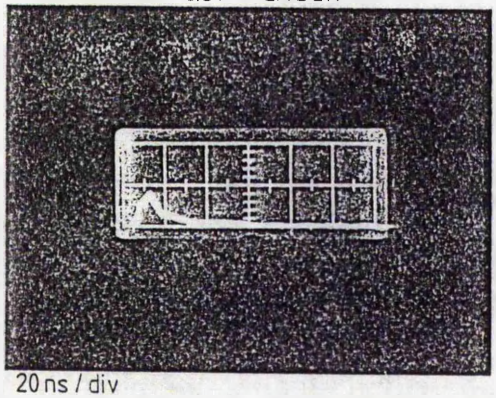

20 ns / div

PHOTOGRAPH 6.38 : LASER

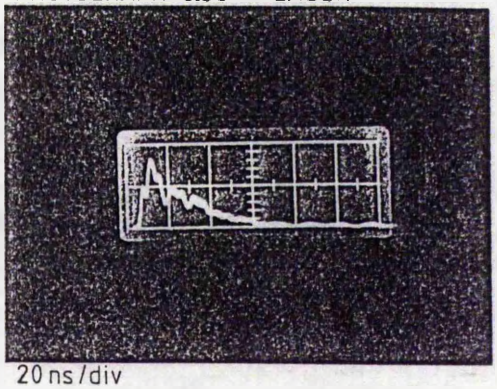

20 ns / div

PHOTOGRAPH 6.39 : LASER

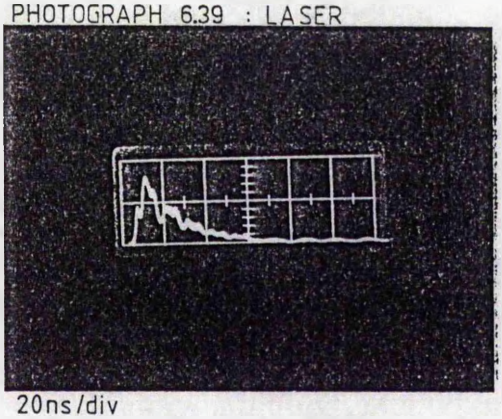

20 ns / div

PHOTOGRAPH 6.40 : LASER

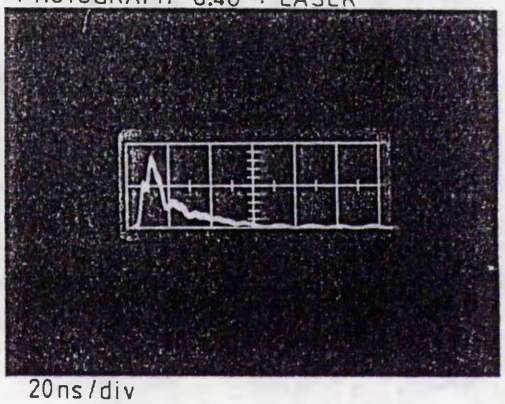

20 ns / div

PHOTOGRAPH 6.41 : LASER

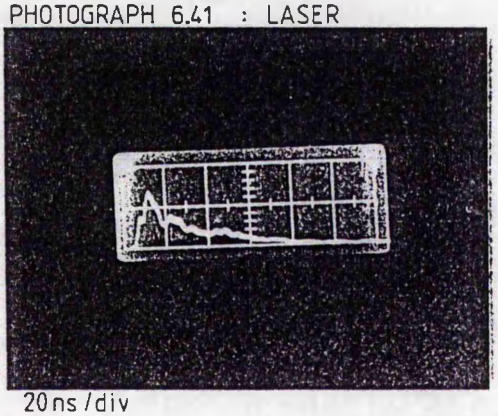

20 ns / div

FIGURE 6.1 : (a) LASER CAVITY VACUUM SYSTEM

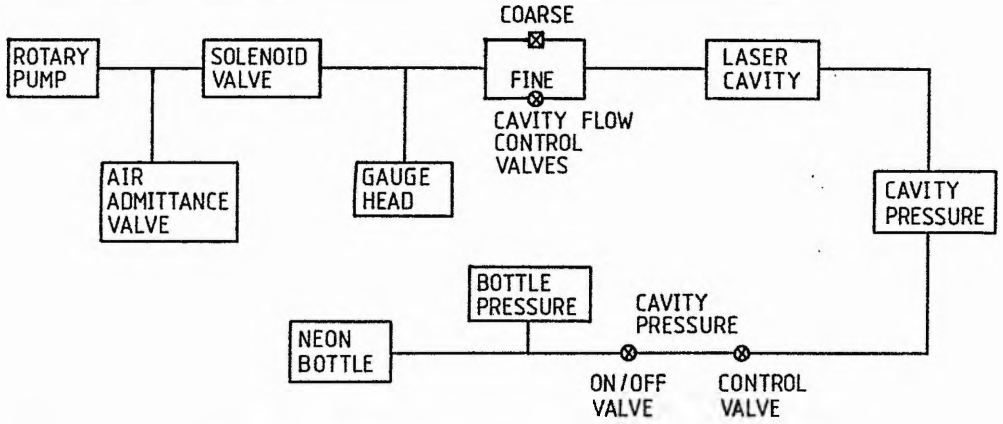

(b) RADIATION GAP VACUUM SYSTEM

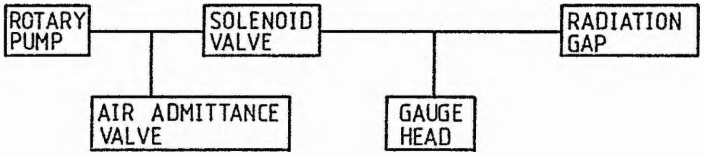

FIGURE 6.2 : HEATER CIRCUIT AND CONNECTIONS

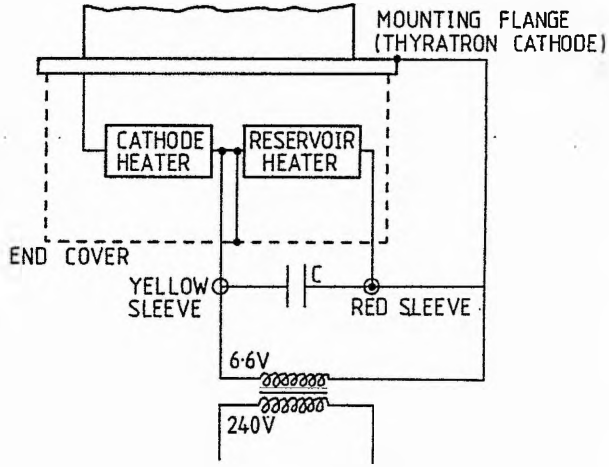

FIGURE 6.3 : THYRATRON GRID SUPPLY

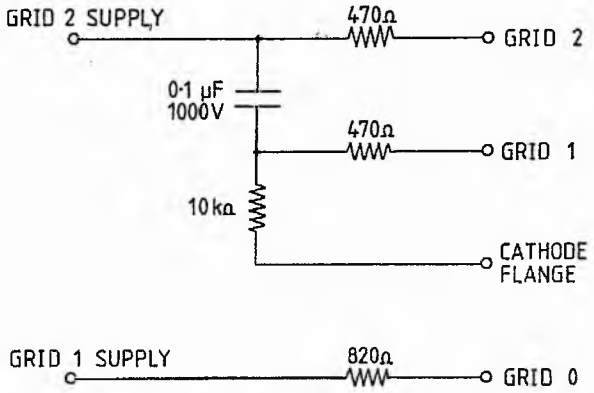

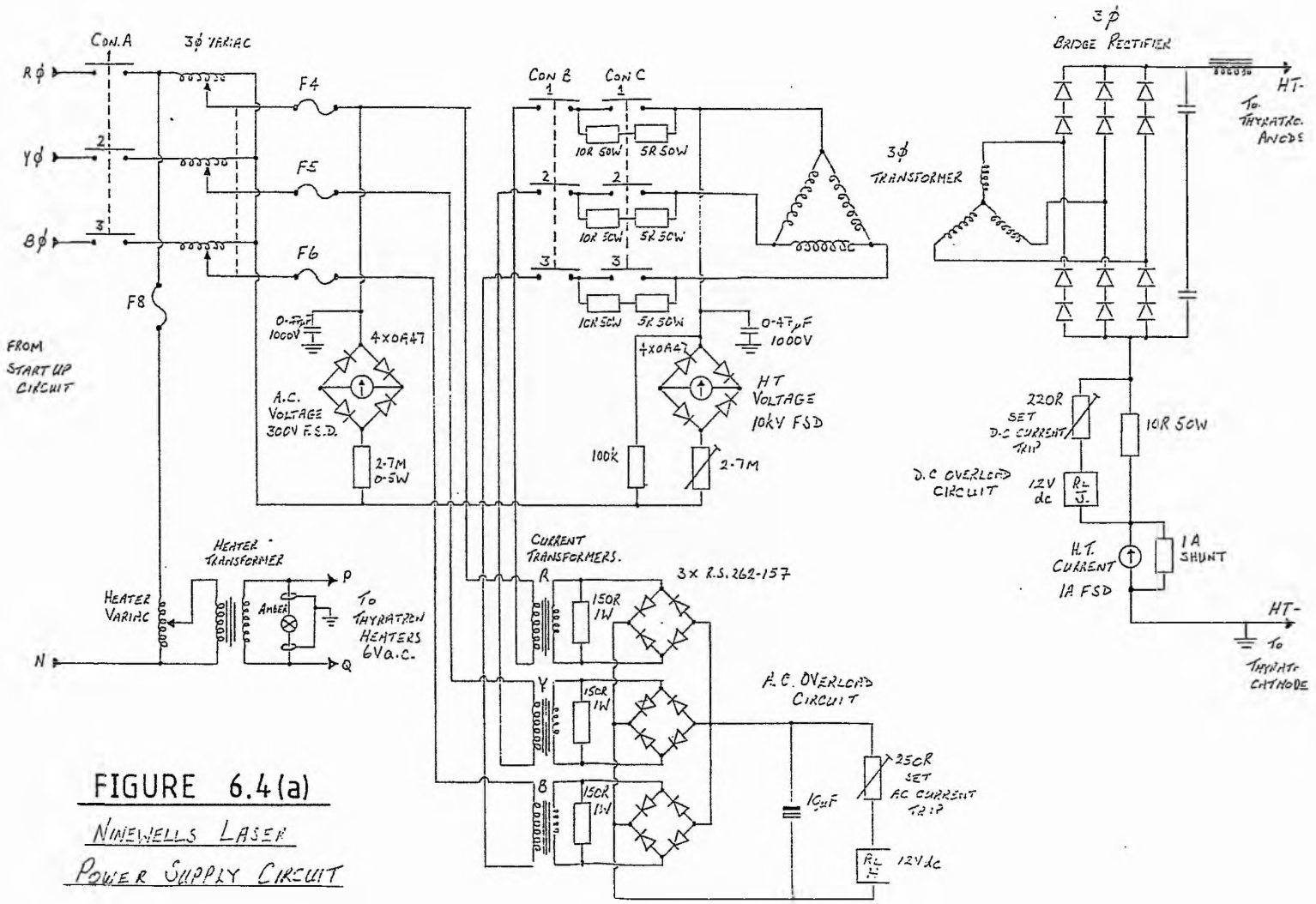

FIGURE 6.4(a)

NINEWELLS LASER

POWER SUPPLY CIRCUIT

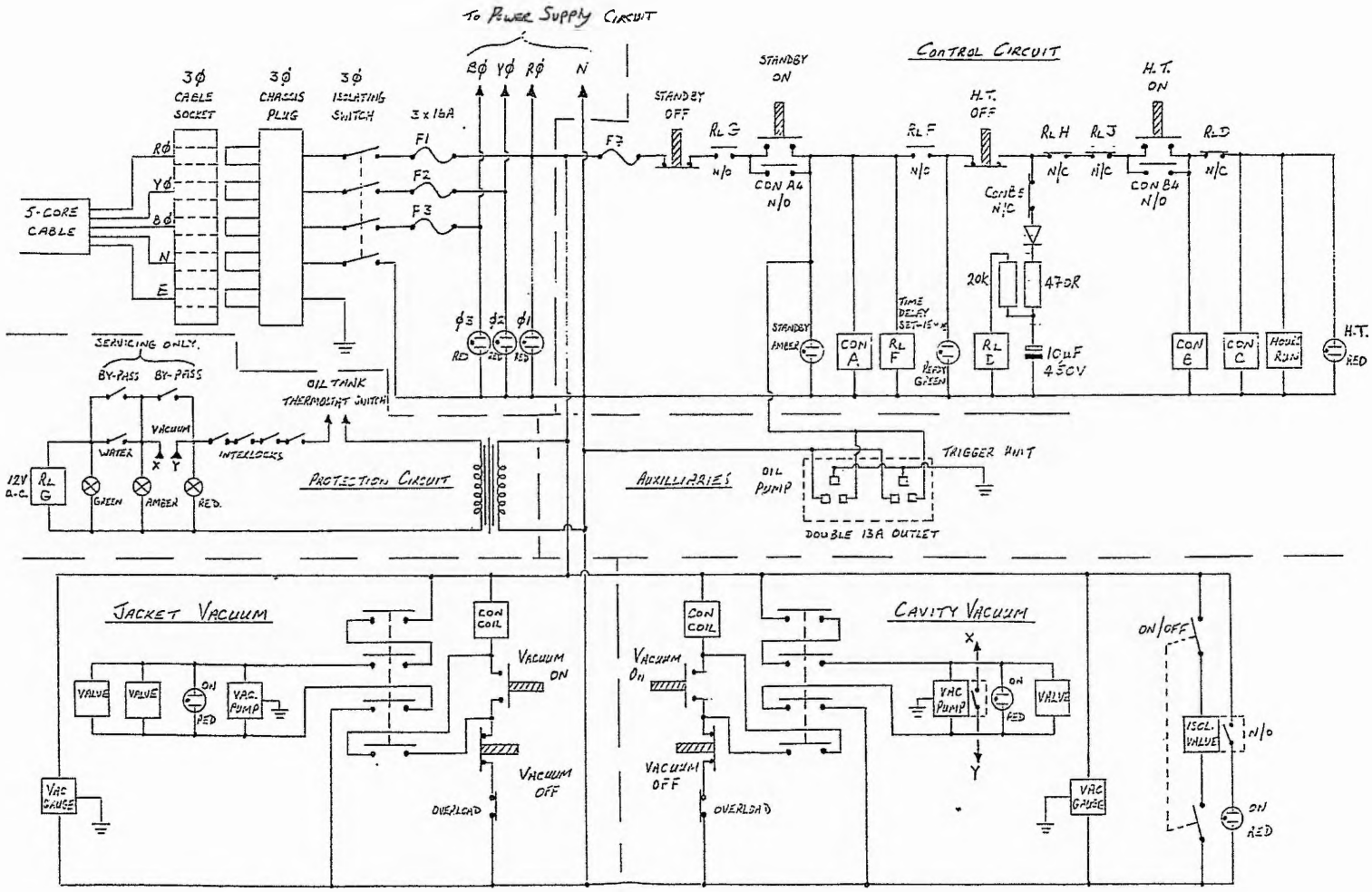

FIGURE 6.4(b) NINEWELLS LASER START UP AND CONTROL CIRCUITRY

FIGURE 6.5 : LASER POWER VARIATION WITH NEON PRESSURE

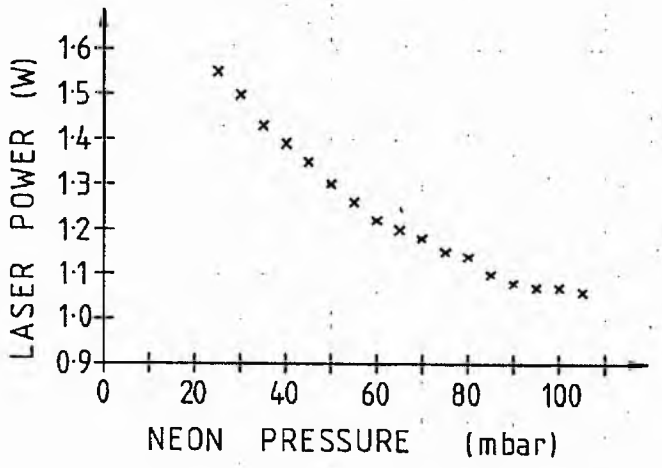

FIGURE 6.6 : PARTIAL ENERGY LEVEL DIAGRAM OF GOLD

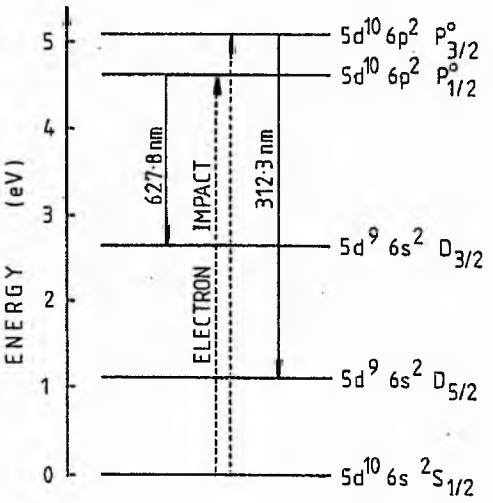

CHAPTER 7

7 DISCHARGES CONFINED BY METAL SEGMENTS

7.1 INTRODUCTION

This chapter describes the experiments carried out with metal-walled discharges and some theories to explain their use. Preliminary experiments were carried out to determine the feasibility of running pulsed discharges in long metal tubes and their operating conditions. The results of these experiments were then used in the design of the metal CVL discharge tubes. Theories to explain the use of discharges confined by metal walls and their application in the copper vapour laser discharge are discussed in Sections (7.3) to (7.6).

7.2 EXPERIMENTS

7.2.1 DISCHARGES IN LONG METAL TUBES

In order to investigate the distance which a pulsed discharge will penetrate into a metal tube, the apparatus shown in Fig. (7.1) was used. A long glass tube enclosed the metal tube. The ends of the glass tube were stopped with rubber bungs, with the electrodes pushed through the bungs. The gap between the electrodes was filled with a continuous length of brass, either a 139 cm long, 3.8 cm O.D., 3.6 cm I.D. tube, or two 70 cm long pieces of gauze wrapped into a tubular shape. The two pieces of gauze touched so that they formed a continuous length of metal. The tube had 2 mm diameter holes drilled every 2 cm. The gauze hole size was 0.25 mm^2. The cathode electrode

was hollow, allowing the tube to be evacuated and then filled with the required gas. A Vacuum General Model 80-6A pressure display module was connected to a Vacuum General Capacitance Manometer to measure pressures from 10 torr down to millitorr. Helium, argon and hydrogen were used in turn. The system was not leaktight. The base pressure reached was 50 mtorr. The circuit shown in Fig. (7.2) was used, with a 0.5 μF capacitor initially. The capacitor was charged through the resistor until the voltage on it was large enough to break down both the spark gap and the gas in the discharge tube. The power supply voltage was kept at 7 kV unless otherwise stated.

Figures (7.3) to (7.5) show the results obtained with the brass tube. In each case, the pressure was reduced gradually from about 1 torr by adjusting the gas admittance and pumping rates. The extent to which the discharge penetrated the tube was measured by observing the length of the glow through the holes in the tube. In each case, the discharge penetrated a constant distance from the cathode, independently of the gas pressure or type. However, as the pressure dropped, the length of the glow from the anode end increased. There was a large pulse-to-pulse variability in the distance from the anode, which was probably due to the circuit used. A discharge over the whole length of the tube was achieved at a much higher pressure in helium than in either argon or hydrogen. With He in the tube, the discharge reached about 26 cm from the anode until the pressure was reduced to 0.95 torr. At this pressure, the discharge suddenly reached the whole way through the tube and continued to do so as the pressure dropped further. The discharge eventually stopped at 0.155 torr when the supply voltage was insufficient to break down the combination of the spark gap and the discharge tube. Argon and hydrogen have the same characteristic pressure dependence (Figs. (7.3) and (7.4)) : a slow increase in the length of the glow as the pressure

is reduced and then a "runaway" effect as the gradient of the curve increases. When the discharge penetrated the whole tube, the intensity of the glow was fairly uniform, apart from a dimmer section extending from the edge of the cathode region for 10 or 15 cm. When the pressure became too low, usually at about 100 mtorr, the discharge stopped. Increasing the supply voltage started the discharge again and enabled a lower pressure to be reached.

The inductance of the discharge loop was reduced by wrapping a coaxial return made of copper foil around the discharge tube, with a narrow gap left to allow the holes in the brass tube to be seen. The spark gap and capacitor were positioned close to the anode to minimize the length of the connecting leads. The effect on the discharge is shown in Fig. (7.5) for hydrogen. Comparing this with Fig. (7.4), it can be seen that reducing the circuit inductance reduced the penetration distance for a given pressure.

The supply voltage was increased from 6.5 kV to 10 kV without any noticeable variation in the length of the glow at the cathode end. The length of the cathode glow was therefore independent of the voltage, gas pressure and type, and was probably dependent principally on the geometry of the electrode and metal tube.

In order to study the structure of the discharge, the brass tube was replaced with the gauze described above. Using hydrogen, the discharge moved further into the tube as the pressure was reduced, until, at 0.2 torr, it reached the whole length. Small flashes of light could be seen at random points on the walls. The density and frequency of these flashes was higher nearer the anode. The discharge could be seen to extend radially out to the gauze walls over the whole length of the tube. Also, striations could be seen running from about 50 cm from the anode to a dimmer region before the start of the cathode glow. These striations varied in position and length from

pulse to pulse, but were typically between 1 and 4 cm long. Occasionally the striations disappeared and the glow became uniform. Between the anode and cathode glows there was a dim region of length 10 to 15 cm. The discharge was much brighter at both the cathode and anode ends than in the middle.

The 0.5 μF capacitor was replaced by a 1.8 nF strontium titanate one in order to increase the PRF of the discharge. Again, using hydrogen at a pressure of about 0.15 torr, the discharge extended over the whole length of the gauze with a similar structure to that described above for the larger capacitor, although the striations were absent. The glow filled the whole cross-section of the tube, apart from the middle region, where it narrowed slightly, moving away from the walls. The small flashes of light at the wall noted above were present again, and increasing the supply voltage caused them to increase in number.

In order to allow observations of the voltage on a long metal tube placed between the electrodes in a pulsed discharge, the apparatus shown in Fig. (7.6) was used. The electrode at one end was a hollow cathode, and at the other was a pin to be used as the anode. The floating metal tube had connections made to it to allow the voltage on it during the discharge to be measured. The ends of the metal tube and the cathode were machined smooth to reduce field enhancement effects. A coaxial return, made from brass gauze, was wrapped round the discharge tube and attached to the anode. The electrodes were connected to the CVL discharge circuit (Fig. (2.2)). In order to reduce the amount of impurities in the discharge, the discharge was only run at 140 Hz. The storage capacitance was either 3.6 nF or 1.8 nF, the peaking capacitance was 1.8 nF and the voltage to which C_s was charged was 6 kV. The power dissipated by the discharge was therefore no more than 9 W. Hydrogen was used to carry

the discharge between the electrodes.

The photographs in Fig. (7.7) show the effect on the cathode and floating tube voltages of changing the gas pressure and C_s:C_p ratio. In Fig. (7.7(a)) and (7.7(b)), the positive spike which occurred after the peak negative voltage was probably due to an arc forming between the electrodes and the metal tube. For the first 300 ns of the discharge, the voltage traces shown in Figs. (7.7(d)) and (7.7(e)) had the same form as the current pulse was expected to have. Current pulses were not obtained because of problems with electrical noise, but it was assumed that the current pulse shape was the same as in Photos. (4.11) and (4.14) in Section (4.4.4), depending on the ratio of C_s to C_p. With C_s at 3.6 nF (twice C_p), the voltage pulse had the double hump shape (Fig. (7.7(d))) which is characteristic of the mismatch in charge transfer between C_s and C_p. However, when C_s was reduced to the same size as C_p, the voltage pulse showed only one peak (Fig. (7.7(f))). Since the voltage pulse did appear to follow the expected current pulse shape, the change in the shape of the pulse must have been due to the improved matching between C_s and C_p, so that there was no after-current.

The discharge circuit was not well matched to the load, so that oscillations in the C_p -L_b loop occurred after the initial negative pulse (Fig. (7.7(h))). The voltage on the floating tube at this point (Fig. (7.7(i))) showed a slightly different form to that of the cathode voltage. There were noticeable positive oscillations, but the voltage did not swing negative after more than 4 μs from the start of the pulse. This showed that current was flowing from the floating tube to the anode (which was earthed), so that the potential difference between the floating tube and anode was small. However, when the cathode voltage became positive, there was little or no current flow from the anode to the floating tube, resulting in a large

potential difference.

7.2.2 METAL SEGMENTS IN THE CVL

With the 3 cm long Mo segments (Section (2.8.4)) placed in the quartz tube in the CVL head, a DC discharge was started with a neon pressure of 40 torr. With a current of over 1 A and over 1 kV across the electrodes, the neon pressure was increased to 170 torr, with no visible sign of arcing between the segments. At this pressure, the discharge was constricted to a diameter of less than 1 cm. When the pressure was reduced again, the discharge expanded.

If a pulsed discharge was started with a neon pressure of 20 torr, filamentary discharges could be seen running over the alumina spacers between the segments, showing that some of the discharge current was being conducted through the segments. The glow on the discharge axis was very weak. Changing the power supply voltage had no apparent effect. Raising the gas pressure increased the number and intensity of the filamentary discharges between segments. In order to make the discharge run down the axis of the segments, the neon pressure had to be reduced to less than 10 torr. Increasing the power supply voltage did not visibly affect the discharge path at low pressure. A thin "cathode dark space" could be seen between the edge of the cathode and the start of the glow. This varied in length up to about 2 cm, depending on the discharge conditions.

Initially, Mo rings flame-sprayed with zirconia were used as the innermost layer in each segment. However, after less than an hour at high temperatures, the rings curled up and obstructed the laser beam. This did not happen to Mo which had not been sprayed. After a few hours at high temperature, the flame-sprayed Mo rings became brittle.

The 3 cm segments were removed and reassembled in the quartz tube

in groups of four, so as to form 12 cm long segments (Fig. (7.8)). Initially, the alumina spacers could "see" the discharge. A 6 cm long gap was left between the cathode electrode and the nearest segment. Alumina segments were used to shield the o-ring round the quartz tube at the cathode end from the heat generated by the cathode. A 2 cm long gap was left between the anode electrode and the nearest metal segment. In these experiments, the circuit shown in Fig. (2.2) was used, with a 9 nF storage capacitance and a 3.6 nF peaking capacitance. Neon was used as the buffer gas.

It was found necessary to start the discharge at a neon pressure of no more than 6 torr in order to avoid visible arcing between the segments. Typically, the discharge was started at low voltage (about 2 kV supply) and the PRF was slowly increased to about 7 kHz, with the pressure kept at 6 torr. To increase the wall temperature, the supply voltage had to be increased. However, increasing the voltage moved the discharge back towards the windows, causing them to overheat. To avoid this, the neon pressure was increased gradually, keeping it as high as possible without causing arcing between segments.

With the 12 cm long segments, an output power of 1 W was achieved for a supply power of 2.36 kW. When the supply power was increased to 2.86 kW, the laser power rose to 8.4 W in twelve minutes. The neon pressure was 32 torr. This power level lasted for five minutes, and then started to drop. Two effects were observed: a gradual drop in power and an occasional flicker in the beam accompanied by a sudden drop in power. Within fifteen minutes, the power had dropped to 5 W. When the laser was disassembled and the segments inspected, the distribution of copper on the inside surface of each segment was as shown in Fig. (5.10). The inner surface of every alumina ring was coated with copper. Also, the zirconia felt had soaked up some copper, thus reducing its effectiveness as a thermal insulator. The

drop in laser power was therefore due to a combination of the copper rapidly migrating from the hot zone, an increasing proportion of the discharge current flowing through the segments via the copper-coated alumina rings and a gradual drop in the wall temperature as the zirconia felt absorbed copper. There were no signs of damage to either the segments or to the alumina rings.

The segments were rearranged so as to shield the alumina rings from the discharge and were refilled with copper. The segment lengths were the same as in Fig. (7.8). The rate of copper loss proved to be too great to run reliable laser power output experiments. Fifty minutes after lasing started, a supply power of 4.3 kW was required to obtain 3 W of laser power.

The use of Mo segments proved to have an unexpected effect on the optical modes of the laser cavity. "Waveguide" laser modes were observed in the form of two thin beams of green light, at slightly different angles, lying on the bottom of the innermost surface of the segments nearest the cathode electrode. The inside of these segments could be seen through the gap between the cathode flange and the coaxial return. When the alignment of the output coupler was adjusted, their intensity changed. Covering the aluminium mirror at the anode end caused them to disappear. The optical path for these beams must have included reflections from the innermost segment walls and the Mo electrodes, as well as from the end mirrors.

The longest segmented arrangement attempted was made up of three groups of segments: two 27 cm lengths (each of nine 3 cm segments) and one 15 cm length at the cathode end. After a discharge had been run, the heating pattern described in Section (5.5.3) and shown in Fig. (5.11) was obtained. This was different from that of the 12 cm segments (Fig. (5.10)). Here, the highest temperatures were nearer the cathode end. This suggests that some of the discharge current in

segments 1 to 9 (Fig. (5.11)) was conducted through the metal and so the dissipation per unit length was less there. The temperatures required for lasing were not achieved with this arrangement.

7.2.3 LONG METAL TUBES IN THE CVL

The results obtained from the 3 cm and 12 cm segments and the experiments described in Section (7.2.1) showed that in order to use still longer metal tubes, the buffer gas pressure had to be reduced. With neon, as described in Section (7.2.2), there were problems associated with reducing the pressure. However, the results described in Section (4.7.3) showed that laser action with hydrogen as the buffer gas at pressures less than 1 torr was possible. Also, the results of Section (7.2.1) showed that a pulsed discharge in hydrogen could be run through a metal tube 140 cm long. Therefore, in order to increase the segment length, it was decided to use hydrogen. From Section (7.2.1), a length to diameter ratio of 40:1 seemed feasible. Two 40 cm lengths of 2.85 cm ID molybdenum rod were used. The Mo tubes were wrapped in zirconia felt and inserted into a quartz tube in the CVL head. The gap between the two Mo tubes was approximately 1 cm. There was 5 cm between the cathode and the nearest Mo tube, and 4 cm between the other tube end and the anode. A single length of copper wire (weight not measured) was placed in each tube. Figure (7.9) shows a schematic diagram of this arrangement.

Observations of the discharge from the cathode end (looking along the discharge axis) together with the discharge voltage pulses showed the following: as contaminants evolved and the pressure increased, a bright glow could be seen between the two Mo tubes; when the glow between the two tubes was brightest, the voltage pulse was most undermatched, whereas when the glow disappeared, the pulse became

overmatched. When the discharge was switched off after running with 1 kW drawn from the power supply, only the Mo tube nearer the anode electrode was red hot (measured as 800°C).

After one more decontamination run which lasted for over two hours, an attempt was made to obtain lasing action. At a PRF of 10 kHz, a supply voltage of 3.5 kV and a supply power of 1.6 kW, lasing was observed, although the power was very low (a few milliwatts). It was not possible to obtain more power because the cathode end window was being coated with a brown material. The anode window appeared to be clean. When the discharge was switched off, the pressure was just over 1 torr, but rapidly dropped to 0.5 torr, showing that over 50% of the buffer gas had been composed of contaminants.

The windows were removed and inspected. The nylon window mounts were damaged, having been partially melted. The o-rings had hardened. The anode window had a brown annular deposit around its rim. The cathode window had a similar deposit plus a copper-coloured deposit in the centre. The elements in these deposits were identified using an electron microprobe (JOEL Superprobe 733). The only element detected on the anode window was Si, from the window itself. The brown material on both windows was lifted off by the electron beam. In the operator's opinion, the material was probably some sort of hydrocarbon. If so, it must have come from the nylon window mounts and/or the o-rings. When the deposits on the cathode window were inspected, Si was again detected. Also present were S, Ni, Cr, Fe and P, showing that sputtering from the stainless steel flange must have occurred. Molybdenum and copper may have been present, but at very low levels. The relative concentrations of these elements was not known.

While the discharge was running, the brown material appeared on

the windows first. It is possible that the addition of the hydrocarbons to the discharge, especially around near the cathode, may have affected the cathode processes. This could then have resulted in material being sputtered from the steel flange and deposited onto the window.

7.3 THEORY

7.3.1 INTRODUCTION

Having demonstrated that a copper vapour laser discharge can operate along the axis of a metal tube, the question arises as to how much influence does the metal wall have on the discharge. In the following sections, it will be argued that the most important properties of the plasma in this respect are the breakdown voltages for various paths (as determined by Paschen's Law), the Debye length and the plasma frequency.

7.3.2 PASCHEN'S LAW

Paschen's Law (Section (1.4.2)) must apply to the gaps between the segments as well as to the gap between the electrodes. If field enhancement effects, due to sharp edges or to preionization, can be neglected, it is possible to estimate the breakdown voltage for two of the possible discharge paths between the electrodes : directly from the cathode to the anode through the gas; from the cathode to the anode via the metal segments. Table (7.1) shows the breakdown voltages (from Fig. (1.11)) at various neon pressures (at room temperature) for the direct route between the electrodes and for the route through the segments for two segment lengths (3 and 12 cm). As

expected, the lower the pressure, the higher is the breakdown voltage through the segments compared with the breakdown voltage directly between the electrodes. Therefore, the lower the pressure, the more likely is breakdown to be achieved directly between the electrodes. Although this agrees with experimental observations, account must also be taken of the fact that the discharge gap is overvolted, so that it is possible for the breakdown voltage for both paths to to be exceeded. Also, there are actually an infinite number of discharge paths between the electrodes, since the discharge current could run onto any segment from the axial discharge and off again into the discharge from any point.

As the wall and plasma temperatures increase, the gas density will decrease. Therefore, the breakdown voltage for the small gaps between the segments will increase as the product pd/T (where T is the gas temperature) decreases, and so moves up the left hand side of the Paschen curve.

7.3.3 DEBYE LENGTH

As discussed in Section (1.2), if a metal tube in contact with a gas discharge is too long (greater than d_{max} in equ. [1.1]), the potential of one end of the tube will become positive with respect to the adjacent plasma. In this case, electrons will be attracted to the positive end of the tube. If the flow of electrons is great enough, an arc will form and the current in the arc will then conduct through the metal walls of the tube. However, under certain circumstances, the electrons in the plasma will be shielded from the positive charges on the walls.

If a positive charge is placed in an initially neutral, uniform plasma, the electrons in the plasma will move towards the charge and

the ions will move away from it. In doing so, the charged particles shield the positive charge so that its electric field has no effect on the rest of the plasma. The distance over which the field of the positive charge extends is given by the Debye length λ_D [1],

$$\lambda_D = [\, k\, T_e\, e_o / n\, e^2 \,])^{1/2} \text{ metres} \quad , \qquad [7.1]$$

where T_e is the electron temperature and n is the electron density. In the case of a metal tube or segment in the CVL, if part of the wall does become positively charged with respect to the adjacent plasma, the electrons in the plasma nearest the wall will be attracted to it. As they move towards the wall, they will tend to shield electrons further away from the field produced by the charges on the wall. If the Debye length is much smaller than the tube radius, the charge distribution in the plasma will be such that the bulk of the plasma will be shielded from the wall charges.

7.3.4 PLASMA FREQUENCY

Calculations can show whether or not the Debye length is short enough compared to the tube radius for the bulk of the plasma to be screened from the walls. However, the above argument will only hold in the case of the CVL if the electrons and ions can move to shield the plasma from the radial electric field on a timescale much shorter than the risetime of the current pulse. A measure of the speed with which the plasma can screen out any perturbation is given by the plasma frequency w_p [1], where

$$w_p = [\, n\, e^2 / m\, e_o \,]^{1/2} \text{ rads/sec} \quad , \qquad [7.2]$$

and n is the electron density (m^{-3}). From this, the response time of the plasma is estimated to be given by

$$t_r = 0.11 \; / \; n^{1/2} \quad \text{secs} \qquad [7.3]$$

7.3.5 CONCLUSION

The arguments put forward in the previous two sections suggest that if the electrons and ions in the plasma can move fast enough, and the Debye length is much less than the tube radius, the electrons in the plasma will be isolated from the electric field produced by the charges on the walls. In effect, the bulk of the plasma will not "know" whether the walls confining the discharge are metal or ceramic.

7.4 DEBYE LENGTH AND PLASMA RESPONSE TIME IN THE CVL

In order to establish the Debye length and plasma response time under various conditions in the CVL discharge, equs. [7.1] and [7.3] were inserted into the computer program which models the CVL discharge (Chapter 3).

Figures (7.10) and (7.11) show how the Debye length and plasma response time vary during the first 500 ns of the discharge when the tube is cold and the initial electron density is low. The current pulse through the laser discharge is also shown. The curves have been drawn for both low and high Ne pressures. Figures (7.12) and (7.13) show the Debye length and plasma response time in the hot zone for different initial electron densities when the wall temperature is near optimum. When the tube is cold, and the neon pressure is 20 torr, the Debye length is greater than 1 mm over most of the first 200 ns of the

discharge (Fig. (7.10)). Of greater importance, however, is the plasma response time, which is greater than 5 ns under the same conditions (Fig. (7.11)). This is not negligible compared with the risetime of the current pulse. It is likely, therefore, that the electric field produced by charges on the walls will penetrate much further into the discharge than the Debye length. When the neon pressure is reduced, both the plasma response time and the Debye length fall (Figs. (7.10) and (7.11)). The plasma forming more than one millimetre away from the tube wall should therefore be shielded from the wall charges during the whole of the discharge. When the tube is hot, the electron/ion density is much higher and the discharge forms more quickly. The Debye length is therefore very small compared to the radius of the tube (Fig. (7.12)) and the plasma response time (Fig. (7.13)) is small compared to the current risetime. It can be seen from Figs. (7.12) and (7.13) that if the electron density at the start of the pulse is increased, the Debye length and the plasma response time become still smaller. Reducing these quantities could be achieved by running the discharge at higher repetition rates.

7.5 MAXIMUM METAL SEGMENT LENGTH IN THE CVL DISCHARGE

Sections (7.3) and (7.4) suggest that arcing will not occur under suitable discharge conditions so that the maximum metal segment length is given by equ. [1.1]. In this section, it will be argued that the segment length can be increased still further.

Assuming discharge conditions such that the walls are isolated from the plasma, positive ions will only move to the walls under random thermal motion. The proof for equ. [1.1] assumes that the ion and electron currents to the walls are equal. However, the slow moving ions will take much longer to reach the walls than the

electrons. During this period, the walls will be more negatively charged than they would be in equilibrium. If the maximum gas temperature is taken to be 4000 K, the average thermal velocity of the ions is 2000 ms^{-1} (equ. [3.6]). Therefore, the time taken for an ion to move directly to the walls from a position on the axis, assuming it collides with no other particles on the way, is 5 us. The ion current to the walls will therefore be less than the electron current during the current pulse as long as the walls are shielded from the plasma. The metal tube will therefore be more negative with respect to the plasma than it would be under equilibrium conditions, resulting in a longer maximum metal segment length than that predicted by equ. [1.1]. However, under conditions where the electric field produced by the charges on the walls can penetrate into the plasma, positive ions will be accelerated to the walls by the radial electric field. In this case, the ion and electron currents will balance each other on a much shorter timescale and the maximum segment length will be correspondingly reduced.

7.6 APPLICATION TO THE CVL DISCHARGE

7.6.1 BEFORE BREAKDOWN

In a CVL, the voltage between the electrodes falls to zero before each pulse. Therefore, the axial plasma potential will also drop to zero. However, there may still be a radial electric field, since the positive ion sheath will only disappear when the plasma fully recombines, which does not happen at high PRFs in the CVL. The potential difference between each segment and the adjacent plasma is therefore dependent on the charge density remaining in the tube from the previous pulse. Therefore, the initial charge on a segment

depends on whether the tube is cold and filled only with the buffer gas, or whether it is hot and there is a large metal vapour density. When the tube is cold, the charge density in the tube is comparatively low, so that the segment potential will be close to the plasma potential at the start of the pulse. It is probably at this point that Paschen breakdown between segments can take place if the sum of the breakdown voltages between the segments is less than the breakdown voltage between the electrodes. When the CVL is hot, the electron/ion density at the start of each discharge is very high (of the order of 10^{10} cm^{-3} or greater). In effect, there is already a plasma between the electrodes. Since the plasma has not totally recombined, there must still be an ion and electron current flowing to the walls. The positive ion sheath will already be in place and so, as the discharge builds up, only high energy electrons will be able to penetrate to the walls.

7.6.2 DISCHARGE DEVELOPMENT

Only when breakdown starts does the DC metal segment theory (Section (1.2)) apply. However, for a pulsed discharge in a long coaxial tube there are added effects that must be taken into consideration, such as the propagation of the ionization wave front and the charging up of the discharge tube walls (Section (1.4.3)). Since the CVL system is coaxial, there is a comparatively large capacitance between the metal segments and the coaxial return. An electron current must therefore flow to the walls to charge this capacitance.

As the discharge develops, the high electron temperature means that more electrons than ions will reach the walls, charging them negatively. The negative charge on the tube walls will repel

electrons and attract positive ions. However, if the Debye length and plasma response time are small compared with the tube radius and current risetime, respectively, the developing plasma will be shielded from the wall potential. As the discharge develops, positive ions will move to the walls. If this flow is fast enough, part of the tube will become positively charged with respect to the plasma during the current pulse. In this case, electrons will move to the part of the tube which is positive with respect to the plasma potential, causing a discharge to form between the cathode electrode and the nearest part of the metal tube. Then, even if the gas does break down, the metal tube and the discharge plasma must be regarded as two conductors in parallel, each with a certain inductance and resistance. The discharge current will divide between them according to the ratio of their impedances and the laser efficiency will be correspondingly reduced. This argument suggests that the current pulse should be as short as possible to ensure that as much of the discharge current as possible has been dissipated in the plasma before the potential of the walls rises above that of the plasma at any point.

7.6.3 AFTERGLOW PROCESSES

By the end of the discharge pulse, when the current has stopped flowing, the walls may still be negative with respect to the plasma. If so, positive ions will flow to them to neutralize their charge. This positive ion current to the walls may increase the plasma recombination rate. A CVL with the discharge confined by a metal tube which is negatively biased by an external circuit would produce a significant improvement in the optimum PRF. In this case, the metal tube would act like the control grid in a thyratron. It could also be used to switch the laser discharge, thus removing the need for a

thyratron.

7.7 CONCLUSION

The copper vapour laser is, at present, limited in its applications and ease of use because of the requirement that the buffer gas be flowed through the laser tube to remove contaminants. For CVLs to gain wider acceptance, the next stage of development should be directed towards the use of materials which are free of contaminants in order that sealed-off tubes may be built. The results described above have shown that metal walls may be used to confine the CVL discharge under certain conditions. Further work will show whether CVLs of this type can compete in terms of power output and efficiency with ceramic-insulated, flowing buffer gas CVLs.

REFERENCES FOR CHAPTER 7

1 : Cherrington B.E.

Gaseous Electronics and Gas Lasers, Pergamon Press (1980)

TABLE 7.1

Ne PRESSURE (torr)	2	5	10	20
BREAKDOWN VOLTAGE (kV) 3 cm SEGMENTS (a)	7.1	5.6	6.2	7.4
BREAKDOWN VOLTAGE (kV) 12 cm SEGMENTS (b)	2.3	2.0	2.4	3.1
BREAKDOWN VOLTAGE (kV) ANODE - CATHODE (c)	1.2	2.3	4.0	6.0

(a) Twenty-three, 3 cm segments; 0.5 cm gap between segments;
2 cm between the anode and the nearest segment;
8 cm between the cathode and the nearest segment.

(b) Six, 12 cm segments; one, 6 cm segment; 0.5 cm gap between segments; 2 cm between the anode and the nearest segment;
7 cm between the cathode and the nearest segment.

(c) 90 cm between electrodes.

FIGURE 7.1 : SCHEMATIC DIAGRAM OF APPARATUS USED TO DETERMINE THE EXTENT OF DISCHARGE PENETRATION INTO A LONG METAL TUBE

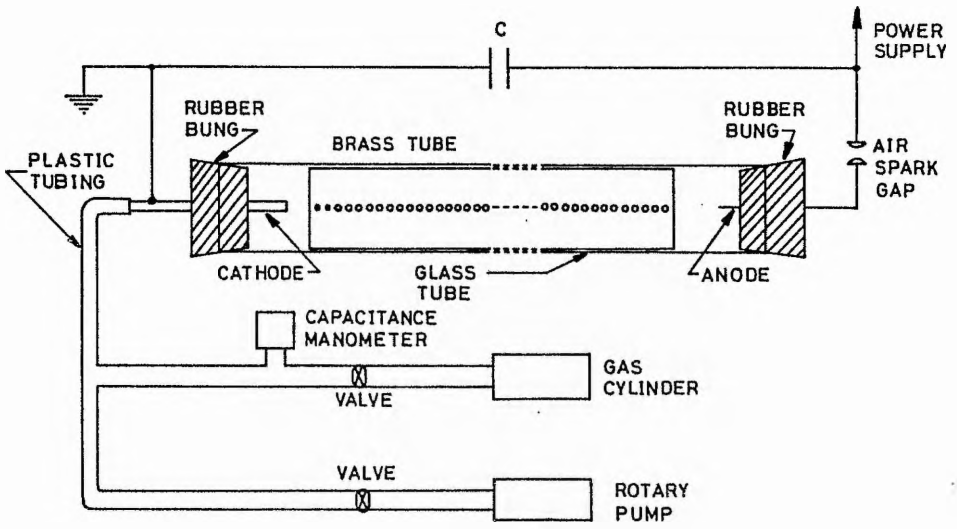

FIGURE 7.2: DISCHARGE CIRCUIT

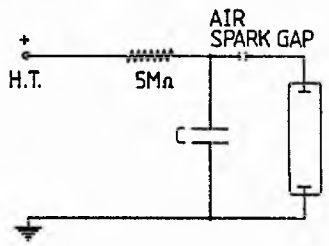

FIGURE 7.3 : DEPENDENCE OF DISCHARGE PENETRATION INTO A METAL TUBE ON ARGON PRESSURE

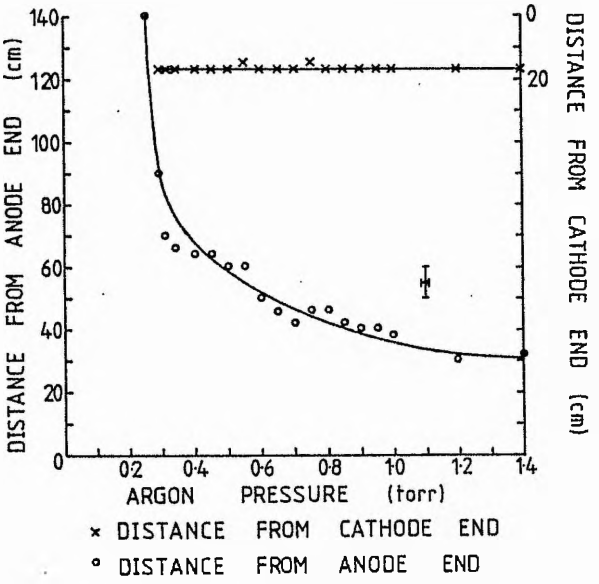

FIGURE 7.4 : DEPENDENCE OF DISCHARGE PENETRATION INTO A METAL TUBE ON HYDROGEN PRESSURE

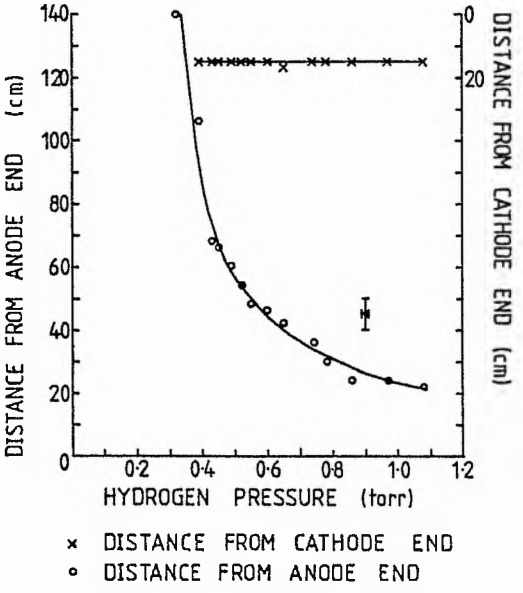

FIGURE 7.5 : DEPENDENCE OF DISCHARGE PENETRATION INTO A METAL TUBE ON HYDROGEN PRESSURE ; LOW INDUCTANCE CIRCUIT

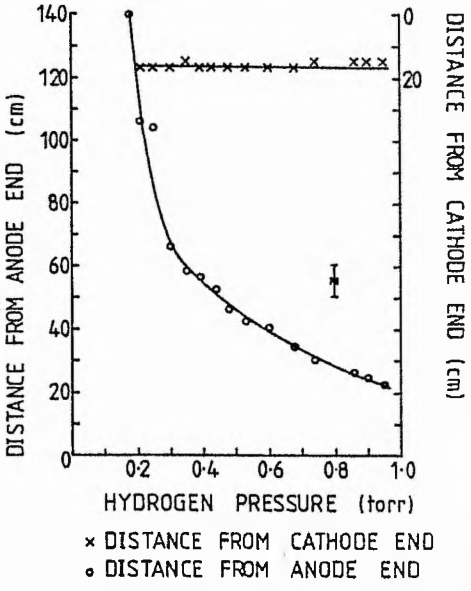

FIGURE 7.6 : SCHEMATIC DIAGRAM OF APPARATUS USED TO DETERMINE THE VOLTAGE ON A FLOATING METAL TUBE IN A PULSED DISCHARGE

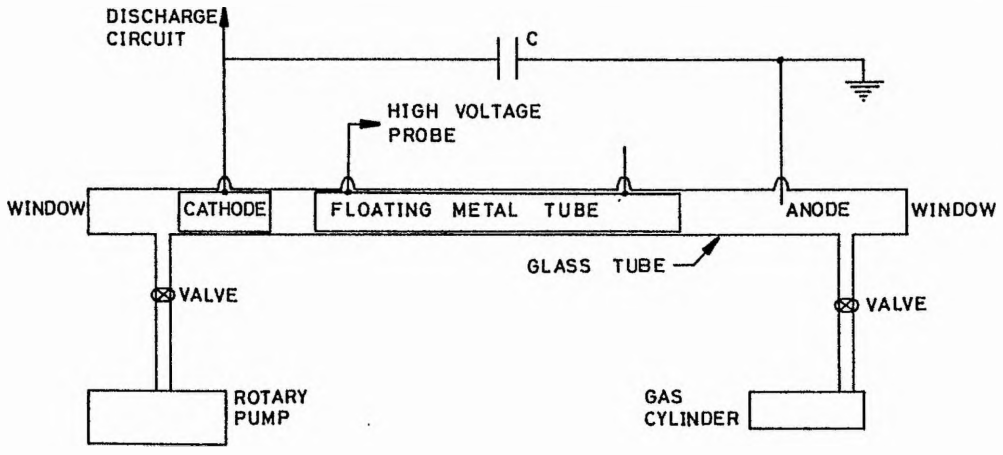

FIGURE 7.7 : VOLTAGES ON THE CATHODE AND A FLOATING METAL TUBE IN A PULSED DISCHARGE UNDER VARIOUS CONDITIONS

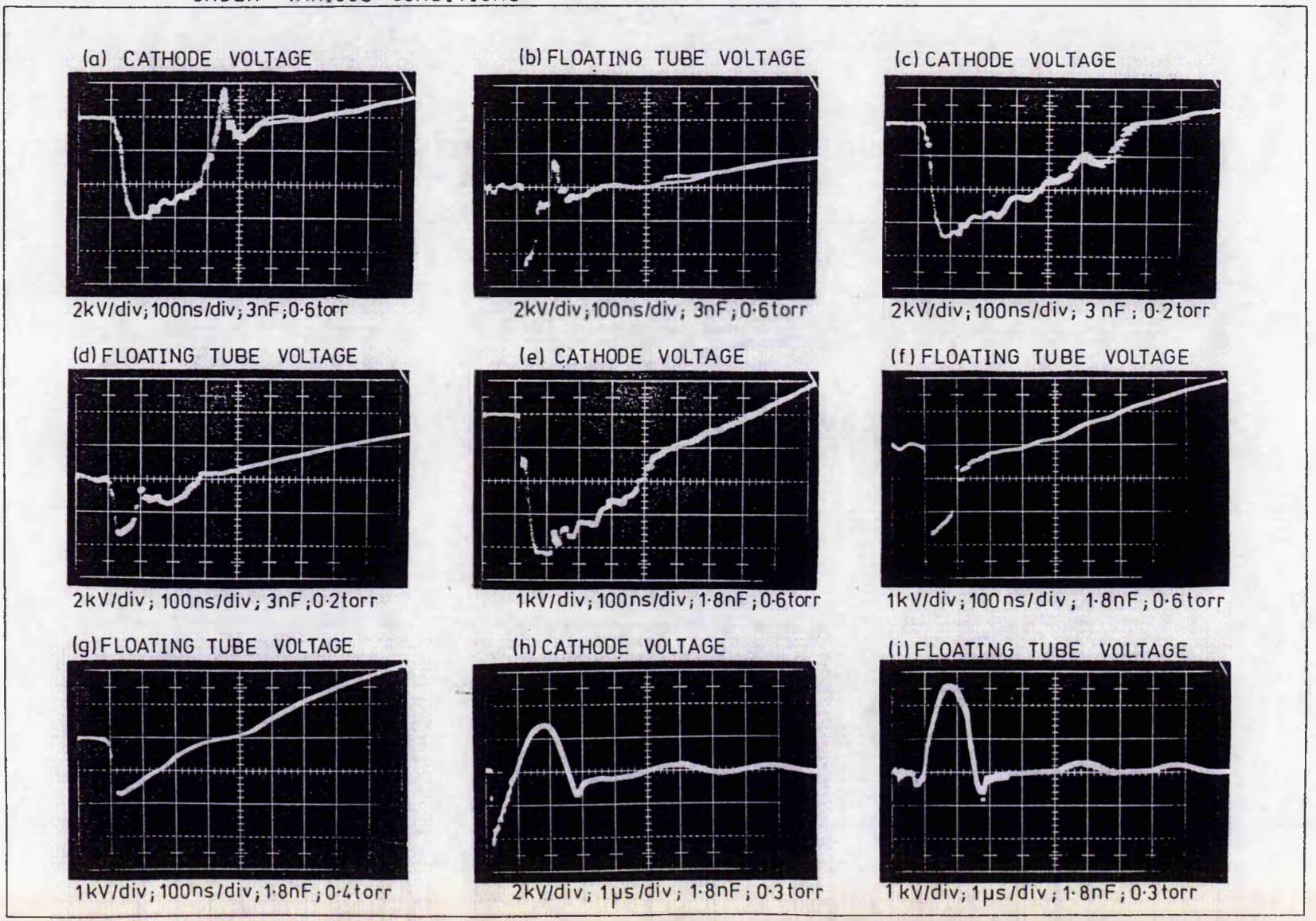

FIGURE 7.8 : SCHEMATIC DIAGRAM OF ARRANGEMENT WHICH FORMED 12cm LONG METAL SEGMENTS IN CVL DISCHARGE TUBE ; SIZES IN cm

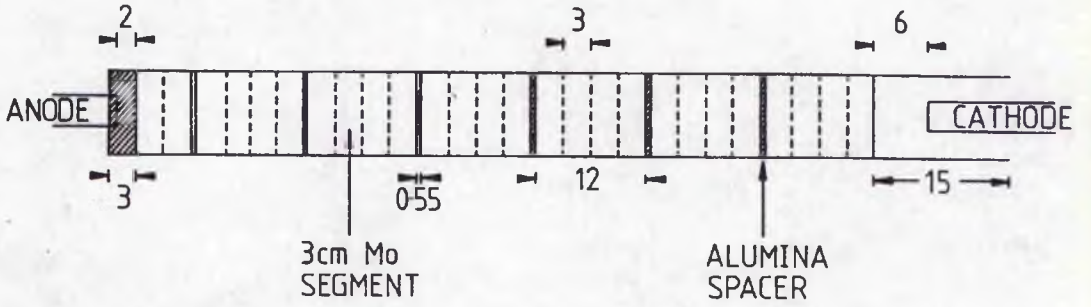

FIGURE 7.9: SCHEMATIC OUTLINE OF THE COPPER VAPOUR LASER WITH THE DISCHARGE CONFINED BY TWO 400mm LONG Mo TUBES

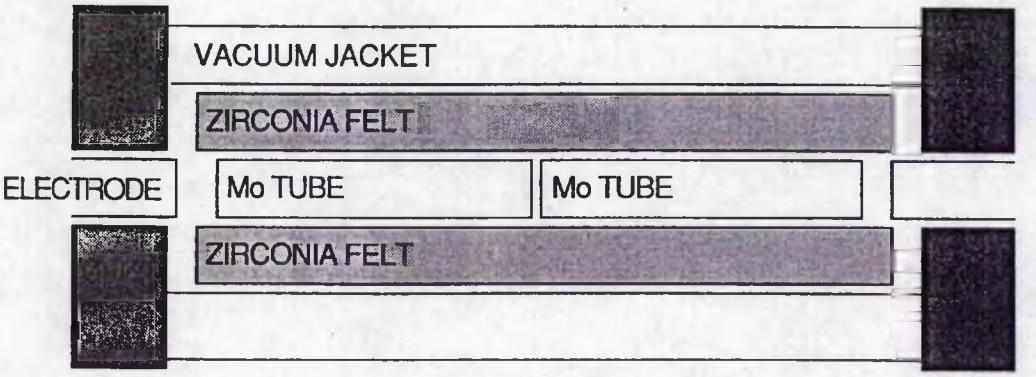

FIGURE 7.10 : VARIATION OF DEBYE LENGTH WITH TIME IN THE CVL DISCHARGE AT 100°C
THE DISCHARGE CURRENT IS ALSO SHOWN
INITIAL ELECTRON DENSITY : 1E7 cm^{-3}
NEON PRESSURE : (a) 2 torr (b) 20 torr

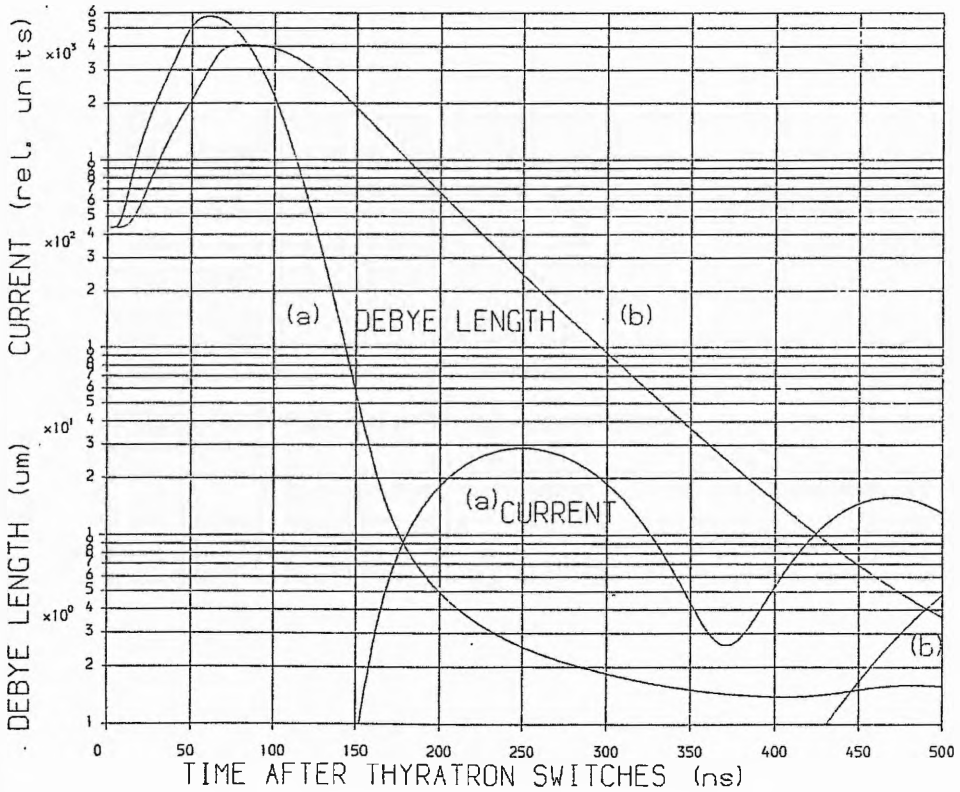

FIGURE 7.11 : VARIATION OF PLASMA RESPONSE TIME WITH TIME IN THE CVL DISCHARGE AT 100°C
THE DISCHARGE CURRENT IS ALSO SHOWN
INITIAL ELECTRON DENSITY : 1E7 cm^{-3}
NEON PRESSURE : (a) 2 torr (b) 20 torr

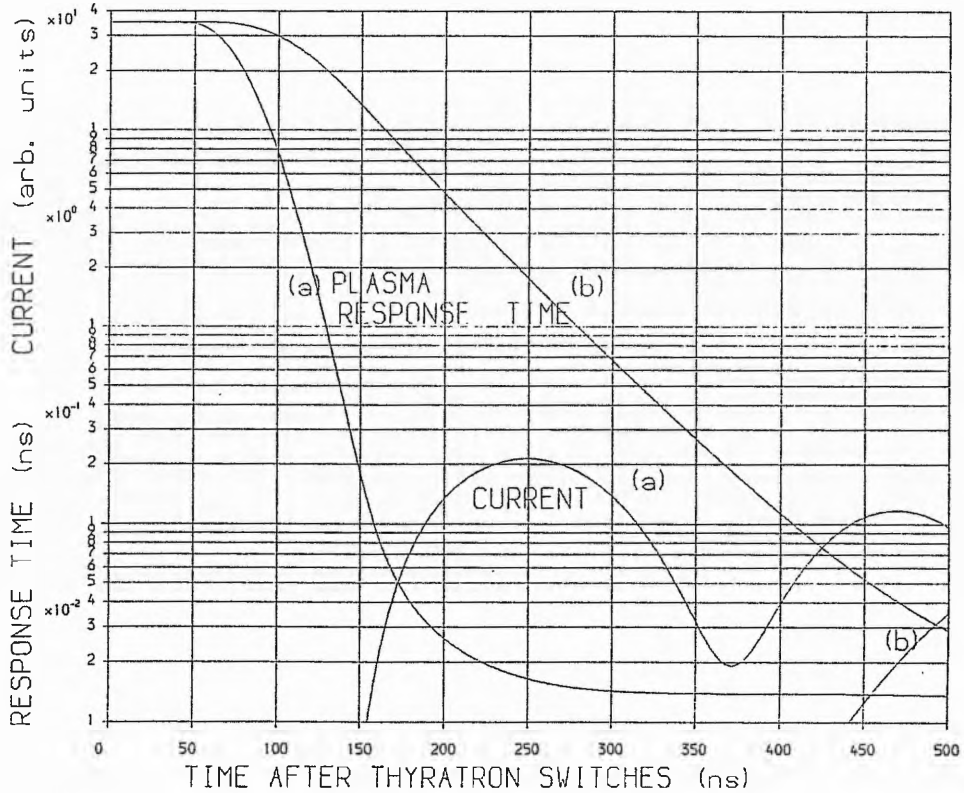

FIGURE 7.12 : VARIATION OF DEBYE LENGTH WITH TIME IN THE HOT ZONE OF THE CVL DISCHARGE. THE DISCHARGE CURRENT IS ALSO SHOWN.
NEON PRESSURE : 20 torr ; WALL TEMPERATURE : 1500°C
ELECTRON DENSITY : (a) 2E11 (b) 2E12 cm^{-3}

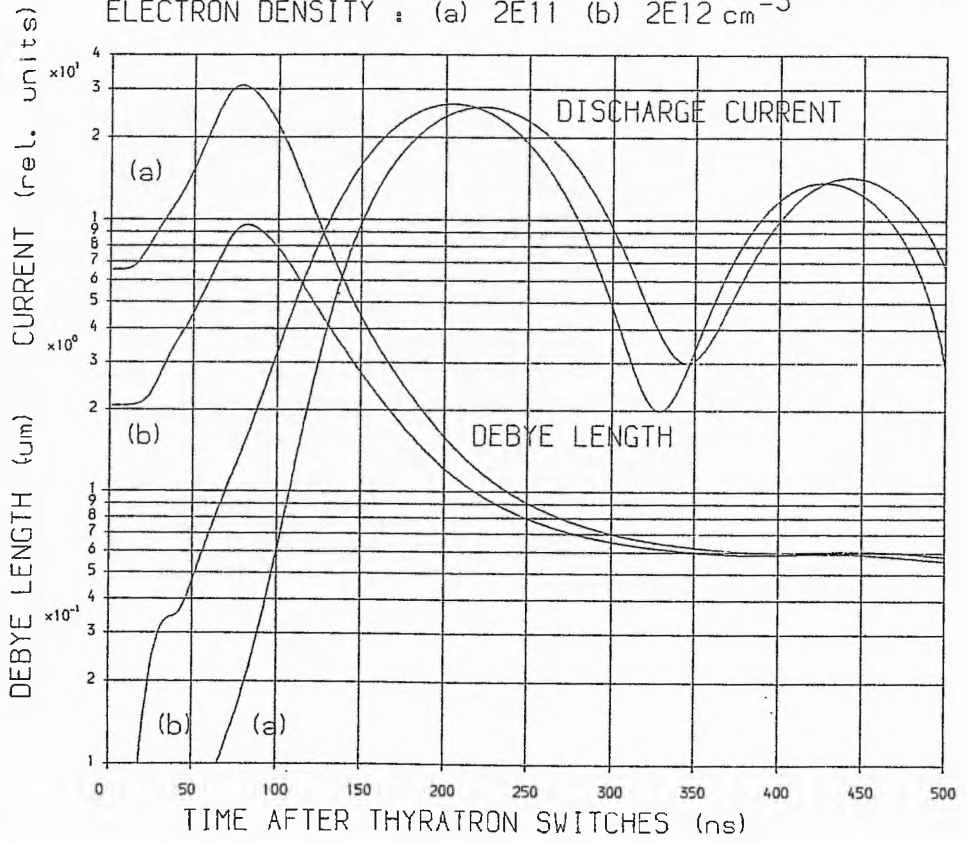

FIGURE 7.13 : VARIATION OF PLASMA RESPONSE TIME WITH TIME IN HOT ZONE OF CVL DISCHARGE DISCHARGE CURRENT IS ALSO SHOWN
NEON PRESSURE : 20 torr ; WALL TEMPERATURE : 1500°C
ELECTRON DENSITY : (a) 2E11 (b) 2E12 cm^{-3}

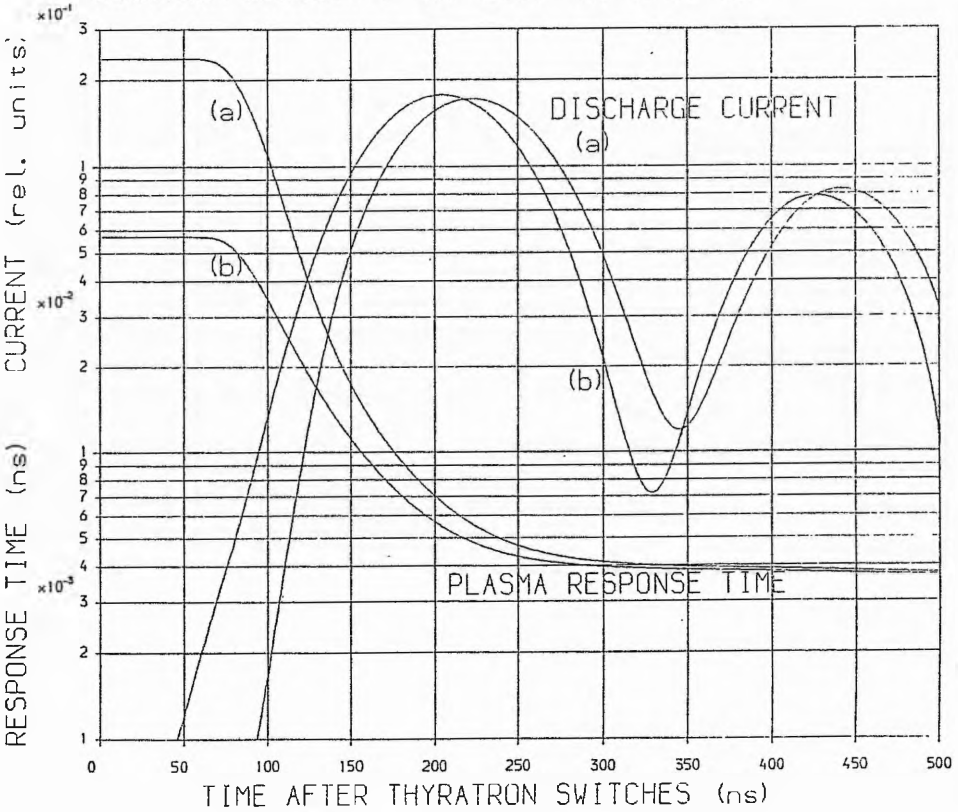

APPENDIX A

A.1 INTRODUCTION

This appendix describes the inductance charging of a capacitor from a DC power supply. It is divided into three sections : a general analysis of inductive charging [1]; a discussion of the effects of magnetic cores and air gaps; and the design of a charging inductor [1,2].

A.2 ANALYSIS OF DC INDUCTIVE CHARGING

The assumptions used in the following analysis are that the effect of circuit inductances outside the charging inductor can be neglected and that the inductance of the charging inductor is constant.

The charging circuit is shown in Fig. (A.1), where V is the power supply voltage, L is the charging inductance, R is the resistance of the inductor and C is the capacitance to be charged. The equation for this circuit, in terms of q, the charge on the capacitor, is

$$L \frac{d^2q}{dt^2} + R \frac{dq}{dt} + \frac{q}{C} = V \quad . \qquad [A.1]$$

Also, the equations

$$q(0) = C\, v(0)$$

and

$$i(0) = (dq/dt)_{t=0} \qquad [A.2]$$

give the initial current i(0) in the inductor and the initial charge

q(0) on the capacitor, when v(0) is the initial voltage on the capacitor. Using Laplace transforms and the initial conditions, equ. [A.1] can be rewritten as

$$L\,[\,s^2q(s) - sq(0) - (dq/dt)_{t=0}\,] + R\,[\,sq(s) - q(0)\,] + q(s)/C = V/s \quad . \qquad [A.3]$$

Rearranged, this becomes

$$q(s) = \frac{CVw_o^2}{s}\,\frac{1}{s^2+2as+w_o^2} + \frac{q(0)\,(s+2a)}{(s^2+2as+w_o^2)} + \frac{i(0)}{(s^2+2as+w_o^2)} \quad , \qquad [A.4]$$

where a and w are given by

$$a = R / 2L \quad ,$$

$$w^2 = 1/LC - R^2/4L^2 = w_o^2 - a^2 \quad .$$

Taking the inverse transform of equ. [A.4], we get

$$q(t) = VC\,[1 - \exp(-at)(\cos(wt) + (a/w)\sin(wt))] + q(0)\exp(-at)\,[\cos(wt) + (a/w)\sin(wt)] + i(0)\exp(-at)\sin(wt)/w \quad . \qquad [A.5]$$

Voltage and current equations can be derived from equ. [A.5] to give

$$v(t) = q(t) / C \qquad [A.6]$$

and

$$i(t) = dq(t)/dt$$

$$= \exp(-at)\left[\frac{(V-v(0))\sin(wt)}{wL} + i(0)(\cos(wt)-(a/w)\sin(wt))\right]. \quad [A.7]$$

Since the duration of the pulse produced by C is very small compared to the period of the charging cycle, the current in the inductor can be assumed to be the same at the beginning and end of each charging cycle. Therefore, we have

$$i(0) = i(T) \quad ,$$

where T is the duration of the charging cycle. Substituting T for t in equ. [A.7], setting it equal to i(0) and rearranging, gives us

$$i(0) = \frac{V-v(0)}{wL} \frac{\sin(wT)}{[\exp(aT)-\cos(wT)+(a/w)\sin(wT)]} . \quad [A.8]$$

This can be substituted into equs. [A.6] and [A.7] to get the following general expressions for the current through L and the voltage on C,

$$i(t) = \frac{V-v(0)\ \exp(-aT)\ [\exp(aT)\sin(wt) + \sin(w(T-t))]}{wL \qquad [\exp(aT)+(a/w)\sin(wT)-\cos(wT)]} , \quad [A.9]$$

and

$$v(t) = V + (V-v(0))\exp(-aT)\left[\frac{\sin^2(wT)}{w^2LC(\exp(aT)-\cos(wT)+(a/w)\sin(wT)}\right.$$

$$\left. - (\cos(wT)+(a/w)\sin(wT))\right] \quad . \qquad [A.10]$$

If the resistance of the inductor can be neglected (effectively R=a=0), then equs. [A.9] and [A.10] become

$$i(t) = \frac{[V-v(0)]\cos[(T-2t)/2\sqrt{LC}]}{\sqrt{(L/C)}\quad \sin(T/2\sqrt{LC})} \quad , \qquad [A.11]$$

and

$$v(t) = V + (V-v(0))\frac{\sin[(2t-T)/2\sqrt{LC}]}{\sin(T/2\sqrt{LC})} \quad . \qquad [A.12]$$

At time t=T, when C is fully charged, we have

$$v(t) = 2V - v(0) \quad . \qquad [A.13]$$

Therefore, if the capacitor is fully discharged at the start of the next charging cycle, it should be possible to charge C up to twice the supply voltage. In practice, however, there are always losses, but if these are kept as low as possible, the voltage on C will be nearly twice the supply voltage.

Resonant charging occurs when the inductor is chosen to satisfy

$$L_R = 1 / (\pi^2 f^2 C) \quad , \qquad [A.14]$$

where f is the charging frequency required. From equ. [A.8], it can be seen that when resonant charging occurs, the current at the beginning

of the charging cycle is zero, since we have

$$f = 1/T = w/2\pi \ .$$

From equ. [A.6], if i(0) is zero, then we get

$$v(t) = V + \exp(-at)[v(0) - V][\cos(wt) + (a/w)\sin(wt)] \quad . \quad [A.15]$$

Equation [A.15] shows that at the start of the charging cycle, the voltage increases slowly, thus allowing plenty of time for the thyratron to deionize.

If L is smaller than L_R, then the current in the circuit will reverse direction and the voltage on the capacitor starts to decrease from its peak value unless a diode is used in series with the charging inductor. This maintains the voltage at its peak value until the capacitor is discharged, assuming that no leakages occur. However, if L is made too small, the inductor core may saturate due to the high peak current (equ. [A.20]). As the charging inductor becomes larger than L_R, the voltage curve becomes increasingly linear, with the voltage still increasing when the capacitor is discharged. However, assuming that the circuit losses are the same, the voltage to which the capacitor is charged is the same as when L_R is used. When linear charging is used, the current in the charging circuit never falls to zero. This can cause the thyratron to fail to recover. Figure (2.12) shows the current and voltage waveforms for L smaller than, equal to, and greater than L_R.

By adding a diode in series with the charging inductor, it is possible to vary the charging frequency over a large range both higher and lower than the resonant charging frequency of the chosen inductor while still achieving voltage doubling. However, there are practical

difficulties with the charging current in that the range of frequencies over which inductive charging can operate depends on the recovery characteristics of the thyratron and the current at which the inductor's core will start to saturate.

A.3 MAGNETIC CORES AND AIR GAPS

By analogy with Ohm's law written in the form

$$i = v / r \quad , \qquad [A.16]$$

the equivalent magnetic circuit equation is

$$\phi = F / R \quad , \qquad [A.17]$$

where ϕ is the magnetic flux, F is the magneto-motive force (MMF) in ampere turns, and R is the magnetic reluctance. The magneto-motive force, F, can be regarded as the force driving the magnetic flux through a medium with magnetic resistance R. The current i which flows through the windings of the coil and the magnetic flux are related by

$$\phi = \mu_o \mu_r N A i / l \quad , \qquad [A.18]$$

where μ_o is the permittivity of free space, μ_r is the relative permittivity of the core material, N is the number of turns in the coil, A is the cross-sectional area of the core and l the mean length of path that the magnetic flux follows. Figure (A.2) shows the relationship between the flux and the current in the inductor. The

inductance of the coil is proportional to the gradient of the curve,

$$L = k \phi / i \quad , \qquad [A.19]$$

where, in an ideal inductor, k is a constant until the core starts to saturate. As the current in the windings of the inductor increases, the magnetic flux increases at the same rate. If the current becomes too large (i_s in Fig. (A.2)), the core starts to become saturated with magnetic flux. Larger and larger increases in current are then required to obtain ever smaller increases in the flux. This saturation causes the inductance to decrease (from equ. [A.19]), which in turn increases the peak current, since we have

$$\hat{i} = V (C/L)^{1/2} \quad . \qquad [A.20]$$

Figure (A.3) shows the effect of saturation in an inductor. In (a), the current waveforms are as expected for a normally operating charging inductor. At a higher average current in (b), the inductor core is becoming saturated at the peak of the current waveform, thus causing the peak current to increase. At a still higher average current, as in (c), the voltage-current characteristics repeat in alternate cycles, with one cycle having a much higher peak current and voltage than the other. In this case, the saturation has lowered the inductance, which increases the current, lowering the inductance still further, thus causing the current to increase rapidly. Also, since the inductance has decreased, the period of the charging circuit

$$t = \pi (LC)^{1/2} \quad , \qquad [A.21]$$

decreases, causing the voltage increase on the capacitor to become

more linear, and the charging current to have time to fall to zero. If there is no charging diode, the voltage will overshoot 2V and the current will go negative. Since the current now starts from zero, the inductance remains higher for longer than on the previous cycle, so the current peak value is smaller. The higher average inductance causes the length of the charging cycle to increase, so that when the capacitor discharges, the voltage on it is significantly less than 2V, and there is still current flowing in the circuit. This allows the next cycle to start from a positive current, so that the saturation level is reached much earlier, causing the current to increase rapidly, and so on. This stable arrangement occurs because there is an alternation between high and low average inductances in each cycle.

The requirement of a charging inductor, therefore, is that it should not saturate at the expected peak charging current, i.e. that its hysteresis curve should be linear. Also, the less area the hysteresis loop encloses, the smaller the losses will be, which will allow the capacitor to be charged closer to twice the supply voltage.

The solution to the problem of saturation is to include an air gap (or gaps) in series with the magnetic flux path. From equ. [A.18], if an air gap is included, the magnetic flux becomes

$$\phi = \frac{N\,i}{(l_m/A_m\mu_o\mu_r) + (l_a/A_a\mu_o)} \quad , \qquad [A.22]$$

where the subscripts m,a denote magnetic material and air respectively. Since $\mu_r \gg 1$, equ. [A.22] is approximately the same as

$$\phi = \mu_o N A_a i / l_a \quad . \qquad [A.23]$$

Since $A_m = A_a$ if fringing effects are neglected, it can be seen from equs. [A.18] and [A.23] that the inclusion of an air gap has the effect of reducing the magnetic flux, as long as the following inequality is satisfied

$$l_a > l_m / \mu_r \quad , \qquad [A.24]$$

and all the other terms are constant.

Figure (A.4) shows a core with an air gap of length l_a. The broken line in Fig. (A.4(a)) shows the average path of the magnetic flux when there is no leakage. Figures (A.4(b)) and (A.4(c)) show the effect on flux leakage of the position of the windings with respect to the air gap. If the windings cover the air gap, the MMF required to drive the magnetic flux round the core is reduced, as is the amount of leakage. Figure (A.4(d)) shows fringing of the magnetic field lines at the air gap (the effect of fringing is not shown in (a),(b),(c)). Fringing is caused by the high magnetic field intensity driving the flux through the air near the sides of the air gap. This increases the effective area of the gap to

$$A = (a + l_a)(b + l_a) \quad , \qquad [A.25]$$

where a,b are the cross-sectional dimensions of the core.

The air gap should be neither too long nor too short. If it is too short, it will not increase the current level at which the core saturates. On the other hand, if it is too long, the inductance of the coil will decrease, since we have

$$L = \mu_o N^2 A_a / l_a \quad . \qquad [A.26]$$

At the same time, the losses due to fringing at the air gap will

increase. As a general guide, the length of the air gap should be less than the dimensions of the cross-section of the core to avoid significant fringing, and at the same time, should be greater than 0.6% of the total magnetic flux path length.

A.4 DESIGN OF A CHARGING INDUCTOR

The peak current in the inductor is calculated by equating the energy stored in the capacitor and inductor half-way through the charging cycle. At this point, the capacitor will be charged to the supply voltage, so it has one quarter of its final energy. However, since a DC power supply is being used, half of the eventual energy to be stored in the capacitor must be in the charging circuit, so that an equal amount of energy must be stored in the inductor. Therefore, we have

$$1/2\ CV^2 = 1/2\ L\hat{i}^2 \quad , \qquad [A.27]$$

where $\hat{i}$ is the peak current flowing through the inductor and V is the power supply voltage. If an inductor can be designed whose core does not saturate at $\hat{i}$, then its inductance will remain constant over the whole of the charging cycle.

The energy stored in the inductor is given by

$$E = B^2 Vol_a / 2\mu_o = 1/2\ L\hat{i}^2 \quad . \qquad [A.28]$$

Therefore, the volume of the air gap is given by

$$Vol_a = \mu_o L \hat{i}^2 / B^2 \quad . \qquad [A.29]$$

Ferrite cores tend to saturate if the magnetic flux density B is greater than 0.32 T, so the inductor is normally designed so that B is less than 0.3 T. Iron cores do not saturate until the flux density is approximately 0.7 T. Equation [A.23] gives an expression for the magnetic flux in an inductor with an air gap. This can be rearranged to give

$$N = B\, l_a / \mu_o \hat{i} \quad , \qquad [A.30]$$

which is the number of turns required to give a specified magnetic flux density, given the current and length of air gap. Equation [A.30] can now be substituted into [A.29] and rearranged to get the following expression for the number of turns required,

$$N = L \hat{i} / B A_a \quad . \qquad [A.31]$$

The process involved in designing a charging inductor is as follows. Choose the required inductance from the resonant charging condition in equ. [A.14]. Using this value, along with the supply voltage and size of capacitance to be charged, the peak current through the inductor can be calculated from equ. [A.20]. Equation [A.29] then allows the calculation of the required volume of air gap, given the maximum magnetic flux density allowed in the core. Finally, either equ. [A.30] or [A.31] will give the number of turns required, taking into account the cross-sectional area of the available cores, and the requirement that the air gap length must be less than the dimensions of the cross-sectional area of the core so as to avoid fringing.

FIGURE A.1 : CHARGING CIRCUIT

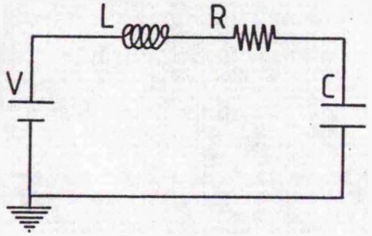

FIGURE A.2 : DEPENDENCE OF MAGNETIC FLUX ON CHARGING CURRENT

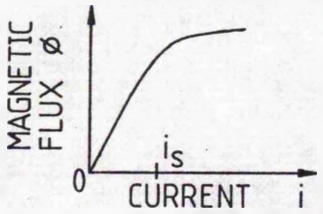

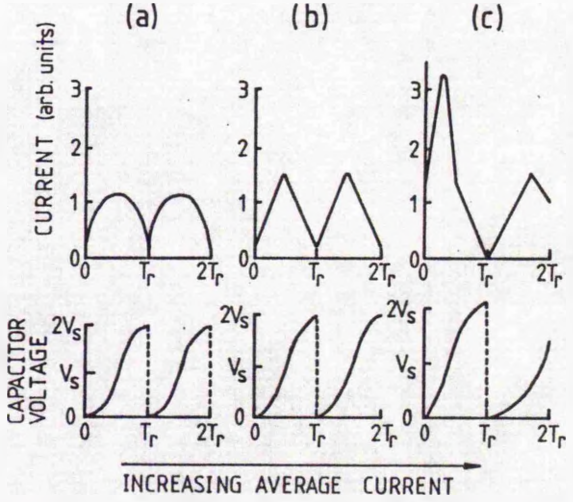

FIGURE A.3 : EFFECT OF SATURATION ON NETWORK CURRENT AND VOLTAGE

FIGURE A.4 : FLUX PATH IN CORE WITH AIR GAP
(a) NO LEAKAGE OF FLUX
(b),(c) EFFECT OF POSITION OF COIL
(d) FRINGING AT AIR GAP

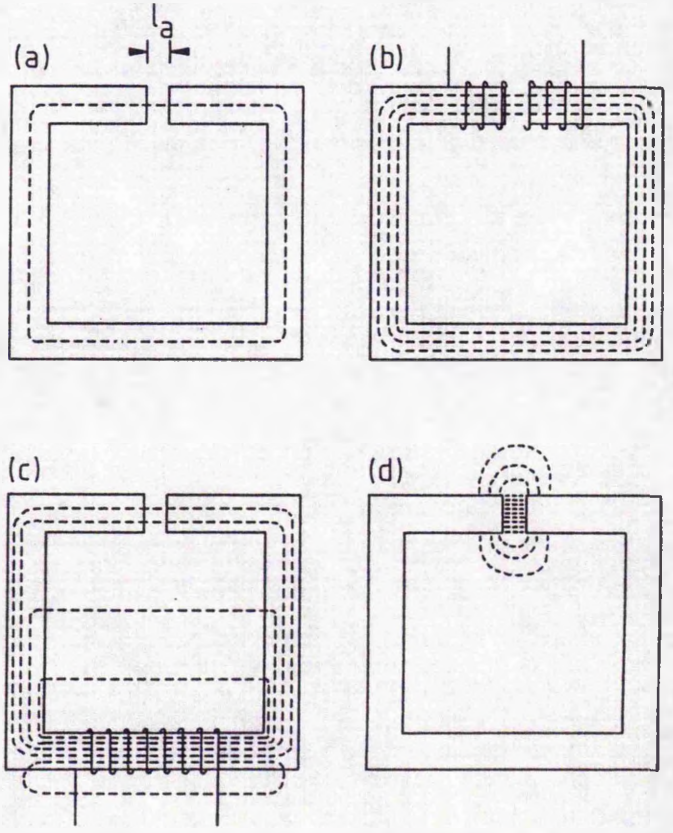

APPENDIX B

B HYDROGEN THYRATRONS

B.1 INTRODUCTION

The thyratron is a gas-filled switch capable of holding off large voltages and conducting large currents at high repetition rates [1,3,4]. The thyratrons which have been used in the CVL discharge circuit have five main components : the cathode, anode, grids, gas reservoir and heaters for the cathode and reservoir. Figure (B.1) shows a schematic diagram of the thyratron. The cathode is coated with a mixture of oxides which have a small work function so that when heated, it emits thermionic electrons. The cathode is heated by the cathode heater and is maintained at earth potential in the circuit used. The anode is the high voltage electrode and is connected to the high voltage components in the discharge circuit. The grids are used to control the switching of the thyratron. The reservoir supplies gas, either hydrogen or deuterium, and significantly extends the operating lifetime of the thyratron by replacing gas which is absorbed in the system. The reservoir itself is a small mass of titanium hydride (or deuteride) which gives off hydrogen when heated by the reservoir heater contained in the base of the thyratron. When the reservoir is at a constant temperature, it maintains a constant gas pressure within the thyratron.

When the thyratron is switched on by applying trigger pulses to the grids, the hydrogen gas breaks down, and the impedance of the thyratron falls to a fraction of an ohm. This allows the energy stored in the external circuit to be discharged through the thyratron

and the load. When this current pulse has ended, the plasma in the thyratron decays until the thyratron has returned to the non-conducting state. Thyratrons can be triggered by low-voltage, low-energy pulses with very little jitter.

Figure (B.2) shows the Paschen curve for hydrogen. Thyratrons operate on the left hand side of this curve, where the breakdown voltage increases as the product pd (torr cm) decreases. This allows narrow gaps and low pressures to hold off very high voltages. At the operating pressure, which is usually a few hundreds of millitorr, the distance between the anode and each grid is such that the breakdown voltage for each gap is greater than both the maximum allowed anode voltage and the breakdown voltage for the anode-cathode gap.

B.2 OPERATION

Figure (B.3) shows ideal current and voltage waveforms for a thyratron, covering the whole sequence of events from triggering to recovery. Initially, there is a large positive voltage on the anode, no current flowing, and a negative bias voltage on the control grid. The bias voltage shields the cathode from the high anode voltage. When a positive pulse is applied to the control grid, the cathode is no longer shielded from the anode and so the gas starts to break down as free electrons are accelerated from the cathode to the anode. As the gas breaks down, the anode and grid voltages fall and the current rises. The rate of rise of the current pulse is determined by the external circuit and the rate of fall of the anode voltage. This period, between triggering and full breakdown, is known as commutation. A large proportion of the total amount of energy dissipated by the thyratron is dissipated during the commutation period. When the gas is fully broken down, the grids and anode will

be at the arc drop voltage (of the order of 100 V, or less) which is determined by the impedance of the plasma and the current flowing in the tube. When the current falls to zero, the anode voltage becomes either positive or negative, depending on the mismatch in impedance between the discharge circuit and the load. Ideally, a small negative voltage on the anode is required, as this stops the thyratron conducting. If the load impedance is greater than the output impedance of the circuit, the anode voltage may remain positive, in which case the thyratron will keep conducting. If conduction does stop, the plasma in the tube starts to diffuse to the walls, where the recombination process mainly occurs. During recovery, the control grid voltage falls towards the bias level, drawing positive ions to it and so speeding up the recombination process. At the same time, the anode voltage increases as the circuit charges up again for the next cycle. If the anode voltage becomes too large too quickly, the thyratron may break down again without a trigger pulse being applied to the control grid. The voltage at which the thyratron hangs-up is called the reignition voltage, and is usually 100 or 200 V. Resonant charging of the circuit storage capacitors is the best charging method because the time taken to reach the reignition voltage is a maximum. The recovery time is the time between the end of the current pulse and the time at which the reignition voltage can be passed without hang-up occurring. The initial gas density determines the plasma density at the start of recovery, and as the plasma density increases, so does the recovery time. Therefore both the initial gas density and the rate of decay of the plasma put an upper limit on the maximum pulse repetition rate.

B.3 DISSIPATION

When the thyratron is triggered. the anode voltage fall at time t is given by

$$e_b = e_{py} - A \exp(t/t_a) \quad , \qquad [B.1]$$

where A is a constant, e_b is the anode potential at a time t after triggering, e_{py} is the initial anode voltage and t_a is the time constant of the fall. The time constant is strongly dependent on the gas density in the thyratron, decreasing with increasing density, but is only weakly dependent on e_{py} and circuit constants. A large proportion of the total anode dissipation occurs during the time taken for the anode voltage to fall to the arc level. Once the arc level is reached, the amount of energy dissipated drops, and remains at a small level until a negative voltage appears on the anode at the start of the recovery period.

The rate of rise of current during commutation is determined by both the rate of fall of the anode voltage and the external circuit. The current rise can therefore be calculated from

$$e_{py} - A \exp(t/t_a) = e_{py} - L\, di/dt - (R+Z)\, i \quad , \qquad [B.2]$$

where R is the load resistance and L and Z are the inductance and impedance of the lumped pulse forming network (Fig. (B.4)). Using Laplace transforms, the current can be shown to be

$$i = A\, [\exp(t/t_a) - \exp(-t/t_c)] \,/\, L(1/t_a + 1/t_c) \quad , \qquad [B.3]$$

where t_c is the circuit time constant (= L/(R+Z)).

The energy dissipated by the thyratron during commutation is obtained by multiplying the current and voltage together and integrating over the commutation period. The duration of the commutation period can be estimated from equ. [B.1] by assuming it is the time taken for e_b to fall to zero. The energy dissipated is therefore given by

$$E = e_{py}^2 \, t_a^2 \, t_c \, / \, (2L \, (t_a + t_c)) \quad . \qquad [B.4]$$

Equation [B.4] can be rewritten to include the peak current, which is determined by the external circuit, to give

$$E = e_{py} \, i_b \, t_a^2 \, / \, 2(t_a + t_c) \quad , \qquad [B.5]$$

where i_b is the peak current ($=e_{py}/(R+Z)$). To obtain the power dissipated, Equation [B.5] is multiplied by the pulse repetition rate. Equation [B.5] shows that the main causes of dissipation during commutation will be a reduction in gas density, which increases the anode fall time constant, or an increase in the load resistance, which decreases the circuit time constant. Since the gas density is inversely proportional to the temperature, the density may vary in different parts of the thyratron. In particular, if the anode is not cooled sufficiently, the gas density will drop near the anode, and thus cause more heat to be dissipated during commutation and so increase the anode temperature still further. During the steady-state conduction period, energy is still dissipated, but provided the maximum recommended values for peak and average anode currents are not exceeded, the heating caused by this is not a problem.

Dissipation at the anode can also be caused by a negative voltage appearing from a reflection at a mismatched load. This field will

accelerate ions from the plasma to the anode, causing heating effects. The peak value of the inverse current is proportional to the amplitude of the negative voltage present during this current flow. The peak inverse current is also directly proportional to the peak forward current pulse, since the forward current pulse determines the ion density in the anode region. It has been shown that the inverse current is independent of the gas pressure [4]. The power dissipated by the inverse current is given by

$$P_{inv} = k\, e_{px}^2\, i_b\, f \quad , \qquad [B.6]$$

where e_{px} is the peak inverse voltage and k is an empirically determined constant which increases with the volume of the grid-anode region in different types of thyratron.

The energy dissipated by the thyratron is therefore governed by the gas density within the thyratron and by the components in the discharge circuit. Provided the circuit is arranged so that the maximum peak and average currents are not exceeded, and the load is matched as closely as possible to the circuit, the main source of dissipation will be in the commutation period. Equation [B.5] shows that in order to reduce dissipation to a minimum during commutation, the anode fall time should be as short as possible. In order for this to happen, the gas pressure in the thyratron must be as high as possible without causing recovery problems and the thyratron must be adequately cooled to ensure that the maximum body temperature is not exceeded.

When the CVL discharge circuit was run, its operating conditions were arranged so that the inverse (reflected) voltage appearing on the thyratron anode after the discharge was always less than -2 kV. However, there were problems with overheating of the anode when the

CX1535 was air-cooled (Section (2.3.3)), due mainly to losses during the commutation period and to inadequate cooling of the thyratron base. The dissipation problems were solved by immersing the CX1535 in oil.

B.4 HOLLOW ANODE THYRATRONS

Conventional thyratrons can only conduct in one direction, so that if there is a large current reversal in the circuit which causes a large negative voltage to appear on the anode, any ions in the grid-anode region which have not recombined will be accelerated towards the anode. If the velocity of these ions is high enough, they can damage the anode when they collide with it by causing the surface to sputter. If the negative voltage is large enough, the grid-anode gap may break down, causing more sputtering. To enable thyratrons to conduct in the reverse direction, a hollow anode structure is used [5]. In this design (Fig. (B.5)), the anode is a hollow box. Since there is a comparatively large volume in this box, the plasma there decays slowly. If the anode voltage then swings negative, there is sufficient plasma for the conduction of electrons from the anode to the cathode to occur. The size and duration of the voltage reversal are limited by the amount of plasma contained within the anode box, since the plasma can only be produced during forward conduction without damaging the thyratron. A hollow anode thyratron (EEV CX1625) was used in both the CVL and GVL discharge circuits (Sections (2.4) and (6.2.3), respectively).

REFERENCES FOR APPENDICES A AND B

1 : Glasoe, Lebacqz, (Editors), PULSE GENERATORS
DOVER PUBLICATIONS (NEW YORK) (1948)

2 : Matsch L.W., CAPACITORS, MAGNETIC CIRCUITS AND TRANSFORMERS
PRENTICE-HALL (1964)

3 : EEV HYDROGEN THYRATRON PRODUCT DATA HANDBOOK (1985)

4 : Marton L. (Editor)
ADVANCES IN ELECTRONICS AND ELECTRON PHYSICS VOL. XIV, 207-264

5 : Menown H., Neale C.V.
"Thyratrons for Short Pulse Laser Circuits"
13th PULSE POWER MODULATOR SYMPOSIUM, BUFFALO, NEW YORK, 1978

FIGURE B.1: TRIPLE GRID THYRATRON

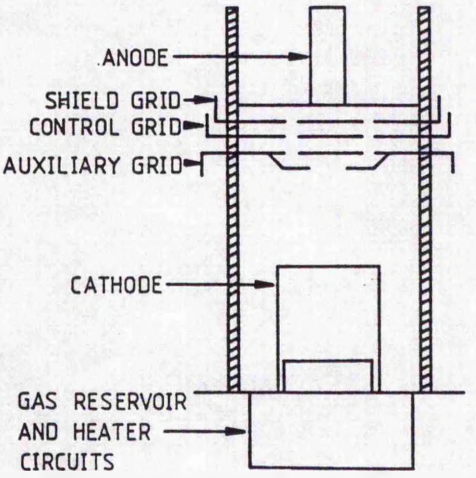

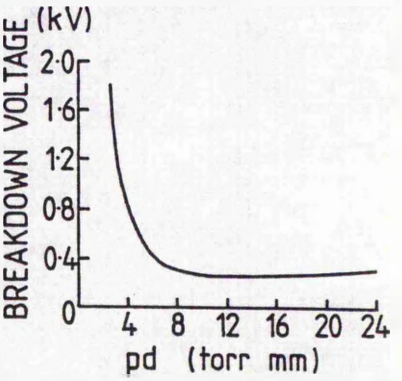

FIGURE B.2: PASCHEN CURVE FOR HYDROGEN

FIGURE B.3: CURRENT AND VOLTAGE WAVEFORMS OVER A CYCLE OF OPERATION OF A THYRATRON

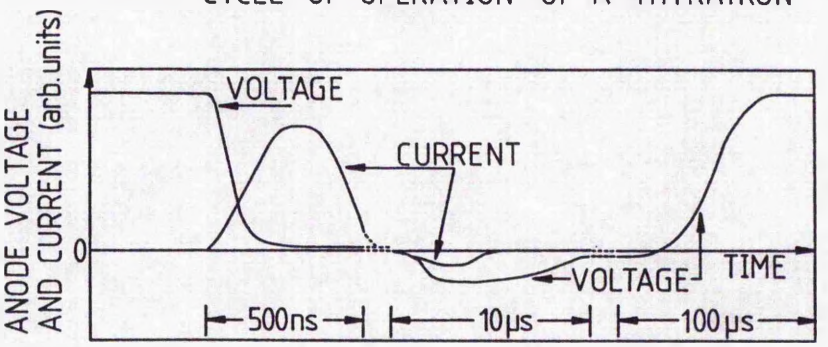

FIGURE B.4: EQUIVALENT CIRCUIT FOR THE DISCHARGING OF A THYRATRON-SWITCHED CIRCUIT

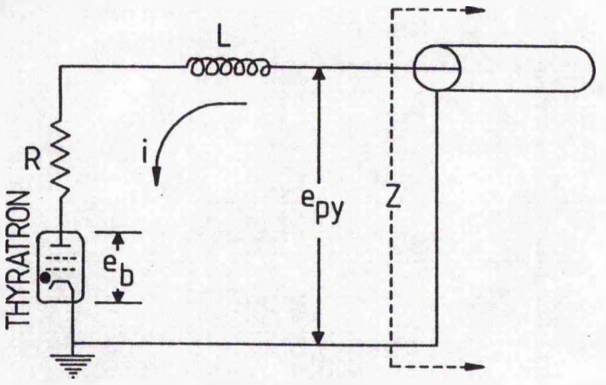

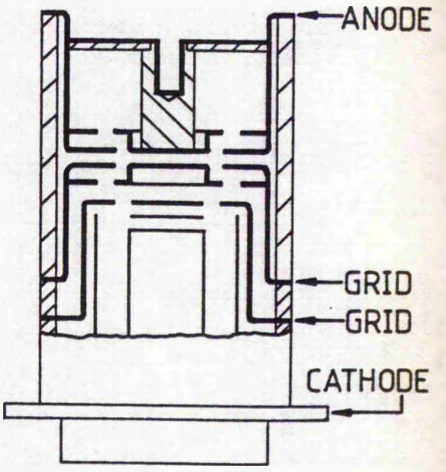

FIGURE B.5: HOLLOW ANODE THYRATRON

APPENDIX C

```
! PROGRAM TO MODEL THE KINETICS OF THE COPPER VAPOUR LASER
! DURING THE DISCHARGE PULSE
!
! INTITIALIZATION OF VARIABLES
!
      implicit none
      real inc,incez
      real zz,dummy,answer,reply
      common reply
      real ne,neold,energy,denergy,dne
      real nscool,nshot
      real debout(500),resout(500)
      real vout(500),fout(500),rpout(500),lpout(500)
      real ilout(500),i2out(500)
      real nm1out(500),nm2out(500),nl1out(500),nl2out(500)
      real npsout(500),nmneout(500),nrneout(500),npsneout(500)
      real laseouty(500),laseoutg(500),lastotal(500)
      real lmax(500),tempout(500)
      real neout(500),cuionout(500),neionout(500),timeout(500)
      real rp,lp,l1,l2,fc,fh,conc,conh,d1,d2,diam,rad,r1,r2
      real rpc,rph,lpc,lph
      real i1,i2,di1,di2,vcs,vcp,dvcs,dvcp,vl,cs,cp
      real vlc,vlh,vc0,vs,ton
      real s0,s1,s2,s3,s4,s5,s6,s7,s8,s9
      real h1,h2
      real pf,psel,pel,pex,pion
      real ve,v1,v2,v3,v4,v5,v6,v7,v8,v9,v10,v11,v12
      real v13,v14,v15,v16,v17,v18,v19
      real ncu,nm1,nm2,nl1,nl2,nps,cuion
      real nep,nne,nmne,nrne,npsne,neion
      real c,k,q,pi,kt
      real me,mcu,mne
      real e0m1,e0m2,e0l1,e0l2,e0ps,el1ps,el2ps
      real e0icu,em1i,em2i,el1i,el2i,epsi
      real e0mne,e0psne,empsne,e0ine,emine,epsine
      real xmtelcu,xmtmcu,xmtlcu,xmtpscu
      real xmtelne,xmtmne,xmtpsne
      real xm10,xm20,xl10,xl20,xps0,xpsl1,xpsl2
      real xm0ne,xps0ne,xpsmne
      real x0m1,x0m2,x0l1,x0l2,x0ps,xl1ps,xl2ps
      real x0icu,xmicu,xlicu,xpsi
      real x0mne,x0psne,xmpsne
      real x0ine,xmine,xpsine
      real xxcu,xxne
      real twall,temp,tempold,tgas,tgasold
      real time,duration,t
      real rionmne,rion0ne,rionpsne,r0mne,rmpsne,r0psne
      real rionrne,r0rne,rrpsne
      real rion0,rionm1,rionm2,rionl1,rionl2,rionps
      real rm1,rm2,rl1,rl2,rl1ps,rl2ps,rps
      real rdm1,rdm2,rdl1,rdl2,rdpsl1,rdpsl2,rdps0
      real rdm0ne,rdps0ne,rdpsmne,rdr0ne,rdpsrne
      real g0,gm1,gm2,gl1,gl2,gps
      real xstimy,xstimg
      real sumy,sumg
      real ly,lg,ll1,ll2,lps0,lpsl1,lpsl2,lpsmne,lr0ne
      real radtrap1,radtrap2
      real rspps0,rspl10,rspl20,rsppsl1,rsppsl2,rspl2m1,rspl1m2
      real rsppsmne,rspr0ne
```

```
      real numouty,numoutg,useabley,useableg
      real angle,cavityl,reflect
      real rlasey,rlaseg,nlasey,nlaseg
! variables for cool zone : same as above, but cz stands for
! cool zone
      real nczrne,nczmne,nczpsne,nczne,nczi
      real necz,neczold,tempcz,tempczold,tgascz,tgasczold
      real vecz,ktcz,energycz
      real h1cz,h2cz
      real v14cz,v15cz,v16cz,v17cz,v18cz,v19cz
      real s4cz,s6cz,s7cz,s8cz
      real pioncz,pexcz,pfcz,pelcz,pselcz
      real rcz0i,rczmi,rczpsi,rcz0m,rcz0ps,rczmps
      real rczri,rcz0r,rczrps
      real xczps0ne,xczpsmne,xczm0ne
      real rdczps0ne,rdczpsmne,rdczm0ne,rczsppsmne
      real rdczpsrne,rdczr0ne,rczspr0ne
      real dnecz,denergycz
!
!********************** SET VALUES OF CONSTANTS *********************
!
! set up duration of program and variables associated with
! timing - zz is used in arrays to store only some results
!
      time = 1.0e-10
      zz = time / 1.0e-9
! length of program
      duration = 300.0
      duration = duration * 1.0e-9 / time
! physical constants
      c = 3.0e10
      k = 1.3807e-23
      pi = 3.14159
      q = 1.602e-19
! masses of particles
      me = 9.109534e-31
      mcu = 1.055e-25
      mne = 3.350855e-26
! energy levels
      e0m1 = 2.23e-19
      e0m2 = 2.63e-19
      e011 = 6.07e-19
      e012 = 6.12e-19
      e0ps = 9.13e-19
      el1ps = 3.06e-19
      el2ps = 3.01e-19
      e0icu = 1.24e-18
      em1i = 1.017e-18
      em2i = 9.77e-19
      el1i = 6.33e-19
      el2i = 6.28e-19
      epsi = 3.27e-19
      e0mne = 2.660e-18
      e0psne = 2.96e-18
      empsne = 3.0e-19
      e0ine = 3.455e-18
      emine = 7.95e-19
      epsine = 4.95e-19
! statistical weights of each level
      g0 = 2.004
      gm1 = 1.22
      gm2 = 0.806
```

```
      gl1 = 0.659
      gl2 = 1.338
      gps = 2.0
!
! cross-sections
!
! cross-sections for ionization and excitation
      x0m1 = 3.3e-16
      x0m2 = 2.2e-16
      x0l1 = 3.5e-16
      x0l2 = 7.5e-16
      x0ps = 2.4e-16
      xl1ps = 4.0e-15
      xl2ps = 4.8e-15
      x0icu = 3.0e-16
      x0mne = 6.0e-18
      x0psne = 2.0e-18
      xmpsne = 6.0e-15
      x0ine = 2.0e-17
! elastic scattering cross-sections
        xxcu = 8.0e-15
        xxne = 3.0e-16
! momentum transfer cross-sections
      xmtelcu = 8.0e-15
      xmtlcu = 1.0e-15
      xmtmcu = 4.0e-16
      xmtpscu = 6.0e-16
      xmtelne = 2.0e-16
      xmtmne = 4.0e-17
      xmtpsne = 4.0e-17
! stimulated emission cross-sections
      xstimy = 2.0e-15
      xstimg = 2.0e-15
!
! lifetimes for spontaneous transitions on the lines between
! the upper levels and the metastable levels
!
! lg is the lifetime of the green transition
! ly is the lifetime of the yellow transition
      lg = 770.0e-9
      ly = 370.0e-9
! lifetimes for transitions from pseudo-state
      lpsl1 = 20.e-9
      lpsl2 = 10.e-9
      lps0 = 100.e-9
! Ne lifetimes
      lpsmne = 2.0e-9
      lr0ne = 2.0e-9
! other constants
      angle = 5.0e-5
      cavityl = 200.0
      reflect = 0.1
! circuit constants
      l1 = 1.2e-6
      l2 = 8.0e-7
      cs = 6.5e-9
      cp = 3.2e-9
      ton = 10.0e-9
      r1 = 1.0
      r2 = 1.0
      vc0 = 10.0e3
      d1 = 0.9
```

```
      d2 = 0.5
      diam = 0.02
      rad = diam / 2.0
! gas, electron and wall temperatures and electron densities
      tgasold = 1800.0
      tgasczold = tgasold / 2.0
      tempold = 1800.0
      tempczold = tempold / 2.0
      neold = 2.0e11
      neczold = 1.0e11
      twall = 1500.0
! Ne pressure
      nep = 20.0
!
! SET INITIAL VALUES OF VARIABLES
!
! initial temperature of electrons and gas temperature
101   temp = tempold
      tempcz = tempczold
      tgas = tgasold
      tgascz = tgasczold
! initial electron densities
      ne = neold
      necz = neczold
! initial populations of Cu metastable levels
      nm1 = 1.0e12
      nm2 = 1.55e11
! initial total amount of energy in each laser pulse
      sumy = 0.0
      sumg = 0.0
! initial number of laser photons in cavity
      nlasey = 0.0
      nlaseg = 0.0
! initial circuit conditions
      vcs = vc0
      vcp = 0.0
      i1 = 0.0
      i2 = 0.0
301   do dummy = 1,35
      print*,' '
      end do
!
! title of program
!
      print*,'COPPER VAPOUR LASER SIMULATION PROGRAM'
      print*,'  '
      print*,'c G.CLARK (1986)'
      do dummy = 1,5
      print*,' '
      end do
!
! routine to change initial variables
!
      call menu(twall,nep,ne,necz,temp,tgas,d2,d1,diam)
      if (reply .le. 6) then
      call change(twall,nep,ncu,nne,necz,ne,temp,tgas)
      end if
      if (reply .eq. 7) then
      call circuit(l1,l2,cs,cp,vc0,r1,r2,ton)
      end if
      if (reply .ge. 8 .and. reply .le. 10) then
      call tube(d1,d2,diam)
```

```
      end if
      if (reply .eq. 11) then
      call xcu(x011,x012,x0m1,x0m2,x0ps,xl1ps,xl2ps,x0icu,xxcu)
      end if
      xmicu = ((e0icu/1.0e-18) ** 2.0) * x0icu
      xlicu = ((e0icu/6.3e-19) ** 2.0) * x0icu
      xpsi = ((e0icu/epsi) ** 2.0) * x0icu
      if (reply .eq. 12) then
      call xne(x0mne,x0ine,x0psne,xmpsne,xxne)
      end if
      xmine = ((e0ine/emine) ** 2.0) * x0ine
      xpsine = ((e0ine/epsine) ** 2.0) * x0ine
      if (reply .eq. 13) then
      call xlase(xstimy,xstimg)
      end if
      if (reply .eq. 14) then
      call xmtcu(xmtelcu,xmtmcu,xmtlcu,xmtpscu)
      end if
      if (reply .eq. 15) then
      call xmtne(xmtelne,xmtmne,xmtpsne)
      end if
      if (reply .eq. 16) then
      call metpop(nm1,nm2,temp)
      end if
      if (reply .eq. 17) then
      call lifetime(lg,ly,lps0,lpsl1,lpsl2,lpsmne,lr0ne)
      end if
      if (reply .gt. 0) goto 301
!
! densities of constituent particles : Cu, Ne atoms
!
      ncu = 1.23e7 * exp(0.0123655 * twall)
      nne = nep * 9.65e18 / tgas
      tgascz = tgas / 2.0
      nczne = nep * 9.65e18 / tgascz
      inc = (tgas * 0.5) / 1.0e3
      incez = (tgascz * 0.5) / 1.0e3
! program variables
      kt = k * temp
      ktcz = k * tempcz
! average velocities of constituent particles (in cm/s)
        ve = ((8.0 * kt / (pi * me)) ** 0.5) * 100.0
      vecz = ((8.0 * ktcz / (pi * me)) ** 0.5) * 100.0
! initial energy of electrons
        energy = 1.5 * kt
      energycz = 1.5 * ktcz
! densities of Cu and Ne energy levels
      if (twall .lt. 1080) then
      ncu = 1.0
      nm1 = 0.0
      nm2 = 0.0
      end if
      nl1 = gl1 * ncu * exp(-e0l1/kt) / g0
      nl2 = gl2 * ncu * exp(-e0l2/kt) / g0
      nps = ncu * exp(-e0ps/kt)
      cuion = 1.0e11
      ncu = ncu - nm1 - nm2 - nl1 - nl2 - nps - cuion
      nmne = nne * exp(-e0mne/kt)
      nrne = nmne
      npsne = nne * exp(-e0psne/kt)
      neion = 1.e6
      nne = nne - nmne - npsne - neion
```

```
      nczmne = nczne * exp(-e0mne/(k*tgascz))
      nczrne = nczmne
      nczpsne = nczne * exp(-e0psne/(k*tgascz))
      nczne = nczne - nczmne - nczrne - nczpsne
! charging voltage on Cs
      vcs = vc0
! lifetimes for spontaneous emission to ground,
! including radiation trapping
      dummy = 1.57e-15 * ncu * 1.0e6 / (tgas ** 0.5)
      if (twall .lt. 1080.0) then
      radtrap1 = 1.0
      else
      radtrap1 = 1.6 / (dummy * rad * ((pi * log(dummy*rad)) ** 0.5))
      end if
      dummy = 3.31e-15 * ncu * 1.0e6 / (tgas ** 0.5)
      if (twall .lt. 1080.0) then
      radtrap2 = 1.0
      else
      radtrap2 = 1.6 / (dummy * rad * ((pi * log(dummy*rad)) ** 0.5))
      end if
      if (radtrap1 .gt. 1.0) then
      radtrap1 = 1.0
      end if
      if (radtrap2 .gt. 1.0) then
      radtrap2 = 1.0
      end if
      l11 = 10.24e-9 / radtrap1
      l12 = 9.60e-9 / radtrap2
! store initial values
!
      tempold = temp
      tempczold = tempcz
      tgasold = tgas
      tgasczold = tgascz
      neold = ne
      neczold = necz
!
      do dummy = 1,10
      print*,'  '
      end do
      print*,'PLEASE WAIT, PROGRAM IS RUNNING'
      do dummy = 1,25
      print*,'  '
      end do
!*********************************************************************
!
!******************  MAIN PROGRAM  ********************************
!
!*********************************************************************
!
      do t=1,duration
!
! routines to calculate voltages and currents in circuit
!
! con is the electrical conductivity of the plasma
! c,h refer to the cool zone and hot zone, respectively
      nscool = (xmtelne * nczne) + (xmtmne * nczmne)
      nscool = nscool + (xmtpsne * nczpsne)
      conc = log(necz*1.0e6) + (2.0*log(q)) + log(vecz/100.0)
      conc = conc - log(3.0*ktcz) - log(nscool*100.0)
      conc = exp(conc)
      nshot = (xmtelne * nne) + (xmtmne * nmne)
```

```
      nshot = nshot + (xmtpsne * npsne)
      nshot = nshot + (xmtelcu * ncu) + (xmtlcu * (nl1 + nl2))
      nshot = nshot + (xmtmcu * (nm1 + nm2)) + (xmtpscu * nps)
      conh = log(ne*1.0e6) + (2.0*log(q)) + log(ve/100.0)
      conh = conh - log(3.0*kt) - log(nshot*100.0)
      conh = exp(conh)
! rp,lp are the plasma resistance, inductance
      rpc = (d1 - d2) * 4.0 / (pi * conc * (diam**2.0))
      rph = d2 * 4.0 / (pi * conh * (diam**2.0))
      rp = rpc + rph
      lpc = 4.*(d1-d2)*me / (necz*1.0e6*(q**2.)*pi*(diam**2.))
      lph = 4. * d2 * me / (ne*1.0e6 * (q**2.) * pi * (diam**2.))
      lp = lpc + lph
! i is the current, vc the capacitor voltage, 1,2 refer to storage
! loop and discharge loop respectively
      vs = vc0 * exp(-t/ton)
      di1 = (vcs - vs + vcp - (r1 * i1)) * time / l1
      di2 = -(vcp + (i2 * (r2 + rp))) * time / (l2 + lp)
      i1 = i1 + di1
      if (i1 .lt. 0.0) then
      i1 = 0.0
      end if
      i2 = i2 + di2
      dvcs = -i1 * time / cs
      dvcp = (i1 - i2) * time / cp
      vcs = vcs + dvcs
      vcp = vcp - dvcp
! vl is the voltage across the laser tube
! vlc and vlh are the voltage drops across each zone
      vlc = (rpc * i2) + (lpc * di2 / time)
      vlh = (rph * i2) + (lph * di2 / time)
      vl = - vlc - vlh
! assume that the electric field in the discharge is linear and
! is given by the voltage across each zone, fc,fh are in V/m
!
      fc = vlc / (d1 - d2)
      fh = vlh / d2
!
! CALCULATE RATE EQUATIONS
!
! set up commonly-used variables to save time in calculations
!
      h1 = ve / 100.0
      h2 = (log(8.0/(pi*kt)) - log(me)) / 2.0
      h2 = exp(h2) * 100.
      h1cz = vecz / 100.0
      h2cz = (log(8.0/(pi*ktcz)) - log(me)) / 2.0
      h2cz = exp(h2cz) * 100.
!
! calculate the average velocities of each group of electrons
!
      v1 = h2 * exp(-e0m1/kt) * (e0m1 + kt)
      v2 = h2 * exp(-e0m2/kt) * (e0m2 + kt)
      v3 = h2 * exp(-e0l1/kt) * (e0l1 + kt)
      v4 = h2 * exp(-e0l2/kt) * (e0l2 + kt)
      v5 = h2 * exp(-e0ps/kt) * (e0ps + kt)
      v6 = h2 * exp(-el1ps/kt) * (el1ps + kt)
      v7 = h2 * exp(-el2ps/kt) * (el2ps + kt)
      v8 = h2 * exp(-e0icu/kt) * (e0icu + kt)
      v9 = h2 * exp(-em1i/kt) * (em1i + kt)
      v10 = h2 * exp(-em2i/kt) * (em2i + kt)
      v11 = h2 * exp(-el1i/kt) * (el1i + kt)
```

```
      v12 = h2 * exp(-el2i/kt) * (el2i + kt)
      v13 = h2 * exp(-epsi/kt) * (epsi + kt)
      v14 = h2 * exp(-e0mne/kt) * (e0mne + kt)
      v15 = h2 * exp(-e0psne/kt) * (e0psne + kt)
      v16 = h2 * exp(-empsne/kt) * (empsne + kt)
      v17 = h2 * exp(-e0ine/kt) * (e0ine + kt)
      v18 = h2 * exp(-emine/kt) * (emine + kt)
      v19 = h2 * exp(-epsine/kt) * (epsine + kt)
      v14cz = h2cz * exp(-e0mne/ktcz) * (e0mne + ktcz)
      v15cz = h2cz * exp(-e0psne/ktcz) * (e0psne + ktcz)
      v16cz = h2cz * exp(-empsne/ktcz) * (empsne + ktcz)
      v17cz = h2cz * exp(-e0ine/ktcz) * (e0ine + ktcz)
      v18cz = h2cz * exp(-emine/ktcz) * (emine + ktcz)
      v19cz = h2cz * exp(-epsine/ktcz) * (epsine + ktcz)
!
! rate of ionization of Cu and Ne atoms
!
      rion0 = ncu * ne * x0icu * v8
      rionm1 = nm1 * ne * xmicu * v9
      rionm2 = nm2 * ne * xmicu * v10
      rionl1 = nl1 * ne * xlicu * v11
      rionl2 = nl2 * ne * xlicu * v12
      rionps = nps * ne * xpsi * v13
      rionmne =  nmne * ne * xmine * v18
      rionrne =  nrne * ne * xmine * v18
      rion0ne = nne * ne * x0ine * v17
      rionpsne = npsne * ne * xpsine * v19
      rcz0i = nczne * necz * x0ine * v17cz
      rczmi = nczmne * necz * xmine * v18cz
      rczri = nczrne * necz * xmine * v18cz
      rczpsi = nczpsne * necz * xpsine * v19cz
! electron energy loss from ionization of atoms
      s0 = nm1 * xmicu * em1i * exp(-em1i / kt)
      s0 = s0 * ne * (em1i + kt)
      s1 = nm2 * xmicu * em2i * exp(-em2i / kt)
      s1 = s1 * ne * (em2i + kt)
      s2 = nl1 * xlicu * el1i * exp(-el1i / kt)
      s2 = s2 * ne * (el1i + kt)
      s3 = nl2 * xlicu * el2i * exp(-el2i / kt)
      s3 = s3 * ne * (el2i + kt)
      s4 = (nmne + nrne) * xmine * emine * exp(-emine / kt)
      s4 = s4 * ne * (emine + kt)
      s5 = ncu * x0icu * e0icu * exp(-e0icu / kt)
      s5 = s5 * ne * (e0icu + kt)
      s6 = nne * x0ine * e0ine * exp(-e0ine / kt)
      s6 = s6 * ne * (e0ine + kt)
      s7 = nps * xpsi * epsi * exp(-epsi / kt)
      s7 = s7 * ne * (epsi + kt)
      s8 = npsne * xpsine * epsine * exp(-epsine / kt)
      s8 = s8 * ne * (epsine + kt)
      pion = h2 *(s0 + s1 + s2 + s3 + s4 + s5 + s6 + s7 + s8)*1.0e6
      s4cz = (nczmne + nczrne) * xmine * emine * exp(-emine/ktcz)
      s4cz = s4cz * necz * (emine + ktcz)
      s6cz = nczne * x0ine * e0ine * exp(-e0ine / ktcz)
      s6cz = s6cz * necz * (e0ine + ktcz)
      s8cz = nczpsne * xpsine * epsine * exp(-epsine / ktcz)
      s8cz = s8cz * necz * (epsine + ktcz)
      pioncz = h2cz * (s4cz + s6cz + s8cz) * 1.e6
!
! rate of excitation to Cu levels
!
      rm1 = ncu * x0m1 * ne * v1
```

```
      rm2 = ncu * x0m2 * ne * v2
      rl1 = ncu * x0l1 * ne * v3
      rl2 = ncu * x0l2 * ne * v4
      rps = ncu * x0ps * ne * v5
      rl1ps = nl1 * xl1ps * ne * v6
      rl2ps = nl2 * xl2ps * ne * v7
! rate of excitation of Ne levels
      r0mne = nne * x0mne * ne * v14
      r0rne = nne * x0mne * ne * v14
      r0psne = nne * x0psne * ne * v15
      rmpsne = nmne * xmpsne * ne * v16
      rrpsne = nrne * xmpsne * ne * v16
      rcz0m = nczne * x0mne * v14cz * necz
      rcz0r = nczne * x0mne * v14cz * necz
      rcz0ps = nczne * x0psne * v15cz * necz
      rczmps = nczmne * xmpsne * v16cz * necz
      rczrps = nczrne * xmpsne * v16cz * necz
! energy loss from excitation of atoms
      s0 = ncu * x0m1 * e0m1 * exp(-e0m1 / kt)
      s0 = s0 * ne * (e0m1 + kt)
      s1 = ncu * x0m2 * e0m2 * exp(-e0m2 / kt)
      s1 = s1 * ne * (e0m2 + kt)
      s2 = ncu * x0l1 * e0l1 * exp(-e0l1 / kt)
      s2 = s2 * ne * (e0l1 + kt)
      s3 = ncu * x0l2 * e0l2 * exp(-e0l2 / kt)
      s3 = s3 * ne * (e0l2 + kt)
      s4 = 2.0 * nne * x0mne * e0mne * exp(-e0mne / kt)
      s4 = s4 * ne * (e0mne + kt)
      s5 = nl1 * xl1ps * el1ps * exp(-el1ps / kt)
      s5 = s5 * ne * (el1ps + kt)
      s6 = nl2 * xl2ps * el2ps * exp(-el2ps / kt)
      s6 = s6 * ne * (el2ps + kt)
      s7 = nne * x0psne * e0psne * exp(-e0psne / kt)
      s7 = s7 * ne * (e0psne + kt)
      s8 = (nmne + nrne) * xmpsne * empsne * exp(-empsne / kt)
      s8 = s8 * ne * (empsne + kt)
      s9 = ncu * x0ps * e0ps * exp(-e0ps / kt)
      s9 = s9 * ne * (e0ps + kt)
      pex = h2*(s0 + s1 + s2 + s3 + s4 + s5 + s6 + s7 + s8 + s9)*1.e6
      s4cz = 2.0 * nczne * x0mne * e0mne * exp(-e0mne / ktcz)
      s4cz = s4cz * necz * (e0mne + ktcz)
      s7cz = nczne * x0psne * e0psne * exp(-e0psne / ktcz)
      s7cz = s7cz * necz * (e0psne + ktcz)
      s8cz = (nczmne + nczrne) * xmpsne * empsne * exp(-empsne/ktcz)
      s8cz = s8cz * necz * (empsne + ktcz)
      pexcz = h2cz * (s4cz + s7cz + s8cz) * 1.0e6
!
! superelastic collision cross-sections using detailed balance
!
      xm10 = (1 + (e0m1 / energy)) * x0m1 * g0 / gm1
      xm20 = (1 + (e0m2 / energy)) * x0m2 * g0 / gm2
      xl10 = (1 + (e0l1 / energy)) * x0l1 * g0 / gl1
      xl20 = (1 + (e0l2 / energy)) * x0l2 * g0 / gl2
      xpsl1 = (1 + (el1ps / energy)) * xl1ps * gl1 / gps
      xpsl2 = (1 + (el2ps / energy)) * xl2ps * gl2 / gps
      xps0 = (1 + (e0ps / energy)) * x0ps * g0 / gps
      xps0ne = (1 + (e0psne / energy)) * x0psne
      xpsmne = (1 + (empsne / energy)) * xmpsne
      xm0ne = (1 + (e0mne / energy)) * x0mne
      xczps0ne = (1 + (e0psne / energycz)) * x0psne
      xczpsmne = (1 + (empsne / energycz)) * xmpsne
      xczm0ne = (1 + (e0mne / energycz)) * x0mne
```

```
!
! rate of deexcitation due to superelastic collisions
!
      dummy = ne * ve
      rdm1 = nm1 * dummy * xm10
      rdm2 = nm2 * dummy * xm20
      rdl1 = nl1 * dummy * xl10
      rdl2 = nl2 * dummy * xl20
      rdpsl1 = nps * dummy * xpsl1
      rdpsl2 = nps * dummy * xpsl2
      rdps0 = nps * dummy * xps0
      rdps0ne = npsne * dummy * xps0ne
      rdpsmne = npsne * dummy * xpsmne
      rdm0ne = nmne * dummy * xm0ne
      rdr0ne = nrne * dummy * xm0ne
      rdpsrne = npsne * dummy * xpsmne
      dummy = necz * vecz
      rdczps0ne = nczpsne * xczps0ne * dummy
      rdczpsmne = nczpsne * xczpsmne * dummy
      rdczm0ne = nczmne * xczm0ne * dummy
      rdczr0ne = nczrne * xczm0ne * dummy
      rdczpsrne = nczpsne * xczpsmne * dummy
!
! change densities to per cubic metre - any odd numerical factors
! appearing in the following equations will be to convert
! from resultant powers of cm to those of metres
!
      ne = ne * 1.0e6
      ncu = ncu * 1.0e6
      nne = nne * 1.0e6
      necz = necz * 1.0e6
      nczne = nczne * 1.0e6
!
! CALCULATE ENERGY FLOW INTO/OUT OF ELECTRON DISTRIBUTION
!
! main energy transfer equations for Maxwellian electron
! distribution - note that PEX and PION are calculated within
! the excitation and ionization routines above
!
! energy gain from electric field
      pf = h2 * (q**2.0) * (fh**2.0) * ne * 1.0e-4 / (3.0 * nshot)
      pfcz = h2cz * (q**2.0) * (fc**2.0) * necz*1.e-4/ (3.0*nscool)
! energy gain from superelastic collisions
      psel = (nl1 * e0l1 * xl10) + (nl2 * e0l2 * xl20)
      psel = psel + (nm1 * e0m1 * xm10) + (nm2 * e0m2 * xm20)
      psel = psel + (nps * e0ps * xps0) + (nps * el1ps * xpsl1)
      psel = psel + (nps * el2ps * xpsl2)
      psel = psel+(npsne*e0psne*xps0ne)+(2.*npsne*empsne*xpsmne)
      psel = (psel + ((rmne + nrne) * e0mne * xm0ne)) * 100.0
      psel = h1 * ne * psel
      pselcz=(nczpsne*e0psne*xczps0ne)+(2.*nczpsne*empsne*xczpsmne)
      pselcz = (pselcz + ((nczmne+nczrne) * e0mne * xczm0ne))*100.
      pselcz = pselcz * necz * h1cz
! energy loss from elastic collisions
      pel = (nne*1.0e-4*xxne/mne) + (ncu*1.0e-4*xxcu/mcu)
      pel = pel + (nne*1.0e-4*xmtelne/mne)
      pel = pel + (ncu*1.0e-4*xmtelcu/mcu)
      pel = log(pel) + log(h1*me) + log(kt) + log(ne)
      pel = 4.0 * exp(pel)
      pelcz = nczne * (xxne + xmtelne) * 1.0e-4 / mne
      pelcz = log(pelcz) + log(h1cz*me) + log(ktcz) + log(necz)
      pelcz = 4.0 * exp(pelcz)
```

```
!
! change energy gain and loss from per second per cubic metre
! to per iteration per cubic centimetre
!
      dummy = time / 1.e6
      pf = pf * dummy
      psel = psel * dummy
      pel = pel * dummy
      pex = pex * dummy
      pion = pion * dummy
      pfcz = pfcz * dummy
      pselcz = pselcz * dummy
      pelcz = pelcz * dummy
      pexcz = pexcz * dummy
      pioncz = pioncz * dummy
!
! change densities back to per cubic cm
!
      ne = ne / 1.0e6
      ncu = ncu / 1.0e6
      nne = nne / 1.0e6
      necz = necz / 1.0e6
      nczne = nczne / 1.0e6
!
! spontaneous emission rates
!
! upper laser levels to ground
      rspl10 = nl1 / ll1
      rspl20 = nl2 / ll2
! pseudo-state to upper laser levels
!
      rsppsl1 = nps / lpsl1
      rsppsl2 = nps / lpsl2
! pseudo state to ground
      rspps0 = nps / lps0
! transition from L2 to M1 : green line
      rspl2m1 = nl2 / lg
! transition from L1 to M2 : yellow line
      rspl1m2 = nl1 / ly
!
! CALCULATE LASER OUTPUT
!
! rate of stimulated emissions between laser levels
!
      if (gm2*nl1 .gt. gl1*nm2) then
      rlasey = nl1 * xstimy * nlasey * c
      else
      rlasey = 0.0
      end if
!
      if (gm1*nl2 .gt. gl2*nm1) then
      rlaseg = nl2 * xstimg * nlaseg * c
      else
      rlaseg = 0.0
      end if
!
! number of laser photons in cavity after stimulated transitions
!
      nlasey = nlasey + (((rspl1m2 * angle) + rlasey) * time)
      nlaseg = nlaseg + (((rspl2m1 * angle) + rlaseg) * time)
!
! number of laser photons coupled out of cavity via end mirrors
```

```
!
      numouty = nlasey * c * (1-reflect) * time / cavityl
      numoutg = nlaseg * c * (1-reflect) * time / cavityl
!
! number of laser photons left in cavity after output coupling
!
      nlasey = nlasey - numouty
      nlaseg = nlaseg - numoutg
!
! sum output power
!
      sumy = sumy + (numouty*3.44e-19)
      sumg = sumg + (numoutg*3.89e-19)
!
! radiative decay in Ne
!
      rczsppsmne = nczpsne / lpsmne
      rsppsmne = npsne / lpsmne
      rspr0ne = nrne / lr0ne
      rczspr0ne = nczrne / lr0ne
!
! calculate new populations of energy levels using rate equations
!
! copper levels
!
      rm1 = rm1 + ((rm1 - rionm1 + rspl2m1 + rlaseg - rdm1) * time)
      rm2 = rm2 + ((rm2 - rionm2 + rspl1m2 + rlasey - rdm2) * time)
      dummy = rl1 - rionl1 - rl1ps - rspl10 + rsppsl1 - rspl1m2
      nl1 = nl1 + ((dummy - rlasey + rdpsl1 - rdl1) * time)
      dummy = rl2 - rionl2 - rl2ps - rspl20 + rsppsl2 - rspl2m1
      nl2 = nl2 + ((dummy - rlaseg + rdpsl2 - rdl2) * time)
      dummy = rps - rsppsO- rionps+ rl1ps + rl2ps- rsppsl1 - rsppsl2
      nps = nps + ((dummy - rdpsl1 - rdpsl2 - rdpsO) * time)
      dummy = rspl10 + rspl20 - rion0 - rm1 - rm2 - rl1 - rl2 - rps
      dummy = dummy + rdm1 + rdm2 + rdl1 + rdl2 + rdpsO + rsppsO
      ncu = ncu + (dummy * time)
! neon levels
!
      dummy = r0rne - rionrne - rrpsne + rdpsrne - rdr0ne
      nrne = nrne + ((dummy + (rsppsmne*0.5) - rspr0ne) * time)
      dummy = r0mne - rionmne - rmpsne + rdpsmne - rdm0ne
      nmne = nmne + ((dummy + (0.5*rsppsmne)) * time)
      dummy = r0psne - rionpsne + rmpsne - rdpsOne - rdpsmne
      npsne = npsne + ((dummy - rsppsmne + rrpsne - rdpsrne) * time)
      dummy = rdm0ne + rdpsOne - rion0ne - r0mne - r0psne
      nne = nne + ((dummy - r0rne + rdr0ne + rspr0ne) * time)
      dummy = rionrne + rionmne + rionpsne + rion0ne
      neion = neion + (dummy * time)
! Ne levels in the cool zone
      dummy = rdczm0ne + rdczpsOne - rcz0i - rcz0m - rcz0ps
      dummy = dummy - rcz0r + rdczr0ne + rczspr0ne
      nczne = nczne + (dummy * time)
      dummy = rcz0m - rczmi - rczmps + rdczpsmne - rdczm0ne
      nczmne = nczmne + ((dummy+(0.5*rczsppsmne))*time)
      dummy = rcz0ps - rczpsi + rczmps - rdczpsOne - rdczpsmne
      dummy = dummy + rczrps - rdczpsrne
      nczpsne = nczpsne + ((dummy - rczsppsmne) * time)
      dummy = rcz0r - rczri - rczrps + rdczpsrne - rdczr0ne
      nczrne = nczrne + ((dummy + (rczsppsmne*.5) - rczspr0ne)*time)
!
! calculate number of new electrons due to ionizations
!
```

```
      dne = rion0 + rionm1 + rionm2 + rionl1 + rionl2 + rionps
      cuion = cuion + (dne * time)
      dne = dne + rionrne
      dne = (dne + rionmne + rion0ne + rionpsne) * time
      dnecz = (rczri + rczmi + rcz0i + rczpsi) * time
      nczi = nczi + dnecz
!
! energy gain or loss of the distribution
!
      denergy = pf + psel - pel - pex - pion
      denergycz = pfcz + pselcz - pelcz - pexcz - pioncz
!
! CALCULATE NEW ELECTRON TEMPERATURE AND VELOCITY
!
      energy = ((energy*ne) + denergy) / (ne+dne)
      ne = ne + dne
      temp = 2.0 * energy / (3.0 * k)
      kt = k * temp
      if (t .lt. 1000.0) then
      tgas = tgas + inc
      nne = nep * 9.65e18 / tgas
      ncu = ncu * (tgas - inc) / tgas
      else
      tgas = tgas - (inc * 0.2)
      nne = nep * 9.65e18 / tgas
      ncu = ncu * (tgas + (inc * 0.2)) / tgas
      end if
      ve = ((8.0 * kt / (pi * me)) ** 0.5) * 100.0
      energycz = ((energycz*necz) + denergycz) / (necz + dnecz)
      necz = necz + dnecz
      tempcz = 2.0 * energycz / (3.0 * k)
      ktcz = k * tempcz
      vecz = ((8.0 * ktcz / (pi * me)) ** 0.5) * 100.0
      if (t .lt. 1000.0) then
      tgascz = tgascz + inccz
      nczne = nep * 9.65e18 / tgascz
      else
      tgascz = tgascz - (inccz * 0.2)
      nczne = nep * 9.65e18 / tgascz
      end if
!
! STORE DATA
!
! send data to output data files; output is
! unformatted - saves space over formatted
!
      if (t*zz .eq. int(t*zz)) then
      debout(t*zz) = 69. * 1.e6 * ((temp/(ne*1.e6)) ** 0.5)
      resout(t*zz) = 0.111 * 1.e9 / ((ne*1.e6) ** 0.5)
      lmax(t*zz) = 1.1 * temp / abs(fh)
      vout(t*zz) = -vl / 200
      timeout(t*zz) = t*time
      fout(t*zz) = vcp
      ilout(t*zz) = i2 * 5.0
      i2out(t*zz) = i2
      rpout(t*zz) = rp
      lpout(t*zz) = lp
      neout(t*zz) = ne
      tempout(t*zz) = temp
      nl1out(t*zz) = nl1
      nl2out(t*zz) = nl2
      nm1out(t*zz) = nm1
```

```
      nm2out(t*zz) = nm2
      npsout(t*zz) = nps
      npsneout(t*zz) = npsne
      if (npsneout(t*zz) .lt. 0.0) then
      npsneout(t*zz) = 0.0
      end if
      nmneout(t*zz) = nmne
      if (nmneout(t*zz) .lt. 0.0) then
      nmneout(t*zz) = 0.0
      end if
      nrneout(t*zz) = nrne
      if (nrneout(t*zz) .lt. 0.0) then
      nrneout(t*zz) = 0.0
      end if
      neionout(t*zz) = neion
      if (neionout(t*zz) .lt. 0.0) then
      neionout(t*zz) = 0.0
      end if
      dummy = nm1 + nm2 + nl2 + nl1 + nps
      cuionout(t*zz) = cuion
      if (cuionout(t*zz) .lt. 0.0) then
      cuionout(t*zz) = 0.0
      end if
      laseouty(t*zz) = numouty*3.44e-19/time
      laseoutg(t*zz) = numoutg*3.89e-19/time
      lastotal(t*zz) = laseouty(t*zz) + laseoutg(t*zz)
      end if

      end do
!*************************************************************************
!
!*************** END OF MAIN PROGRAM ***********************************
!
!*************************************************************************
!
      do dummy = 1,30
      print*,'  '
      end do
      print*,'TOTAL ENERGY IN EACH LASER PULSE'
      print*,'  '
      print*,'YELLOW AT 578nm (joules) = ',sumy
      print*,'GREEN AT 510nm (joules) = ',sumg
      do dummy = 1,10
      print*,'  '
      end do
!
! graphics routine
!
      duration = duration * time
401   call choose
! set up for graphics
      if (reply .gt. 0) then
      call paper(1)
      call frame
! maximum metal segment length
      if (reply .eq. 1) then
      call filnam('qe8.grd;1',9)
      call pspace(0.2,1.0,0.2,0.8)
      call map(0.0,300.0e-9,0.0,50.0)
      call ptjoin(timeout,lmax,1,299,0)
      end if
! plasma resistance
```

```
      if (reply .eq. 2) then
      call mapyl(0.0,duration,1.0,1.0e4)
      call axeyl
      call grayl
      call ptjoin(timeout,rpout,1,500,0)
      end if
! plasma inductance
      if (reply .eq. 3) then
      call mapyl(0.0,duration,2.0e-10,2.0e-7)
      call axeyl
      call grayl
      call ptjoin(timeout,lpout,1,500,0)
      end if
! electron density
      if (reply .eq. 4) then
      call mapyl(0.0,duration,1.0e11,1.0e15)
      call axeyl
      call grayl
      call ptjoin(timeout,neout,1,500,0)
      end if
! electron temperature
      if (reply .eq. 5) then
      call map(0.0,duration,0.0,1.0e5)
      call axes
      call gratic
      call ptjoin(timeout,tempout,1,500,0)
      end if
! Cu excited state densities
      if (reply .eq. 6) then
      call mapyl(0.0,duration,2.0e11,2.0e14)
      call axeyl
      call grayl
      call ptjoin(timeout,nl1out,1,500,0)
      call ptjoin(timeout,nl2out,1,500,0)
      call ptjoin(timeout,nm1out,1,500,0)
      call ptjoin(timeout,nm2out,1,500,0)
      call ptjoin(timeout,npsout,1,500,0)
      end if
! Ne excited state densities
      if (reply .eq. 7) then
      call mapyl(0.0,duration,1.0e11,1.0e14)
      call axeyl
      call grayl
      call ptjoin(timeout,nmneout,1,500,0)
      call ptjoin(timeout,nrneout,1,500,0)
      call ptjoin(timeout,npsneout,1,500,0)
      end if
! Cu and Ne ion densities
      if ( reply .eq. 8) then
      call mapyl(0.0,duration,1.0e11,1.0e15)
      call axeyl
      call grayl
      call ptjoin(timeout,cuionout,1,500,0)
      call ptjoin(timeout,neionout,1,500,0)
      end if
! laser output power
      if (reply .eq. 9) then
      call map(1.0e-7,3.0e-7,0.0,8.0e2)
      call axes
      call gratic
      call ptjoin(timeout,i2out,100,300,0)
      call ptjoin(timeout,laseouty,100,300,0)
```

```
      call ptjoin(timeout,laseoutg,100,300,0)
      call ptjoin(timeout,lastotal,100,300,0)
      end if
! voltage and current for discharge loop
      if (reply .eq. 10) then
      call map(0.0,duration,-1.4e4,4.0e3)
      call axes
      call gratic
      call ptjoin(timeout,fout,1,500,0)
      call ptjoin(timeout,ilout,1,500,0)
      end if
! Debye length
      if (reply .eq. 11) then
      call filnam('debgrd.grd;1',12)
      call pspace(0.1,0.95,0.1,0.8)
      call mapyl(0.0,duration,0.1,40.0)
      call ptjoin(timeout,debout,1,500,0)
      end if
! plasma response time
      if (reply .eq. 12) then
      call filnam('resgrd.grd;1',12)
      call pspace(0.1,0.95,0.1,0.8)
      call mapyl(0.0,duration,3.0e-3,0.3)
      call ptjoin(timeout,resout,1,500,0)
      end if
! switch off graphics
      call grend
      end if
      if (reply .gt. 0.0) goto 401
      print*,' '
      print*,'ENTER 0 TO FINISH, ANY OTHER NUMBER TO RETURN TO START'
      read*,answer
      duration = duration / time
      if (answer .gt. 0) goto 101
      do dummy = 1,35
      print*,' '
      end do
      stop
      end
! graph menu subroutine
      subroutine choose
      implicit none
      real reply,dummy
      common reply
501   print*,' '
      print*,'ENTER A NUMBER FOR A GRAPH OR TO CONTINUE'
      print*,' '
      print*,'   1 : MAXIMUM METAL SEGMENT LENGTH'
      print*,'   2 : PLASMA RESISTANCE'
      print*,'   3 : PLASMA INDUCTANCE'
      print*,'   4 : ELECTRON DENSITY'
      print*,'   5 : ELECTRON TEMPERATURE'
      print*,'   6 : Cu EXCITED STATE DENSITIES'
      print*,'   7 : Ne EXCITED STATE DENSITIES'
      print*,'   8 : Cu AND Ne ION DENSITIES'
      print*,'   9 : LASER OUTPUT POWER'
      print*,'  10 : VOLTAGE AND CURRENT IN LASER LOOP'
      print*,'  11 : DEBYE LENGTH'
      print*,'  12 : PLASMA RESPONSE TIME'
      print*,'   0 : CONTINUE'
      read*,reply
      do dummy = 1,35
```

```
      print*,' '
      end do
      if (reply .lt. 0 .or. reply .gt. 12) goto 501
      return
      end
!
! subroutine to present menu for changing initial variables
!
      subroutine menu(twall,nep,ne,necz,temp,tgas,d2,d1,diam)
      implicit none
      real dummy,reply,twall,nep,ne,necz,temp,tgas,d2,d1,diam
      common reply
551   print*,' '
      print*,'ENTER A NUMBER TO CHANGE A CONSTANT OR TO RUN'
      print*,' '
      print*,'   1 : WALL TEMPERATURE',int(twall),'C'
      print*,'   2 : Ne PRESSURE',int(nep),'torr'
      print*,'   3 : INITIAL HOT ZONE ELECTRON DENSITY',ne,' /cc'
      print*,'   4 : INITIAL COOL ZONE ELECTRON DENSITY',necz,' /cc '
      print*,'   5 : INITIAL ELECTRON TEMPERATURE',int(temp),'K'
      print*,'   6 : INITIAL GAS TEMPERATURE',int(tgas),'K'
      print*,'   7 : CIRCUIT CONSTANTS'
      print*,'   8 : LENGTH OF ACTIVE ZONE',int(100.*d2),'cm'
      print*,'   9 : LENGTH OF DISCHARGE ZONE',int(100.*d1),'cm'
      print*,'  10 : DIAMETER OF DISCHARGE',int(100.*diam),'cm'
      print*,'  11 : Cu CROSS-SECTIONS'
      print*,'  12 : Ne CROSS-SECTIONS'
      print*,'  13 : STIMULATED EMISSION CROSS-SECTIONS'
      print*,'  14 : Cu MOMENTUM TRANSFER CROSS-SECTIONS'
      print*,'  15 : Ne MOMENTUM TRANSFER CROSS-SECTIONS'
      print*,'  16 : INITIAL Cu METASTABLE POPULATIONS'
      print*,'  17 : EXCITED LEVEL LIFETIMES'
      print*,'   0 : RUN PROGRAM'
      read*,reply
      do dummy = 1,8
      print*,' '
      end do
      if (reply .lt. 0 .or. reply .gt. 17) then
      do dummy = 1,35
      print*,' '
      end do
      end if
      if (reply .lt. 0 .or. reply .gt. 17) goto 551
      return
      end
!
! subroutine to alter the initial densities
!
      subroutine change(twall,nep,ncu,nne,necz,ne,temp,tgas)
      implicit none
      real necz,ncu,nne,ne,twall,nep,reply,temp,tgas
      common reply
      if (reply .eq. 1) then
631   print*,' '
      print*,'ENTER NEW WALL TEMPERATURE (C)'
      read*,twall
      if (twall .lt. 0.0 .or. twall .gt. 2000.0) goto 631
      ncu = 1.23e7 * exp(0.0123655 * twall)
      end if
      if (reply .eq. 2) then
632   print*,' '
      print*,'ENTER NEW Ne PRESSURE (torr)'
```

```
      read*,nep
      if (nep .lt. 0.1 .or. nep .gt. 760.0) goto 632
      nne = nep * 9.65e18 / tgas
      end if
      if (reply .eq. 3) then
633   print*,' '
      print*,'ENTER INITIAL HOT ZONE ELECTRON DENSITY (cc)'
      read*,ne
      if (ne .lt. 1.0e3 .or. ne .gt. 1.0e15) goto 633
      end if
      if (reply .eq. 4) then
634   print*,' '
      print*,'ENTER INITIAL COOL ZONE ELECTRON DENSITY (cc)'
      read*,necz
      if (necz .lt. 1.0e3 .or. necz .gt. 1.0e15) goto 634
      end if
      if (reply .eq. 5) then
635   print*,' '
      print*,'ENTER INITIAL ELECTRON TEMPERATURE (K)'
      read*,temp
      if (temp .lt. 300.0 .or. temp .gt. 5.0e3) goto 635
      end if
      if (reply .eq. 6) then
636   print*,' '
      print*,'ENTER INITIAL GAS TEMPERATURE (K)'
      read*,tgas
      if (tgas .lt. 300.0 .or. tgas .gt. 5.0e3) goto 636
      nne = nep * 9.65e18 / tgas
      end if
      return
      end
! subroutine to change tube dimensions
      subroutine tube(d1,d2,diam)
      implicit none
      real d1,d2,diam,reply
      common reply
      print*,' '
      if (reply .eq. 8) then
641   print*,'ENTER NEW ACTIVE ZONE LENGTH IN METRES'
      read*,d2
      if (d2 .lt. 0.1 .or. d2 .gt. d1) goto 641
      end if
      if (reply .eq. 9) then
642   print*,'ENTER NEW DISCHARGE ZONE LENGTH IN METRES'
      read*,d1
      if (d1 .lt. d2 .or. d1 .gt. 2.0) goto 642
      end if
      if (reply .eq. 10) then
643   print*,'ENTER NEW DISCHARGE DIAMETER IN METRES'
      read*,diam
      if (diam .lt. 0.005 .or. diam .gt. 0.04) goto 643
      end if
      return
      end
!
! subroutine to alter Cu cross-sections
!
      subroutine xcu(x0l1,x0l2,x0m1,x0m2,x0ps,xl1ps,xl2ps,x0icu,xxcu)
      implicit none
      real x0l1,x0l2,x0m1,x0m2,x0ps,xl1ps,xl2ps,x0icu,xxcu,dummy,dum
670   do dum = 1,15
      print*,' '
```

```
      end do
      print*,'ENTER A NUMBER : 0 RETURNS TO MAIN MENU'
      print*,'  '
      print*,'   1 : 2P(1/2) CROSS-SECTION',x011,'sq.cm.'
      print*,'   2 : 2P(3/2) CROSS-SECTION',x012,'sq.cm.'
      print*,'   3 : 2D(5/2) CROSS-SECTION',x0m1,'sq.cm.'
      print*,'   4 : 2D(3/2) CROSS-SECTION',x0m2,'sq.cm.'
      print*,'   5 : IONIZATION FROM GROUND',x0icu,'sq.cm.'
      print*,'   6 : 2S TO PSEUDO STATE',x0ps,'sq.cm.'
      print*,'   7 : 2P(1/2) TO PSEUDO STATE',xl1ps,'sq.cm.'
      print*,'   8 : 2P(3/2) TO PSEUDO STATE',xl2ps,'sq.cm.'
      print*,'   9 : ELASTIC COLLISIONS',xxcu,'sq.cm.'
      print*,'   0 : RETURN TO INITIALIZATION MENU'
      read*,dummy
      do dum = 1,10
      print*,' '
      end do
      if (dummy .lt. 0 .or. dummy .gt. 9) goto 670
      if (dummy .eq. 1) then
671   print*,'  '
      print*,'ENTER YELLOW LASER LEVEL EXCITATION CROSS-SECTION'
      read*,x011
      if (x011 .lt. 1.0e-18 .or. x011 .gt. 1.0e-14) goto 671
      end if
      if (dummy .eq. 2) then
672   print*,'  '
      print*,'ENTER GREEN LASER LEVEL EXCITATION CROSS-SECTION'
      read*,x012
      if (x012 .lt. 1.0e-18 .or. x012 .gt. 1.0e-14) goto 672
      end if
      if (dummy .eq. 3) then
673   print*,'  '
      print*,'ENTER 2D(5/2) EXCITATION CROSS-SECTION'
      read*,x0m1
      if (x0m1 .lt. 1.0e-18 .or. x0m1 .gt. 1.0e-14) goto 673
      end if
      if (dummy .eq. 4) then
674   print*,'  '
      print*,'ENTER 2D(3/2) EXCITATION CROSS-SECTION'
      read*,x0m2
      if (x0m2 .lt. 1.0e-18 .or. x0m2 .gt. 1.0e-14) goto 674
      end if
      if (dummy .eq. 5) then
675   print*,'  '
      print*,'ENTER GROUND IONIZATION CROSS-SECTION'
      read*,x0icu
      if (x0icu .lt. 1.0e-18 .or. x0icu .gt. 1.0e-15) goto 675
      end if
      if (dummy .eq. 6) then
676   print*,'  '
      print*,'ENTER GROUND TO PSEUDO STATE CROSS-SECTION'
      read*,x0ps
      if (x0ps .lt. 0.0 .or. x0ps .gt. 1.0e-14) goto 676
      end if
      if (dummy .eq. 7) then
677   print*,'  '
      print*,'ENTER 2P(1/2) TO PSEUDO STATE CROSS-SECTION'
      read*,xl1ps
      if (xl1ps .lt. 0.0 .or. xl1ps .gt. 1.0e-14) goto 677
      end if
      if (dummy .eq. 8) then
678   print*,'  '
```

```
      print*,'ENTER 2P(3/2) TO PSEUDO STATE CROSS-SECTION'
      read*,xl2ps
      if (xl2ps .lt. 0.0 .or. xl2ps .gt. 1.0e-14) goto 678
      end if
      if (dummy .eq. 9) then
679   print*,'  '
      print*,'ENTER ELASTIC COLLISIONS CROSS-SECTION'
      read*,xxcu
      if (xxcu .lt. 1.0e-18 .or. xxcu .gt. 1.0e-14) goto 679
      end if
      if (dummy .gt. 0) goto 670
      return
      end
!
! subroutine to change Ne cross-sections
!
      subroutine xne(x0mne,x0ine,x0psne,xmpsne,xxne)
      implicit none
      real x0mne,x0ine,x0psne,xmpsne,xxne,dummy,dum
690   do dum = 1,15
      print*,' '
      end do
      print*,'ENTER A NUMBER : 0 RETURNS TO MAIN MENU'
      print*,'  '
      print*,'   1 : GROUND TO METASTABLE',x0mne,'sq.cm.'
      print*,'   2 : GROUND TO PSEUDO STATE',x0psne,'sq.cm.'
      print*,'   3 : METASTABLE TO PSEUDO',xmpsne,'sq.cm.'
      print*,'   4 : IONIZATION FROM GROUND',x0ine,'sq.cm.'
      print*,'   5 : ELASTIC COLLISIONS',xxne,'sq.cm.'
      print*,'   0 : RETURN TO INITIALIZATION MENU'
      read*,dummy
      do dum = 1,10
      print*,' '
      end do
      if (dummy .lt. 0 .or. dummy .gt. 5) goto 690
      if (dummy .eq. 1) then
691   print*,'  '
      print*,'ENTER METASTABLE STATE EXCITATION CROSS-SECTION'
      read*,x0mne
      if (x0mne .lt. 1.0e-18 .or. x0mne .gt. 1.0e-14) goto 691
      end if
      if (dummy .eq. 2) then
692   print*,'  '
      print*,'ENTER GROUND TO PSEUDO STATE CROSS-SECTION'
      read*,x0psne
      if (x0psne .lt. 1.0e-18 .or. x0psne .gt. 1.0e-14) goto 692
      end if
      if (dummy .eq. 3) then
693   print*,'  '
      print*,'ENTER METASTABLE TO PSEUDO STATE CROSS-SECTION'
      read*,xmpsne
      if (xmpsne .lt. 1.0e-18 .or. xmpsne .gt. 1.0e-14) goto 693
      end if
      if (dummy .eq. 4) then
694   print*,'  '
      print*,'ENTER GROUND IONIZATION CROSS-SECTION'
      read*,x0ine
      if (x0ine .lt. 1.0e-18 .or. x0ine .gt. 1.0e-16) goto 694
      end if
      if (dummy .eq. 5) then
695   print*,'  '
      print*,'ENTER ELASTIC COLLISION CROSS-SECTION'
```

```
      read*,xxne
      if (xxne .lt. 1.0e-18 .or. xxne .gt. 1.0e-14) goto 695
      end if
      if (dummy .gt. 0) goto 690
      return
      end
! subroutine to alter circuit constants
      subroutine circuit(l1,l2,cs,cp,vc0,r1,r2,ton)
      implicit none
      real l1,l2,cs,cp,vc0,dummy,r1,r2,ton,dum
710   do dum = 1,15
      print*,' '
      end do
      print*,'ENTER A NUMBER : 0 RETURNS TO MAIN MENU'
      print*,'  '
      print*,'   1 : INDUCTANCE OF C1-C2 LOOP',int(1.e9*l1),'nH'
      print*,'   2 : INDUCTANCE OF C2-LASER LOOP',int(1.e9*l2),'nH'
      print*,'   3 : STORAGE CAPACITOR (C1)',int(1.e10*cs)/10,'nF'
      print*,'   4 : PEAKING CAPACITOR (C2)',int(1.e10*cp)/10,'nF'
      print*,'   5 : C1 CHARGING VOLTAGE',int(vc0*1.e-3),'kV'
      print*,'   6 : RESISTANCE OF C1-C2 LOOP',int(r1),'ohms'
      print*,'   7 : RESISTANCE OF C2-LASER LOOP',int(r2),'ohms'
      print*,'   8 : THYRATRON SWITCH-ON TIME',int(ton*1.e9),'ns'
      print*,'   0 : RETURN TO INITIALISATION MENU'
      read*,dummy
      do dum = 1,10
      print*,' '
      end do
      if (dummy .lt. 0.0 .or. dummy .gt. 8) goto 710
      print*,'  '
      if (dummy .eq. 1) then
711   print*,'  '
      print*,'ENTER C1-C2 INDUCTANCE (H)'
      read*,l1
      if (l1 .lt. 50.0e-9 .or. l1 .gt. 2.0e-6) goto 711
      end if
      if (dummy .eq. 2) then
712   print*,'  '
      print*,'ENTER C2-LASER INDUCTANCE (H)'
      read*,l2
      if (l2 .lt. 100.0e-9 .or. l2 .gt. 20.0e-6) goto 712
      end if
      if (dummy .eq. 3) then
713   print*,'  '
      print*,'ENTER STORAGE CAPACITANCE (F)'
      read*,cs
      if (cs .lt. 1.0e-9 .or. cs .gt. 20.0e-9) goto 713
      end if
      if (dummy .eq. 4) then
714   print*,'  '
      print*,'ENTER PEAKING CAPACITANCE (F)'
      read*,cp
      if (cp .lt. 100.0e-12 .or. cp .gt. 10.0e-9) goto 714
      end if
      if (dummy .eq. 5) then
715   print*,'  '
      print*,'ENTER CHARGING VOLTAGE ON STORAGE CAPACITOR (V)'
      read*,vc0
      if (vc0 .lt. 1.0e3 .or. vc0 .gt. 25.0e3) goto 715
      end if
      if (dummy .eq. 6) then
716   print*,'  '
```

```
      print*,'ENTER R1'
      read*,r1
      if (r1 .lt. 0.0 .or. r1 .gt. 10.0) goto 716
      end if
      if (dummy .eq. 7) then
717   print*,'  '
      print*,'ENTER R2'
      read*,r2
      if (r2 .lt. 0.0 .or. r2 .gt. 10.0) goto 717
      end if
      if (dummy .eq. 8) then
718   print*,'  '
      print*,'ENTER THYRATRON SWITCHING TIME (SECS)'
      read*,ton
      if (ton .lt. 1.e-9 .or. ton .gt. 100.e-9) goto 718
      end if
      if (dummy .gt. 0) goto 710
      return
      end
! subroutine to change stimulated emission cross sections
      subroutine xlase(xstimy,xstimg)
      implicit none
      real xstimy,dum,xstimg,dummy
751   do dum = 1,20
      print*,' '
      end do
      print*,'ENTER A NUMBER : 0 RETURNS TO MAIN MENU'
      print*,' '
      print*,'   1 : YELLOW CROSS-SECTION',xstimy,'sq.cm.'
      print*,'   2 : GREEN CROSS-SECTION',xstimg,'sq.cm.'
      print*,'   0 : RETURN TO INITIALIZATION MENU'
      read*,dummy
      do dum = 1,15
      print*,' '
      end do
      if (dummy .lt. 0 .or. dummy .gt. 2) goto 751
      if (dummy .eq. 1) then
752   print*,' '
      print*,'ENTER YELLOW LASER CROSS-SECTION'
      read*,xstimy
      if (xstimy .lt. 1.0e-17 .or. xstimy .gt. 1.0e-14) goto 752
      end if
      if (dummy .eq. 2) then
753   print*,' '
      print*,'ENTER GREEN LASER CROSS-SECTION'
      read*,xstimg
      if (xstimg .lt. 1.0e-17 .or. xstimg .gt. 1.0e-14) goto 753
      end if
      if (dummy .gt. 0) goto 751
      return
      end
! subroutine to change Cu momentum transfer cross-sections
      subroutine xmtcu(xmtelcu,xmtmcu,xmtlcu,xmtpscu)
      implicit none
      real xmtelcu,xmtmcu,xmtlcu,xmtpscu,dummy,dum
810   do dum = 1,20
      print*,' '
      end do
      print*,'ENTER A NUMBER : 0 RETURNS TO MAIN MENU'
      print*,'  '
      print*,'   1 : ELASTIC MOMENTUM TRANSFER',xmtelcu,'sq.cm.'
      print*,'   2 : 2D MOMENTUM TRANSFER',xmtmcu,'sq.cm.'
```

```
      print*,'   3 : 2P MOMENTUM TRANSFER',xmtlcu,'sq.cm.'
      print*,'   4 : PSEUDO MOMENTUM TRANSFER',xmtpscu,'sq.cm.'
      print*,'   0 : RETURN TO INITIALIZATION MENU'
      read*,dummy
      do dum = 1,10
      print*,' '
      end do
      if (dummy .lt. 0 .or. dummy .gt. 4) goto 810
      if (dummy .eq. 1) then
811   print*,'  '
      print*,'ENTER ELASTIC MOMENTUM TRANSFER CROSS-SECTION'
      read*,xmtelcu
      if (xmtelcu .lt. 1.0e-17 .or. xmtelcu .gt. 1.0e-13) goto 811
      end if
      if (dummy .eq. 2) then
812   print*,'  '
      print*,'ENTER METASTABLE MOMENTUM TRANSFER CROSS-SECTION'
      read*,xmtmcu
      if (xmtmcu .lt. 1.0e-17 .or. xmtmcu .gt. 1.0e-14) goto 812
      end if
      if (dummy .eq. 3) then
813   print*,'  '
      print*,'ENTER LASER LEVELS MOMENTUM TRANSFER CROSS-SECTION'
      read*,xmtlcu
      if (xmtlcu .lt. 1.0e-17 .or. xmtlcu .gt. 1.0e-14) goto 813
      end if
      if (dummy .eq. 4) then
814   print*,'  '
      print*,'ENTER PSEUDO LEVELS MOMENTUM TRANSFER CROSS-SECTION'
      read*,xmtpscu
      if (xmtpscu .lt. 1.0e-17 .or. xmtpscu .gt. 1.0e-14) goto 814
      end if
      if (dummy .gt. 0) goto 810
      return
      end
! subroutine to change Ne momentum transfer cross-sections
      subroutine xmtne(xmtelne,xmtmne,xmtpsne)
      implicit none
      real xmtelne,xmtmne,xmtpsne,dummy,dum
860   do dum = 1,20
      print*,' '
      end do
      print*,'ENTER A NUMBER : 0 RETURNS TO MAIN MENU'
      print*,'  '
      print*,'   1 : ELASTIC MOMENTUM TRANSFER',xmtelne,'sq.cm.'
      print*,'   2 : METASTABLE MOM. TRANS.',xmtmne,'sq.cm.'
      print*,'   3 : PSEUDO LEVEL MOM. TRANS.',xmtpsne,'sq.cm.'
      print*,'   0 : RETURN TO INITIALIZATION MENU'
      read*,dummy
      do dum = 1,10
      print*,' '
      end do
      if (dummy .lt. 0 .or. dummy .gt. 3) goto 860
      if (dummy .eq. 1) then
861   print*,'  '
      print*,'ENTER ELASTIC MOMENTUM TRANSFER CROSS-SECTION'
      read*,xmtelne
      if (xmtelne .lt. 1.0e-17 .or. xmtelne .gt. 1.0e-14) goto 861
      end if
      if (dummy .eq. 2) then
862   print*,'  '
      print*,'ENTER METASTABLE MOMENTUM TRANSFER CROSS-SECTION'
```

```
      read*,xmtmne
      if (xmtmne .lt. 1.0e-18 .or. xmtmne .gt. 1.0e-14) goto 862
      end if
      if (dummy .eq. 3) then
863   print*,' '
      print*,'ENTER PSEUDO LEVEL MOMENTUM TRANSFER CROSS-SECTION'
      read*,xmtpsne
      if (xmtpsne .lt. 1.0e-18 .or. xmtpsne .gt. 1.0e-14) goto 863
      end if
      if (dummy .gt. 0) goto 860
      return
      end
! subroutine to change initial metastable populations
      subroutine metpop(nm1,nm2,temp)
      implicit none
      real nm1,nm2,temp,dummy,gm1,gm2,de,k,dum
      gm1 = 1.22
      gm2 = 0.806
      de = 4.0e-20
      k = 1.38e-23
910   do dum = 1,20
      print*,' '
      end do
      print*,'ENTER A NUMBER : 0 RETURNS TO MAIN MENU'
      print*,' '
      print*,'   1 : 2D(5/2) POPULATION',nm1,'per cc'
      print*,'   2 : 2D(3/2) POPULATION',nm2,'per cc'
      print*,'   3 : BOTH TOGETHER'
      print*,'   0 : RETURN TO INITIALIZATION MENU'
      read*,dummy
      do dum = 1,10
      print*,' '
      end do
      if (dummy .lt. 0.0 .or. dummy .gt. 3) goto 910
      if (dummy .eq. 1) then
911   print*,' '
      print*,'ENTER LOWER METASTABLE LEVEL POPULATION'
      read*,nm1
      if (nm1 .lt. 0.0 .or. nm1 .gt. 1.0e15) goto 911
      end if
      if (dummy .eq. 2) then
912   print*,' '
      print*,'ENTER UPPER METASTABLE LEVEL POPULATION'
      read*,nm2
      if (nm2 .lt. 0.0 .or. nm2 .gt. 1.0e15) goto 912
      end if
      if (dummy .eq. 3) then
913     print*,' '
      print*,'ENTER LOWER METASTABLE LEVEL POPULATION'
      print*,'THE UPPER LEVEL POPULATION WILL BE CALCULATED'
      print*,'AUTOMATICALLY FROM THE RATIO OF THE'
      print*,'STATISTICAL WEIGHTS OF THE TWO LEVELS'
      read*,nm1
      if (nm1 .lt. 0.0 .or. nm1 .gt. 1.0e15) goto 913
      nm2 = nm1 * gm2 * exp(-de/(k*temp)) / gm1
      end if
      if (dummy .gt. 0) goto 910
      return
      end
! subroutine to change lifetimes of excited levels
      subroutine lifetime(lg,ly,lpsl1,lpsl2,lpsmne,lr0ne)
      implicit none
```

```
      real lg,ly,lpsl1,lpsl2,lpsmne,lr0ne,dummy,dum
940   do dum = 1,20
      print*,' '
      end do
      print*,'ENTER A NUMBER : 0 RETURNS TO MAIN MENU'
      print*,' '
      print*,'   1 : 2P(1/2)-2D(3/2) LIFETIME',ly,' secs'
      print*,'   2 : 2P(3/2)-2D(5/2) LIFETIME',lg,' secs'
      print*,'   3 : PSEUDO STATE TO 2P(1/2)',lpsl1,' secs'
      print*,'   4 : PSEUDO STATE TO 2P(3/2)',lpsl2,' secs'
      print*,'   5 : PSEUDO TO METASTABLE NEON',lpsmne,' secs'
      print*,'   6 : RESONANCE TO GROUND NEON',lr0ne,'secs'
      print*,'   0 : RETURN TO INITIALIZATION MENU'
      read*,dummy
      do dum = 1,10
      print*,' '
      end do
      if (dummy .lt. 0.0 .or. dummy .gt. 6) goto 940
      if (dummy .eq. 1) then
941     print*,' '
      print*,'ENTER YELLOW SPONTANEOUS LIFETIME'
      read*,ly
      if (ly .lt. 1.0e-9 .or. ly .gt. 1.0e-5) goto 941
      end if
      if (dummy .eq. 2) then
942   print*,' '
      print*,'ENTER GREEN SPONTANEOUS LIFETIME'
      read*,lg
      if (lg .lt. 1.0e-9 .or. lg .gt. 1.0e-5) goto 942
      end if
      if (dummy .eq. 3) then
943     print*,' '
      print*,'ENTER PSEUDO TO 2P(1/2) LIFETIME'
      read*,lpsl1
      if (lpsl1 .lt. 1.0e-9 .or. lpsl1 .gt. 1.0e-6) goto 943
      end if
      if (dummy .eq. 4) then
944     print*,' '
      print*,'ENTER PSEUDO TO 2P(3/2) LIFETIME'
      read*,lpsl2
      if (lpsl2 .lt. 1.0e-9 .or. lpsl2 .gt. 1.0e-6) goto 944
      end if
      if (dummy .eq. 5) then
945     print*,' '
      print*,'ENTER PSEUDO TO METASTABLE NEON LIFETIME'
      read*,lpsmne
      if (lpsmne .lt. 1.0e-9 .or. lpsmne .gt. 1.0e-6) goto 945
      end if
      if (dummy .eq. 6) then
946   print*,' '
      print*,'ENTER RESONANCE TO GROUND NEON LIFETIME'
      read*,lr0ne
      if (lr0ne .lt. 1.0e-9 .or. lr0ne .gt. 1.0e-6) goto 946
      end if
      if (dummy .gt. 0) goto 940
      return
      end
```

APPENDIX D

```
! PROGRAM TO CALCULATE RADIAL TEMPERATURES IN THE CVL
! FOR DIFFERENT INPUT POWERS
! INSULATION IS MADE UP FROM AN INNER ALUMINA TUBE WRAPPED IN
! ZIRCONIA FELT WITH A RADIATION SHIELD IN THE VACUUM GAP

      implicit none
      real rinner,router,tinner,touter
      real p,a2,a3,s,ez,eshield,l,t0,t1,t2,t3,tave,pi,dummy
      real r0,r1,r2,r3,kal,kzi,kza,power,sf,diff
      real temp0(50),temp2(50)

! PROGRAM TITLE
      do dummy=1,10
      print*,' '
      end do
      print*,'CVL THERMAL INSULATION PROGRAM : CERAMIC INSULATION'
      print*,' '
      print*,' '

! SET UP CONSTANTS

! s is Stephan's constant
      s = 5.67e-8

! sf is the radiation shape factor
      sf = 0.74

! eshield is the emissivity of the radiation shield
11    print*,'ENTER EMISSIVITY OF RADIATION SHIELD'
      read*,eshield
      print*,' '
      if (eshield .le. 0.0 .or. eshield .ge. 1.0) goto 11

! ez is the emissivity of the zirconia felt (assumed)
      ez = 0.5

      pi = 3.14159

! diff is the increment used in the iterations
      diff = 0.001

! r0, r1 are the inner and outer radii of the alumina tube
! r2 is the outer radius of the zirconia insulation
! and r3 is the radius of the heat shield
      r0 = 10.0e-3
      r1 = 14.0e-3
      r2 = 28.0e-3
      r3 = 38.0e-3

! kal is the thermal conductivity of alumina
      kal = 5.6

! l is the normalized length of the hot zone in metres
      l = 0.01

      a2 = 2 * pi * r2 * l
      a3 = 2 * pi * r3 * l

! t3 is the temperature of the heatshield in degrees Kelvin
```

```
      t3 = 400.0

! ********************** MAIN PROGRAM **********************

! p is the input power in watts
      do p = 1,50

! power radiated directly is reduced due to shape factor
      power = p * sf

! t2 is the temperature of the outer zirconia boundary
! t0 is the temperature of the inner alumina wall
      dummy = (1/ez) + ((a2/a3) * ((1/eshield)-1))
      dummy = (dummy * power / (a2*s)) + (t3**4.0)
      t2 = dummy**0.25

! move inwards through the zirconia felt in 0.5mm steps,
! calculating the thermal conductivity and temperature at
! each step
! rinner, router are the inner and outer radii of each 'segment'
! tinner, touter are the inner and outer temperatures
      router = r2
      rinner = router - 0.5e-3
      touter = t2

      do rinner=r2-0.5e-3,r1,-0.5e-3

! kzi is the initial 'guess' at the felt's conductivity
! kza is the actual value
      kzi = (1.6e-4 * touter) - 0.06
101   kzi = kzi + diff

      dummy = p * log(router/rinner) / (2 * pi * kzi * l)
      tinner = dummy + touter

      tave = (tinner + touter) / 2.0
      kza = (1.6e-4 * tave) - 0.06

! if the 'guess' and the actual value do not agree, 'guess' again
      if (kza - kzi .gt. diff) goto 101

      touter = tinner
      router = rinner

      end do

      t1 = tinner

      dummy = p * log(r1/r0) / (2 * pi * kal * l)
      t0 = dummy + t1

! store results in arrays
      temp0(p) = t0
      temp2(p) = t2

      end do

! ********************END OF MAIN PROGRAM ******************

! graphics routines

      call paper(1)
```

```
      call filnam('ceramic.grd;1',13)
      call pspace(0.1,0.95,0.1,0.8)
      call map(0.0,50.0,400.0,2000.0)
      call gratic
      call scales

! routine to draw the curves

      call positn(1.0,temp0(1))
      do p = 1,50
      call join(p,temp0(p))
      end do

      call positn(1.0,temp2(1))
      do p = 1,50
      call join(p,temp2(p))
      end do

      call grend

      stop
      end
```

```
! PROGRAM TO CALCULATE THE RADIAL TEMPERATURES IN THE LASER
! FOR DIFFERENT INPUT POWERS. ONLY METAL SEGMENTS ARE USED.
! THE RESULTS ARE NORMALIZED TO 1cm
! THIS VERSION HAS BEEN ALTERED TO INCLUDE CONDUCTION BETWEEN
! ADJOINING RINGS IN A SEGMENT AND GASEOUS CONDUCTION

      implicit none
      real sf,p,power,ad,ea,eb,eold,em,l
      real ashield,tshield,rshield,eshield
      real w,x,y,z,space,de,pi,s,dummy,kmo,kg,zz,num
      real dummy2,dummy3,dummy4,dummy5
      real r(20),a(20),t(20),temp(20,200),pow(200)

! PROGRAM TITLE
      do dummy = 1,10
      print*,' '
      end do
      print*,'PROGRAM TO CALCULATE RADIAL TEMPERATURE GRADIENT'
      print*,'IN THE CVL WITH METAL SEGMENTS USED AS INSULATION'
      print*,' '

! SET UP CONSTANTS
! de is the difference between ea and eb
      de = 0.001

! s is Stephan's constant
      s = 5.67e-8

! em is the initial assumed emissivity
      em = 0.3

! eshield is the emissivity of the radiation shield
      print*,' '
11    print*,'ENTER THE EMISSIVITY OF THE RADIATION SHIELD'
      read*,eshield
      print*,' '
      if (eshield .le. 0.0 .or. eshield .ge. 1.0) goto 11

      pi = 3.14159

! k is the thermal conductivity (mo = molybdenum ; g = buffer gas)
      kmo = 84.0
      kg = 8.0e-2

! include/exclude gaseous conduction processes
      print*,'ENTER 0.0 IF GASEOUS CONDUCTION IS TO BE EXCLUDED'
      read*,dummy
      print*,' '
      if (dummy .eq. 0.0) then
      kg = 0.0
      end if

! r(z) are the radii of the radiation shields
! rshield is the radius of the radiation shield
      rshield = 38.0e-3
21    print*,'ENTER NUMBER OF RADIATION SHIELDS'
      read*,num
      print*,' '
      if (num .le. 0.0 .or. num .ge. 20.0) goto 21

      r(num) = 28.0e-3
```

```
31    print*,'ENTER SPACING BETWEEN SHIELDS IN MILLIMETRES'
      read*,space
      print*,' '
      space = space / 1.0e3
      if (space .le. 0.0) goto 31
      if (space*(num-1) .ge. 28.0e-3) goto 31

      do z = num-1,1,-1
      r(z) = r(z+1) - space
      end do
      print*,'INNER WALL RADIUS IS',r(1)*100.0,'cm'
      print*,' '

! l is the length of the radiation shield segment in metres
41    print*,'ENTER LENGTH OF SEGMENT IN CENTIMETRES'
      read*,l
      l = l * 0.01
      print*,' '

      if (l .eq. 0.03) then
      sf = 0.92
      else
      if (l .eq. 0.12) then
      sf = 0.94
      else
      sf = 0.0
      end if
      end if
      if (sf .eq. 0.0) goto 41

! tshield is the temperature of the radiation shield
      tshield = 400.0

! ad is the area of the dimple in contact with the surrounding ring
51    print*,'AREA OF CONTACT BETWEEN RINGS IN SQUARE MILLIMETRES?'
      read*,ad
      print*,'  '
      if (ad .lt. 0.0 .or. ad .ge. 100.0) goto 51
      ad = ad / 1.0e6

! a(z) are the surface areas of the molybdenum rings in one segment
! and ashield is the area of the radiation shield that the outer
! molybdenum ring radiates to
      do z = 1,num
      a(z) = 2 * pi * r(z) * 0.01
      end do
      ashield = 2 * pi * rshield * 0.01

! this routine calculates the inner and outer temperatures of the
! laser for different input powers, p is the input power in watts

! ***************************** MAIN PROGRAM ************************

      do p = 1.0,60.0

      power = p / 2.0

      eb = em
91    ea = eb
      x = power * ((1 / eshield) - 1) / (ashield * s)
      t(num) = ((power/(a(num)*s*ea)) + x + (tshield**4.0)) ** 0.25
```

```
      eb = (1.35e-4 * t(num)) - 0.048
      if (eb-ea .gt. de .or. ea-eb .gt. de) goto 91
      eold = ea

      power = power / 0.74

      do z = num-1,1,-1

92    ea = eb
      t(z) = t(z+1)
      w = 2 * pi * kg * 0.01 / log(r(z+1)/r(z))
      x = a(z) * s / ((1/ea) + (a(z) * ((1/eold) - 1) / a(z+1)))
      y = ad * kmo / (r(z+1) - r(z))
      zz = t(z+1) ** 4.0
93    t(z) = t(z) + 0.5
      dummy2 = (x * ((t(z)**4.0)-zz)) + (w * (t(z)-t(z+1)))
      dummy3 = y * (t(z)-t(z+1))
      dummy5 = dummy2 + dummy3
      dummy4 = (dummy2*power/(dummy5*sf))+(dummy3*power/dummy5)
      dummy = dummy5 - dummy4
      if (dummy .lt. 0.0) goto 93
      eb = (1.35e-4 * t(z)) - 0.048
      if (eb-ea .gt. de .or. ea-eb .gt. de) goto 92
      eold = ea
      power = dummy4
      end do

      pow(p) = power

      do z = 1,num
      temp(z,p) = t(z)
      end do

      end do

! ************************** END OF MAIN PROGRAM ******************

! graphics routines
      call paper(1)
      call filnam('segrad.grd;1',12)
      call pspace(0.1,0.95,0.1,0.8)
      call map(0.0,50.0,400.0,2000.0)
      call gratic
      call scales

! routine to draw the curves
      do z = 1,num,num-1
      call positn(pow(1),temp(z,1))
      do p = 1.0,60.0
      call join(pow(p),temp(z,p))
      end do
      end do

      call grend
      stop
      end
```

```
! PROGRAM TO CALCULATE THE RADIAL TEMPERATURES IN THE LASER
! FOR DIFFERENT INPUT POWERS. ONLY METAL SEGMENTS ARE USED.
! THE RESULTS ARE NORMALIZED TO 1cm
! THIS VERSION HAS BEEN ALTERED TO INCLUDE CONDUCTION BETWEEN
! ADJOINING RINGS IN A SEGMENT AND GASEOUS CONDUCTION
! THE INNER 10 RINGS ARE FLAME-SPRAYED ON THE OUTSIDE

      implicit none
      real sf,p,power,ad,ea,eb,eold,em,l
      real ashield,tshield,rshield,eshield
      real w,x,y,z,space,de,pi,s,dummy,kmo,kg,zz,num
      real dummy2,dummy3,dummy4,dummy5
      real kzr,ezr,th
      real r(20),a(20),t(20),temp(20,200),pow(200)

! PROGRAM TITLE

      do dummy = 1,10
      print*,' '
      end do
      print*,'PROGRAM TO CALCULATE RADIAL TEMPERATURE GRADIENT'
      print*,'IN THE CVL WITH FLAME-SPRAYED METAL SEGMENTS'
      print*,'USED AS INSULATION'
      print*,' '

! SET UP CONSTANTS

! de is the difference between ea and eb
      de = 0.001

! s is Stephan's constant
      s = 5.67e-8

! em is the initial assumed emissivity
! ezr is the emissivity of the sprayed zirconia layer
      em = 0.3
      ezr = 0.5

! eshield is the emissivity of the radiation shield
      print*,' '
11    print*,'ENTER THE EMISSIVITY OF THE RADIATION SHIELD'
      read*,eshield
      print*,' '
      if (eshield .le. 0.0 .or. eshield .ge. 1.0) goto 11

      pi = 3.14159

! k is the thermal conductivity (mo = molybdenum ; g = buffer gas ;
! zr = zirconia layer)
      kmo = 84.0
      kg = 8.0e-2
      kzr = 2.0

! include/exclude gaseous conduction processes
      print*,'ENTER 0.0 IF GASEOUS CONDUCTION IS TO BE EXCLUDED'
      read*,dummy
      print*,' '
      if (dummy .eq. 0.0) then
      kg = 0.0
      end if
```

```
! r(z) are the radii of the radiation shields
! rshield is the radius of the radiation shield
      rshield = 38.0e-3
21    print*,'ENTER NUMBER OF RADIATION SHIELDS'
      read*,num
      print*,' '
      if (num .le. 0.0 .or. num .ge. 20.0) goto 21

      r(num) = 28.0e-3

31    print*,'ENTER SPACING BETWEEN SHIELDS IN MILLIMETRES'
      read*,space
      print*,' '
      space = space / 1.0e3
      if (space .le. 0.0) goto 31
      if (space*(num-1) .ge. 28.0e-3) goto 31

      do z = num-1,1,-1
      r(z) = r(z+1) - space
      end do
      print*,'INNER WALL RADIUS IS',r(1)*100.0,'cm'
      print*,' '

! th is the thickness of the sprayed zirconia layer
      th = 1.2e-4

! l is the length of the radiation shield segment in metres
41    print*,'ENTER LENGTH OF SEGMENT IN CENTIMETRES'
      read*,l
      l = l * 0.01
      print*,' '

      if (l .eq. 0.03) then
      sf = 0.92
      else
      if (l .eq. 0.12) then
      sf = 0.94
      else
      sf = 0.0
      end if
      end if
      if (sf .eq. 0.0) goto 41

! tshield is the temperature of the radiation shield
      tshield = 400.0

! ad is the area of the dimple in contact with the surrounding ring
51    print*,'AREA OF CONTACT BETWEEN RINGS IN SQUARE MILLIMETRES?'
      read*,ad
      print*,' '
      if (ad .lt. 0.0 .or. ad .ge. 100.0) goto 51
      ad = ad / 1.0e6

! a(z) are the surface areas of the molybdenum rings in one segment
! and ashield is the area of the radiation shield that the outer
! molybdenum ring radiates to
      do z = 1,num
      a(z) = 2 * pi * r(z) * 0.01
      end do
      ashield = 2 * pi * rshield * 0.01

! this routine calculates the inner and outer temperatures of the
```

```
! laser for different input powers, p is the input power in watts

! ************************** MAIN PROGRAM ************************

      do p = 1.0,60.0

      power = p / 2.0

      eb = em
91    ea = eb
      x = power * ((1 / eshield) - 1) / (ashield * s)
      t(num) = ((power/(a(num)*s*ea)) + x + (tshield**4.0)) ** 0.25
      eb = (1.35e-4 * t(num)) - 0.048
      if (eb-ea .gt. de .or. ea-eb .gt. de) goto 91
      eold = ea

      power = power / 0.74

      do z = num-1,num-4,-1

92    ea = eb
      t(z) = t(z+1)
      w = 2 * pi * kg * 0.01 / log(r(z+1)/r(z))
      x = a(z) * s / ((1/ea) + (a(z) * ((1/eold) - 1) / a(z+1)))
      y = ad * kmo / (r(z+1) - r(z))
      zz = t(z+1) ** 4.0
93    t(z) = t(z) + 0.5
      dummy2 = (x * ((t(z)**4.0)-zz)) + (w * (t(z)-t(z+1)))
      dummy3 = y * (t(z)-t(z+1))
      dummy5 = dummy2 + dummy3
      dummy4 = (dummy2*power/(dummy5*sf))+(dummy3*power/dummy5)
      dummy = dummy5 - dummy4
      if (dummy .lt. 0.0) goto 93
      eb = (1.35e-4 * t(z)) - 0.048
      if (eb-ea .gt. de .or. ea-eb .gt. de) goto 92
      eold = ea
      power = dummy4
      end do

      do z = num-5,1,-1

      t(z) = t(z+1)
      w = 2 * pi * kg * 0.01 / log(r(z+1)/r(z))
      x = a(z) * s / ((1/ezr) + (a(z) * ((1/eold) - 1) / a(z+1)))
      y = ad / (((r(z+1)-r(z)) / kmo) + (th / kzr))
      zz = t(z+1) ** 4.0
94    t(z) = t(z) + 0.5
      dummy2 = (x * ((t(z)**4.0)-zz)) + (w * (t(z)-t(z+1)))
      dummy3 = y * (t(z)-t(z+1))
      dummy5 = dummy2 + dummy3
      dummy4 = (dummy2*power/(dummy5*sf))+(dummy3*power/dummy5)
      dummy = dummy5 - dummy4
      if (dummy .lt. 0.0) goto 94
      eold = (1.35e-4 * t(z)) - 0.048
      power = dummy4
      end do

      pow(p) = power

      do z = 1,num
      temp(z,p) = t(z)
      end do
```

```
      end do

! ************************** END OF MAIN PROGRAM ******************

! graphics routines

      call paper(1)
      call filnam('flame.grd;1',11)
      call pspace(0.1,0.95,0.1,0.8)
      call map(0.0,50.0,400.0,2000.0)
      call gratic
      call scales

! routine to draw the curves

      do z = 1,num,num-1

      call positn(pow(1),temp(z,1))

      do p = 1.0,60.0
      call join(pow(p),temp(z,p))
      end do

      end do

      call grend

      stop
      end
```